NUMERICAL INVESTIGATION OF 2D DAM-BREAK FAILURES BY USING GIS APPLICATIONS

A THESIS SUBMITTED TO
THE GRADUATE SCHOOL OF NATURAL AND APPLIED SCIENCES
OF
MIDDLE EAST TECHNICAL UNIVERSITY

BY

AMMAR ASHRAF

IN PARTIAL FULFILLMENT OF THE REQUIREMENTS
FOR
THE DEGREE OF DOCTOR OF PHILOSOPHY
IN
CIVIL ENGINEERING

JULY 2021

Approval of the thesis:

NUMERICAL INVESTIGATION OF 2D DAM-BREAK FAILURES BY USING GIS APPLICATIONS

submitted by **AMMAR ASHRAF** in partial fulfillment of the requirements for the degree of **Doctor of Philosophy** in **Civil Engineering, Middle East Technical University** by,

Prof. Dr. Halil Kalıpçılar
Dean, Graduate School of **Natural and Applied Sciences**

Prof. Dr. Ahmet Türer
Head of the Department, **Civil Engineering**

Prof. Dr. Zafer Bozkuş
Supervisor, **Civil Engineering, METU**

Examining Committee Members:

Prof. Dr. İsmail Aydın
Civil Engineering, METU

Prof. Dr. Zafer Bozkuş
Civil Engineering, METU

Prof. Dr. A. Melih Yanmaz
Civil Engineering, METU

Assoc. Prof. Dr. Yakup Darama
Civil Engineering, Atılım University

Assoc. Prof. Dr. A. Ersin Dinçer
Civil Engineering, Abdullah Gül University

Date: 12.07.2021

I hereby declare that all information in this document has been obtained and presented in accordance with academic rules and ethical conduct. I also declare that, as required by these rules and conduct, I have fully cited and referenced all material and results that are not original to this work.

Name Last name : Ammar Ashraf

Signature :

ABSTRACT

NUMERICAL INVESTIGATION OF 2D DAM-BREAK FAILURES BY USING GIS APPLICATIONS

Ashraf, Ammar
Doctor of Philosophy, Civil Engineering
Supervisor: Prof. Dr. Zafer Bozkuş

July 2021, 197 Pages

In this study, the dam-break analysis of Ondokuz Mayıs Dam, İhsaniye Dam, and Avcıdere Dam is performed using full momentum HEC-RAS and dynamic wave FLO-2D model. The breach hydrograph for each dam was obtained by modeling the reservoir with dynamic wave routing in HEC-RAS. Three breach hydrographs (S1, S2, and S3) were calculated for each dam using a different set of breach parameters. The breach hydrographs were routed over the floodplain using both HEC-RAS and FLO-2D models. For Ondokuz Mayıs Dam, an accuracy check is performed for elevation data by comparing the Land Registry (Tapu Kadastro) and DSI data, and a new Digital Elevation Model (DEM) is developed using both datasets which is used in flood modeling later. Model calibration is done for Ondokuz Mayıs Dam; by using the flow depth of 2.735 m observed in the Engiz Creek in the year 2010. The calibration was done by varying the roughness values using the trial-and-error method. The calibrated model is then used for the breach hydrograph routing simulations. For Ihsaniye Dam and Avcıdere Dam, roughness values were selected based on the land use Google Earth images. The results of the routing analysis are presented in terms of inundation maps of maximum flow depth, maximum velocity and arrival time of maximum depth. For each dam, comparison of flow depth is presented at selected sections in populated areas. Moreover, the effect of sensitivity of grid resolution, roughness values, and breach hydrograph on the results are also presented. Flood hazard maps are prepared for each breach hydrograph to identify the risk-prone areas in the three dam sites. It was observed that in case of Ondokuz Mayıs Dam breach, Ondokuz Mayıs District will be at high hazard level, for İhsaniye Dam breach, Yalakdere Town will be at a high hazard level, and for Avcıdere Dam breach, Yalakdere town and southern part of Avcıköy town will be at a high hazard level. Flood damages caused by dam breach were also calculated in terms of losses to buildings and agriculture for the relevant areas. From the dam breach modeling results, it was concluded that there is a need to develop emergency action plans for the relevant areas, and the population in the affected areas should be educated about it, so that loss of lives and property can be avoided.

Keywords: Dam Breach, Breach hydrograph, Two-dimensional flood modeling, HEC-RAS, FLO-2D

ÖZ

CBS UYGULAMALARI KULLANILARAK 2-B BARAJ YIKILMALARININ SAYISAL İNCELENMESİ

Ashraf, Ammar
Doktora, İnşaat Mühendisliği
Tez Yöneticisi: Prof. Dr. Zafer Bozkuş

Temmuz 2021, 197 Sayfa

Bu çalışmada, Ondokuz Mayıs Barajı, İhsaniye Barajı ve Avcıdere Barajı'nın baraj-yıkılma analizi, tam momentum denklemli HEC-RAS (2D) ve dinamik dalga FLO-2D modeli kullanılarak yapılmıştır. HEC-RAS'ta her baraj için rezervuar dinamik dalga ötelemesi ile modellenerek gedik hidrografı elde edilmiştir. Her Baraj için farklı bir gedik parametresi seti kullanılarak üç gedik hidrografı (S1, S2 ve S3) hesaplanmıştır. Gedik hidrografları, hem HEC-RAS hem de FLO-2D modelleri kullanılarak taşkın yatağı üzerinden ötelendi. Ondokuz Mayıs Barajı için Tapu Kadastro ve DSİ verileri karşılaştırılarak kot verileri için doğruluk kontrolü yapılmış ve daha sonra taşkın modellemesinde kullanılmak üzere, her iki veri seti ile yeni bir Sayısal Yükseklik Modeli (SYM) geliştirilmiştir. Ondokuz Mayıs Barajı için 2010 yılında Engiz Deresinde gözlemlenen 2.735 m akış derinliği kullanılarak model kalibrasyonu yapılmıştır. Deneme yanılma yöntemi ile pürüzlülük değerleri değiştirilerek kalibrasyon yapılmıştır. Kalibre edilen model daha sonra gedik hidrograflarının öteleme simülasyonları için kullanılmıştır. İhsaniye Barajı ve Avcıdere Barajı için arazi kullanımı Google Earth görüntüleri baz alınarak pürüzlülük değerleri seçilmiştir. Öteleme analizlerinin sonuçları, taşkın haritalarında maksimum akış derinliği, maksimum hız ve maksimum derinliğe ulaşma zamanı cinsinden sunulmuştur. Her baraj için, yerleşim alanlarında seçilen enkesitlerde akış derinliği karşılaştırması sunulmaktadır. Ek olarak, ızgara çözünürlüğü, pürüzlülük değerleri ve gedik hidrografı hassasiyetinin sonuçlara etkisi de sunulmaktadır. Üç baraj yerinde riske açık alanları belirlemek için her bir gedik hidrografı için taşkın tehlike haritaları hazırlanmıştır. Ondokuz Mayıs Barajı yıkılması durumunda Ondokuz Mayıs Mahallesi'nin yüksek tehlike seviyesinde olacağı, İhsaniye Barajı için Yalakdere Beldesinin yüksek tehlike seviyesinde olacağı, Avcıdere Barajı için ise Yalakdere Beldesi ve Avcıköy'ün güney kesiminin yüksek tehlike seviyesinde olacağı gözlemlendi. Baraj yıkılmasından kaynaklanan sel zararları, ilgili alanlar için bina ve tarımsal kayıplar açısından da hesaplanmıştır. Baraj yıkılması modelleme sonuçlarından, ilgili alanlar için acil durum eylem planlarının geliştirilmesine ihtiyaç olduğu ve etkilenen bölgelerdeki nüfusun bu konuda eğitilmesi gerektiği ve böylece can kayıplarının azaltılacağı sonucuna varılmıştır.

Anahtar Kelimeler: Baraj yıkılması, gedik hidrografı, İki boyutlu taşkın modelleme, HEC-RAS, FLO-2D.

Dedicated to my Parents

ACKNOWLEDGMENTS

Foremost, I would like to express my sincerest gratitude to my advisor Dr. Zafer Bozkuş for his continuous support, motivation, patience, and immense knowledge. Without his guidance this research could not have been possible.

I would also like to thank my thesis committee members, Dr. İsmail Aydın, Dr. A. Melih Yanmaz, Dr. Yakup Darama, and Dr. A. Ersin Dinçer for their valuable suggestions, assistance in data acquisition and guidance for the completion of this study. I am also very grateful to all the members for providing me with the financial support as it was quite helpful and made it possible for me to complete this study.

This study would not have been possible without the data provided by the DSI and Tapu Kadastro, and SUFEN, Turkey Distributor of FLO-2D. I am very grateful for their support.

I would like to express my very great appreciation to to Higher Education Commission, Pakistan for providing me with the scholarship to study in Middle East Technical University. It had been a life-changing experience and I have learned a lot from it.

I would also like to extend my thanks to Muhammad Amjad, Mansoor Ahmed, Hassaan Bin Altaf, Uzair Hashmi, Rabela Junejo, and KM Sifatullah for their support and motivation during my stay at METU.

Finally, I would like to dedicate this thesis to my parents, as without their prayers and support, it would not have been possible for me.

TABLE OF CONTENTS

LIST OF TABLES

TABLES

LIST OF FIGURES

FIGURES

LIST OF ABBREVIATIONS

ABBREVIATIONS

DEM	Digital elevation model
DSI	State Hydraulic Works, Turkey
DBIP	Dam-Break inundation perimeter
ED	Escape direction
SES	Safe evacuation spots
SER	Secondary evacuation route
CZ	Concentration zone
MER	Main evacuation route
F-Statistic	Fit Statistic
FEMA	Federal Emergency Management Agency, US
HEC-RAS 1D	HEC-RAS One-dimensional model
HEC-RAS	HEC-RAS Two-dimensional model
IDW	Inverse Distance Weighing
JRC	Joint Research Center, Italy
RMSE	Root Mean Square Error
S1	Breach Hydrograph for Scenario 1
S2	Breach Hydrograph for Scenario 2
S3	Breach Hydrograph for Scenario 3
TSB	Turkey Insurance Association
TOB	Ministry of Agriculture and Forestry, Turkey
USACE	United States Army Corps of Engineers, US
US	United States

LIST OF SYMBOLS

SYMBOLS

A	Area of the building, m^2
A_r	Referenced wet area, m^2
A_s	Predicted wet area, m^2
A_o	Overlap of reference and predicted wet area, m^2
$A_k(H)$	Grid face area as a function of H, m^2
B_t	Breach top width, m
B_b	Breach bottom width, m
B_{ave}	Average breach width, m
BF	Structure unit price, TL
C	Courant number
C_b	Reservoir size coefficient
D	Non-dimensional empirical constant that depends upon the geometry and bottom/wall surface
DR	Damage factor
FD	Economic damage value calculated for the relevant floods, TL
H	Water surface elevation, m
H_b	Breach depth, m
K	A coefficient (0.6 x 0.5 x 1.18)
Max	Maximum
Q_n	Discharge in north direction, m^3/sec
Q_e	Discharge in east direction, m^3/sec
Q_s	Discharge in south direction, m^3/sec
Q_w	Discharge in west direction, m^3/sec
Q_{ne}	Discharge in northeast direction, m^3/sec
Q_{nw}	Discharge in northwest direction, m^3/sec
Q_{se}	Discharge in southeast direction, m^3/sec

Q_{sw}	Discharge in southwest direction, m^3/sec
R	Hydraulic radius, m
S_f	Friction slope component
S_o	Bed slope pressure gradient
V	Depth-averaged velocity in one of the eight flow directions x, m/sec
V_w	Reservoir volume at the start of dam failure, m^3
V_{er}	Volume of material eroded from the dam embankment, m^3
V_{out}	Volume of water that passes through the breach, m^3
V_o	Volume of water released, m^3
d	Reservoir depth, m
W_c	Dam crest width, m
Z	Breach side slope factor
Z_1	Average slope of the upstream face of dam
Z_2	Average slope of the downstream face of dam
c	Wave celerity, m/sec
c_f	Bottom friction coefficient
c_j	Intermediate coefficient
d_x	Estimated flow depth, m
d_i^p	Predicted flow depth, m
d_i^r	Referenced flow depth, m
e	Square of eccentricity of the earth
f	Coriolis parameter
g	Gravitational acceleration value, m/sec^2
g_o	Gravitational acceleration at equator, m/sec^2
h	Flow depth, m
h_d	Height of dam, m
h_w	Depth of water above the bottom of the breach, m
i	Excess rainfall intensity

k	Normal gravity constant
l	Length of dam crest, m
n	Roughness values, s/m$^{1/3}$
n_k	Unit normal vector at cell face k
q	Source/sink flux term
s	Sample size
t	Time, hr
t_p	Time to peak discharge, hr
t_f	Failure time, hr
u	Velocity components in x direction, m/sec
u_*	Shear velocity, m/sec
v	Velocity components in y direction, m/sec

Greek Symbols

$\Omega(H)$	Volume of cell as a function of H, m^3
ΔT	Computational time step, sec
ΔX	Average cell size, m
Δx	Width of the square grid element, m
Δt	Difference between consecutive time steps, sec
v_t	Coefficient for horizontal eddy viscosity
Θ	Theta implicit weighing factor
φ	Latitude
ω	Sidereal angular velocity of earth, 0.00007292115855306587/s
β	Coefficient (5/3 for a wide channel)

Superscripts

b,c	Coefficients computed from the regression analysis

n, n+1	timesteps

Subscripts

k	cell face
x	Location in the cell
j	cell

CHAPTER 1

INTRODUCTION

1.1 General Overview

A dam is a barrier that is used to store water for various purposes such as municipal use, agricultural use, hydropower, flood protection, and recreation (Zhang et al., 2016). The classification of dam can be based on their size, structure type, construction method and material. Structure wise dams can be classified as gravity dam, buttress dam, arch dam, etc. Based on the construction material, dam can be classified as embankment dam (earth-fill dam and rockfill dam), concrete dam, cemented sand and gravel dam, masonry dam, etc., (FEMA, 2013). For the dam size classification, International Commission on Large Dams (ICOLD) has marked 15 m as a reference dam height to differentiate the large dams from the smaller ones (ICOLD, 1998b).

Every dam poses a certain danger because of the possibility of its failure, which can produce catastrophic floods in the downstream floodplain (Říha et al, 2020). Dam failure can occur due to design flaws, operational shortcomings, earthquakes, overtopping, seepage, and many other factors (Vinet, 2017). From 1975 to 2011, about 70% of the dam failure in the United States was due to overtopping, 14% was due to seepage, while the rest was due to human-related issues, animal activities, and other factors (FEMA, 2013). Worldwide as least one event of dam failure occurs every year. Since the year 2000, 46 dams have failed worldwide, resulting in about loss of 392 lives. In the last two years alone, some of the notable dam-breaks with fatalities are, Tiware Dam in India, 2019 (23 fatalities), Brumadinho Dam in Brazil, 2019 (270 fatalities), Swar Chaung Dam in Myanmar, 2018 (4 fatalities), Xe-Pian

Xe-Namnoy Dam in Laos, 2018 (36 fatalities), Panjshir Dam in Afghanistan, 2018 (10 fatalities), Patel Dam in Kenya, 2018 (47 fatalities). Most of these dams breached with overtopping mode of failure caused by hydrological events (Wikipedia, 2020).

The flood hydrographs resulting from a dam-break are significantly different from those produced by rainfall, as they have higher flow rates and take a shorter time to peak (Khosravi, et al., 2019). This makes dam failure a catastrophic event, resulting in many casualties, economical, and environmental damages. These losses can be minimized by utilizing the knowledge of dam-break modeling. From the numerical modeling, the flooding zone and the flooding time can be estimated, which can be helpful in creating evacuation plans for hazardous areas. With the availability of high-speed computing systems and GIS-based numerical models, which utilize the digital terrain datasets, dam breach modeling has developed into the cost-effective and most attractive option (Issakhov & Imanberdiyeva, 2019).

Dam breach modeling is a two-step process. In the first step, a set of breach parameters are used to estimate the breach hydrograph, and in the second step, the breach hydrograph is routed over the downstream area (Zhang et al., 2016). A significant number of dam-break studies had been performed, using one-dimensional and two-dimensional models. For hazard assessment studies, one-dimensional models can capture the flow processes in channels adequately, while flow over a floodplain is better represented by the two-dimensional models (Falter et al., 2013, DRIP, 2018). In the one-dimensional (1D) models, cross-section data depicts the geometry and physical properties of the channel. The flow is simulated in one direction, and the water surface elevation, flow velocity, and momentum is assumed to be constant over the entire cross-section. (Jam & Engle, 2012). Some of the 1D models used to perform the dam-break studies since the 1970’s are DAMBRK, FLDWAV, SMPDBK, HEC-1, HEC-RAS 1D, and MIKE11 (Bozkuş & Güner, 2001; Bozkuş & Bağ, 2011; Bozkuş & Kasap, 1998, DRIP, 2018).

For dam breach modeling, recent development has focused on two-dimensional (2D) modeling for breach hydrograph routing and physically-based modeling of the dam breach erosion process. The 2D model uses the dynamic wave form or the simplified form of shallow water equation to route flow over floodplains, which are flat and wide, and also can be used to solve channel flows (FEMA, 2013). Some widely used 2D models for dam breach modeling are DSS-WISE, MIKE FLOOD, MIKE 21, LISFLOOD-FP, TELEMAC-2D, FLO-2D, and HEC-RAS (Salt, 2019; Zolghadr Et Al., 2011 ; Shustikova Et Al., 2020; Şahin, 2016; Ünal, 2019)

In 2D models, computations are carried out at a grid scale. The grid cells represent the terrain in terms of the elevation data and roughness values data. Most of the 2D models are raster based, which means that the underlying terrain is presented in terms of a single elevation values for each grid. In these type of models, as the grid size is changing, the shape of the underlying terrain is also changing (Jam & Engle, 2012). On the other hand HEC-RAS uses sub grid bathymetric approach to capture the details of the underlying terrain by computing the hydraulic properties for each computational grid from the available bathymetric data. The grid face capture the variation in the terrain in more details which are then incorporated in the model calculations (G. W. Brunner, 2016).

The 1D models are relatively faster to run with typical simulation runtimes less than an hour. 1D models can be time consuming to build but can be modified quickly and the results files are smaller in size. It also requires more interpolation and interpretation of results. On the other hand, for a 2D model the simulation can take hours to weeks to run. The model runtimes for the 2D models is inversely proportional to the grid resolution, the finer the computational grid, the larger the model runtime, and vice versa. In 2D models less interpolation of results is required, no advance identification of flow path is required, more complex flow path can be modeled, and results are more readily accessible/explicable (Babister et al., 2012; Dimitriadis et al., 2016; Morales-Hernández et al.,2016; Shustikova et al., 2019).

2D models calculate the inundation maps of flow depth and flow velocity over the terrain in the 2D grid system. Based on the simulation results, flood hazard maps can be prepared. Flood hazard maps are also useful to enhance the awareness of the public, municipalities, and other government organizations about the possibility of flooding. It shows the area which are at different hazard levels and can help device emergency action plan accordingly (Environment Agency, 2018). Furthermore, these inundation maps can be quite helpful in mitigation planning, emergency action plans and consequence assessment (SEPA, 2018).

The results of dam break modelling such as characteristics of the dam breach floods, and the inundation extents of the affected area are quite helpful in the devising the emergency action plans. This information can be used in the development of the warning systems and evacuation plans for the flood-prone areas (G. W. Brunner, 2016; FEMA, 2017; Říha et al., 2020).

1.2 Motivation and Contribution to the Study

In addition to all the advantages associated with a dam, it also poses a threat to no match. The breach hydrographs resulting from the dam failure are way different from the flood hydrographs resulting from hydrological events. In the majority of the cases the dam failure is a sudden event, which causes flood peaks higher than hydrological floods, and in a relatively much shorter interval of time. Dam break modeling has been an efficient tool is simulating scenarios of dam failure, so that possible protective measures can be taken based on the modeling output.

In recent times the use of 2D numerical modeling has increased in flood modeling simulations. 2D models make use of the detailed topographic data of the floodplain and provides better flood inundation results than 1D models. The advantages of 2D models come with a higher computational cost in comparison to 1D models. The grid resolution of the 2D model, determines the computational effort, as finer the grid resolution the higher the computational cost. The type of terrain also plays an essential part in the selection of appropriate grid resolution for flood simulations.

In this study, 2D dam breach modeling is done for three different types of terrains (for the Ondokuz Mayıs Dam; first it is a meandering valley and then a relatively flat floodplain, for İhsaniye Dam; the downstream area consists of a straight valley, and for the Avcıdere Dam; the downstream area is a meandering valley) using two different types of hydraulic models, HEC-RAS and FLO-2D.

Both the models will be analyzed for the sensitivity of the computational grid resolution (from finer to coarser resolution) to the inundation results. The results of this study will be helpful in evaluating each model's performance at different types of terrain. The results will be helpful for carrying out the 2D flood modeling for similar types of terrains. For the three dams, the calculated inundation results can be used for the preparation of emergency action plans, so that loss of life and property can be avoided.

1.3 Objectives of the Study

The main objective of this study is to determine the threat posed by dam failure to the downstream areas of the three dams: Ondokuz Mayıs Dam, İhsaniye Dam, and Avcıdere Dam. The results can be then used to devise the dam break risk management plans and hazard mitigation measures.

The objectives which will be covered in this study are.

- To model reservoir in 2D with HEC-RAS using a different set of breach parameters and failure modes to obtain breach hydrographs for each dam.
- For the Ondokuz Mayıs Dam, a quality check of the elevation data will be performed by comparing the elevation data obtained from Tapu Kadastro and DSI. Model calibration is also done for Ondokuz Mayıs Dam; Engiz Creek, using the flow measurement records of the Engiz Creek.
- Breach hydrograph routing will be carried out in HEC-RAS and FLO-2D and results will be compared for 5 m grid resolution for the three dams.
- The sensitivity of grid resolution to model output will be analyzed for the three terrains with both HEC-RAS and FLO-2D. The results of coarser

resolution (10 m, 25 m and 50 m) will be compared with the results of 5 m resolution for each model separately.

- The sensitivity of roughness values and breach hydrograph to the model output will also be analyzed in both models.
- Flood hazard maps will be prepared.
- Flood damages will be calculated.
- Recommendations based on the inundation results will be made for the hazard mitigation measure to minimize the damages.

1.4 Thesis Outline

In this thesis, there are 6 chapters. A brief description of each chapter is given below.

Chapter 1: In this chapter, a brief overview is presented along with this study's objectives.

Chapter 2: In the literature review chapter, the discussion is made for the type of dams, dam classification systems, the history of dam breach modeling, components of dam breach modeling, numerical model brief overview, and the methods for dam-break risk management.

Chapter 3: This chapter covers the basic methodology, assumptions, governing equations, and solution algorithm used in the HEC-RAS and FLO-2D.

Chapter 4: In this chapter, details are presented for the study area, hydrological and hydraulic data, elevation data preparation, roughness vale selection, breach parameters, flood hazard maps, and flood damage calculation.

Chapter 5: Th results of this study are presented in this chapter. The discussion is made for the breach hydrographs, the model calibration study of Ondokuz Mayıs Dam, breach hydrograph routing results of both HEC-RAS and FLO-2D are discussed. The inundation results are analyzed for their sensitivity to grid resolution, roughness values and breach hydrographs. Flood hazard maps and the calculated flood damages for the three dams are also presented.

Chapter 6: The last chapter includes the conclusions drawn from the simulation results. It also includes the recommendation based on the study results.

CHAPTER 2

LITERATURE REVIEW

Dams are constructed with the purpose of storing water to be used for the benefit of society in different ways, such as for irrigation, flood protection, water supply, hydropower generation, recreation and many more. The classification of dams can be done as discussed below.

2.1 Classification of Dams

2.1.1 Types of Dams

Dams can be categorized based on the type of construction material used. It can be an embankment dam or a concrete /masonry dam. Dams that consist of more than one component are known as composite dams, such as an embankment dam with a masonry spillway. The selection of the type of dam at a particular location depends upon several factors such as foundation geology, topography, the shape of the valley, the construction material availability, the type of spillway, seismicity of the area, and method of construction. The majority of the dams listed worldwide are mostly embankment dams and at second number are concrete dams, for example in the United States, about 87% of the constructed dams until 2009 were embankment dams (Figure 2-1).

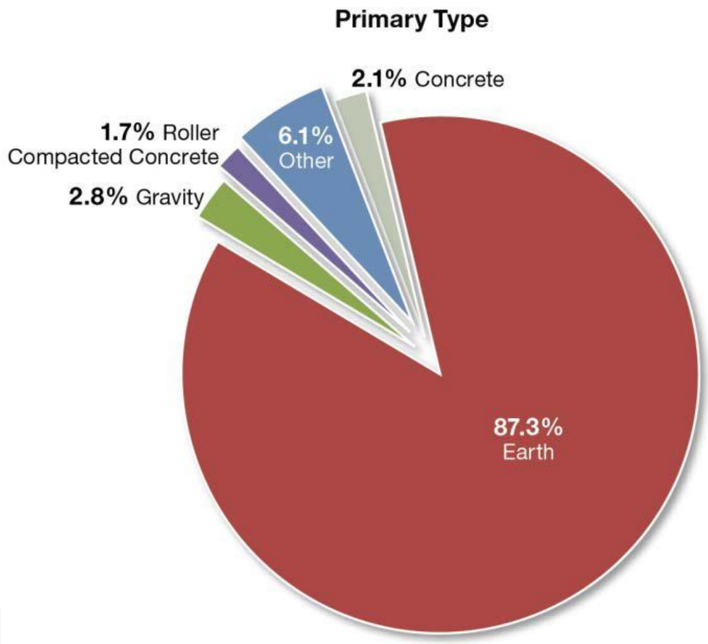

Figure 2-1 Percent of dams by primary type (USACE, 2009)

Concrete Dams:

Concrete dams comprise of concrete gravity, hollow gravity, single/multi-arch, buttress, and roller-compacted concrete dams (RCC). The construction material used in the construction of these dams is typically concrete or masonry components.

Embankment Dams:

Embankment dams are built with earthen materials which are available at or near the dam site. The dam body is filled with earth, rock, clay, or other materials which are erosion resistant. Figure 2-2 shows the different types of embankment dams. The most common types of embankment dams are earth-fill and rock-fill dams. On the upstream face of the embankment dams, typically there is cladding, for protecting the dam from water erosion. The seepage problem in these types of dams is controlled by constructing a center core of impervious material, permeable filters at downstream, and cut-off wall under the dam.

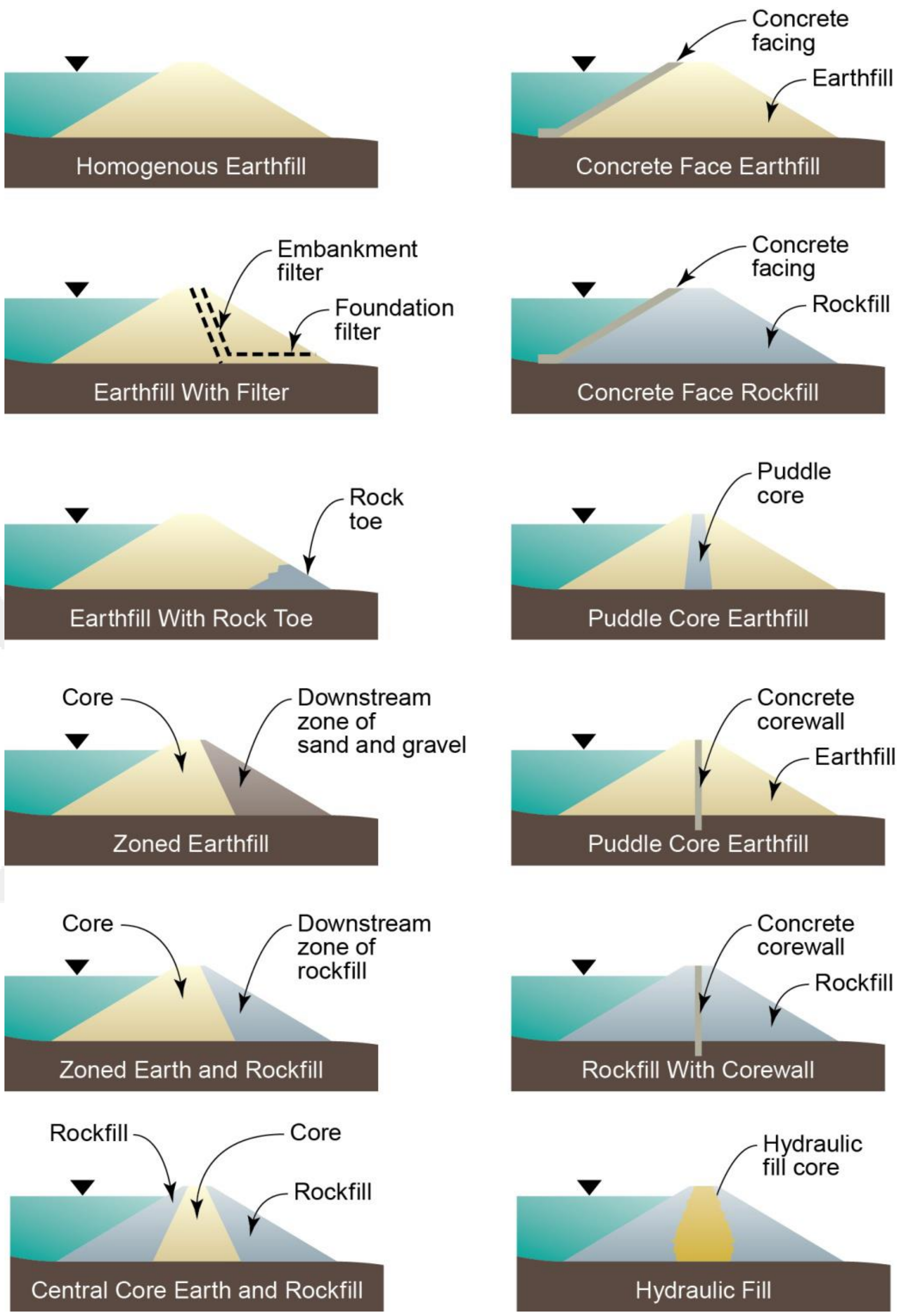

Figure 2-2 Types of embankment dams (Foster et al, 1998)

2.1.2 Dam Classification Systems

The state agencies in the US classify the dams, in terms of the size and hazard potential to regulate the dam design and dam-break modeling.

2.1.3 Dam Size Classification System

A classification system based on dam size was developed in 1979 by USACE for implementing the Dam Inspection Act (Pl 92-367). In this system, the dam properties such as the height of the dam, volume of the reservoir were used for classification. The dams were categorized into small, intermediate, and large dams. Table 2-1 gives the dam size classification system. (FEMA, 2013)

Table 2-1 Dam size classification system (USACE, 1979)

Category	Dam Height and Storage Volume	
	Height (m)	Storage (10^4 m^3)
Small	8 - 12	6 – 123
Intermediate	12 - 30	123 – 6170
Large	> 30	> 6170

2.1.4 Dam Hazard Potential Classification System

The hazard potential classification of dams in the US is based on the impact of dam failure on life and property (FEMA, 2013). FEMA recommended that the hazard potential classification can be based on the effect of failure during both normal and flood flow conditions, also furthers recommendations suggesting that the rating should be based on the probable worst-case failure scenario.

Table 2-2 shows the classification system suggested by FEMA for of hazard potential of dams and Table 2-3 gives the USACE system for hazard potential classification.

Table 2-2 FEMA Hazard Potential Classification System (FEMA, 2004b)

Hazard Potential	Loss of life	Economic, Environmental, lifeline losses
Low	None expected	Low and generally limited to owner
Significant	None expected	Yes
Hight	Probable. One or more expected	Yes

Table 2-3 USACE Dam Hazard Potential Classification System for Civil Works Projects (USACE, 1997)

Category	Hazard Potential Classification		
	Low	Significant	High
Direct loss of life	None expected (due to rural location with no permanent structures for human habitation)	Uncertain (rural location with few residences and only transient or industrial development)	Certain (one or more extensive residential, commercial or industrial development)
Lifeline losses	No disruption of services – repairs are cosmetic or rapidly repairable damage	Disruption of essential facilities and access	Disruption of critical facilities and access
Property Losses	Private agricultural lands, equipment and isolated building	Major public and private facilities	Extensive public and private facilities
Environmental Losses	Minimal incremental damage	Major mitigation required	Extensive mitigation cost or impossible to mitigate

These systems are used worldwide for the hazard level identification of dams.

2.1.5 Probable Life Loss

The public perception is greatly influenced by the loss of life in terms of any disaster. Probable loss of life is an essential consideration in emergency action planning and hazard potential classification. In case of a dam failure, the probable loss of life is determined based on the number of habitable structures and roads located in the affected areas (FEMA, 2013). Generally hazard potential classification systems do not account for people who are passer-by, non-overnight or occasional in the probable loss of life analysis (FEMA, 2004a).

2.2 Dam Failure

The dam failure can take place due to many mechanisms such as overtopping, piping (dam body and foundation), landslide, earthquake, structural failure, and equipment failure (G. Brunner, 2014). Historically, the majority of dams that have failed have been embankment dams, triggered by flooding.

Costa (1985) collected the data for all types of dams that have failed till 1985. It was observed that 34% of dams have failed because of overtopping, 30% by foundation defects, 28% due to piping/seepage, and 8% were caused by other forms of failure. For embankment dams, Costa (1985) stated that 35% have failed because of overtopping, 38% due to piping and seepage, 21% from foundation defects, and 6% from other modes of failure. Table 2-4 shows dam types and their failure modes.

Table 2-4 Possible Failure Modes for Various Dam Types (Costa, 1985)

Failure Mode	Embankment	Concrete Gravity	Concrete Arch	Concrete Buttress	Concrete Multi-Arch
Overtopping	✓	✓	✓	✓	✓
Piping/seepage	✓	✓	✓	✓	✓
Foundation defects	✓	✓	✓	✓	✓
Sliding	✓	✓		✓	
Overturning		✓	✓		
Cracking	✓	✓	✓	✓	✓
Equipment Failure	✓	✓	✓	✓	✓

With the provision of abundant benefits, the failure of a dam also accounts for catastrophic loss of life and property. From the historical record of dam failure, it can be seen that at least one event of dam failure occurs every year. Dam failure can occur due to design and operational shortcomings, earthquakes, overtopping, seepage, and many other factors (Vinet, 2017). Flood resulting from dam failure are different from those originating from hydrological events, as they have more significant peaks in a smaller amount of time.

2.3 Dam-Break Modeling

2.3.1 History of Dam-Break Research

The risk associated with the failure of the dam has highlighted the importance of research in dam failure problems. Luo et al. (2012) divided the past research in dam failure into three periods based on the contents and the characteristics of the research: First period (1850 to 1950), Second period (1950 to 1990), and the Third period (from 1990 onwards). In the first period, the main focus was on the testing of the physical models of the dam-break and the theoretical solutions of dam-break problems.

During the second period, field tests and laboratory experiments were carried out to study the dam-break process. In this time period, computer was also used in the Dam-Break study and various dam-break models were also developed such as DAMBRK, BREACH, FLDWAV, SMPDBK, MIKE and many more (D. L. Fread, 1989; George & Nair, 2015; Wing et al., 2019).

In the third period from 1990 onwards, the continuous improvement in computing systems has helped in the up-gradation of the hydraulic models resulting in improvement in the forecasting of dam failures, such as HEC-RAS 1D/2D, FLO-2D, DSS-WISE, MIKE FLOOD, MIKE 21, LISFLOOD-FP, TELEMAC-2D and many more (G. Brunner, 2014; G. W. Brunner, 2016) .

2.3.2 Components of Dam-Break Modeling

Dam-Break modeling consists of two components: a) Estimation of breach hydrograph, b) Routing of breach hydrograph on the downstream flood plain. The dam breach hydrograph is characterized by two main parameters: a) The magnitude of peak discharge Q_p, b) Time to peak discharge t_p (Figure 2-3). The magnitude of the peak discharge directly affects the area to be inundated and flood wave propagation on the downstream floodplain. The time to peak discharge is important in terms of the available time to warn the people at risk (Kalinina, et al., 2016).

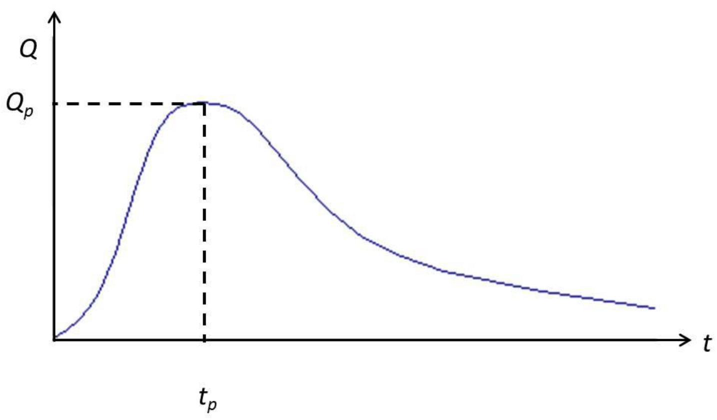

Figure 2-3 Scheme of a breach hydrograph (Kalinina et al., 2016)

The accurate estimation of the Q_p and t_p is important in risk evaluation studies as it is the primary input (Wahl, 2010).

The methods used for the estimation of breach hydrograph are discussed below.

2.3.2.1 Methods for Estimation of Dam Breach Hydrograph

The methods available in the literature to compute the dam breach hydrograph can be classified into three groups ranging from simpler to more complex methods (Wahl, 2010).

1. Methods that directly predict the peak discharge.
2. Methods that make use of breach parameters to predict the breach development and compute the outflow based on the breach progression.
3. Methods that compute the breach erosion process, the breach formation and the outflow in great detail.

Methods that directly predicts the peak discharge: The peak outflow from a dam-break can be directly estimated using the empirical equation developed from the regression analysis of data from historical dam failures. Typically regression equations are in the form of power-law relationships as shown in equation 2.1 (Manville, 2001).

$$Q_p = \alpha V_w^b h_w^c \tag{2.1}$$

where V_w is the reservoir volume at the start of dam failure (m^3/s) and h_w is the height of water from breach bottom elevation (m), a, b, c are the coefficients computed from the regression analysis.

MacDonald and Langridge-Monopolis, (1987) developed a relationship for the peak discharge from dam-break by utilizing data sets from 42 dams (embankment dams). Costa (1985) derived an equation for peak outflow from the regression analysis of data from 31 dams (embankment and concrete dams). Froehlich (1995) used the available discharge data from 22 dams in regression analysis to develop an equation for peak outflow. Table 2-5 gives some empirical equations used for the estimation of peak outflow Q_p (m^3/s) and Time to peak t_p (h).

Table 2-5 Empirical equation for estimation of peak discharge (Kalinina et al., 2016)

	Equation	Reference
Peak outflow (m^3/s)	$Q_p = 1.15(V_w H_w)^{0.41}$	MacDonald and Langridge-Monopolis (1984)
	$Q_p = 0.763(V_w H_w)^{0.42}$	Costa (1985)
	$Q_p = 0.607 V_w^{0.295} H_w^{1.24}$	Froehlich (1995b)
Time to peak (h)	$t_p = 0.0179\ (V_{er})^{0.364}$ where $V_{er} = 0.00348\ (V_{out}\ H_w)^{0.852}$	MacDonald and Langridge-Monopolis (1984)
	$0.25 \leq t_p \leq 1$	Singh and Snorrason (1982, 1984)

Methods that predict breach development directly and the outflow analytically: This approach makes use of the regression methods which are developed based on the historical dam failure data. The aim is to predict the breach parameters in relation to the dam and reservoir characteristics.

Breach parameters can be divided in to geometric and hydrographic groups. The shape for embankment dam breach is often trapezoidal, described in terms of geometric parameters such as breach depth H_b, breach top width B_t, breach bottom width B_b, average breach width B_{ave}, and breach side slope factor Z, as shown in Figure 2-4. Out of these five geometric parameters, combination of any three parameters defines the breach size and shape. Among the hydrographic parameters are peak outflow discharge Q_p, b) Failure time t_f. With the start of breaching, the outflow increases until it reaches Q_p, and then decreases until the water level in the reservoir drops (Chinnarasri et al, 2004). The time it take from the inception of breach to its completion is defined as Failure time t_f (Singh & Snorrason, 1984).

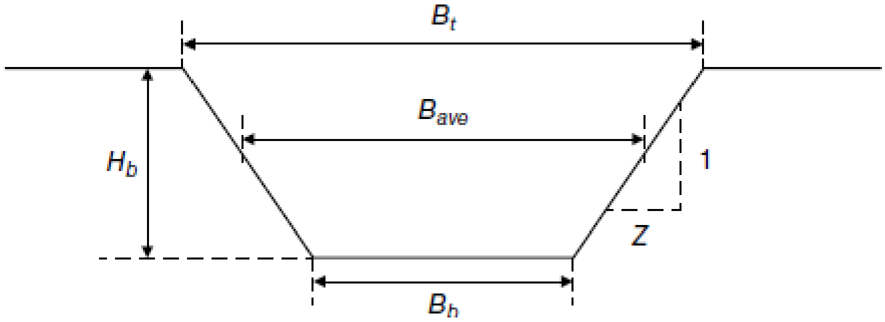

Figure 2-4 Geometric parameters of an idealized dam breach. (Xu & Zhang, 2009)

In these methods, the analysis of the dam-breach formation process is carried out separately from the analysis of the flow through the breach. Although the breach formation process is mostly common for embankment dams, these methods are presented to provide a general overview. The dam-breach formation is modeled with regression methods that are based on historical data and aim to predict the parameters characterizing the breach development as a function of dam and reservoir characteristics without simulating the erosion processes.

The breach is described in terms of estimated parameters such as breach width and breach formation time. The breach opening is treated as a weir control, with the outflow calculated using the weir equations. Some of the empirical equations for breach width and breach formation time are given in Table 2-6, where V_o is the volume of water released (m^3), d is the reservoir depth (m). These methods do not account for the erosion process.

Table 2-6 Empirical equations for estimation of the parameters of the breach-formation process (Kalinina et al., 2016)

	Equation	Reference
Breach Width (m)	$B = 3(H_w)$	Bureau of reclamation (1988)
	$B = 13.3(V_0 H_w)^{0.25}$	Froehlich (1987)
Breach formation time (h)	$t_b = 3.84(V_0)^{0.364} d^{-0.9}$	Froehlich (1995a)
	$t_b = 0.011B$	Bureau of reclamation (1988)
	$t_b = B/(4H_w + 61)$	Lawrence Von Thun and Gillette (1990)

Methods that model the erosion processes, the breach development and the flow in detail: In these methods. Breach hydrograph is computed by simulating the breach erosion process and the associated flow hydraulics. This method is generally used for embankment dams (earth fill or rockfill dams). One of the models which estimate the breach width and formation time based on the erosion process is BREACH model developed by the National Weather Service (Fread, 1988). One of the limitations of these types of models is that it does not account for the dynamic effects of flow in the reservoir which can be crucial in some cases (Kalinina et al., 2016).

2.3.2.2 Downstream Routing Analysis

After the estimation of the dam breach outflow hydrograph, the flood wave is routed over the downstream terrain to determine the impact of flood at any concerned location in the floodplain. The key components in the dam-break flood simulation are;

a) Input; the breach hydrograph, the topography of the downstream floodplain, and Land use shapefile

b) Model type, flow equations and the numerical methods to solve them,

c) Output; the arrival time of the flood wave, the maximum flow depth, the time to maximum flow depth, and the maximum flow velocity.

2.4 Numerical Models

In this section, a brief discussion is made for the hydraulic model in terms of 2D vs 1D, numerical solution procedures, and numerical schemes used.

2.4.1 2D vs 1D

Traditionally dam-break modeling has been done by 1D models which solve either fully dynamic or simplified form of 1D cross-section averaged shallow water equations across the cross-sections. 1D models generally yield meaningful results for areas with confined floodplains/channels where the flow is along a single direction without any major divergence. Confined floodplains consist of rivers located in mountainous ranges to wide coastal plains. As the flow enters into unconfined flat regions errors might be introduced into the unsteady flow simulations. 1D models give output in terms of depth and discharge at the provided cross-sections along the river. Some of the one-dimensional models used to perform the dam-break studies since the 1970's are DAMBRK, FLDWAV, SMPDBK, HEC-1, HEC-RAS 1D, and MIKE11 (Bozkuş & Güner, 2001; Bozkuş & Bağ, 2011; Bozkuş & Kasap, 1998, DRIP, 2018).

The areas downstream of the dam may consist of both confined and unconfined floodplains. An example of it would be a dam located on a mountainous river that flows into a large valley from an alluvial fan. ID models are based on certain assumptions such as flow velocity is uniform over the cross-section which does not hold well and can affect the accuracy of the model (DRIP, 2018).

For dam-break, the flow rate generally exceeds the capacity of the downstream channels and spreads significantly across the downstream terrain. Therefore, 2D models can be considered as most accurate for dam breach modeling depending upon the availability of fine-resolution terrain data. 2D models solve either the dynamic wave form or the simplified form of shallow water equation to route flow over unconfined/confined floodplains, (FEMA, 2013). With the recent developments in computing systems, the use of 2D models for dam failure studies has increased. Some widely used two-dimensional models for dam breach modeling are DSS-WISE, MIKE FLOOD, MIKE 21, LISFLOOD-FP, TELEMAC-2D, FLO-2D, and HEC-RAS (Salt, 2019; Zolghadr et al., 2011 ; Shustikova et al., 2020; Şahin, 2016; Ünal, 2019).

2.4.2 Numerical Solution Procedures

The solution of numerical modeling initiates with the discretization process, in which the differential form of shallow water equations is replaced by algebraic equations which are relationships representing the calculated variable at a finite set of points in the time and space domain. In hydrodynamic modeling software's there are three primary methods to solve the shallow water equations or their simplified forms: (Néelz & Pender, 2009)

- Finite Difference
- Finite Volume
- Finite Element

A brief explanation of each of these methods is given below.

Finite Difference: In the finite difference method, the representation of equations as a continuum is replaced by a set of piecewise equations at the points in the domain. This method is the most direct approach for mapping the differential equations to the individual elements in the domain. The finite difference method is typically applied on a structured grid with points at a regular spacing to improve the efficiency of the method. In this method, computation are carried out at the cell center and mass is conserved globally (Robinson et al., 2019).

Finite Element: The finite element method converts the continuum field equations into the equation for each element. This is done as the field in each element are approximated as a simple function e.g., a linear polynomial with a finite number of degrees of freedom. This method uses a set of linear equations to explain the approximate behavior of flow locally in the element. With the compilation of the contribution from all the elements, the finite element method forms a large matrix which is solved with the well-known matrix solvers. The finite element method is quite general and has been used successfully to study many problems. It can adapt easily to the higher-order elements rather than being confined to only linear elements. The higher-order elements improve the accuracy of the representation of the unknown in the element. In Finite element methods, the computations are carried out at Gauss points (special location inside the element) and mass is conserved at the global scale.

Finite Volume: In the finite volume method, the solution domain is subdivided in a similar manner as in the finite element method, however the numerical basis varies substantially. The main feature of the finite-volume method is that it performs flux evaluations across the element boundaries. This feature is also applicable to nonlinear problems that appear frequently in transport problems (i.e., water quality or sediment transport). The computations are carried out typically at the center of each element or center of each face between the elements and mass is conserved both globally and locally.

2.4.3 Implicit and Explicit Schemes

The discretization of the partial differential equations is accomplished using numerical approximation schemes: implicit and explicit. The main difference in these solution schemes is how the solution advances in time. In the explicit schemes, known variables at the current timestep are used to directly compute the dependent variable in the next time step. For the implicit schemes, the known variables at both the present and the next time step are used in the coupled set of equations to be solved with iterative or matrix solver techniques for obtaining the solution for the dependent variable.

Explicit schemes are typically easier to program, less complex to represent, easier to split for parallelization, and takes less computational effort for each solution step. Also explicit schemes have a larger number of solution steps because of the smaller time step requirement. While for implicit schemes a significantly larger time step can be selected without affecting the stability of the solution, however any error analysis should be performed to find out its impact on the solution accuracy.

Therefore, implicit schemes can require orders of magnitude fewer solution time steps than explicit methods. The main benefit of implicit methods is the ability to select a significantly larger time step without affecting stability, though an error analysis must be performed to determine its effects on accuracy.

2.5 Literature Review of the Studies

Some of the studies related to dam-break and flood inundation modeling are reviewed in this segment as under.

M.S. Horritta, (2002) tested 1D and 2D hydraulic models (HEC-RAS, TELEMAC-2D, and LISFLOOD-FP) for simulating the flood events of the River Severn (UK) in 1998 and 2000. The models were calibrated and the performance for each model was evaluated against the observed data.

Horritt, Bates, & Mattinson, (2006) investigated the effect of mesh resolution and topographic data quality on the performance of 2D finite volume model for a 7 km reach of Thames River (UK). The model out was found to be more sensitive to mesh resolution in comparison to topographic sampling.

Urzică et al., (2021) used HEC-RAS 2D for dam-break analysis of Cal Alb reservoir in Baseu Basin (Romania), for the purpose of testing the flood control capacity of the system. The dam was breached using the piping process and the downstream 2D flow area comprises of average cell size of 64 m^2. The results obtained were analyzed in terms of flood severity on the downstream settlements. The analysis showed that the multi-reservoir system of the Baseu River has a vital role in flood protection and contribution to the action plan for dam failure.

Quirogaa et al., (2016) studied the floods event of 2014 in the Bolivian Amazonia using HEC-RAS 2D. The results were used in identifying the areas exposed to the different hazard levels.

Farooq et al., (2019) used the HEC-RAS 2D model for calibration and validation of 2010 floods in the area of Swat Valley in Pakistan. Flood hazard maps were prepared for different return periods to help the policy maker in devising the mitigation measures for Swat Valley.

Pinos & Timbe, (2019) developed flood inundation maps for the mountainous river basin of Santa Barbara river in Ecuador, using four 2D models (Iber 2D, HEC-RAS 2D, PCSWMM 2D, and Flood Modeller 2D). Model's performance was evaluated in terms of flood extent and maximum water levels against flood events of 25 and 50 years return period.

Ongdas et al., (2020) simulated various flood scenarios for the Yesil river (Kazakhstan) using HEC-RAS 2D. The model sensitivity to mesh resolution was studied with no significant differences found in the model output. The model was calibrated and then inundation maps for floods of 10-, 20-, and 100-year return period were obtained.

Zeleňáková et al., (2019) used HEC-RAS 2D to perform flood modeling of Slatvinec stream in Slovakia. The simulation results were used to identify the flood risk areas and in the cost evaluation of the flood damages.

Anees et al., (2016) discussed the numerical techniques for flood modeling. It was suggested that HEC-RAS 1D and FLO-2D were accurate and economical for channel and floodplain modeling. The need for the development of 3D model for floodplains was also discussed.

Akkaya & Doğan, (2016) carried out coupled 1D/2D flood modeling of Meric and Tunca rivers at Edirne city center (Turkey) using MIKE 11, and MIKE 21, coupled by using MIKE FLOOD. Flood inundation maps for 2, 25, 50, 100, and 500 return periods were developed. The use of a drainage channel as a flood management measure was also studied.

Shrestha et al., (2020) utilized HEC-RAS 2D and MIKE 21 to perform flood modeling of Deer Creek (Missouri) for the purpose of evaluating the flood extent. The models were calibrated for peak discharges along with the creek and flood inundation maps were obtained for flood hydrographs with different return periods. The compromise between the resources and accuracy is assessed while comparing the capabilities of each model.

Pilotti et al., (2014) carried out the dam-break analysis of the Cancano Dam (Italy) in alpine regions using the 1D Pilotti et al. (2011) model and FLO-2D models. The results obtained were verified against the measurements made in the laboratory study.

Haltas et al. (2016) studied the dam-break scenarios for Alibey Dam (Istanbul) and Porsuk Dam (Eskisehir). Both the dams were breached using HEC-RAS (1D) with three sets of breach parameters to obtain the breach hydrograph. The FLO-2D model was used to route the breach hydrograph over the floodplain. The results were displayed in the form of flow depth, flow velocity and arrival time for maximum flow depth maps. It was noticed that the peak flow rate of the flood hydrographs had a substantial impact on the flow depth, flow velocities, arrival time and inundation areas.

Zaifoğlu, (2018) carried out a flood modeling study for Nicosia by using the coupling of MIKE 11, MIKE 21 in MIKE FLOOD. The model was calibrated for the flood event of 2010. After the model calibration, the flood hydrograph of the 500 year return period was used to study the effect of several flood protection measures and recommendations were made for flood management.

Ünal (2019) performed dam-break analyses for Berdan Dam (Mersin) using HEC-RAS model. In this study, a computational grid size of 100 m x 100 m was used for all the simulations. The dam was breached using overtopping and piping failure scenarios. In addition to the breach hydrograph, the sensitivity of manning's roughness parameter on the flood routing was also studied. The results were presented in the form of maximum flow depth, flow velocity, arrival time, and Water surface elevation maps. A comparison of results was also presented at the different sections near the populated areas. It was observed that the possible flood will severely impact downstream populated areas.

Salt (2019) compared dam breach modeling simulation results using HEC-RAS and DSS-WISE lite 2D models for Rancho Cielito Dam (USA). A computational grid size of 20 ft was used for both model in all the simulations. The results demonstrate some minor differences in the inundation boundaries at flat areas. There was no significant effect observed on the inundation results due to the different numerical schemes used by the models. The simulation time for DSS-WISE Lite was about 100 times faster than that of HEC-RAS 2D. In DSS-WISE Lite some potential features to alter flow were not captured in the terrain file, resulting in vastly different flow characteristics in these areas than the HEC-RAS model.

Şahin (2016) performed the two-dimensional dam breach analysis for the Osmangazi Dam and Sungurlu Dam by using the FLO-2D model. Different dam breach scenarios were modeled. The simulations were carried out at DEM resolution (5 m and 10 m), and grid resolution (10 m, 20 m, 25 m, 30 m, 40 m, 50 m, 75 m, and 100 m). The results were then presented in the form of maximum flow depth, flow velocity, maximum water surface elevation maps. The variation in maximum flow depth and arrival time were also presented at control points. Flood hazard maps were prepared for the downstream area of both dams.

Kiyici (2019) studied the storm event in the Terme river (July 2012) using the LISFLOOD-FP model. The available data was used to calibrate the model. The simulations were performed at 5 m, 10 m, 50 m, and 100 m grid resolution to study the effect of spatial resolution on the results. The sensitivity analysis of the roughness parameter was also carried out. The flow depth obtained from the coarser grid simulations was then compared with the 5 m grid simulation. The outcomes from the LISFLOOD-FP model were found to be quite familiar with the results of a previous study conducted by using the MIKE-21 model.
Khosravi et al. (2019) studied the probable failure of the Sefid-Roud Dam (Iran) using the HEC-RAS model. The dam was breached using an overtopping mode of failure, and the breach flood hydrograph was routed on the downstream floodplain. The 100 m x 100 m grid cells were used in the simulation over terrain with a spatial resolution of 1 m. The results show that the flood arrival time is too short of executing any evacuation plans in highly populated areas. The modeling results were considered to play a vital role in the development of plans for flood management and risk analysis in the downstream area.

Haltas et al., (2016) performed the numerical simulation for a hypothetical dam failure of Ürkmez Dam (Izmir). The dam was breached, and the breach hydrograph was routed in the narrow valley downstream using the HEC-RAS 1D model. The breach flood hydrograph at the last cross-section was used as an inflow hydrograph into the FLO-2D model, to route the flood over the floodplain. The results of the two-dimensional simulation were presented in the form of maps of maximum flow depth, velocity, and arrival time. The dam breach simulation results were then matched with the experimental data obtained from the distorted physical model study, which were found to be quite similar.

Yalçın (2020) studied the effects of topography and land cover on the flood modeling results by using the HEC-RAS model on Kilicozu Creek's floodplain in Kirsehir. The sensitivity of mesh resolution, digital terrain model resolution, and Manning's roughness layer was studied over a wide range. Mesh sizes ranging from 2 m x 2m to 25 m x 25 m were used. The flood modeling was done on 19 different configurations, composed of varying mesh resolution, Terrain spatial resolution and Manning's roughness layer for 500-year return period floods. The results obtained were compared with the model simulation results of the finest resolution.

Shustikova et al., (2019) performed flood modeling for the Sechia River (Italy) using HEC-RAS and LISFLOOD-FP. In the study, grid sizes ranging from 25 m to 100 m were used over the complex terrain of 1 m spatial resolution. The simulation results obtained at different grid sizes were compared. The distribution of flood characteristics over the complex terrain was analyzed. The best results were obtained at 25 m grid, and at a coarser grid size, it was noted that both models miscalculate the flow depth and inundation extents. It was suggested that specific terrain features in an area could cause ambiguities in the simulation results for large-scale models.

Beden et al. (2018) carried out a comparative study of flood simulation using MIKE-21 and FLO-2D models for the Mert River (Samsun). Flood hydrographs of 100 years, 500 years, and 1000 years a return period was used as inflow into the models. The results obtained from both the models were matched to comprehend the advantages and limitations of both models in flood plain modeling. It was observed that there is consistency in the results obtained from both the models and the result reliability mostly depends upon the quality of the available data.

2.6 Dam-Break Risk Management

Despite all the improvements in engineering knowledge and construction quality, dam failure can occur, caused by natural hazards, human actions or loss of dam strength capacity as it ages. Dam failure incidents are a serious threat to public safety, economical, and environmental resources. Over time a lot of dam failure incidents have taken place resulting in loss of life and property. these incidents have highlighted the significance of dam-break risk management, which is an important contribution to the protection of the population, property, and environmental resources along the downstream valley.

Almeida & Viseu (1997) stressed that the dam and the downstream area should be taken as a combined system, with the risk induced by the dam failure should concern both the dam reservoir and the downstream area.

Dam-break risk management consists of two essential parts, risk assessment and risk mitigation (Figure 2-5). Risk assessment deals with the process of risk analysis and risk evaluation. Risk mitigation deals with measures to minimize the human losses, economic and environmental damages resulting from dam failure,

Risk analysis is a structured process that investigates both the extent and likelihood of consequences linked with dam failure. Dam risk analysis includes different types of uncertainties: such as some major hazards resulting in dam failure, predicting and characterizing the chain of events resulting from major events (ranging from the physical response of the dam and the downstream area to human response), vulnerability assessment of the downstream areas through the estimation of the damages in terms of lives lost, the monetary damages and other probable adverse outcomes.

Risk evaluation is the process of identifying the magnitude of the risk, and its comparison with the acceptable risk criteria. The main task of the risk evaluation process is the development of criteria for decision guidance for the comparison of the risk analysis conclusions.

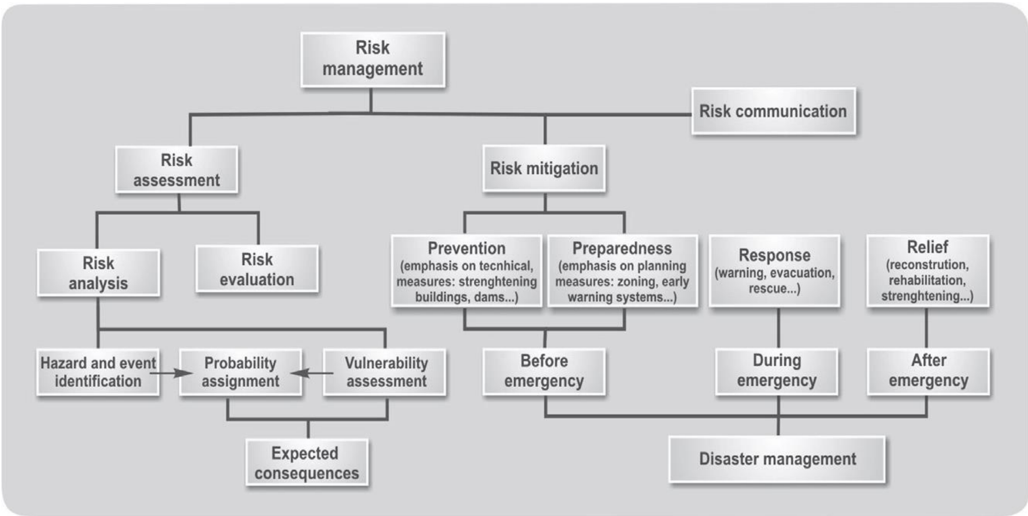

Figure 2-5 The dam risk management general process (Wrachien & Mambretti, 2009)

As the risk analysis outcome shows that the estimated risk is intolerable, then risk mitigation is employed for emergency planning. The planning is carried out for both internal i.e., at the dam site (to minimize the chances of occurrence of an accident) and external, at the downstream valley (to minimize the loss of lives and property). Therefore, methodologies and resources must be defined to enable the successful performance of the five general key aspects of an emergency plan: detection, decision, notification, warning, and evacuation.

Hazard mitigation aims at organizing the prevention measures, namely safety control requirements, to be enforced at the dam site, and emergency preparedness measures, to be implemented in the downstream valley. Issues to be addressed are safety monitoring of dam, emergency planning and preparedness, early warning systems as well as rescue and relief measures for post-event actions.

2.6.1 Dam-Break Risk Mitigation and Response to Hazard

The risk mitigation process aims at the organization of the preventive measures, both at the dam site (by applying structural and non-structural measures for dam safety) and at the downstream valley (to minimize the loss of life and property)

The hazard exposure can be controlled by implementing long-term structural measures for valley preparedness, such as land-use planning and valley risk zoning. Emergency plans, a non-structural measure can be developed to reduce the vulnerability of the downstream valley population.

The emergency action plan is prepared for the pre-emergency phase of the disaster management cycle. It highlights the potential emergency conditions at the dam and presents the action to be taken to reduce the loss of life and property. It provides the measures which the dam owner will undertake to moderate the problems at the dam. It also provides the information and procedures to the dam owner for the issuance of the early warning and messages to the relevant authorities in the downstream areas in case of an emergency. It also contains flood inundations maps to highlight the areas at greater risk in case of emergency.

Emergency action plan generally consists of five essential components:(USBR, 1995, 1998):

- detection of the occurrence of an extreme event or of a dam abnormal behavior;
- decision at the dam site, which is the establishment of procedures to respond to the event or to the dam abnormal behavior;
- notification system;
- warning to the population at risk;
- evacuation of the population at risk.

The dam owner is generally responsible for the first three components, while for the warning and evacuation of the population at risk local authorities are responsible. The efficiency of valley response procedures can be assessed by carrying out field exercises and simulations. The public should be well informed about the risk as it a crucial component in public risk mitigation. The criteria for the selection of the specific risk mitigation measures should be based on social equity, efficacy, and cost-efficiency, among others (Figure 2-6).

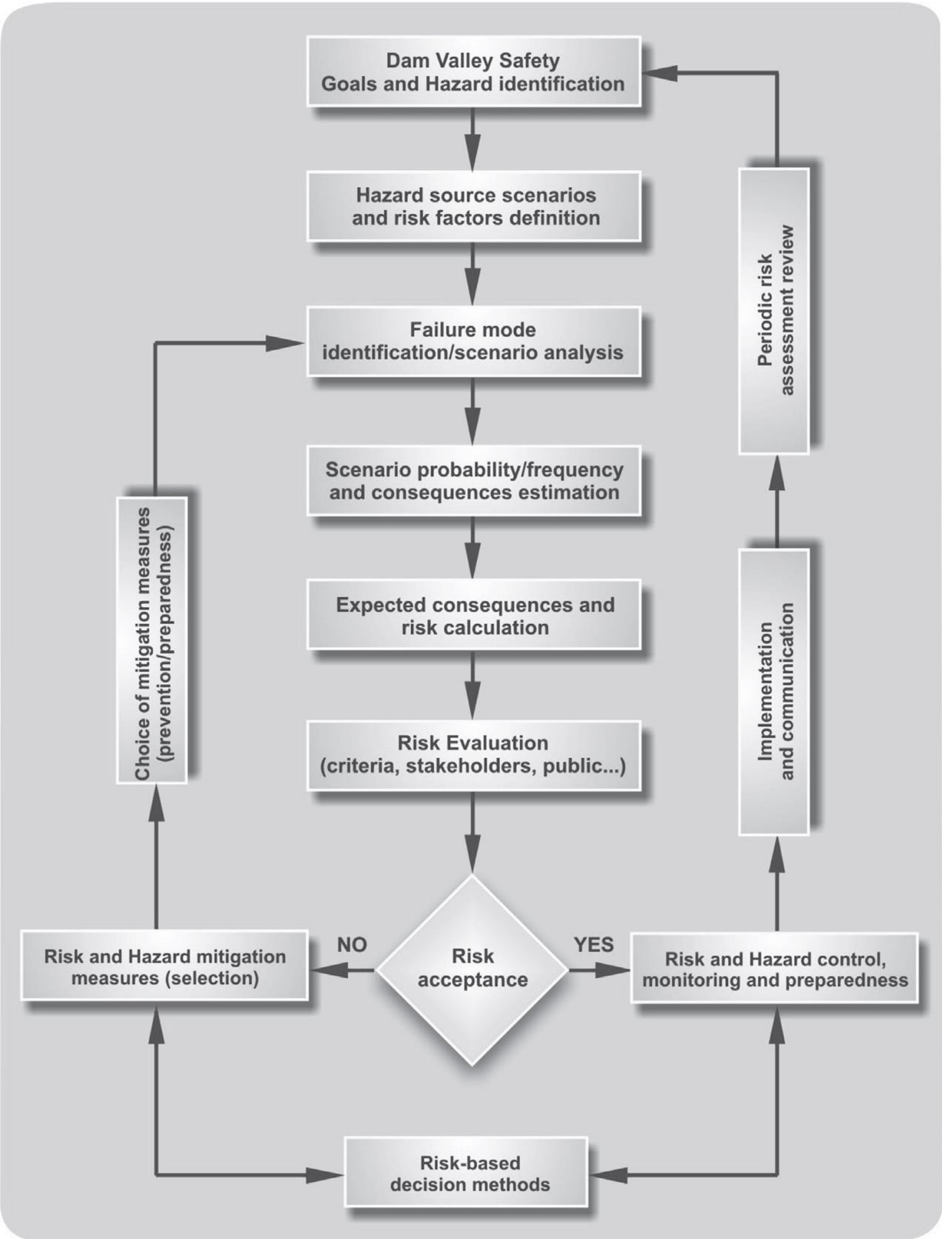

Figure 2-6 The dam risk management operational process (Wrachien & Mambretti, 2009)

2.6.2 Detection of the Hazard

The first mandatory step during emergency events is the detection of a real problem that can affect the dam's safety. The dam safety monitoring systems along with the visual inspection of the dam body are the key aspects in the detection of the problem. The purpose of the dam monitoring system is to provide information regarding the abnormal structural behavior or occurrence of an extreme event. The information is used for taking emergency actions in due time and without compromising safety. A dam safety monitoring system consists of visual inspection, instrumentation, data collection, and data evaluation and management.

2.6.3 Decision at the Dam Site

After an emergency situation is encountered or reported, the responsible person at the dam should classify the scale of the emergency level. Typically, there are three to four emergency levels defined in the emergency action plan, with the following set of situations:

Emergency level 0: Minor incident which does not compromise the safety of dam structure;

Emergency level 1: Unusual event, progressing slowly, possible discharge from dam might have effects in the downstream area;

Emergency level 2: rapidly developing event which may compromise the structural safety, leading to probable dam failure and flash floods in the downstream;

Emergency level 3: Imminent dam failure or in progress, the occurrence of flash flood in the downstream.

The specific information for decision-making for each emergency level is provided in the emergency action plan in terms of the condition of dam and the appropriate response level.

2.6.4 Notification System

The notification system is an effective way of communication between the dam owner and concerned authorities (dam safety authority, downstream civil protection authorities). The effectiveness of the notification systems depends upon two key elements: the design of notification system devices and the identification of the responsible person to alert the authorities.

In recent times, automated systems have taken over the processes of data acquisition, notification and even issuance of a warning, along with some human assistance. A typical flow diagram of a fully automated system is shown in Figure 2-7. The automated system monitors the dam continuously and issues the notification messages to a pre-defined list of responsible personal and experts in case of need of correction measures and warning the population downstream by early warning system in case of emergency level exceedance.

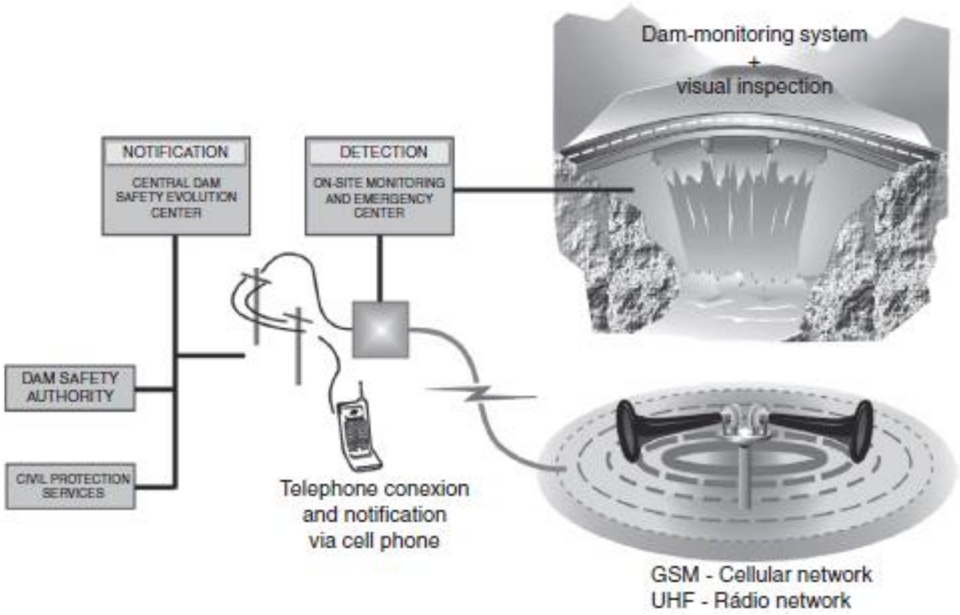

Figure 2-7 Typical flow diagram of a fully automated data acquisition, notification and warning system (Viseu et al, 2007)

2.6.5 Warning the Population at Risk

The warning system is commonly implemented to minimize the impact caused by floods on the population and the welfare in the most dangerous zones of the downstream areas. It also plays a vital role in crisis management and helps in reducing the risk in flood-prone areas. Warning systems are generally divided into the following categories (Viseu et al, 2007).

- Use of the audible system for public warning.
- Direct personal notifications via cell phone, social media, also including the door-to-door warning.
- News broadcast via television and radio networks.

The warning system is commonly implemented between the dam and the population in the most dangerous zone of the downstream valley.

Early warning systems are non-structural instruments intended to minimize flood impacts on populations and welfare, which can also play an important role in crisis management and be a competitive alternative to structural modification projects in order to reduce risk in dam-break flood-prone areas. Warning systems can be generally divided into the following types (Viseu et al, 2007):

public warning using audible systems as well as adopting visible systems (strobe lights and billboards);

personal direct notification via telephone or cell phones, also including the door to- door warning and, nowadays, the use of short message service (SMS) in mobile phones via cellular diffusion;

television or radio station news broadcasts.

For the selection of warning system for downstream areas, distance from the dam body, the geographic dispersion of population (densely populated urban areas, small rural areas. dispersed dwellings, etc.) and the proximity of civil protection services must be taken into consideration. Figure 2-8 shows an example of an early warning system in the downstream areas.

In the densely populated area, which is at higher risk because of the short arrival time of the flood wave, a warning system based on sirens should be envisaged. For areas with a small population and located outside of the dangerous zone, the use of load speakers and personal warnings can be envisaged. Television and radio networks are also very effective means to inform the public during an emergency.

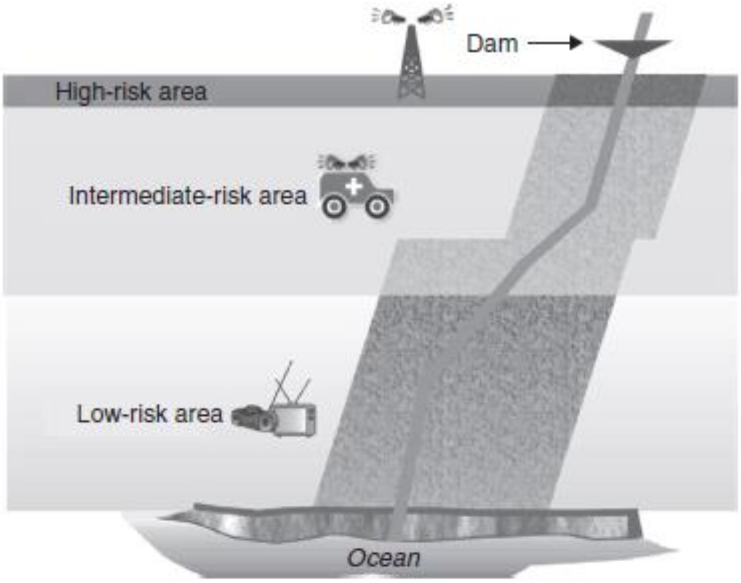

Figure 2-8 Example of a joint early warning system solution for a valley downstream of a dam (Wrachien & Mambretti, 2009)

No single warning system is enough to meet the desired outcome as each system has its own advantages and disadvantages. The main aspect to be considered is the reliability of the warning system is reliable and the surety that the message is clearly understood by the general public.

2.6.6 Evacuation of the Population at Risk

The factors affecting the survival possibilities can be divided into three groups (Funnemark et al, 1998)

Dam-break flow characteristics: Flow depth and velocity, water temperature etc.

Warning time: warning system reliability, distance to dam, decision regarding the start of evacuation.

Evacuation efficiency: Public awareness regarding the actions to be taken in case of dam-break, training and quality of civil protection teams, fraction of more vulnerable people (elderly, disabled persons, and children).

The aim of the evacuation plan is to relocate the people to safer areas in case of any hazard. The execution of the plan is the responsibility of local authorities.

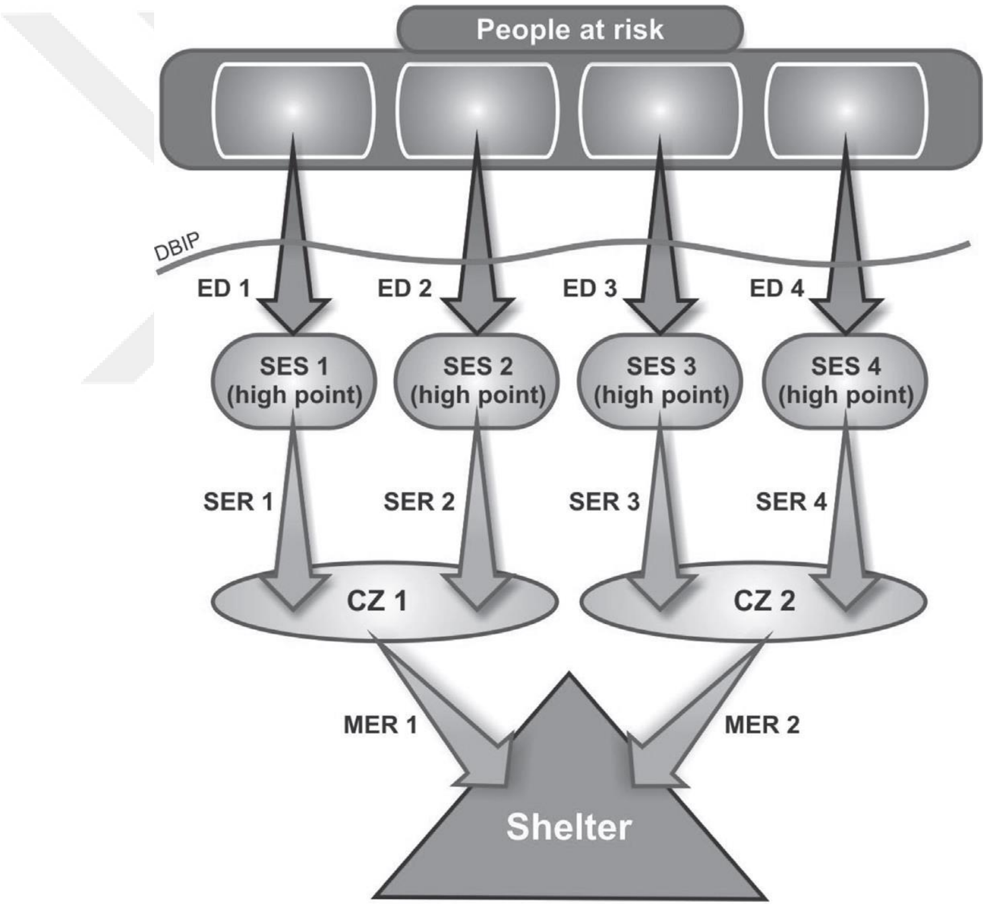

Figure 2-9 Typical flow diagram for population evacuation (Viseu et al, 2007)

DBIP - Dam-Break inundation perimeter, ED - Escape direction, SES - Safe evacuation spots, SER - Secondary evacuation route, CZ - Concentration zone, MER - Main evacuation route

The local authorities will make use of the inundation maps (highlighting the flooded areas in case of dam-break) to identify the evacuation routes for the public out of water path and also designate emergency transportation for transfer of people to shelters (Figure 2-9). The success of evacuation plans largely depends upon the level of organization, preparedness, testing and public awareness in a crisis context. The strategies for risk communication need to be appropriately selected, tested and effectively implemented.

In the next chapter, a general introduction of the hydraulic models used in this study is presented.

CHAPTER 3

HYDRAULIC MODELS

In this chapter, a brief explanation of HEC-RAS and FLO-2D model in terms of input and output, governing equations, numerical methods, computational grid, computational timestep, and solution algorithm is provided.

3.1 HEC-RAS

HEC-RAS 2D is a part of the HEC-RAS model used to carry out unsteady flow simulations in the 2D flow area. The 2D component was introduced in February 2016, with the release of HEC-RAS version 5.0. HEC-RAS 2D solves either diffusive wave equations or 2D Saint-Venant Equations. In general, the model with the diffusive wave equation is faster but less accurate in some cases. The model with the full momentum equation is slower but more accurate.

In HEC-RAS 2D simulation is performed over the 2D flow area computational mesh, using an implicit finite volume scheme. The computational mesh can be either structured or unstructured and can have three to eight polygon sides. (Compass PTS JV, 2019)

For HEC-RAS 2D, unsteady flow simulation output is created by RAS Mapper in the form of grid results of water surface elevation, depth, velocity, arrival time, and inundation boundary polygons, etc.

3.1.1 Input

The input data files required to set up a model include the projection file for the study area, terrain data, land use data, Geometric data, inflow data, and boundary conditions. In a model project file, there can be different plans with associated geometric data and unsteady flow data. Each geometric data can also have a different computational mesh size. Figure 3-1 shows how the data files work together in a model for three plans and geometries.

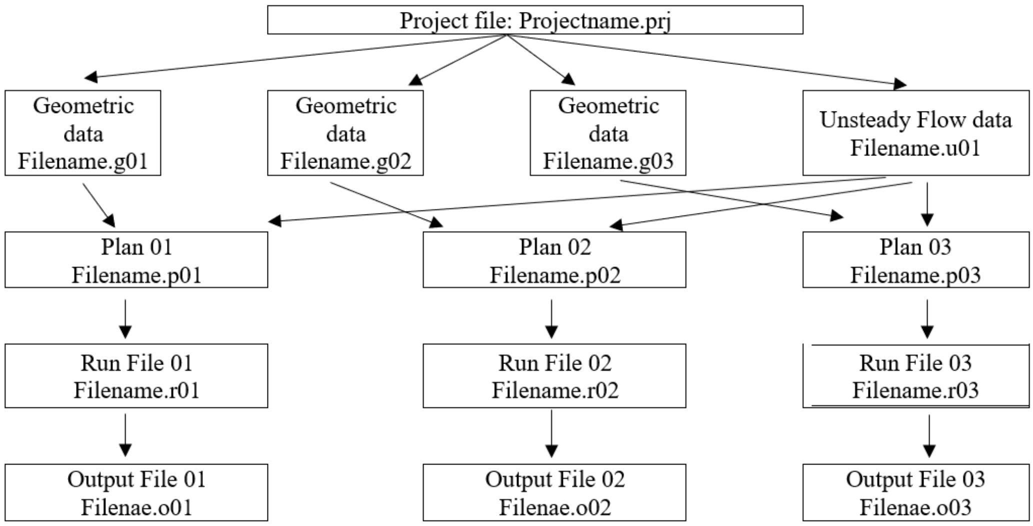

Figure 3-1 Schematic Diagram of HEC-RAS 2D Project data files (Compass PTS JV, 2019)

3.1.2 Output

The results obtained from the HEC-RAS 2D simulations are processed into grid-based maps using RAS Mapper, a GIS tool of HEC-RAS. The results can be displayed at any desired time, at minimum or maximum values of variables such as Depth, Velocity, Water Surface Elevation, Arrival Time, duration, Froude number and inundation maps, etc.

3.1.3 Governing Equation

3.1.3.1 Assumptions

The assumptions made to derive the two-dimensional Shallow Water Equations are the following:

- Incompressible fluid flow
- Hydrostatic pressure distribution
- Vertical component of the flow and velocity are neglected.
- The wavelengths are much larger than the water depth.
- Roughly flat bottom and small bed channel slope
- Manning's equation is used in calculating bed friction.
- The flow can be described as continuous functions of the velocity and water surface elevation.

3.1.3.2 Conservation of Mass

With the assumption of incompressible flow, the continuity equation for 2D unsteady flow can be written as:

$$\frac{\partial H}{\partial t} + \frac{\partial (hu)}{\partial x} + \frac{\partial (hv)}{\partial y} + q = 0 \qquad (3.1)$$

where H is the water surface elevation, h is the flow depth, t is the time, q is the term for source/sink flux, u and v are the velocity components in x and y direction, respectively.

In recent times with the advances in remote sensing, high-resolution topographic data is supplied. The topographic data is presented in the form of computational grids in 2D models. To prevent the loss of terrain information, computational grid size should be same as that of topographic data. This results in very large and infeasible computational times.

HEC-RAS uses sub-grid bathymetric approach as suggested by Casulli (2008), in which coarser grid cell can be used while minimizing the loss of fine bathymetric details and also reducing the computation times. In this approach cross-sectional area, volume, and hydraulic radius, are computed for each computational grid from the fine bathymetric data. This method is suitable for many applications as the free water surface is flatter than the bathymetry, so the spatial variability in the free surface elevation can be computed effectively with coarser computational grid.

Using Gauss Divergence theorem and integrating over a horizontal region (cell), the mass conservation equation for sub-grid bathymetry can be written as:

$$\frac{\Omega(H^{n+1}) - \Omega(H^{n})}{\Delta t} + \sum_{k} V_k . n_k A_k \,(H) + Q = 0 \tag{3.2}$$

where Ω(H) is the volume of cell as a function of H, Δt is the difference between consecutive time steps, V_k and n_k is the average velocity and unit normal vector at cell face k, A_k (H) is the face area as a function of H. The first term is obtained by integrating the first term of mass equation using a numerical method based on the orthogonality of the cells. The second term represents the summation over the vertical faces of the volumetric region.

3.1.3.3 Conservation of Momentum

The Conservation of momentum equation used in HEC-RAS are given as:

$$\frac{\partial u}{\partial t} + u\frac{\partial u}{\partial x} + v\frac{\partial u}{\partial y} = -g\frac{\partial H}{\partial x} + v_t\left[\frac{\partial^2 u}{\partial x^2} + \frac{\partial^2 u}{\partial y^2}\right] - c_f u + fv \tag{3.3}$$

$$\frac{\partial v}{\partial t} + u\frac{\partial v}{\partial x} + v\,\frac{\partial v}{\partial y} = -g\frac{\partial H}{\partial x} + v_t\left[\frac{\partial^2 v}{\partial x^2} + \frac{\partial^2 v}{\partial y^2}\right] - c_f v + fu \tag{3.4}$$

where u and v are velocity component in x and y direction, t is the time, g is gravitational acceleration value, v_t is the coefficient for horizontal eddy viscosity, c_f is the coefficient for bottom friction, f is Coriolis parameter. The terms from left to right are unsteady acceleration, convective acceleration, barotropic pressure, eddy diffusion, bottom friction, and Coriolis effect.

The gravitational acceleration value is computed using the Somigliana formula as:

$$g = g_o\left(\frac{1 + ksin^2\varphi}{\sqrt{1 - e^2sin^2\varphi}}\right) \tag{3.5}$$

where φ is the latitude, g_o is the gravitational acceleration at equator (9.7803267715 m/s^2), k is the normal gravity constant (0.0019318514), and e is the eccentricity of the earth (0.0066943800).

The coefficient for horizontal eddy viscosity v_t is calculated as:

$$v_t = Dhu_* \tag{3.6}$$

where D is a non-dimensional empirical constant that depends upon the geometry and bottom/wall surface. u_* is the shear velocity, which is computed as:

$$u_* = \sqrt{gRS} = \frac{\sqrt{g}}{C}|V| = \frac{n\sqrt{g}}{R^{1/6}}|V| \tag{3.7}$$

where R is hydraulic radius, S is the energy slope computed using Chezy formula and further simplified by Manning formula.

The bottom friction coefficient c_f is computed as:

$$c_f = \frac{n^2\sqrt{g}}{R^{4/3}}|V| \tag{3.8}$$

and for the Coriolis parameter f following equation is used:

$$f = 2\omega sin\varphi \tag{3.9}$$

where ω is the Earth's sidereal angular velocity (0.00007292115855306587/s) and φ is the latitude.

3.1.4 Numerical Methods

HEC-RAS uses a hybrid discretization scheme to take the advantage of grid orthogonality by combining finite difference and finite volume method. Then solution of the hydraulic equation is accomplished by using Newton like solution technique. A brief explanation of the numerical methods is as under.

The discretization of mass conservation equation is done using finite difference and finite volume approximations depending upon the local orthogonality of the grids, while for the momentum equation, the discretization type depends upon the terms.

The Mass conservation equation is discretized using Crank- Nicolson method at time steps n and n+1 as:

$$\frac{\Omega(H^{n+1}) - \Omega(H^{n})}{\Delta t} + \sum_{k} \pm A_k(H)(1-\theta)(u_N)_k^n + \theta(u_N)_k^{n+1}) + Q = 0 \quad (3.10)$$

where Ω(H) is the volume of cell as a function of H, Δt is the difference between consecutive time steps, V_k and n_k is the average velocity and unit normal vector at cell face k, A_k (H) is the face area as a function of H and θ is the user defined theta implicit weighing factor. The summation term sign is chosen based on the orientation of the velocity on the face k. θ value ranges from 0.5 to 1.0, with lower limit of HEC-RAS set at 0.6. Smaller values produce a more accurate model while higher values produce a more stable model (G. W. Brunner, 2018).

The momentum equations are applied on the grid faces, where the velocity calculations are done. The variables in the acceleration, pressure gradient and bottom friction terms are discretized using the Semi implicit scheme. Other terms in the momentum equation are calculated based on the θ-method, however their impact is smaller and so these terms are treated as explicit function. The discretized form of acceleration terms is:

$$\frac{DV}{Dt} \approx \frac{V^{n+1} - V_x^n}{\Delta t} \tag{3.11}$$

where V^{n+1} is the velocity at computational face and V_x^n is the velocity at location x.

The Barotropic pressure gradient terms are discretized as:

$$-g\nabla H \approx -g\sum_j c_j((1-\theta)H_j^n + \theta H_j^{n+1} \tag{3.12}$$

where H is the cell center water elevation, c_j is the intermediate coefficient computed for each cell. The θ scheme is used to compute the water surface elevation at cells.

3.1.5 Computational Grid

The computational grid can be generated by defining the dx and dy size for the grid. The created grid is orthogonally aligned away from the boundary and polygonal at the boundary of the 2D flow area. The grid can have up to eight sides. The shape of a grid can be manually changed if desired. The hydraulic properties are computed for each grid such as area, volume, and hydraulic radius. The center of the grid is represented with a point.

In HEC-RAS 2D, the water elevation is computed at the center of the grid element, while the velocity is computed perpendicular to the faces of the grid element, and the velocity vector is computed at the grid face points.

3.1.6 Computational Time Step

The computational time step can be estimated using the Courant formula. For the Shallow water equation, the maximum courant number of 3 can be tolerated for a suitable solution. For rapidly varying flood waves with respect to time and space, a stable solution can be obtained by using a computational time step which results in Courant number 1.0 for high velocities areas. The following equations are used for calculating the computation interval for the Saint Venant equations:

$$C = \frac{V\Delta T}{\Delta X} \leq 1.0 \text{ (With a max C= 3.0)} \tag{3.13}$$

Or

$$\Delta T \leq \frac{\Delta X}{V} \text{ with C = 1.0} \tag{3.14}$$

where C is the Courant number, V is the flood wave velocity (m/sec), ΔT is the computational time step (sec) and ΔX is the average cell size (m).

3.1.7 Solution Algorithm of HEC-RAS

The solution algorithm for HEC-RAS 2D is given below. (G. W. Brunner, 2016)

1. Pre-Computation of the geometry, local orthogonality and sub grid-bathymetric data.
2. Computations starts with the initial condition provided at time-step n=0.
3. For the next time step n+1, boundary conditions are provided.
4. Initial guess is made for Water surface elevation ($H^{n+1} = H^n$) and velocity (u_N^{n+1}= u_N^n) and (v_N^{n+1}= v_N^n).
5. Explicit terms are computed, e.g., diffusion Laplacian field.
6. Computations are made for θ–averaged water elevation (H = (1 - Θ) $H = (1-\theta)H_j^n + \theta H_j^{n+1}$) and hydraulic properties for sub-grid bathymetry (Grid face area, water surface area, manning's n, hydraulic radii, etc.)
7. A system of equation is compiled for the continuity at cells.
8. Iterations are done using the system of equations to obtain a solution for H^{n+1}.
9. Velocity u_N^{n+1} is computed.
10. If the residual error is higher than the given tolerance, then the solver go back to step 6; if not, the solution proceeds.

11. The obtained solution is accepted.
12. Increment n, if there are more time steps go back to step 3, otherwise the solution is completed.

Figure 3-2 shows the solution algorithm of HEC-RAS.

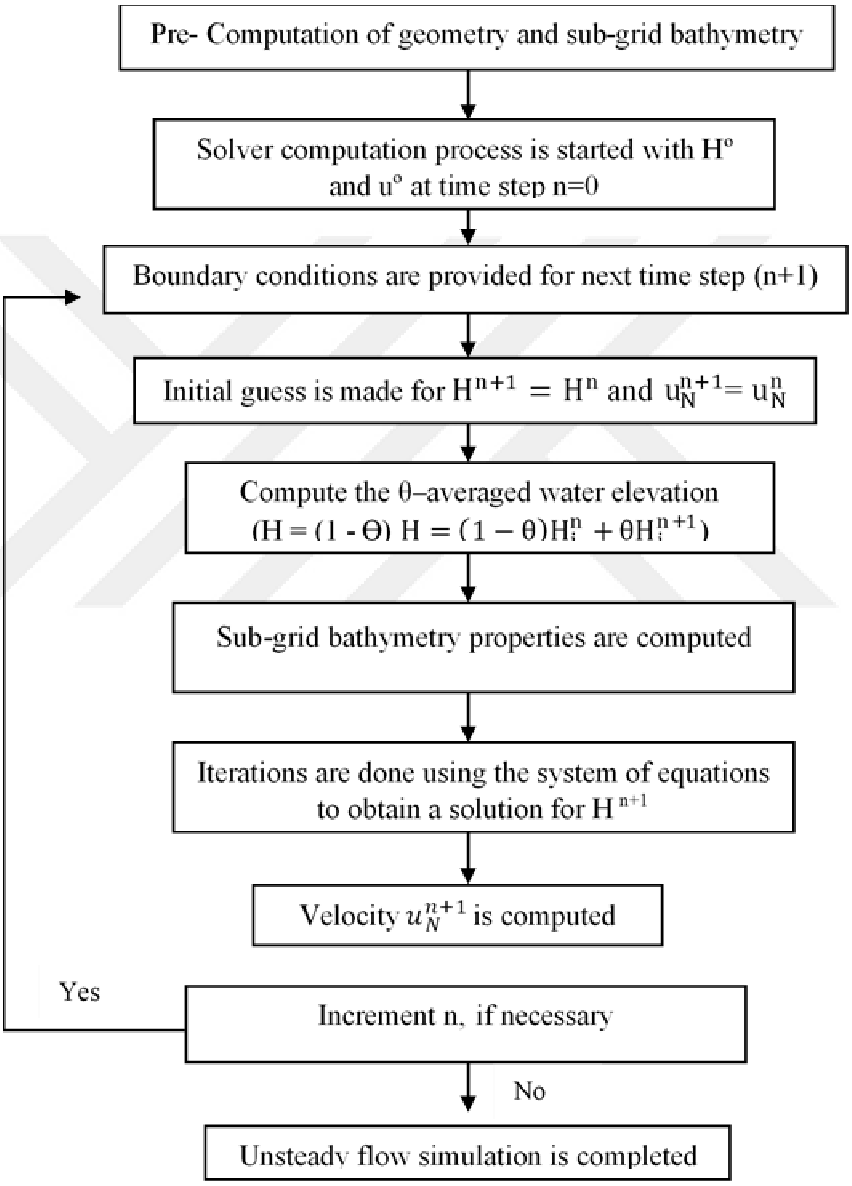

Figure 3-2 Solution Algorithm of HEC-RAS

3.2 FLO-2D

FLO-2D is a simple volume conservation model designed to model flood routing over floodplains, in channels and alluvial fans. It was first introduced in 1988. The model simulates the flood volume in eight directions over a series of tiles for overland flow. The movement of the flood wave over the flood plain is monitored by area topography, inflow hydrograph and resistance to flow (FLO-2D Reference Manual, 2012).

FLO-2D model uses an explicit finite difference numerical scheme to model the flow over a system of square grid elements. The square grid can be easily created and edited for large-scale models. Flows in river bends, hydraulic jumps, around complicated hydraulic structures cannot be simulated with the FLO-2D model in detail (Compass PTS JV, 2019).

3.2.1 Input

The input data files needed to set up a model include the elevation data, land use shapefile, hydrological data and boundary conditions. FLO-2D model consists of a series of ASCII files that are arranged according to the component being modeled. The Grid Developer system of FLO-2D is used to build the input data files using the input data.

3.2.2 Output

FLO-2D gives out put in the form of ASCII files. The MAPPER program is used to create the grid element plot maps of Water surface elevation, Depth, Velocity, Arrival time and Hazard maps. In grid elements plots, each grid has a color assigned to it depending upon the value of the variable for which the plot is created. Profile plot of flow depth can also be obtained in the MAPPER program by drawing a profile line over the desired area. The shapefiles of the desired output features are also created by MAPPER software, which can be imported into GIS software.

3.2.3 Governing Equations

3.2.3.1 Assumptions

The basic assumptions made in the derivation of governing equations in FLO-2D are:

1. Flow is steady for the timestep duration.
2. Pressure distribution is hydrostatic.
3. Hydraulic roughness is based on steady, uniform turbulent flow resistance.
4. A channel element is characterized by uniform channel geometry and roughness.

The governing equations used in the FLO-2D model are given below.

3.2.3.2 Conservation of Mass and Momentum

The governing equations used in the FLO-2D model are the continuity equation and the Momentum equation (Dynamic wave momentum Equation):

$$\frac{\partial h}{\partial t} + \frac{\partial hV}{\partial x} = i \tag{3.15}$$

$$S_f = S_0 - \frac{\partial h}{\partial x} - \left(\frac{V_x}{g}\right)\frac{\partial V_x}{\partial x} - \left(\frac{1}{g}\right)\frac{\partial V_x}{\partial t} \tag{3.16}$$

where h is the flow depth, V is the depth-averaged velocity in one of the eight flow directions x, i is the excess rainfall intensity, S_f is the friction slope component based on Manning's equation, S_o is the bed slope pressure gradient, g is the gravitational acceleration constant, $(V_x/g)\ \partial V_x/\partial x$ is the convective acceleration term and $(1/g)\ \partial V_x/\partial t$ is the local acceleration term.

As FLO-2D is a multi-direction flow model, average flow velocities across a boundary of grid element are calculated by applying the equation of motion over one direction at a time. The calculation is carried out in eight potential flow directions (north, east, south, west, northeast, southeast, southwest, and northwest). Each velocity computation is computed independently of the other seven directions. The strict criteria for the stability of this explicit numerical scheme is based on the magnitude of the variable computational time step.

3.2.4 Numerical Method

FLO-2D model solves the differential form of the continuity and momentum equations with a central, explicit finite difference numerical scheme. In this algorithm, the momentum equation is solved for the flow velocity across the grid element boundary one direction at a time. The solution of momentum equation differential form results from its discrete representation when applied at a point. Explicit numerical schemes are simple to formulate but are limited by strict numerical stability criteria to small timesteps. Finite difference schemes can take longer simulation time for simulating very slow rising or steep rising flood waves, abrupt slope variation, ponded flow areas and split flows.

3.2.5 Computational Grid

The FLO-2D model solution domain consists of uniform square grid elements. The grid is developed from rasterized terrain data and land use shapefile. The multiple elevation points are aggregated by the interpolation method into a single elevation value for each grid. The Manning's roughness values are computed from the land use shapefile for each grid. The elevation and roughness values can be modified for any area of interest, after the grid system has been developed. In the computational procedure for overland flow, the discharge calculations are made for each boundary in the potential eight flow directions with one direction at a time (Figure 3-3). The calculations begin with a linear estimation of flow depth at the boundary of the grid element. The estimated flow depth is obtained by averaging the flow depths between the two grid elements, that are sharing discharge in one of the possible eight directions. The flow velocity is computed by averaging hydraulic parameters (roughness parameter, slope, flow area, wetted perimeter, water surface elevation) between two grid elements. The calculated velocity is then multiplied with the average flow area between two elements to compute the discharge for each time step.

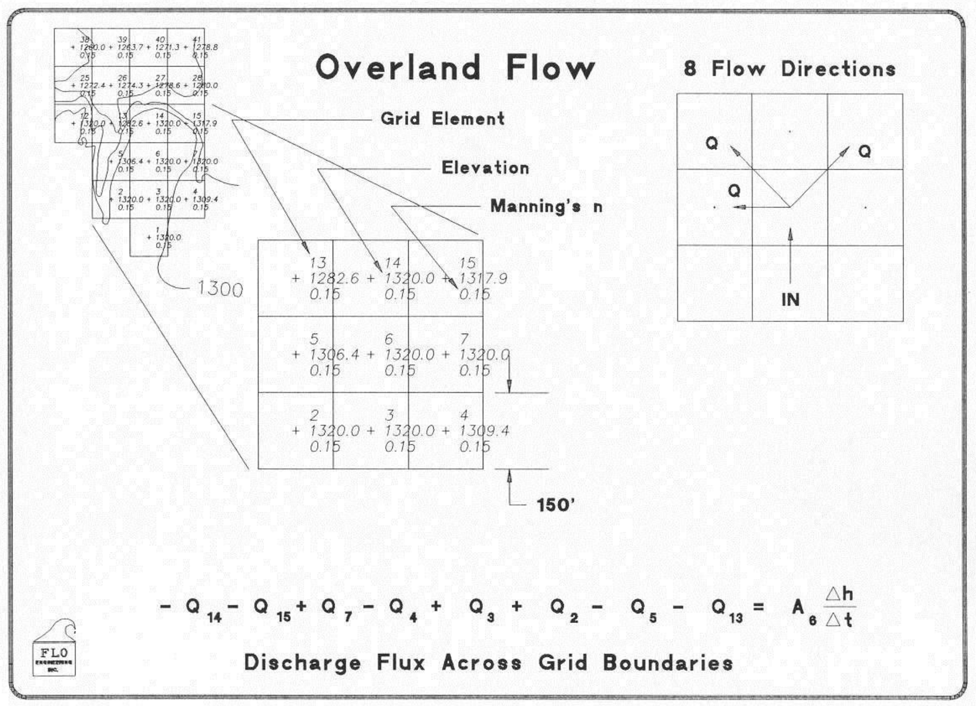

Figure 3-3. Discharge flux across the boundaries of grid element (FLO-2D reference manual, 2012)

3.2.6 Computation Time Step

The numerical stability of the FLO-2D flood routing scheme is based on sufficiently small computations timestep. For efficient flood routing (Finite Difference), the criteria for numerical stability control the timestep to avoid surging and also allows the timestep to be large enough to complete the simulation in a reasonable period.

FLO-2D uses variable timestep, which varies depending on whether the criteria for numerical stability is exceeded or not. In order to ensure that the solution is stable, the criterion for numerical stability is to check for each grid element on each timestep. If the stability criteria are exceeded, the timestep is decreased and the earlier computations are discarded for that timestep. The numerical stability for most explicit schemes is subjected to the Courant-Friedrich-Lewy (CFL) condition (Jin & Fread, 1997). In the CFL condition, flood wave celerity is related to the model time and spatial increment. The physical explanation of the CFL condition is that a fluid particle should not travel more than one spatial increment (Δx) in one timestep (Δt) (Fletcher, 1990). FLO-2D uses the CFL condition for floodplain routing, channel routing, and street routing. The timestep (Δt) is controlled by:

$$\Delta t = C \, \Delta x / (\beta V + c) \tag{3.17}$$

where C is the Courant number ($C \leq 1.0$), Δx is the width of the square grid element, V is the computed average velocity, β is a coefficient (5/3 for a wide channel), c is the computed wave celerity.

3.2.7 Solution Algorithm

The solution algorithm used in FLO-2D consists of following steps:

1. The average flow geometry, roughness, and slope between two grid elements are computed.
2. The estimated flow depth (d_x) from the previous timestep i is used to compute the flow velocity across a grid element boundary for the next timestep (n+1) using a linear estimate.

$$d_x^{n+1} = d_x^n + d_{x+1}^n \tag{3.18}$$

3. The diffusive wave equation is used to compute the first estimate of the velocity. The only unknown variable is the velocity of overland flow, channel flow or street flow.
4. The predicted velocity is then used as a seed in the Newton-Raphson method to solve the dynamic wave equation for the current timestep's solution velocity.
5. The discharge Q across the grid element boundary is calculated by multiplying the velocity by the flow area of the cross-section.
6. The sum of the discharge in all the flow directions is done to determine the net change in discharge in or out of the grid element for the timestep.

$$\Delta Q_x^{n+1} = Q_n + Q_e + Q_s + Q_w + Q_{ne} + Q_{se} + Q_{sw} + Q_{nw} \tag{3.19}$$

   Furthermore, the change in flow depth is obtained by dividing the volume (net discharge * timestep) with the available storage area within the grid element.

$$\Delta d_x^{n+1} = \Delta Q_x^{n+1} \Delta t / A_{surf} \tag{3.20}$$

   where ΔQ_x is the net change in discharge in the eight flow directions for the grid element for the timestep Δt between the time n and n + 1.
7. The criterion for numerical stability is then checked for the flow depth of new grid element. If any of the stability criteria are surpassed, the simulation time is reset to the previous one, the timestep is reduced, all the previous timestep computations are discarded and the velocity computations begin again. The simulation continues with increasing timesteps until the stability criteria are exceeded.

Figure 3-4 shows the solution algorithm of FLO-2D.

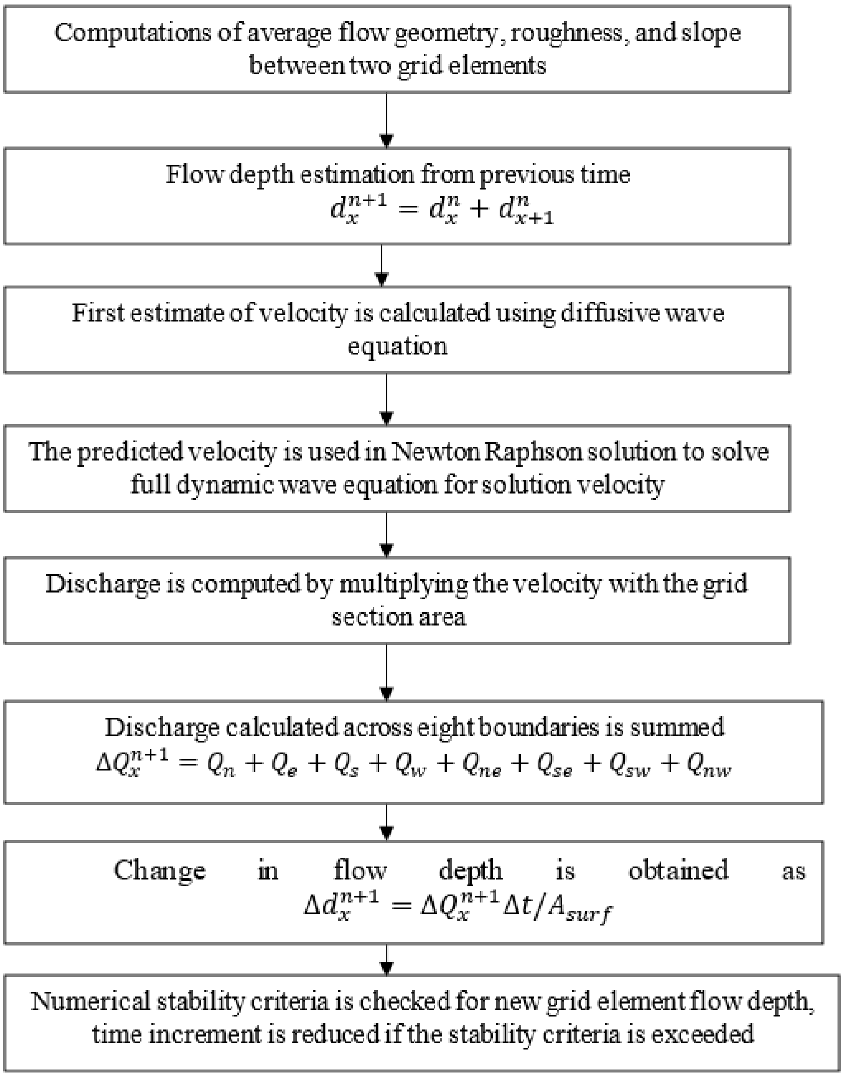

Figure 3-4 Solution Algorithm of FLO-2D

3.3 Comparison of HEC-RAS and FLO-2D

The main differences in HEC-RAS and FLO-2D are based on their governing equations, computational methods, and grid approach. In HEC-RAS, If the grid size is larger than any terrain feature that can influence the flow direction, then the model will not consider the terrain feature in its computations and route the flow in the neighboring cells, resulting in leakage effect, which is a known limitation of the model (Forest, 2020)). In FLO-2D, there is a limitation is that it cannot simulate rapidly varying flow, shock waves, or hydraulic jumps, these discontinuities are smoothed out in the flow profile calculations (FLO-2D Reference Manual).

Table 3-1 lists the comparison of the governing equations and their methods of discretization.

Table 3-1 Comparison of Governing equations of HEC-RAS and FLO-2D

Equation	**Form/Term**	**HEC RAS**	**FLO 2D**
Continuity Equation	Form	Shallow water, 2D Implicit	Shallow water, 2D Explicit
Conservation of Momentum	Form	Full form, 2D Mixed implicit-explicit	Conservative form, 2D Explicit
	Unsteady Acceleration	Semi-implicit	Explicit
	Convective Acceleration	Semi-implicit	Explicit
	Pressure	Mixed implicit/explicit	Explicit
	Gravity	Included, Adjusted for location, Mixed implicit/explicit	Explicit
	Eddy diffusion	Explicit	Not included
	Bottom friction	Implicit	Explicit
	Coriolis effect	Implicit	Not Included

Table 3-2 presents a summary of the main differences in HEC RAS and FLO-2D

Table 3-2 Summary of difference in HEC-RAS and FLO-2D

Model	HEC-RAS	FLO-2D
Governing equations	2D Shallow water equation	Dynamic Wave momentum Equation
Numerical method	The hybrid discretization scheme to take the advantage of grid orthogonality by combining finite difference and finite volume method, Implicit/mixed	Central, finite difference Explicit
2D flow area	Structured or unstructured grids (up to 8 sides) uniform square or rectangle, hexagonal, adaptive grid	Uniform square grids
Elevation values in grid	For each grid element, sub-grid bathymetric approach calculates the hydraulic radius, volume and cross-sectional area	Grid element has one elevation value obtained by interpolation of 2 or more elevation points from the surrounding grids
Roughness values	Extracted from land use shapefile along the cell face	Computed by taking averaged between two grid elements values
Discharge calculation	The water surface elevation is computed for each cell at the cell center, The model computes discharge across a cell face using water surface elevations of adjacent cells	The model computes the discharge across each of the boundaries in the eight potential flow directions
Results grid elements	The Grid can be partially wet or dry depending upon the sub-grid bathymetry	There is one value for each grid element

The comparison of both model's performance is made in this study by carrying out the flood simulation with the same input data as discussed in Results and Discussion Chapter.

CHAPTER 4

METHODOLOGY

4.1 Study Area

In this study, bam breach modeling is carried out on the following dams:

- Ondokuz Mayıs Dam (Samsun Province)
- Avcıdere Dam (Koceli province)
- İhsaniye Dam (Koceli province)

4.1.1 Ondokuz Mayıs Dam

Ondokuz Mayıs Dam is situated in Samsun province, to the south of Ondokuz Mayıs District at a distance of 5.5 km. The coordinates for the dam are 41 ° 27' 36.12" N (latitude) and 36 ° 1'51.29 " E (longitude)

The Ondokuz Mayıs Dam is constructed on Engiz Creek. The Engiz Creek is formed by the merger of Erikli and Kösedik Creeks, originating from the Kocadağ District. The Engiz Creek travels about 32 km and falls into the Black Sea through the Ondokuz Mayıs District.

The project area is located in the Bafra Plain (Kızılırmak Basin), which is one of the most favorable plains of Turkey in terms of soil resources. The natural vegetation is the area is composed of low meadow grasses, beech, oak, chestnut, and scotch pine (DSI, 2013).

The main purpose of the dam is to supply water for municipal and agricultural usage. The supply of muncipal water will be done for Ondokuz Mayıs District, Bafra District, and four towns in the Bafra Plain. The water supply for irrigation is planned for area of 7555 ha located on the right and left banks of Engiz Creek. Irrigation will be done by the pressurized irrigation system. The population of the Ondokuz Mayıs District is 25,893 (Year 2019). The characteristics of the Ondokuz Mayıs Dam are given in Table 4-1.

Table 4-1 Characteristics of Ondokuz Mayıs Dam

Location	Samsun Province (Ondokuz Mayıs District)
River	Engiz Creek
Purpose	Municipal and Agricultural usage
Type	Clay-core rockfill
Crest Elevation	168.00 m
Crest Length	507.10 m
Crest Width	10.00 m
Thalweg Elevation	87.25 m
Height from Thalweg	80.75 m
Height From foundation	89.75 m
Embankment Volume	3 888 527 m^3
Minimum water level	106.30 m
Normal water level	163.75 m
Maximum water level	166.80 m
Minimum Water Level Lake Volume	2.00 hm^3
Normal Water Level Lake Volume	59.27 hm^3
Maximum Water Level Lake Volume	65.93 hm^3
Active Lake Volume	57.27 hm^3
Drainage Area	133.50 km^2
Annual Total Flow	70.60 hm^3

4.1.2 İhsaniye Dam

İhsaniye Dam is located in the Karamürsel District of Kocaeli Province. İhsaniye Dam is built on Sulu Creek, which is a side branch of Yalak Creek. The coordinates for the dam are 40°37'44.13" N (latitude) and 29°35'30.78" E (longitude).

On the dam downstream, there is Yalakdere Town located at distance of about 3.5 km from dam location, with Sulu Creek passing through it. İhsaniye Dam is planned for the purpose of supplying water for agriculture and municipal use. İhsaniye Dam along with the Avcıdere Dam will irrigate an area of 2024 ha. The characteristics of İhsaniye Dam are given in Table 4-2.

Table 4-2 Characteristics of İhsaniye Dam

Location	Kocaeli Province (Karamürsel District)
River	Sulu Creek
Purpose	Municipal and Agricultural usage
Type	Roller compacted concrete
Crest Elevation	234.50 m
Crest Length	203.00 m
Crest Width	8.00 m
Thalweg Elevation	171.50 m
Height from Thalweg	63.00 m
Height From foundation	69.00 m
Embankment Volume	135 000 m^3
Minimum water level	204.00 m
Normal water level	232.00 m
Maximum water level	234.37 m
Minimum Water Level Lake Volume	1.00 hm^3
Normal Water Level Lake Volume	8.94 hm^3
Maximum Water Level Lake Volume	10.17 hm^3
Active Lake Volume	7.94 hm^3
Drainage Area	37.80 km^2
Annual Total Flow	18.43 hm^3

4.1.3 Avcıdere Dam

Avcıdere Dam is located in the Karamürsel District of Kocaeli province. Avcıdere Dam is planned On the Avcı Creek. Sulu Creek and Avci Creek both merges downstream of Yalakdere Town to form Yalak Creek. Avcıdere Dam and İhsaniye Dam are located on the two side branches of the same creek. The coordinates for the Avcıdere Dam are 40°35'57.41" N (latitude) and 29°35'9.27" E (longitude).

On the downstream side of the dam, there is Avcıköy Town (Population 241) on the right side of the Avcı Creek at about 1 km distance and Yalakdere Town (Population

765) at about 3 km distance also on the right side of the Avcı Creek. It is planned to supply water for agricultural and municipal use. The characteristics of the Avcıdere Dam are given in Table 4-3.

Table 4-3 Characteristics of Avcıdere Dam

Location	Kocaeli Province (Karamürsel District)
River	Avcı Creek
Purpose	Municipal and Agricultural usage
Type	Concrete faced rockfill
Crest Elevation	236.00 m
Crest Length	293.00 m
Crest Width	8.00 m
Thalweg Elevation	148.00 m
Height from Thalweg	88.00 m
Height From foundation	92.00 m
Embankment Volume	1 400 000 m^3
Minimum water level	204.00 m
Normal water level	232.00 m
Maximum water level	234.54 m
Minimum Water Level Lake Volume	4.695 hm^3
Normal Water Level Lake Volume	16.93 hm^3
Maximum Water Level Lake Volume	17.28 hm^3
Active Lake Volume	12.24 hm^3
Drainage Area	36.80 km^2
Annual Total Flow	17.93 hm^3

The location of the Ondokuz Mayıs Dam, İhsaniye Dam, and Avcıdere Dam is shown in Figure 4-1.

Figure 4-1 Location of Ondokuz Mayıs Dam (Samsun Province), İhsaniye Dam, and Avcıdere Dam (Kocaeli province) Source: Google Earth.

4.2 Data Collection

In order to perform the dam breach simulations of the three dams, the following data was collected from different governmental institutes:

Hydraulics and Hydrological data: The hydrologic and hydraulic of the respective dams were collected from State Hydraulic Works, DSI (Devlet Su İşleri Genel Müdürlüğü), Turkey.

Elevation Data: Elevation for İhsaniye Dam and Avcıdere Dam located in Karamürsel District were collected from DSI at a scale of 1/5000 in form of point data shapefiles. For Ondokuz Mayıs Dam, elevation data in the form of point data shapefiles was obtained from Tapu Kadastro (Harita Dairesi Başkanlığı, Ankara) and DSI at a scale of 1/5000. The point data shapefiles were converted in DEM by using GIS software.

Land Use Data: Land use shapefiles for the relevant areas were created using Google Earth Images. The shapefiles were then assigned roughness parameters by using ARC GIS software. For Ondouz Mayıs Dam, the calibration of the roughness values is carried out against the flow measurement record of Engiz Creek. The calibrated roughness values were then used in breach hydrograph routing. For İhsaniye and Avcıdere Dam, the roughness values are selected by analyzing the land-use patterns from the google earth images.

4.3 Input Data Preparation

4.3.1 Digital Elevation Model (DEM) Preparation

Elevation data in the format of point shapefiles is converted into the Digital Elevation Model (DEM) using the spatial analyst tool in ARC GIS software. The DEM for the Ondokuz Mayıs Dam region is developed from the elevation point data of Tapu Kadastro and DSI is shown in Figure 4-2. The DEM for İhsaniye Dam and Avcıdere Dam region developed from DSI data is shown in Figure 4-3.

In HEC-RAS software, DEM data can be used in Raster format, while for FLO-2D the DEM is converted into ASCII data format. The coordinate reference system for Ondokuz Mayıs Dam is WGS_1984_UTM_Zone_37N and for İhsaniye Dam and Avcıdere Dam the coordinate reference system is WGS_1984_UTM_Zone_35N.

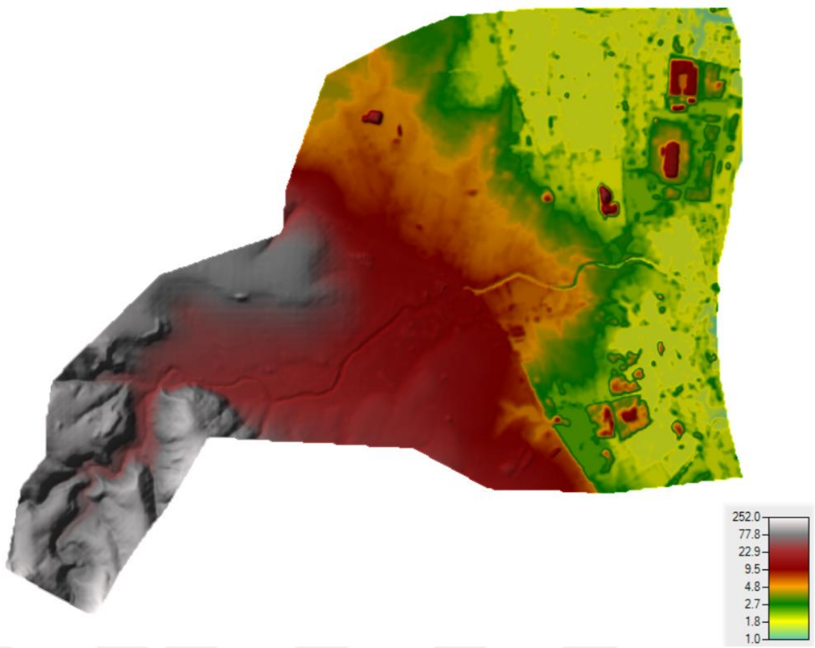

Figure 4-2 Ondokuz Mayıs Dam region (DEM)

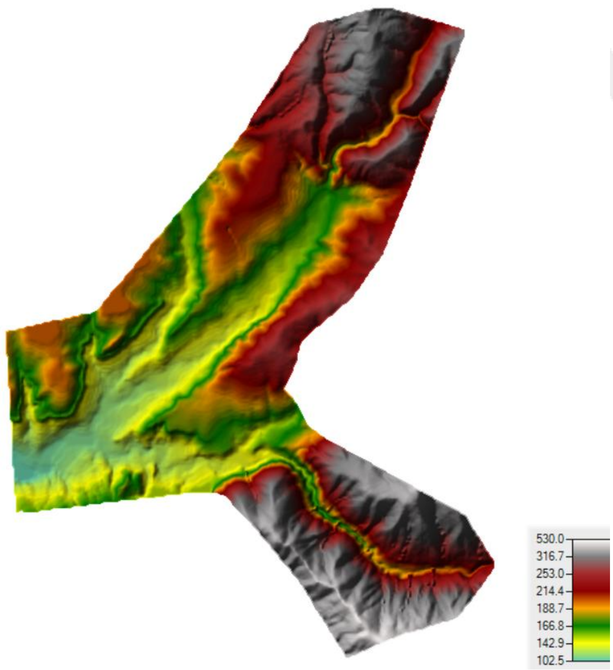

Figure 4-3 İhsaniye Dam and Avcıdere Dam region (DEM)

4.3.1.1 DEM Verification

In this part, the quality of elevation data for the Ondokuz Mayıs Dam area is checked by comparing the elevation data of Tapu Kadastro with the DSI data. The data provided by DSI covers approximately 6 km of Engiz Creek, located downstream region of Ondokuz Mayıs Dam. DSI data consist of irregularly spaced points (distance between points varies from 2 m to more than 20 m), while Tapu Kadastro data consists of regularly spaced points (distance between points is 20 m). Both data sets were converted into DEM using the interpolation techniques available in the Spatial Analyst Tool of ARC GIS Software. The interpolation methods used in the generation of DEM are Inverse Distance Weighting (IDW), Kriging, Natural Neighbor, Spline. After the DEM is created, the cross-section of the exact location is compared from both data sets.

Figure 4-4 shows the DEM developed from topographic data of Tapu Kadastro and DSI, Samsun. It also shows the Engiz Creek and the location of the gauging station. A closeup of the area where the obtained topographic data overlaps for both Tapu Kadastro and DSI is also shown.

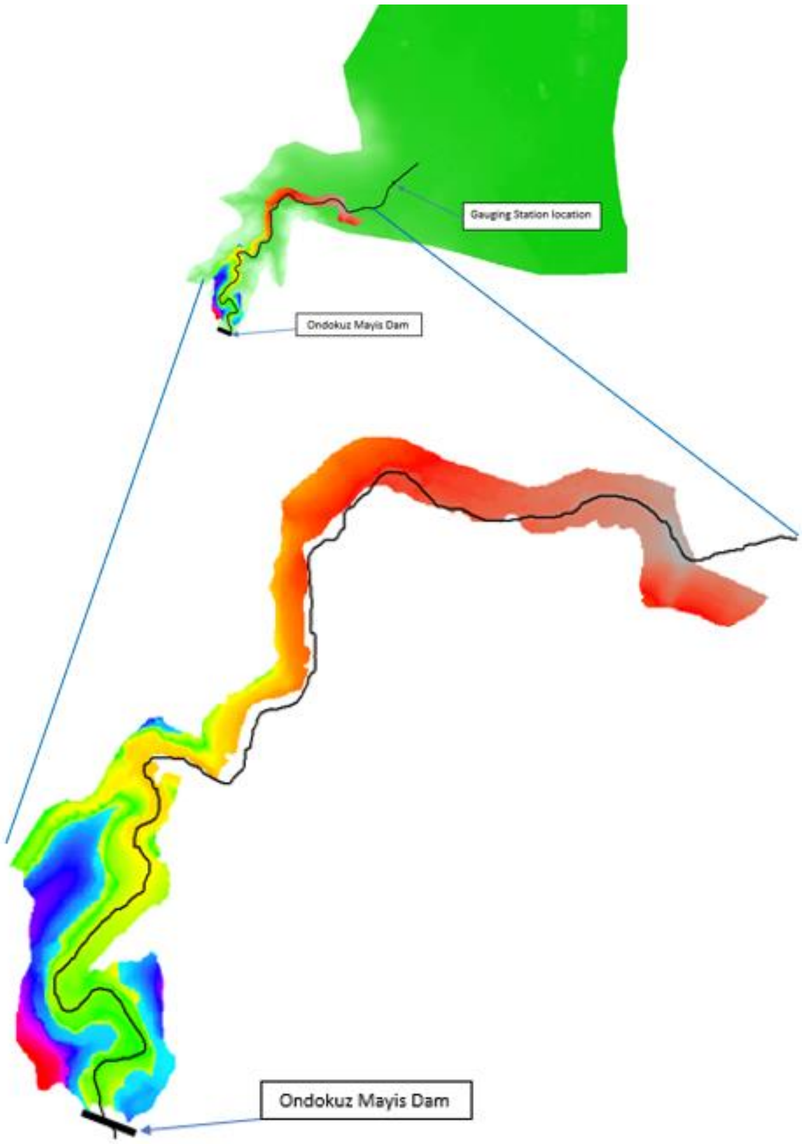

Figure 4-4 DEM of Ondokuz Mayıs District (Green DEM: Tapu Kadastro data, Multi-Color DEM: DSI Samsun data/overlap DEM, Blackline: Engiz Creek)

The locations where cross-sections were taken for comparison is shown in Figure 4-5.

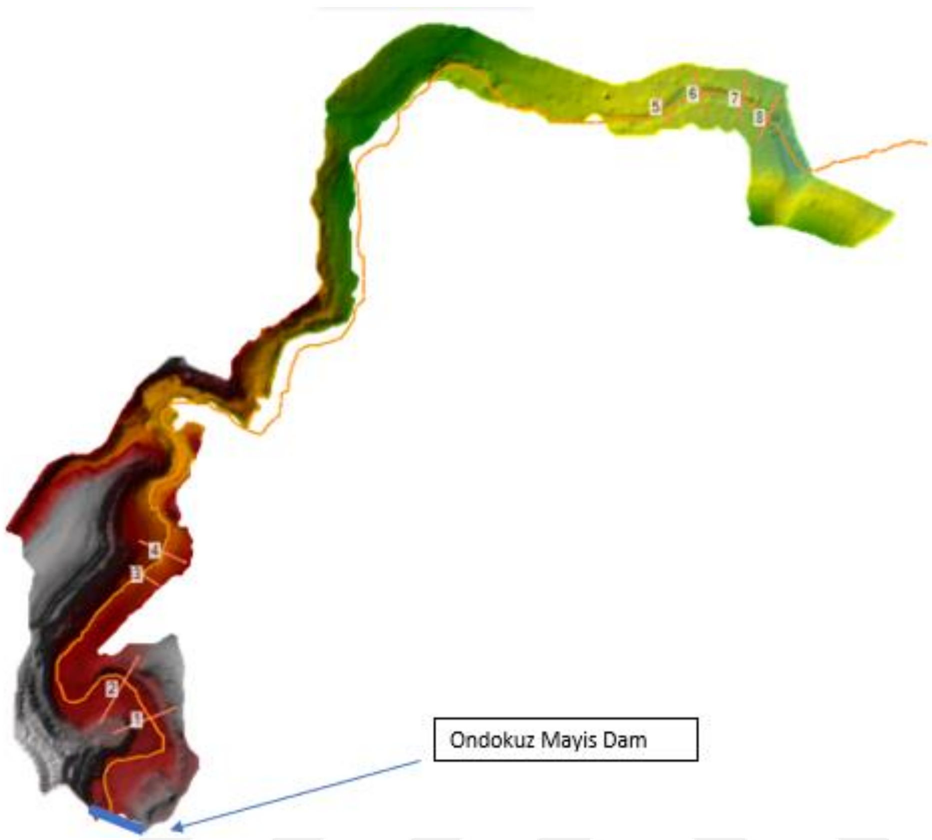

Figure 4-5 Location of the cross-sections for comparison

From the comparison, it was seen the cross-sections obtained from the Natural Neighbor method for DSI data and the IDW method for Tapu Kadastro data show similar profiles in comparison to other interpolation methods. The profile comparison of the cross-sections is presented in Figures 4-6 to 4-13.

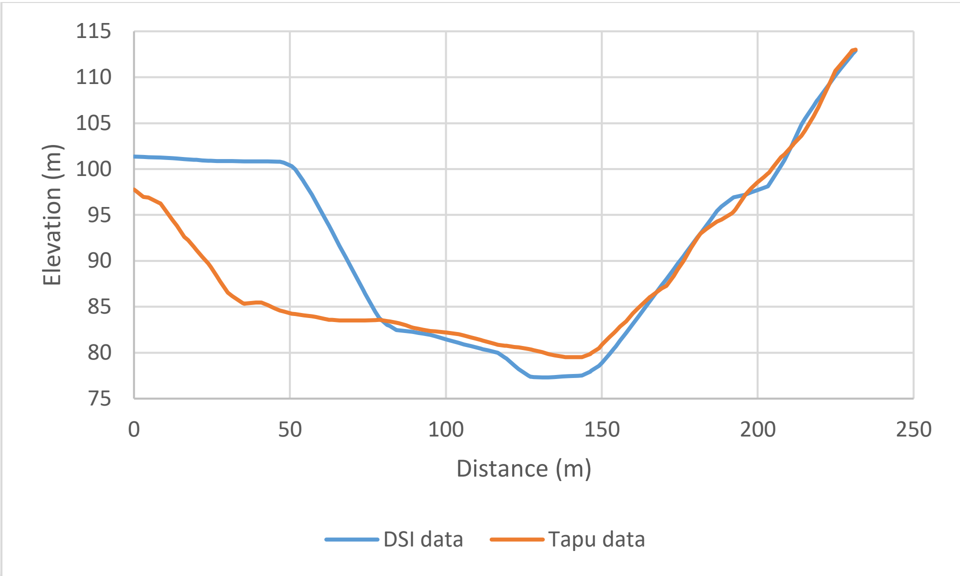

Figure 4-6 Comparison of Tapu Kadastro and DSI elevation data at Cross-section 1

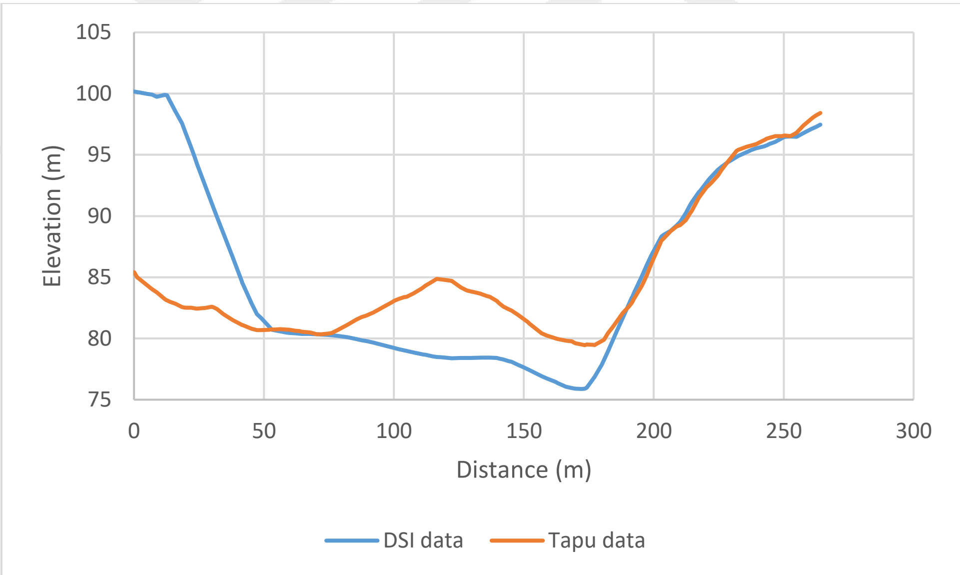

Figure 4-7 Comparison of Tapu Kadastro and DSI elevation data at Cross-section 2

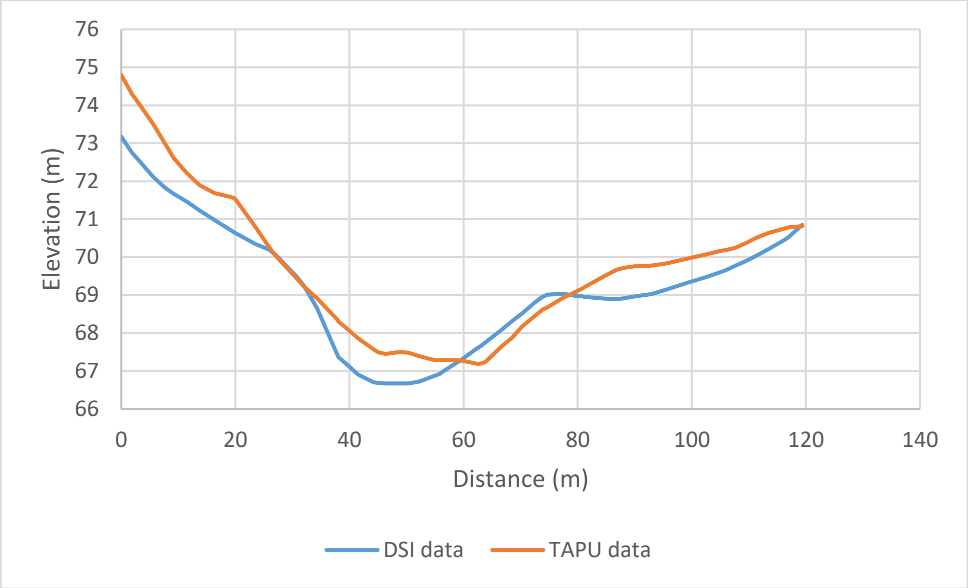

Figure 4-8 Comparison of Tapu Kadastro and DSI elevation data at Cross-section 3

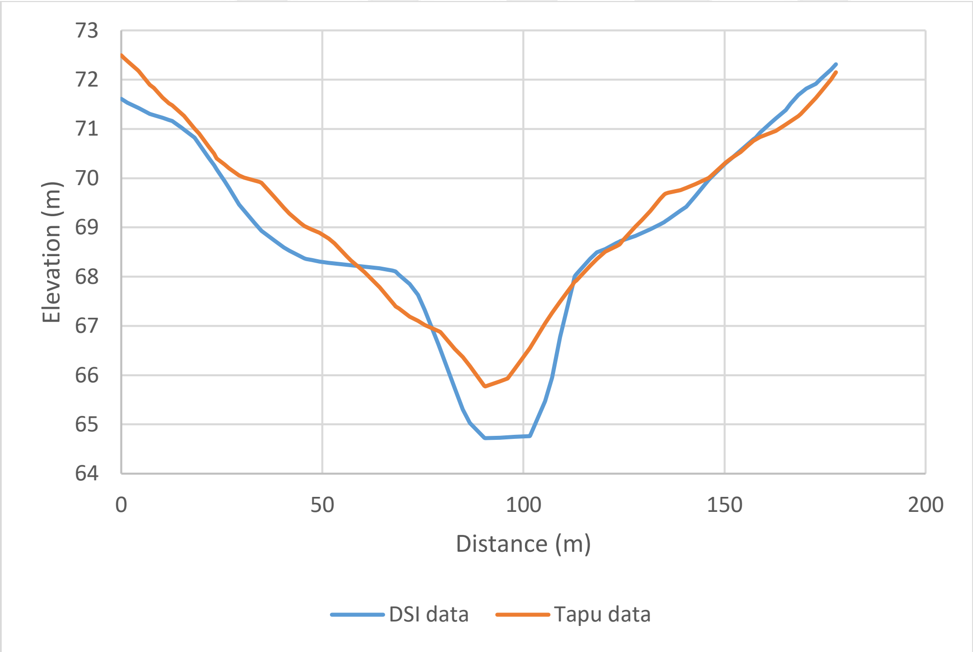

Figure 4-9 Comparison of Tapu Kadastro and DSI elevation data at Cross-section 4

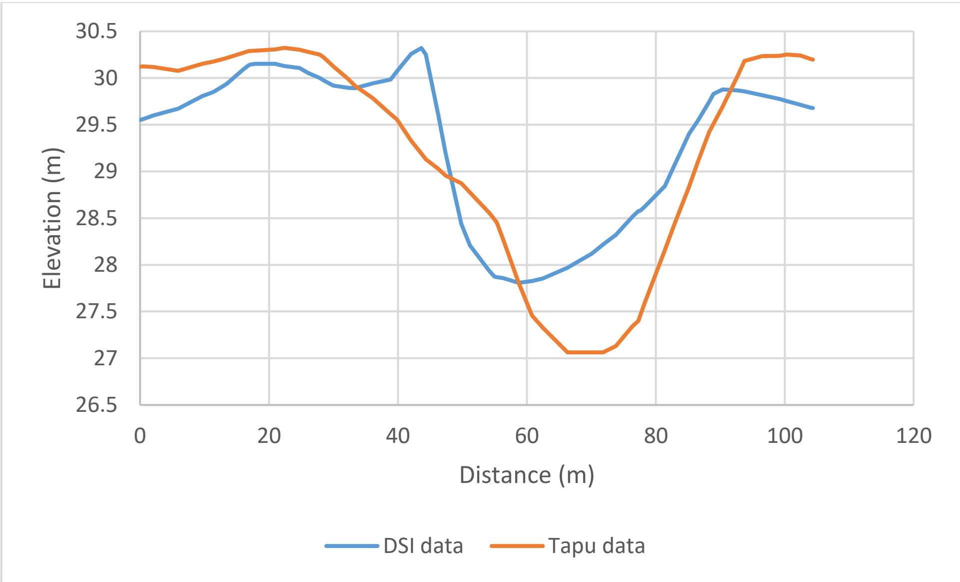

Figure 4-10 Comparison of Tapu Kadastro and DSI elevation data at Cross-section 5

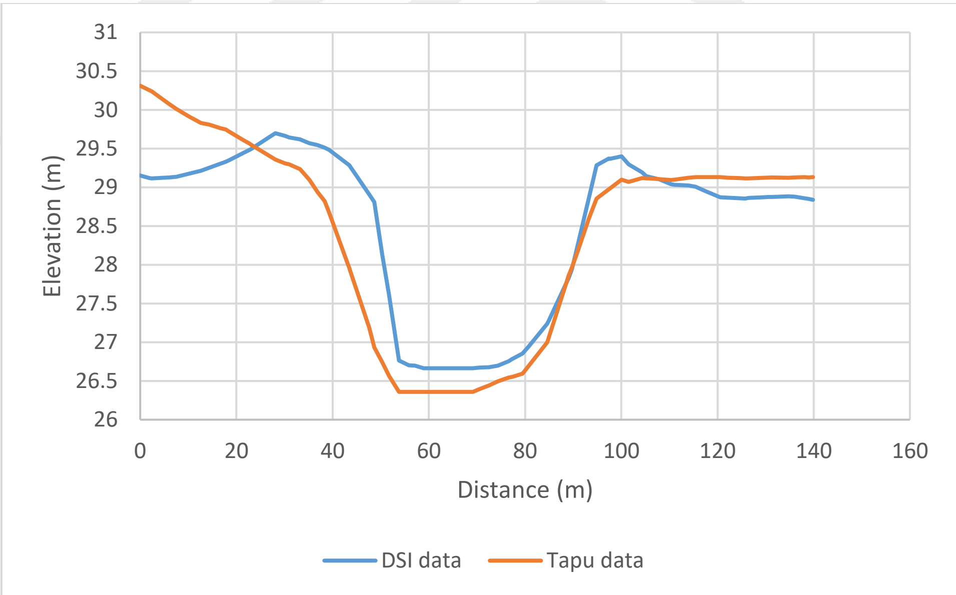

Figure 4-11 Comparison of Tapu Kadastro and DSI elevation data at Cross-section 6

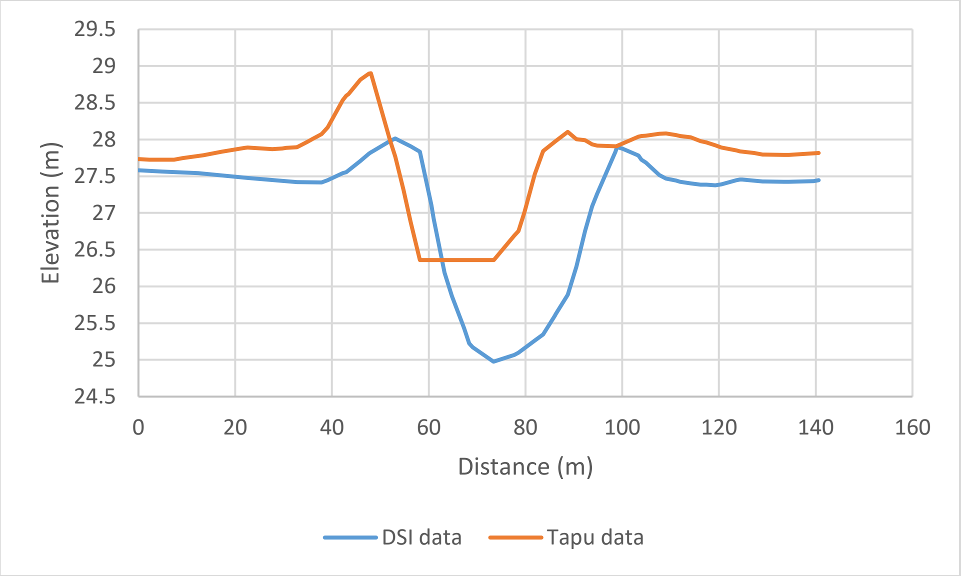

Figure 4-12 Comparison of Tapu Kadastro and DSI elevation data at Cross-section 7

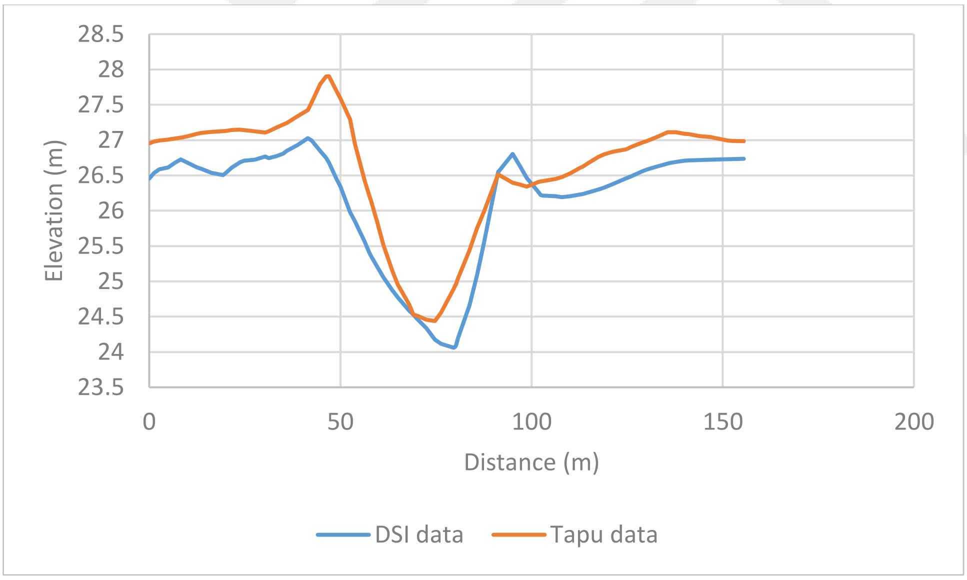

Figure 4-13 Comparison of Tapu Kadastro and DSI elevation data at Cross-section 8

It can be seen from Cross-sections 1 and 2, located downstream of Ondokuz Mayıs Dam, the difference in the elevation is significant. The reason behind it can be that in the hilly regions, there is a rapid variation in elevation in comparison to relatively flatter terrain. To capture the surface variation in more detail in the hilly region, the density of the elevation point data is crucial, i.e., the denser the point data in the hilly region, the better the terrain details will be captured and vice versa. DSI point data has a greater density of points placed over the terrain, so the hilly terrain is captured in a better way in comparison to Tapu Kadastro point data in which the points are placed at a regular interval of 20 m. The graphs for the Cross-sections 3 to 8 show almost similar terrain profiles. This region is relatively flat in comparison to the hilly region just downstream of the dam.

Other than the comparison of the cross-section profile, the Tapu Kadastro DEM is subtracted from DSI DEM using Raster Calculator in ARC GIS to obtain a raster map of elevation differences between the two data sets (Figure 4-14).

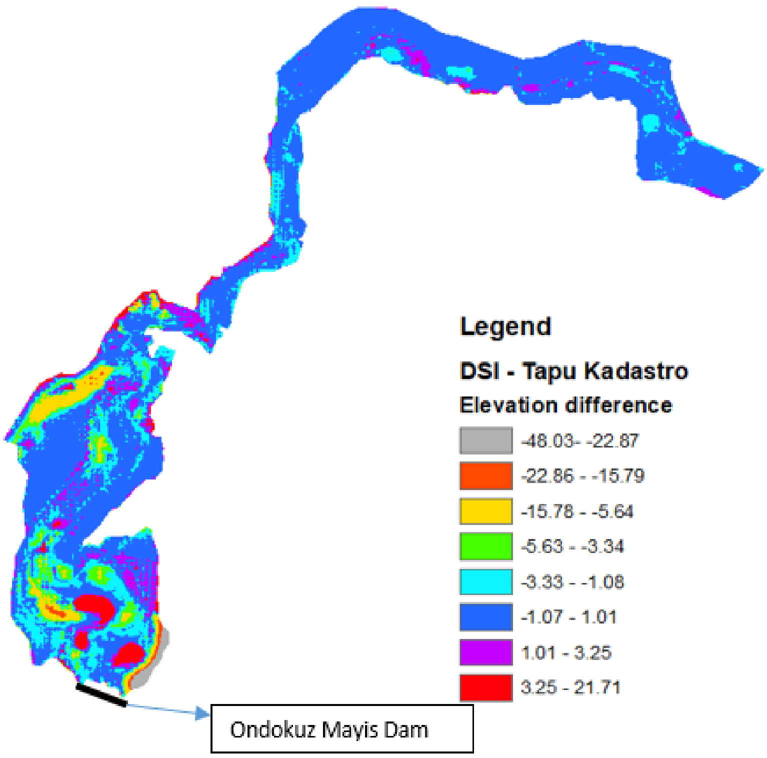

Figure 4-14 Elevation Difference between DSI and Tapu Kadastro data (Negative values show the area in which Tapu Kadastro elevation data has a higher elevation in comparison to DSI data. Positive values shows higher DSI values in comparison to Tapu Kadastro Data)

It can be seen that in the majority of the DEM area, the elevation differences are in the range of about ± 1 m. More significant differences are observed in the hilly region just downstream of the dam.

In order to better capture the topographic details in the hilly region just downstream of the dam, DSI data was incorporated into Tapu Kadastro data using the Editor Tool in ARC GIS and a DEM is developed from the combined elevation data. This new DEM is then used in the model calibration and the breach flood routing simulations of the Ondokuz Mayıs Dam region.

4.3.2 Land Use Shapefile

In order to incorporate the effect of the land use into the hydraulic model, shapefiles were created using the Google Earth software. The shapefile is then imported into ARC GIS software to assign the roughness values according to the land use. The Manning’s Roughness parameters used for both dam sites were obtained from Chow, (1959).

The roughness values for the Ondokuz Mayıs Dam region were selected from model calibration as discussed in Section 5.3.1, while the roughness values for İhsaniye and Avcıdere Dam regions are selected based on the land-use in Google earth images.

The Sensitivity of roughness values on flood routing is also analyzed by multiplying the base roughness values by 0.8 and 1.2. Table 4-4 shows the values of the Manning’s roughness parameter used for Ondokuz Mayıs Dam and Figure 4-15 shows the land use shapefile of Ondokuz Mayıs region.

Table 4-4 Ondokuz Mayıs Dam land use roughness values

Area Description	0.8*base n	Base n	1.2*base n
Channel (Reach 1)	0.0320	0.0400	0.0480
Channel (Reach 2)	0.0168	0.0210	0.0252
Highway	0.0128	0.0160	0.0192
Residential Area	0.0960	0.1200	0.1440
Cultivated Land	0.0320	0.0400	0.0480

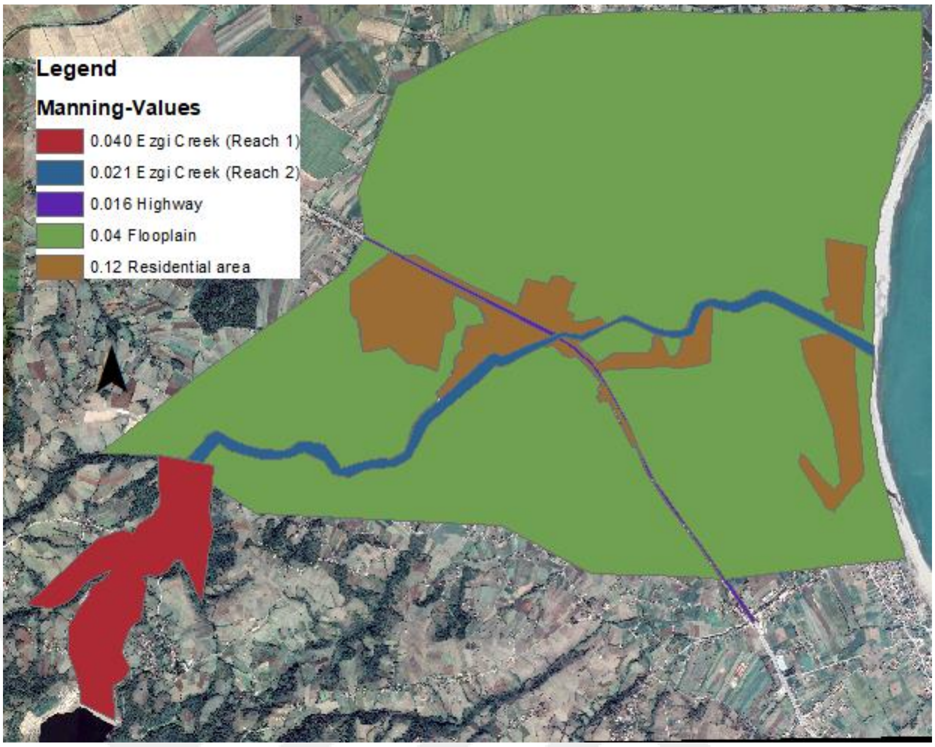

Figure 4-15 Ondokuz Mayıs Dam downstream land use shapefile

Table 4-5 shows the values of the roughness parameter used for İhsaniye Dam and Avcıdere Dam regions. Figure 4-16 shows the land use shapefile for İhsaniye Dam and Avcıdere Dam.

Table 4-5 İhsaniye Dam and Avcıdere Dam land use roughness values

Area Description	**0.8*base n**	**Base n**	**1.2*base n**
Channel	0.0360	0.0450	0.0540
Hill Bush Cover	0.0400	0.0500	0.0600
Residential Area	0.0960	0.1200	0.1440
Forest/ Trees	0.0480	0.0600	0.0720
Cultivated land	0.0320	0.0400	0.0480

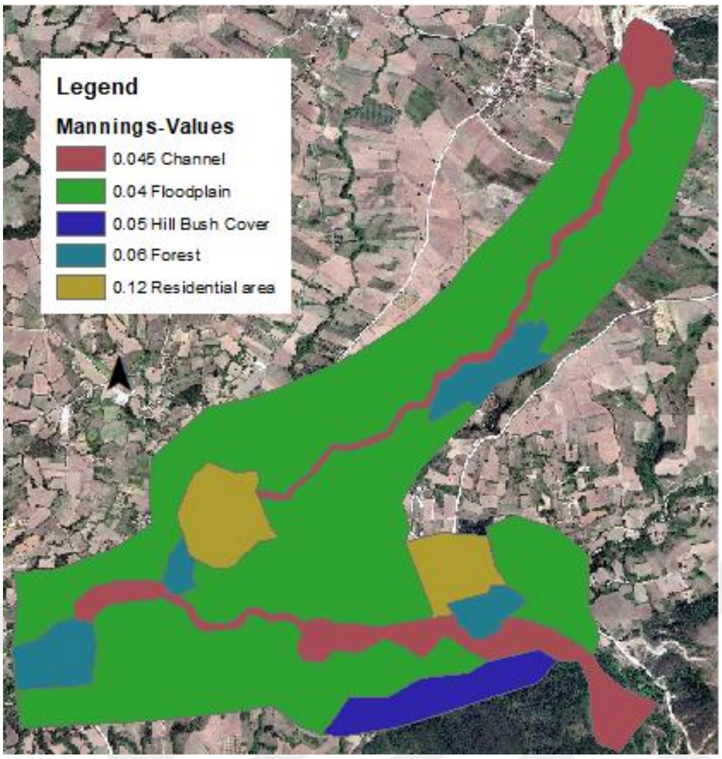

Figure 4-16 İhsaniye Dam and Avcıdere Dam Land use shapefile

4.3.3 Grid Size

In this study, flood routing simulations for breach hydrograph are carried out at grid sizes of 5 m, 10 m, 25 m, and 50 m in both HEC-RAS and FLO-2D. In both models, square-shaped uniform grid sizes were generated to examine the difference in both model's ability to simulate the breach hydrograph over a dry floodplain.

4.3.4 Boundary Conditions

In both models, for routing of breach hydrograph on floodplain an upstream boundary condition of inflow hydrograph and a downstream boundary condition of normal depth were used.

4.4 Breach Parameters

In dam breach analysis, the first thing is the estimation of breach parameters. These parameters are used to compute the breach outflow hydrograph, which will be used to perform downstream routing. Breach parameters are critical in the risk assessment of the dam, as it directly affects the peak flow rates coming out of dam breach. The parameters also affect the possible warning time available to the downstream areas.

The estimation of breach parameters including breach location, breach dimension, and time of failure helps in the assessment of the potential risk to the dam. These parameters must be estimated for each type of dam failure scenario to be studied. The breach parameters that are linked with the hydrological event will be different from those for failure on a sunny day with a normal reservoir level. Unfortunately, the breach size, location, and time of formation are the most uncertain parts of data in a dam failure analysis (G. Brunner, 2014).

4.4.1 Breaching Parameters Estimation

The HEC-RAS software requires the following information to describe the dam breach:

Failure Location: It is the stationing of the centerline of the breach in the dam. The location of breach failure is based on a lot of factors e.g. failure type, dam type and shape, and driving forces of failure. In general, all factors about the dam, including any past information regarding seepage, a foundation problem, and the breach location place is the most possible for each type of failure.

Failure Mode: Failure mode is the mechanism that deals with the start and growth of the breach. The hydraulic computations in HEC-RAS are limited to failure modes of overtopping and piping. All other failure modes can be modeled using one of these methods. Overtopping failures in dams start from the dam’s top and grow to maximum sizes, whereas a piping failure can start at any location and grow to the maximum sizes. The final size of breach and time of breach formation is very much critical in the computation of the outflow hydrograph than the actual breach initiation mode.

Breach Shape: The breach shape is described in terms of Breach width, Breach height, right and left side slopes H: V. HEC-RAS requires breach bottom width (W_b) as breach width for input. For breach height (h_b) the extent from the top of the dam to the average breach invert elevation is used. The side slopes are entered in H: V. A general description of a breach is shown in Figure 4-17.

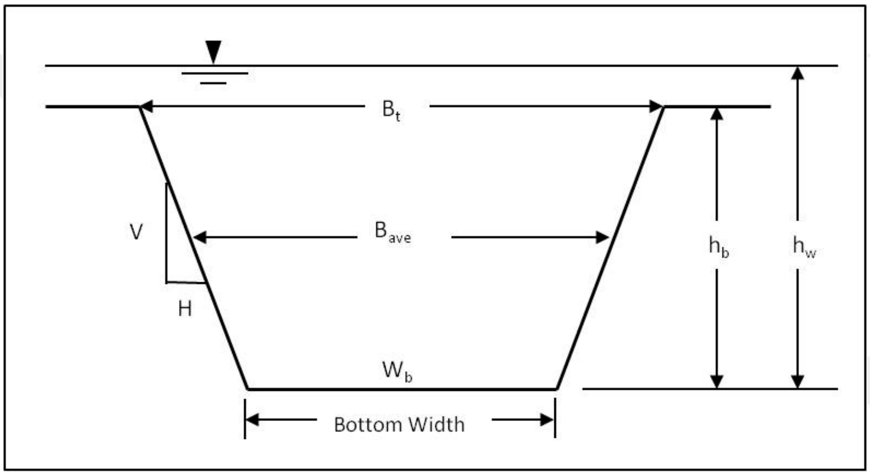

Figure 4-17 Description of the Breach Parameters (G. W. Brunner, 2016)

Breach Development Time: The critical breach development time for HEC-RAS can be explained as below.

Overtopping Failure: In HEC-RAS for overtopping failure mode, breach start time is when the erosion process has reached the upstream face of dam. At this point, the outflow will start to increase from dam breach. When the breach is fully formed and any considerable erosion has halted, then the breach development time for HEC-RAS ends. The ending of breach development time should not account for the time to completely drain the reservoir.

Piping Failure: For piping failure mode in HEC-RAS, Breach formation time starts when a substantial amount of flow and material are coming out downstream of the piping hole. The breach formation time is considered to have ended when the breach is fully formed and there is no significant erosion.

Figure 4-18 demonstrates the example breach process for overtopping and pipping failure of dam.

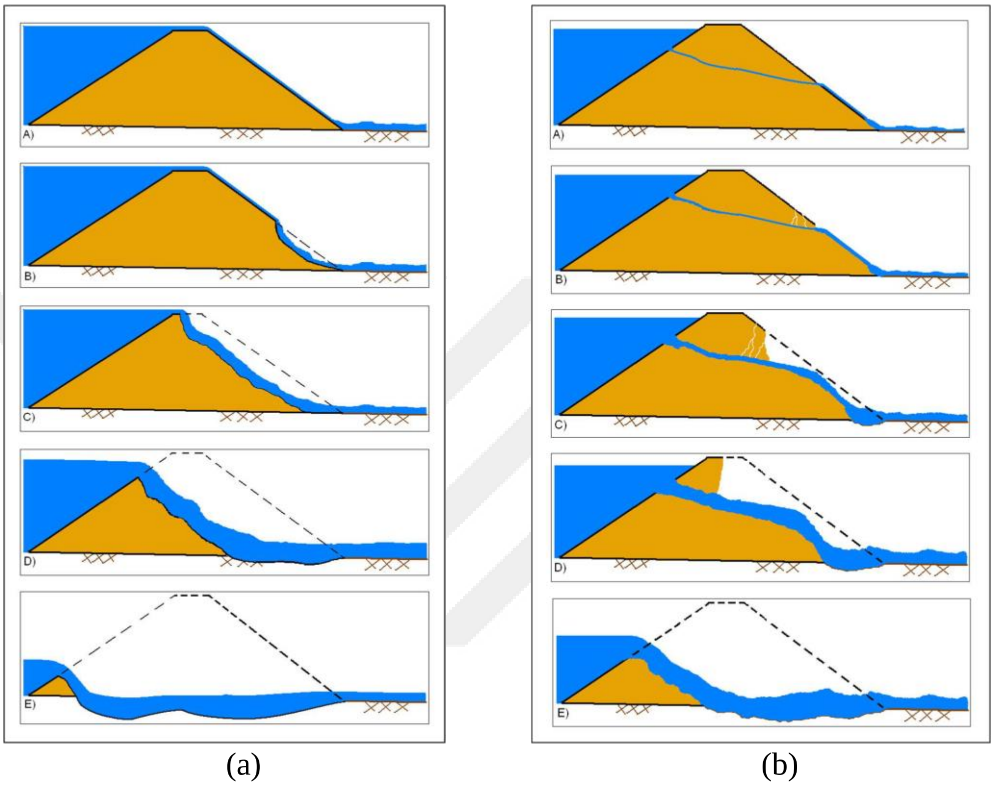

Figure 4-18 Example Breach Process for (a) Overtopping Failure (b) Piping Failure (G. W. Brunner, 2016)

Trigger Mechanism: pool elevation; pool elevation plus duration; or clock time

Weir and Piping Coefficients: weir coefficients are used to compute overtopping/weir flow, and an orifice coefficient is used to compute piping/pressure flow.

Regression Equations: Several regression equations have been developed by researchers for breach dimensions (Breach width, side slopes, etc.) and for failure time. These equations were developed based on the data from earthen dams, earthen dams with impervious cores, and rockfill dams. So, these equations do not directly apply to earthen dams with concrete cores or concrete dams.

Some of the regression equations that have been widely used for dam safety analysis are discussed as under:

- Froehlich (1995 a)
- Froehlich (2008)
- MacDonald and Langridge-Monopolis (1984)
- Von Thun and Gillette (1990)
- Xu and Zhang (2009)

Froehlich (1995 a): Froehlich used data sets from 63 embankment dams (earthen, zoned, with core wall and rockfill dams) to develop the regression equations for the prediction of average breach width, failure time and side slopes.

The data used by Froehlich had the following ranges:

- Height of the dams: 3.66 – 92.96 meters
  (with 90% < 30 meters, and 76% < 15 meters)
- Volume of water at breach time: 0.0130 – 660.0 m^3 x 10^6
  (with 87% < 25.0 m^3 x 10^6, and 76% < 15.0 m^3 x 10^6)

Froehlich's regression equations for average breach width and failure time are:

$$B_{ave} = 0.1803 K_o V_w^{0.32} h_b^{0.19} \tag{4.1}$$

$$t_f = 0.00254 V_w^{0.53} H_b^{-0.90} \tag{4.2}$$

where B_{ave} is average breach width (meters), K_o is constant (1.4 for overtopping failures, 1.0 for piping), V_w is reservoir volume at the time of failure (cubic meters), H_b is the height of the final breach (meters), t_f is breach formation time (hours), Froehlich states that the average side slopes for overtopping failure are 1.4H:1V and 0.9H:1V otherwise (i.e., piping/seepage)

Froehlich (2008): Froehlich updated the breach equations from 1995 based on the new data sets. For these equations, date sets from 74 embankment dams (earthen, zoned, with core wall and rockfill dams) were used. The ranges of the data sets used were:

- Height of the dams: 3.05 – 92.96 meters
  (with 93% < 30 meters, and 81% < 15 meters)
- Volume of water at breach time: 0.0139 – 660.0 $m^3 \times 10^6$
  (with 86% < 25.0 $m^3 \times 10^6$, and 82% < 15.0 $m^3 \times 10^6$)

The updated Froehlich equations for breach width and failure time are:

$$B_{ave} = 0.27 K_o V_w^{0.32} H_b^{0.04} \tag{4.3}$$

$$t_f = 63.2 \sqrt{\frac{V_w}{g H_b^2}} \tag{4.4}$$

where B_{ave} is average breach width (m), K_o is constant (1.3 for overtopping failures, 1.0 for piping), V_w is reservoir volume at the time of failure (cubic meters), H_b is the height of the final breach (m), g is the gravitational acceleration (9.80665 m/sec), t_f is breach formation time (seconds), Froehlich's also estimated that the average side slopes for overtopping failures to be 1.0 H:1V and 0.7 H:1V otherwise (i.e., piping/seepage)

MacDonald and Langridge-Monopolis (1984): MacDonald and Langridge-Monopolis developed a relationship for breach formation factor (a product of the volume of water coming out of dam and water height above the dam) by utilizing data sets from 42 dams (earth-fill, earth-fill with clay core, rockfill). The breach formation factor is then related to the volume of material eroded from dam body.

The ranges for the data used by MacDonald and Langridge-Monopolis are as under:

- Height of the dams: 4.27 – 92.96 meters
  (with 76% < 30 meters, and 57% < 15 meters)
- Breach Outflow Volume: 0.0037 – 660.0 $m^3 \times 10^6$
  (with 79% < 25.0 $m^3 \times 10^6$, and 69% < 15.0 $m^3 \times 10^6$)

The MacDonald and Langridge-Monopolis regression equations for volume of material eroded and breach formation time, are following:

Earthfill dams:

$$V_{er} = 0.0261(V_{out} * h_w)^{0.769} \tag{4.5}$$

$$t_f = 0.0179(V_{er})^{0.364} \tag{4.6}$$

Earth-fill with clay core or rockfill dams:

$$V_{er} = 0.0261(V_{out} * h_w)^{0.769}(4.7) \tag{4.7}$$

where V_{er} is the volume of material eroded from the dam embankment (cubic meters), V_{out} is the volume of water that passes through the breach (cubic meters), h_w is the depth of water above the bottom of the breach (meters), t_f is breach formation time (hours).

For the calculation of breach bottom width, the dam geometry is used with the following equation (State of Washington, 1992):

$$B_b = \frac{V_{er} - h_b^2(ZW_c + Zh_b.Z_3/3)}{h_b(W_c + h_b Z_3/2)} \tag{4.8}$$

where B_b is the bottom width of the breach (meters), h_b is the height from the bottom of the breach to the top of the dam (meters), W_c is dam crest width (meters), Z_3 is Z_1 + Z_2 (Z_1 is the average slope (Z_1:1) of the upstream face of dam, Z_2 is the average slope (Z_2:1) of the downstream face of dam, Z is side slopes of the breach (Z:1), 0.5 for the MacDonald method. MacDonald and Langridge-Monopolis stated that the breach should be trapezoidal with side slopes of 0.5H:1V.

Von Thun and Gillette (1990): Von Thun and Gillette utilized data sets of 57 dams from both the Froehlich (1987) and the MacDonald and Langridge-Monopolis (1984) to develop the regression equations. The data that Von Thun and Gillette used for their regression analysis had the following ranges:

- Height of the dams: 3.66 – 92.96 meters
  (with 89% < 30 meters, and 75% < 15 meters)

- Volume of water at breach time: 0.027 – 660.0 $m^3 \times 10^6$
(with 89% < 25.0 $m^3 \times 10^6$, and 84% < 15.0 $m^3 \times 10^6$)

The equation for the average breach width is:

$$B_{ave} = 2.5h_w + C_b \tag{4.9}$$

where B_{ave} is average breach width (meters), h_w is the depth of water above the bottom of the breach (meters), and C_b is a coefficient, which is a function of reservoir size.

Von Thun and Gillette developed two different sets of equations for the breach development time. The first set of equations calculates the breach development time as a function of water depth above the breach bottom:

$$t_f = 0.02h_w + 0.25 \quad \text{(erosion resistant)} \tag{4.10}$$

$$t_f = 0.015h_w \quad \text{(easily erodible)} \tag{4.11}$$

where t_f is breach formation time (hours), h_w is the depth of water above the bottom of the breach (meters).

The second set of equations calculates the breach development time as a function of water depth above the bottom of the breach and average breach width:

$$t_f = \frac{B_{ave}}{4h_w} \quad \text{(erosion resistant)} \tag{4.12}$$

$$t_f = \frac{B_{ave}}{4h_w + 61.0} \quad \text{(easily erodible)} \tag{4.13}$$

Von Thun and Gillette proposed to use breach side slopes of 1.0H:1.0V for all embankment dams, except for those with cohesive soils, for which the side slopes can be used on the order of 0.5H:1V to 0.33H:1V.

Xu and Zhang (2009): Xu and Zhang used datasets of 45 dams to develop an equation for average breach width and about 28 dams for the failure time equation. The ranges of the data used by Xu and Zhang used for regression analysis are:

- Height of the dams: 3.2 – 92.96 meters
  (with 78% < 30 meters, and 58% < 15 meters)
- Volume of water at breach time: 0.105 – 660.0 m^3 x 10^6
  (with 80% < 25.0 m^3 x 10^6, and 67% < 15.0 m^3 x 10^6)

Xu and Zhang's equation for the average breach width is:

$$\frac{B_{ave}}{H_b} = 0.787 \left[\frac{h_d}{h_r}\right]^{0.133} \left[\frac{V_w^{1/3}}{h_w}\right]^{0.652} e^{B_3} \qquad (4.14)$$

where B_{ave} is average breach width (meters), V_w is reservoir volume at the time of failure (cubic meters), H_b is the height of the final breach (meters), h_d is the height of the dam (meters), h_r is 15 meters, is considered to be a reference height for distinguishing large dams from small dams, h_w is the height of the water above the breach bottom elevation at the time of the breach (meters), B_3 is $b_3+b_4+b_5$ coefficient that is a function of dam properties, b_3 is -0.041, 0.026, and -0.226 for dams with core walls, concrete faced dams, and homogeneous/zoned-fill dams, respectively, b_4 is 0.149 and -0.389 for overtopping and seepage/piping, respectively, b_5 is 0.291, -0.14, and -0.391 for high, medium, and low dam erodibility, respectively.

The breach development time equation developed by Xu and Zhang gives greater breach development time than that of the four equations explained above. It is because of the fact that it includes more of the initial and post erosion period than what is commonly used in HEC-RAS. Because of this, the breach development time equation of Xu and Zhang should not be used in HEC-RAS. However, it is shown here for the method completeness:

$$\frac{T_f}{T_r} = 0.304 \left(\frac{h_d}{h_r}\right)^{0.707} \left(\frac{V_w^{1/3}}{h_w}\right)^{1.228} e^{B_5} \qquad (4.15)$$

where T_f is breach formation time (hours),T_r is 1 hour (unit duration), V_w is reservoir volume at the time of failure (cubic meters), h_d is the height of the dam (meters), h_r is fifteen meters, which is considered to be a reference height for distinguishing large dams from small dams, h_w is the height of the water above the breach bottom elevation at the time of the breach (meters), B_5 is b_3+b_4+b_5 coefficient that is a function of dam properties, b_3 is -0.327, -0.674, and -0.189 for dams with the core walls, concrete faced dams, and homogeneous/zoned-fill dams, respectively, b_4 is -0.579 and -0.611 for overtopping and seepage/piping, respectively, and b_5 is -1.205, -0.564, and 0.579 for high, medium, and low dam erodibility, respectively.

4.5 Performance Measures

Two statistics are used to measure the degree of matching and variation between model simulation results, including Fit statistic (F) and Root Mean Square Errors. A brief explanation of these statistics is given below.

4.5.1 Fit Statistic (F-Statistic)

The F statistic is commonly used for assessing the variation in flood inundation extent. It shows how the change in grid resolution and roughness parameter is affecting the flood inundation area in comparison to the reference inundation area. (Bates & De Roo, 2000; Horritt, MS., & Bates, 2001). F statistic is calculated as follows:

$$F = \frac{A_o}{A_r + A_s - A_o} \tag{4.16}$$

where A_r is the referenced wet area, A_s is the predicted wet areas, and A_o is the overlap of reference and predicted wet areas. F-statistic varies from 0 to 1, with 1 for a perfect fit and 0 for no overlap.

In this study, F-statistic is calculated for both HEC-RAS and FLO-2D simulation results. The inundation map obtained for the 5 m grid simulation is considered as a reference map for each model.

4.5.2 Root Mean Square Error (RMSE)

The RMSE is used to measure the difference in flow depth along the river centerline at different grid resolutions in comparison to flow depth obtained at 5 m grid resolution for both models. RMSE is calculated as follows:

$$RMSE = \sqrt{\frac{\sum_i^n (d_i^p - d_i^r)^2}{s}} \tag{4.17}$$

where d_i^p and d_i^r are the predicted and referenced flow depths, respectively, and s is the sample size. This RMSE value is useful for gauging the overall agreement of flow depth between predicted and reference values.

4.6 Flood Hazard Mapping

Based on the Simulation results Flood hazard maps are prepared using FLO-2D software. Flood hazard maps are beneficial in representing flood-prone areas under extreme conditions according to the hazard level. It also helps in the planning of mitigation and response (Sinha, 2005).

Flood hazard maps are also useful to increase the awareness of the public, municipalities, and other government organizations about the possibility of flooding. It shows the area which are at different hazard levels and can help device emergency action plan accordingly (Environment Agency, 2018)

In this study, Flood hazard maps are prepared using Mapper ++ software which is provided with the FLO-2D pro Model. The method used to develop hazard maps is based on (García et al, (2003, 2005)).

At a specific location, the flood hazard level is a function of flood probability (Frequency) and intensity. Flood frequency is inversely proportional to the magnitude of the flood. The frequency of occurrence of large floods is low. Flood intensity is determined by the flow depth and Velocity. The discrete combined function of flood frequency and intensity is shown in Figure 4-19.

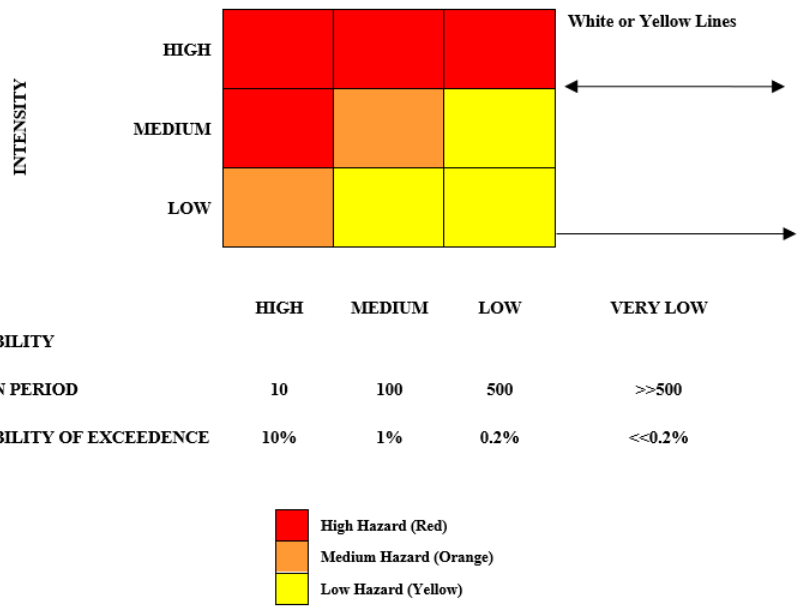

Figure 4-19 Flood hazard level classification (Garcia et al., (2003, 2005))

The flood hazard map consists of three hazard levels high, medium, and low. The high hazard level (red) shows the area in which the population is at risk both inside and outside of the houses. There is a possibility of buildings being destroyed. At medium hazard level (orange) the person outside of their houses is in danger and structures may be destroyed or suffer damage based on construction characteristics.

In low hazard areas (yellow), there is very low or no danger to the population, and the structure might suffer minor damage.

4.7 Flood Damage

Flood damages include all types of damages that are caused by flooding. It covers a wide range of detrimental effects on humans, environment, public infrastructure, industrial production, cultural heritage, and the economy. Different terminologies are used to explain the type of flood damages but they are mainly categorized into direct and indirect damages and into tangible and intangible damages (Smith K, 1998; Parker, Get al, 1987; Penning-Rowsell et al, 2003; Messner & Meyer, 2005)

Direct Damages: The harm caused by the direct contact of floodwater to humans, the environment, and the property is included in direct damages. It ranges from loss of human life, damage to the commercial and residential buildings, loss of agricultural crops and livestock, loss of ecological goods, and direct health impacts.

Indirect Damages: Indirect damages are the ones caused by the disruption of the economy; the additional cost of emergency actions taken to prevent flood damages. It covers the loss of commercial activities (production and consumption activities) and the cost of emergency services.

Tangible Damages: The type of damages which can be simply expressed in terms of monetary value are known as Tangible damages. It covers losses in property, commercial production, etc.

Intangible Damages: Casualties, loss of ecological goods, and all other types of damages that are difficult to assess in terms of monetary value are expressed in terms of intangible damages.

Table 4-6 represents the type of flood damages and how they are evaluated.

Table 4-6 Types of flood damages (Source: (Penning-Rowsell et al., 2003; Smith & Ward, 1998)

		Measurement	
		Tangible	**Intangible**
Form of Damages	**Direct**	Physical damage to assets: • Buildings • Contents • Infrastructure	• Loss of life • Health effects • Loss of ecological goods
	Indirect	• Loss of industrial production • Traffic disruption • emergency costs	• Inconvenience of post-flood recovery • Increased vulnerability of survivors

Smith & Ward (1998) categorized the damages incurred from the flood as primary and secondary damages. With primary being the one which takes place because of the event itself such as the loss in production of a company which is in flood-affected area, while the secondary damages are caused by the primary damages e.g. losses induced by consumers or suppliers because of loss in production and by the people influenced outside of the affected area due to halt in production.

4.7.1 Flood Damage Calculation

Flood damage calculations are done by the methods used in “Flood management Reports of Ministry of Agriculture and Forestry, Republic Of Turkey”. The results from the breach hydrograph simulations were used in the damage calculations. The shapefiles were created in GIS software in order to determine the area of buildings and agricultural land under flooding. In this study, the damage calculations are done for the buildings and the agricultural areas by using the following method.

4.7.2 Flood Damages for Buildings

The economic loss value of the structure that comes in contact with floodwater is calculated using the formula as given in the Basin Flood Management Plan reports by the Ministry of Agriculture and Forest (TOB, 2019) as below:

$$\mathrm{FD} = DR \times A \times BF \times K \qquad (4.18)$$

where, Z is the economic damage value calculated for the relevant flow (TL), DR is the damage factor, A is the area of the building (m^2), BF is the structure unit price (TL / m^2), and K is a coefficient (0.6 x 0.5 x 1.18).

Damage factor: After the calculation of the water depths, the Damage factor is determined by using the "Depth - Damage" curves published in 2017 by the Joint Research Center (JRC) as shown below in Figure 4-20.

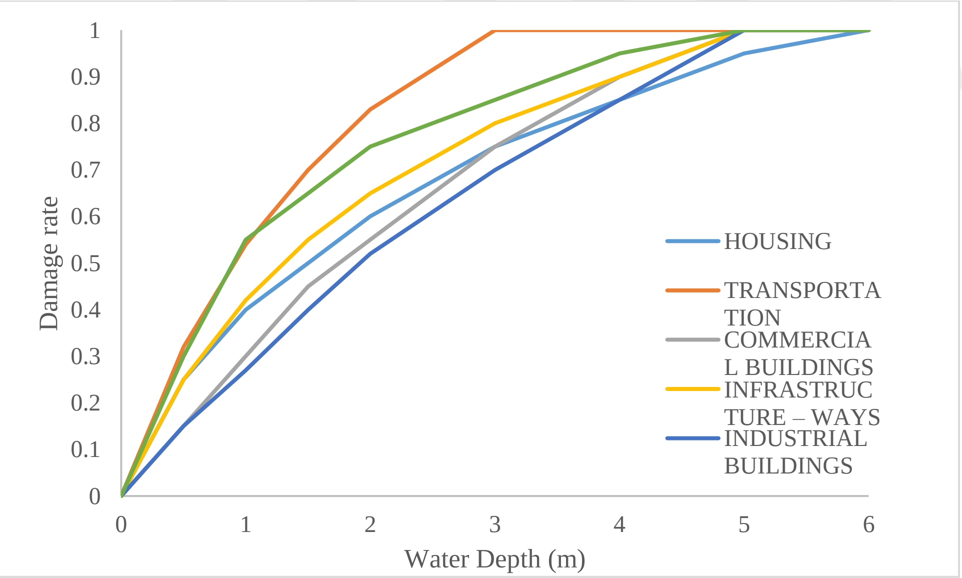

Figure 4-20 Depth - Damage Curve (JRC, 2017)

Area of the building: The area of the buildings is calculated from the shapefiles created by using GIS software.

Structure Unit Price: The building unit costs are taken from the document titled "Mimarlik Ve Mühendislik Hizmet Bedellerinin Hesabinda Kullanilacak 2020 Yili Yapi Yaklaşik Birim Maliyetleri Hakkinda Tebliğ" published by the Ministry of Environment and Urbanization, Turkey.

4.7.3 Flood Damages for Agriculture

In order to calculate the flood damages to agricultural land, firstly flood depths and inundated areas are calculated for the respective areas. In Turkey, Agricultural products are divided into four categories in terms of their sensitivity to floods by the Turkey Insurance Association (TSB), as presented in Table 4-7. In the table, the 1st category is the most resistant to flooding and the 4th class is the most sensitive to flooding. It was observed that the products in the 1st sensitivity class received 0.4, meaning 40% of the products will de damages, the products in the 2nd sensitivity class receive 0.6 (60% of the products will be damaged) and the products in the 3rd sensitivity class received 0.8 (80% of the products will be damaged), while in 4th sensitivity class all of the products will be damaged.

Table 4-7 Flood and Floods Product Sensitivity Classes Table (TSB, 2018)

Accuracy Class	Products
1	Altıntop, Pistachio, Pear, Avocado, Quince, Almond, Walnut, Mulberry, Apple, Plum, Hazelnut, Jujube, Fig, Apricot, Chestnut, Cherry, Kiwi, Lemon, Tangerine, Medlar, Banana, Pomegranate, Nectarine, Orange, Peach, Persimmon, Sour Cherry, Loquat, Olive
2	Raspberry, Blackberry, Grape, Blueberry, Pickled Vine Leaves (Grape (Wine Rack)), Pickled Vine Leaves, Pickled Vine Leaves Drying Rack))
3	Anise, Barley, Barley , Safflower, Safflower , Sunflower (Snack), Sunflower , Sunflower (Oil), Broad Bean (Feed), Wheat, Wheat , Vines, Rye , Rye , Tea, Black Cumin, Millet, Bean , Bean (Dry), Seedling (Strawberry), Seedling (Vegetable), Seedling (Ornamental Plant), Seedling (Field), Vetch, Vetch (Koca), Vetch (Hungarian), Vetch (Hungarian Certified Seed), Vetch , Poppy Capsule (Fall), Poppy Capsule (Summer), Poppy Capsule + Grain (Autumn), Poppy Capsule + Grain (Summer), Carrot (Certified Seed), Animal Beet, Animal Beet , Thyme, Flax (Fiber), Cumin, Rapeseed (Canola), Rapeseed (Canola) , Sainfoin, Birdseed, Lentil (Red), Lentil (Green) , Corn , Corn (Silage), Corn (Grain), Damson, Chickpea, Chickpea , Beet (Red) , Potato, Potato , Sar Garlic (Dry), Onion (Shallot), Onion , Onion (Dry), Sorghum (Grain), Sorghum (Silage), Soy, Soy , Sesame, Sugar beet , Sugar beet, Hops , Triticale, Triticale , Tobacco, Oilfield, Feed Pea, Feed Pea , Peanut, Clover, Clover , Oats, Oats , Purslane , Broad Bean , Pea , Cowpea , Buckwheat, Cress , Dill , Celery , Lettuce , Parsley , Fenugreek, Cabbage , Arugula , Radish , Leek , Quinoa, Spinach , Chard , Turnip , Peanut
4	Anise, Barley, Barley , Safflower, Safflower , Sunflower (Snack), Sunflower , Sunflower (Oil), Broad Bean (Feed), Wheat, Wheat , Vines, Rye , Rye , Tea, Black Cumin, Millet, Bean , Bean (Dry), Seedling (Strawberry), Seedling (Vegetable), Seedling (Ornamental Plant), Seedling (Field), Vetch, Vetch (Koca), Vetch (Hungarian), Vetch (Hungarian Certified Seed), Vetch , Poppy Capsule (Fall), Poppy Capsule (Summer), Poppy Capsule + Grain (Autumn), Poppy Capsule + Grain (Summer), Carrot (Certified Seed), Animal Beet, Animal Beet , Thyme, Flax (Fiber), Cumin, Rapeseed (Canola), Rapeseed (Canola) , Sainfoin, Birdseed, Lentil (Red), Lentil (Green) , Corn , Corn (Silage), Corn (Grain), Damson, Chickpea, Chickpea , Beet (Red) , Potato, Potato , Sar Garlic (Dry), Onion (Shallot), Onion , Onion (Dry), Sorghum (Grain), Sorghum (Silage), Soy, Soy , Sesame, Sugar beet , Sugar beet, Hops , Triticale, Triticale , Tobacco, Oilfield, Feed Pea, Feed Pea , Peanut, Clover, Clover , Oats, Oats , Purslane , Broad Bean , Pea , Cowpea , Buckwheat, Cress , Dill , Celery , Lettuce , Parsley , Fenugreek, Cabbage , Arugula , Radish , Leek , Quinoa, Spinach , Chard , Turnip , Peanut

After the products are divided into classes according to their sensitivity levels, an evaluation is made that how much damage each class will suffer. Flood and Flood Guarantee Premium Price Table published by TSB was used in the evaluation. The letters in Table 4-8 represent the danger zones with Z being the most dangerous zone and A, the safest zone.

Table 4-8 Flood and Flooding Coverage Unit Price Table (TSB, 2018)

Product Sensitivity Class	Flood and Flood Danger Zones and Premium Prices (%) (Common Insurance Rate Standard)											
	A	B	C	D	E	F	G	H	I	J	K	L
1	0.04	0.06	0.08	0.11	0.13	0.19	0.25	0.32	0.38	0.50	0.63	0.76
2	0.06	0.09	0.13	0.16	0.19	0.28	0.38	0.47	0.57	0.76	0.95	1.13
3	0.08	0.13	0.17	0.21	0.25	0.38	0.50	0.63	0.76	1.01	1.26	1.51
4	0.11	0.16	0.21	0.26	0.32	0.47	0.63	0.79	0.95	1.26	1.58	1.89
Product Sensitivity Class	M	N	O	P	R	S	T	U	V	Y	Z	
1	0.88	1.07	1.26	1.58	2.00	2.52	3.15	3.89	4.73	5.46	6.30	
2	1.32	1.61	1.89	2.36	2.99	3.78	4.73	5.83	7.09	8.19	9.45	
3	1.76	2.14	2.52	3.15	3.99	5.04	6.30	7.77	9.45	10.92	12.60	
4	2.21	2.68	3.15	3.94	4.99	6.30	7.88	9.71	11.81	13.65	15.75	

Unit prices of agricultural products were obtained using the values published on the TURKSTAT website. There is information about crops cultivated in agricultural fields in 2015, 2016, 2017 and 2018. While calculating the economic loss, the most valuable crop among the planted crops in the last four years was considered as the worst scenario. The information provided above is used in estimating the losses to crops caused by flood water for the study area.

CHAPTER 5

RESULTS AND DISCUSSIONS

In this chapter, the results of the dam-break analysis for the Ondokuz Mayıs Dam. İhsaniye Dam and Avcıdere Dam are presented. Firstly, the process of calculating the dam breach hydrograph from HEC-RAS for each dam using different set of breach parameters is discussed and then the breach hydrograph is routed over the downstream floodplain using HEC-RAS and FLO-2D.

The model results are presented in the form of inundation maps of maximum flow depth, maximum flow velocity, and maximum depth arrival time. The values of maximum flow depth and arrival time for maximum flow depth are presented at control points located in the populated areas. The sensitivity of grid resolution, roughness parameter, and breach hydrograph (peak flow and time to peak) to the flood inundation results is also presented. Flood hazard maps are developed for the study areas, and flood damage analysis is also done using the simulation results.

For each site, the computation time is selected based on the time the peak of breach hydrograph takes to reach the boundaries of the 2D flow area. The Specification of the computer system used for simulations is Intel® Core (TM) i7 CPU, 3.4 GHz Processor, 16 GB RAM with 64-BIT Operating System.

5.1 Breach Hydrograph Calculation

In 2D dam-break modeling, the breach hydrograph at the dam location can be obtained by modeling the reservoir using either level pool routing or full dynamic wave routing. In the level pool routing, the water surface slope is not captured within the reservoir during the breach simulation, instead the model assumes that water surface elevation is decreasing at the same rate at all locations in the reservoir. The level pool routing is not an accurate representation of the real condition during the dam breach event. On the other hand, full dynamic wave routing is known to be the most accurate methodology for modeling the reservoir and should be preferred when the reservoir bathymetry is available (G. Brunner, 2014).

In this study, breach hydrographs were obtained from HEC-RAS using the dynamic wave routing method for modeling the reservoir in 2D. For each dam, different sets of breach parameters and failure modes were used. The model was set up for each dam using the geometric, hydraulic, and hydrological data. The dam reservoir is defined by a 2D flow area. The reservoir was connected with the downstream area through the dam connection. On the upstream end of the reservoir, the inflow hydrograph was used as the inflow boundary condition, and on the downstream boundary, normal depth was used as the boundary condition. After setting up the model, breach parameters were entered via breach plan data. The simulations were run with the desired breach hydrograph output interval. After the simulation is completed the breach hydrograph at dam location is obtained from the DSS viewer in HEC-RAS.

The dams were breached using the overtopping and piping failure modes. In the case of overtopping failure, a Q-catastrophic hydrograph was used as an inflow boundary condition, while piping failure is assumed to occur on a sunny day.

The breach parameters were selected from the possible ranges given by the federal agencies in the United States as presented in Table 5-1.

Table 5-1 Summary of Possible ranges of breach parameters (USACE, 2014; Gee, 2009)

Type of Dam	Average Breach Width B_{ave}	Horizontal component of breach side slope H:V	Failure time T_f (hrs)	Agency
Embankment	(0.5 to 3.0) x h_d* (0.5 to 5.0) x h_d (1.0 to 5.0) x h_d (2.0 to 5.0) x h_d	0 to 1.0 0 to 1.0 0 to 1.0 0 to 1.0 (slightly larger)	0.5 to 4.0 0.1 to 4.0 0.1 to 1.0 0.1 to 1.0	USACE (1980) USACE (2007) FERC (1988) NWS (Fread, 2006)
Concrete Gravity	Multiple Monoliths Usually ≤ 0.5 *l***	Vertical Vertical Vertical	0.1 to 0.5 0.1 to 0.3 0.1 to 0.2	USACE (2007) FERC NWS
Concrete Arch	Entire Dam (0.8 x *l*) to *l* Entire Dam (0.8 x *l*) to *l*	valley wall slope 0 to valley walls 0 to valley walls 0 to valley walls	≤ 0.1 ≤0.1 ≤ 0.1 ≤ 0.1	USACE (1980) USACE (2007) FERC NWS
Slag/Refuse	0.8 x *l*) to *l* (0.8 x *l*) to *l*	1.0 to 2.0	0.1 to 0.3 ≤ 0.1	FERC NWS

* h_d is the height of the dam,
***l* is the length of the dam crest.

Each dam is breached using three different sets of breach parameters and failure modes. The resulting breach hydrographs are categorized as: Scenario-1 (S1), Scenario-2 (S2), and Scenario-3 (S3) according to the hydrograph features. For all the three dams, S1 refers to the breach hydrograph with the highest peak flow in the shortest time, S3 has the smallest peak flow with the longest time to the peak. The peak flow and time to peak for the S2 hydrograph are averaged between S1 and S3 hydrographs. Further details are presented below for each dam.

5.1.1 Ondokuz Mayıs Dam

Ondokuz Mayıs Dam is a clay-core rock-filled dam. In this study, the dam is breached with both overtopping and piping failure modes. Three scenarios with the different sets of breach parameters were used as can be seen in Table 5-2. The breach hydrograph S1 refers to the worst-case scenario with failure mode as overtopping. For this scenario it was assumed that when the breach starts the reservoir is at its maximum water level with no outflow, and there is an inflow of Q-catastrophic at the upstream end of the reservoir. For S1, the final breach size is selected as largest and breach formation time is the smallest, among the three scenarios. For the S2 breach hydrograph, all the conditions are the same as for S1, except that the final breach size is smaller than S1 and the breach formation time is greater than S1. For the S3 breach hydrograph, the failure mode was selected as piping, the reservoir is at its normal reservoir level with no outflow and inflow. S3 breach hydrograph has the smallest final breach size and longest breach formation time among the three scenarios.

Table 5-2 Breach parameters for Ondokuz Mayıs Dam

Breach hydrograph	**S1**	**S2**	**S3**
Mode of failure	Overtop	Overtop	Piping
Bottom width (m)	110	92	60
Breach formation timing (hr)	0.5	1	2
Peak Flow (m^3/sec)	62592	50993	22179
Time to Peak Flow (hr)	0.33	0.67	1.50

The three breach hydrographs S1, S2, and S3 are presented in Figure 5-1.

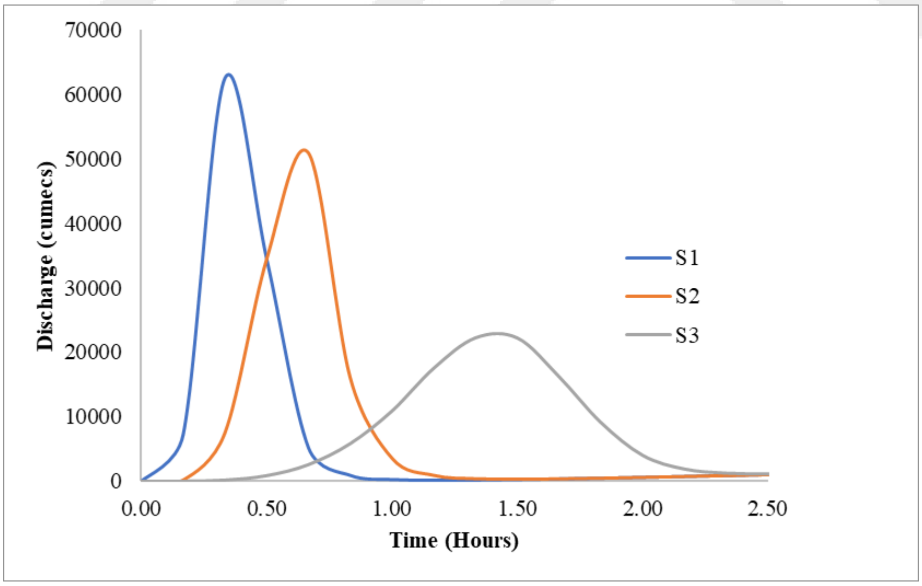

Figure 5-1 Breach hydrograph for Ondokuz Mayıs Dam

These hydrographs are then used as inflow hydrographs for flood routing over the downstream floodplain.

5.1.2 İhsaniye Dam

İhsaniye Dam is a roller-compacted concrete dam. Concrete dams usually fail all of a sudden with failure time ranging from 0.1 to 0.5 hours, depending upon the type of concrete dam (FERC, 1988 ; ICOLD, 1998a). In this study, İhsaniye Dam is breached with the assumption of an overtopping mode of failure. The breach parameters used to obtain the breach hydrograph for İhsaniye Dam are given in Table 5-3. S1 breach hydrograph refers to the worst-case scenario, with the assumption that the dam reservoir is at maximum water level with no outflow from it, and there is an inflow of Q-catastrophic at the upstream end of the reservoir. The final breach size is the largest and breach formation time is the smallest among the three scenarios. S2, breach hydrograph is obtained with the same assumption as of S1, but with final breach size and breach formation time in between S1 and S3. S3 breach hydrograph is based on the same assumptions as S1 has but has the smallest breach size and longest breach formation time among the three scenarios.

Table 5-3 Breach parameters for İhsaniye Dam

Breach hydrograph	**S1**	**S2**	**S3**
Mode of failure	Overtop	Overtop	Overtop
Bottom width (m)	60	50	35
Breach formation timing (hr)	0.25	0.37	0.5
Peak Flow (m^3/sec)	13535	10584	8485
Time to Peak Flow (hr)	0.17	0.25	0.33

The three breach hydrographs S1, S2 and S3 are shown in Figure 5-2.

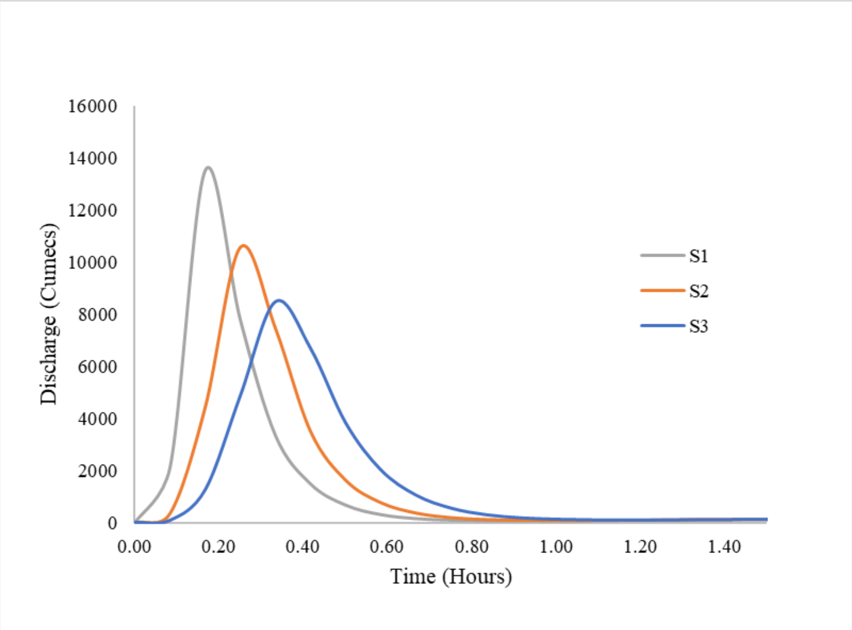

Figure 5-2 Breach hydrograph for İhsaniye Dam

These hydrographs are then used in both HEC-RAS and FLO-2D models as inflow hydrographs for flood routing over the downstream floodplain.

5.1.3 Avcıdere Dam

Avcıdere Dam is a concrete-faced rockfill dam. The failure modes used to obtain the breach hydrographs included both Overtopping and Piping modes. For all three scenarios, it is assumed that dam reservoir is at maximum water level and there is no outflow from the reservoir. In addition to these assumptions for S1, it is assumed there is an inflow of Q-catastrophic at the upstream end of the reservoir and the final breach size is the largest and breach formation time is the smallest among the three scenarios. S2 also uses the same assumptions as for S1 with breach dimension and breach formation time in between S1 and S3. S3 uses the piping failure mode, with the assumption that the reservoir is at maximum water level, with no outflow and inflow, and the final breach size is smallest and breach formation time is the largest among the three scenarios. The breach parameters used to obtain the breach hydrograph for Avcıdere Dam are given in Table 5-4.

Table 5-4 Breach parameters for Avcıdere Dam

Breach hydrograph	**S1**	**S2**	**S3**
Mode of failure	Overtop	Overtop	Piping
Bottom width (m)	30	25	20
Breach formation timing (hr)	0.5	1	2
Peak Flow (m^3/sec)	19758	10587	6324
Time to Peak Flow (hr)	0.33	0.58	1.08

The calculated breach hydrographs are presented in Figure 5-3.

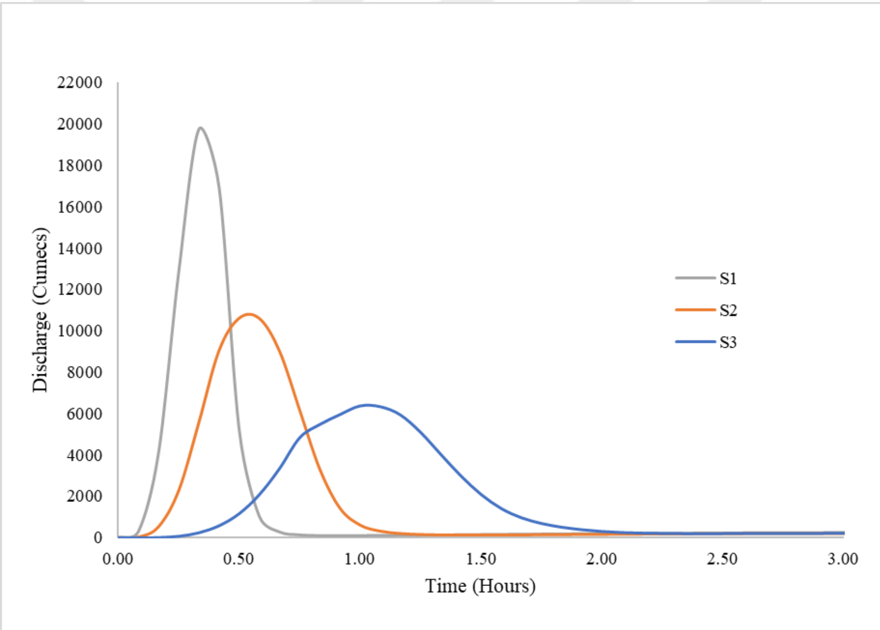

Figure 5-3 Breach hydrograph for Avcıdere Dam

These hydrographs are then used as inflow hydrographs for flood routing over the downstream floodplain.

5.2 Breach Hydrograph Routing: Ondokuz Mayıs Dam

In this part of the analysis, the results of the model calibration for Engiz Creek, breach hydrograph routing, sensitivity of grid resolution, the sensitivity of roughness values and breach hydrograph are also presented.

5.2.1 Model Calibration for Engiz Creek

Model calibration is a useful practice to achieve the simulation results which are the best match with the observed data. For the Ondokuz Mayıs Dam, model calibration is done for Engiz Creek using the flow measurement record of an active gauging station located downstream of the Ondokuz Mayıs Dam.

From the flow data measurement record of Engiz Creek (available online at https://www.dsi.gov.tr/Sayfa/Detay/744), it was seen that there is an active gauging station D15A026, located just upstream of Ondokuz Mayıs District (at about 1.3 km from the district). The flow data record shows the average daily discharge values and gauging station rating curves for each year.

For the model calibration, the peak flood of 211 m^3/sec observed in the year 2010 was selected, as the topographic data is based on the measurements made in the year 2011. The flow measurement record book shows a rating curve with a maximum discharge of 77 m^3/sec for the year 2010. To obtain the flow depth at 211 m^3/sec, the rating curves provided in the flow measurement record from the year 2005 to 2015 were plotted on a single graph (Figure 5-4) to determine if any rating curve matches with that of the year 2010.

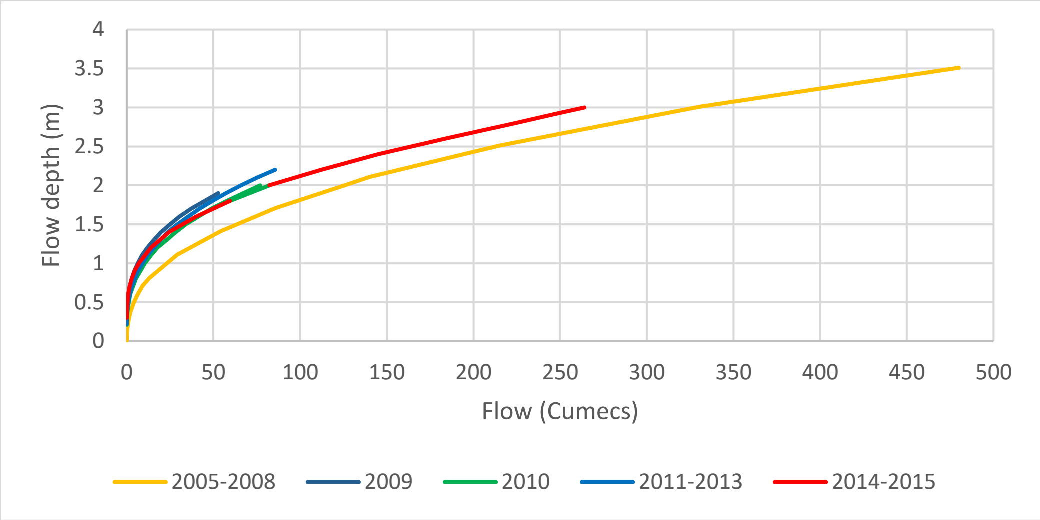

Figure 5-4 Rating curve at gauging station for years 2005 to 2015

It was observed that the rating curves of the years 2010 and 2015 are almost identical (Figure 5-5), so the rating curve of 2015 is used to determine the flow depth. The rating curve for year 2015 gives a flow depth of 2.735 m against the flow of 211 m^3/sec. This flow depth value is then used as a reference value for model calibration.

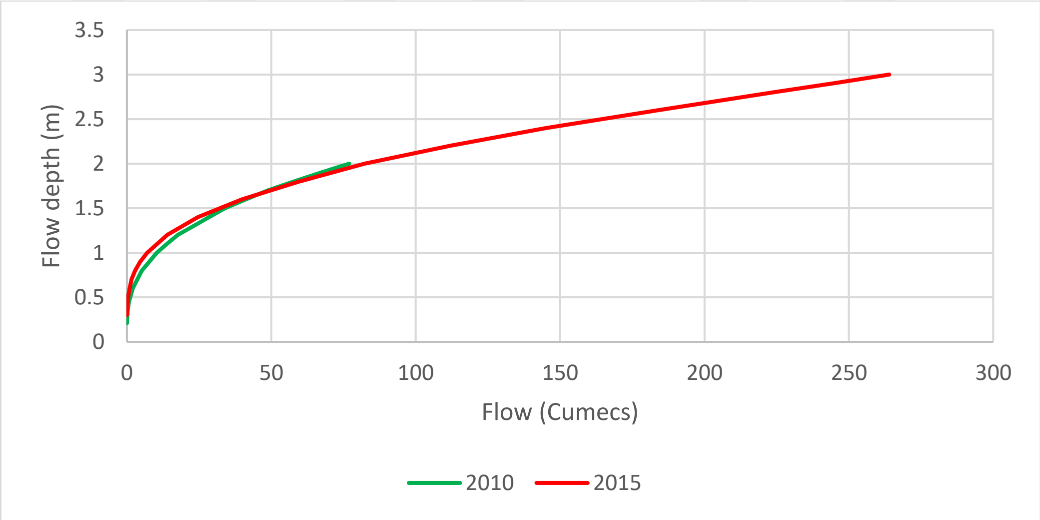

Figure 5-5 Rating curve at gauging station (D150A26) for years 2010 and 2015

The inflow hydrograph for the model calibration was obtained by breaching the dam with such parameters that the breach flow passing through the gauging station should be closer to 211 m^3/sec. It was observed that for the breach hydrograph (Figure 5-6) with a peak flow of 220 m^3/sec at the dam site, a flow of 218 m^3/sec is observed at the gauging station, which is closer to the required flow rate. This breach hydrograph is then used in the model calibration.

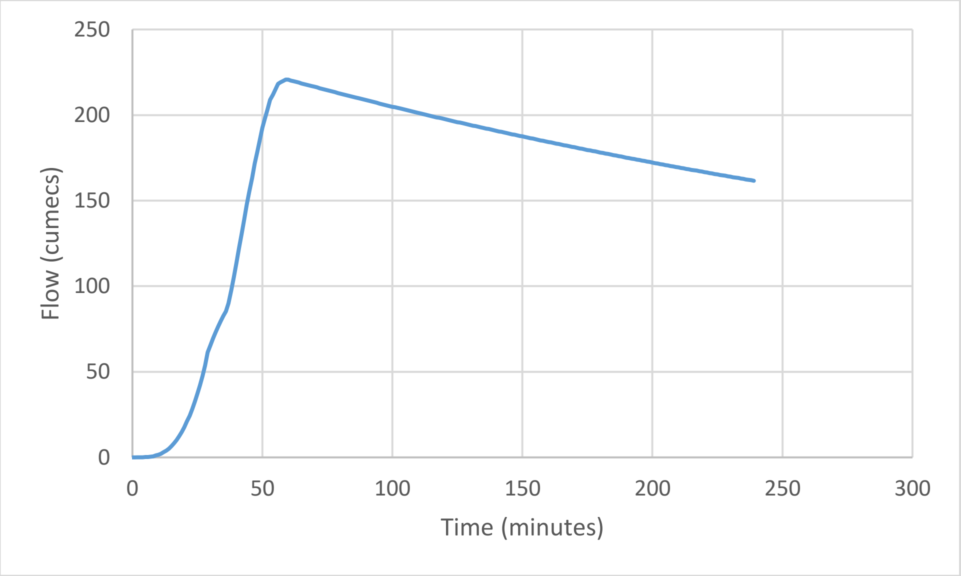

Figure 5-6 Ondokuz Mayıs Dam breach hydrograph for model calibration

After obtaining the inflow breach hydrograph, the flood modeling simulation was performed by altering the roughness values to calibrate the model against the reference flow depth at the gauging station. The length of Engiz Creek between the dam and the gauging station was divided into two reaches; Reach 1 consists of the channel section located in the hilly terrain just downstream of the dam and Reach 2 covers the remaining length of the channel (Figure 4-15).

It was observed that that for roughness value (Chow, 1959) of 0.040 (Reach 1) and 0.021 (Reach 2), a flow depth of 2.744 m is obtained at the gauging station, which is closer to the observed flow depth of 2.735 m. Table 5-5 gives the flow depth at the gauging station for different roughness values.

Table 5-5 Roughness values and flow depth at the gauging station

Roughness value	**Reach 1**	0.040			
	Reach 2	0.025	0.023	0.021	0.020
Flow depth (m)		2.773	2.758	2.744	2.728

Figure 5-7 Maximum flow depth for Peak Discharge of 220.72 m3/sec shows the maximum flow depth map against a peak discharge of 220.72 m^3/sec.

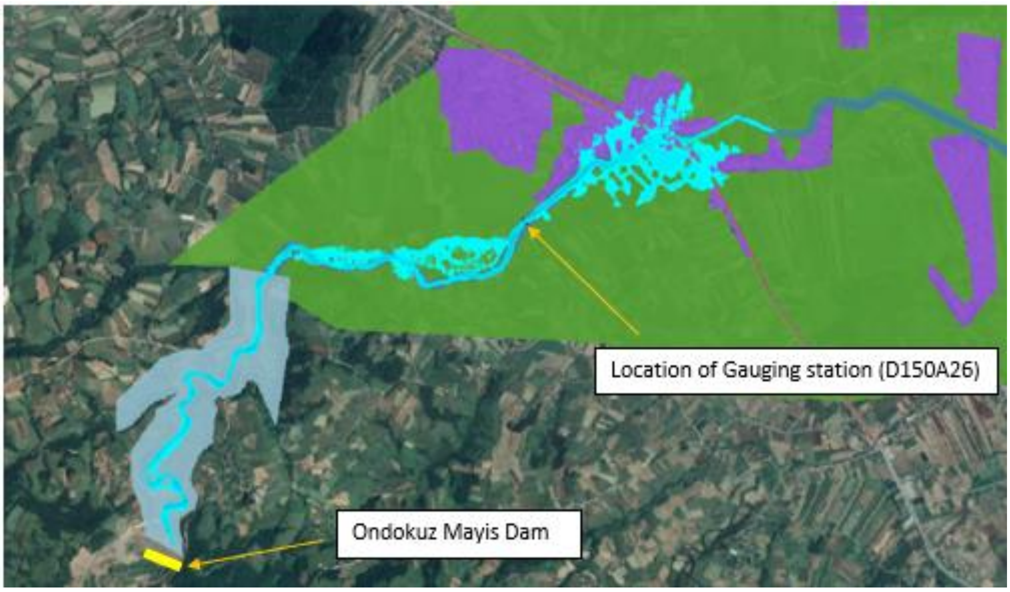

Figure 5-7 Maximum flow depth for Peak Discharge of 220.72 m3/sec

The model calibration was performed in HEC-RAS at 5m grid resolution. The calibrated roughness values are then used in breach hydrograph routing.

5.2.2 Breach Hydrograph Routing

The routing of the breach hydrograph was carried out with HEC-RAS and FLO-2D models. The breach hydrograph was used as an inflow hydrograph with the modified DEM and the calibrated roughness values in the breach hydrograph routing.

The simulation results obtained at 5 m grid resolution are presented in the form of inundation maps of maximum flow depth, maximum velocity and arrival time of maximum depth. Firstly, a comparison of results is made between HEC-RAS and

FLO-2D at selected location in the floodplain. Figure 5-8 shows the location of section in the vicinity of Ondokuz Mayıs District. Then the results of sensitivity of grid resolution, Manning's roughness parameter, and breach hydrograph are presented at the selected locations.

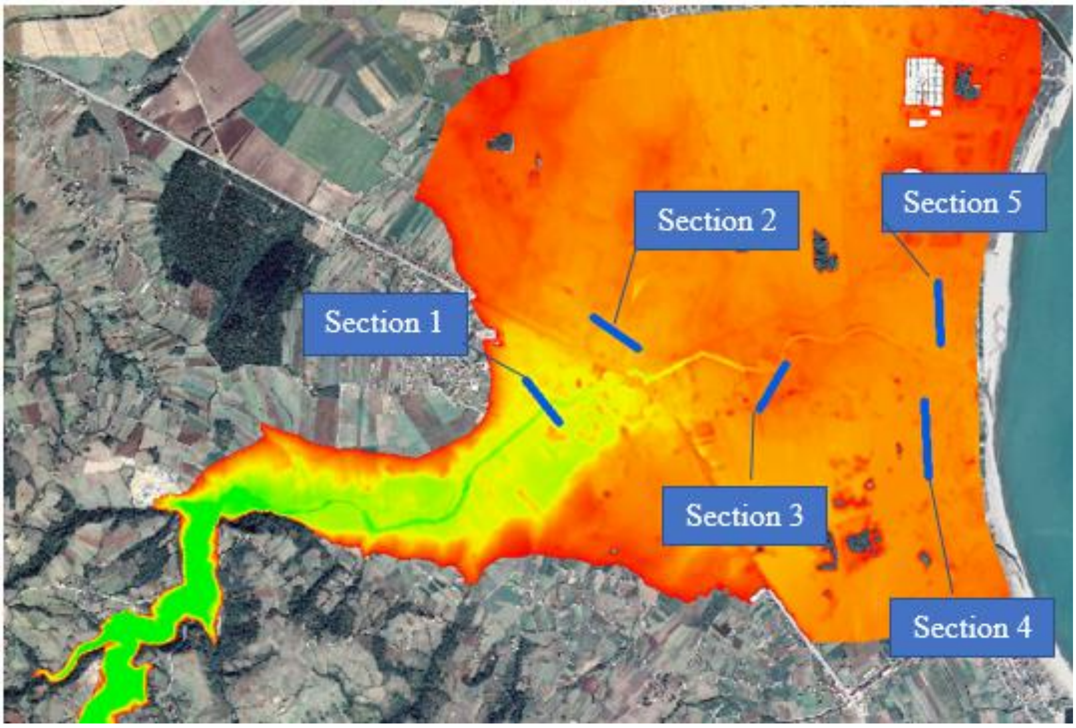

Figure 5-8 Location map of sections in Ondokuz Mayıs District

Figure 5-9 to Figure 5-11 shows the inundation maps of maximum flow depth, maximum velocity and arrival time of max depth for both HEC-RAS and FLO-2D at 5 m grid resolution.

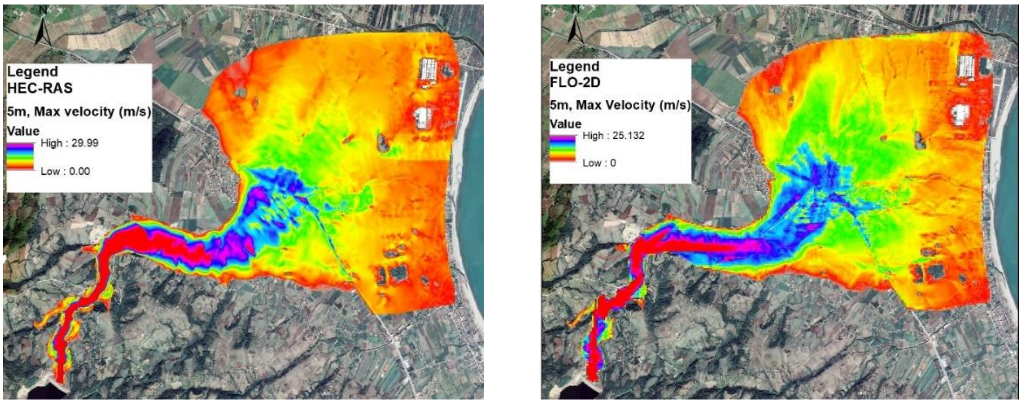

(a) (b)

Figure 5-9 Max flow depth for S1 at 5 m (Ondokuz Mayıs Dam) (a) HEC-RAS (b) FLO-2D

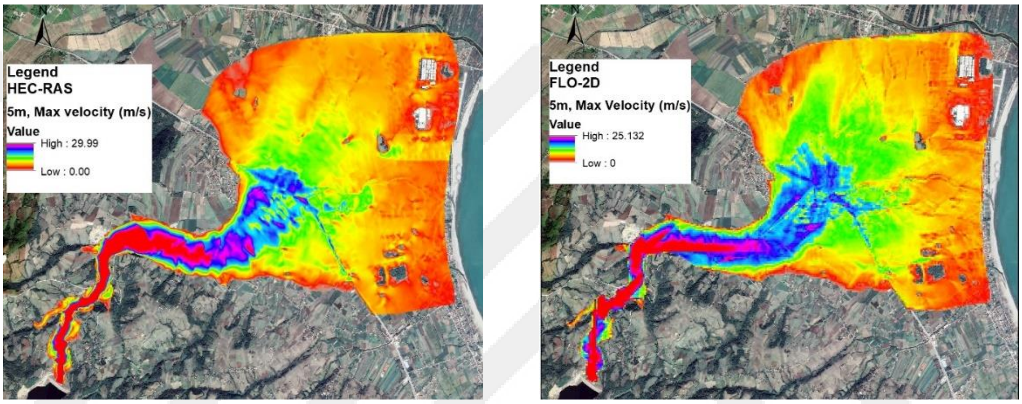

(a) (b)

Figure 5-10 Max flow velocity for S1 5 m (Ondokuz Mayıs Dam) (a) HEC-RAS (b) FLO-2D

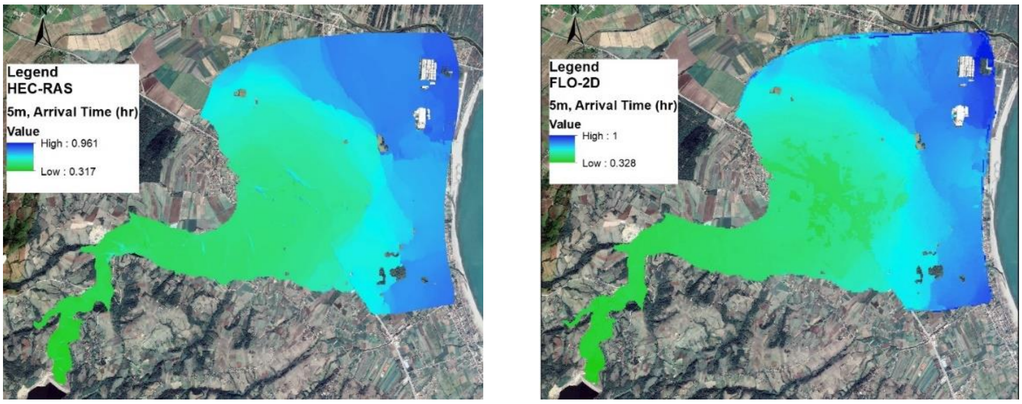

(a) (b)

Figure 5-11 Arrival time for Max depth for S1 at 5 m (Ondokuz Mayıs Dam) (a) HEC-RAS (b) FLO-2D

Figure 5-12 to Figure 5-16 shows the comparison of maximum flow depths for HEC-RAS and FLO-2D at Sections 1 to 5 in Ondokuz Mayıs District.

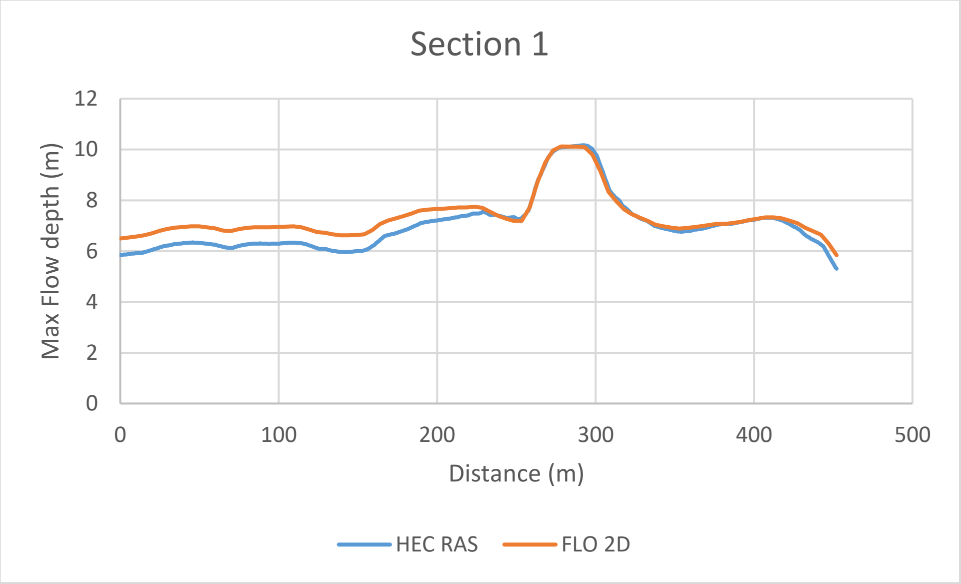

Figure 5-12 Comparison of Max Flow depth at Section-1 for HEC-RAS and FLO-2D (S1, 5 m)

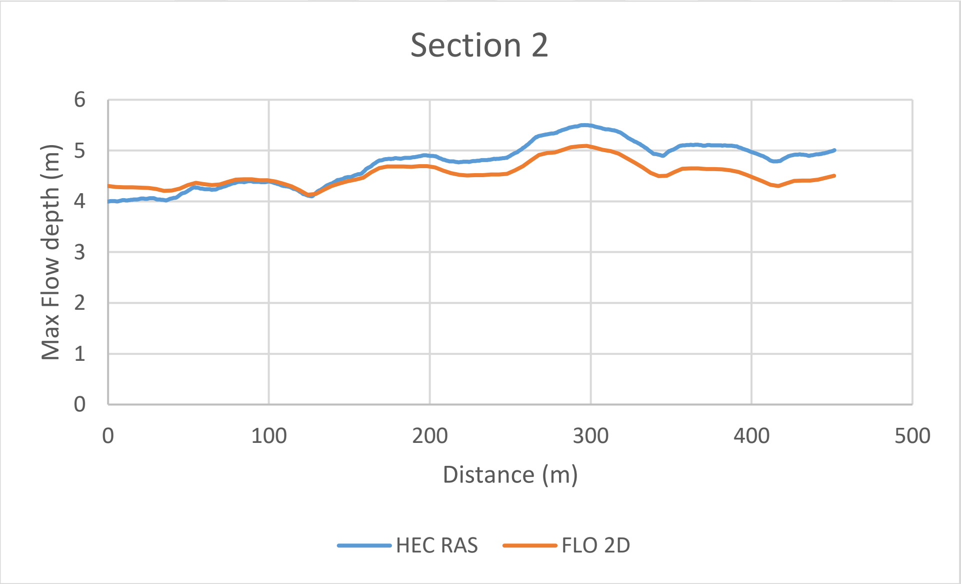

Figure 5-13 Comparison of Max Flow depth at Section-2 for HEC-RAS and FLO-2D (S1, 5 m)

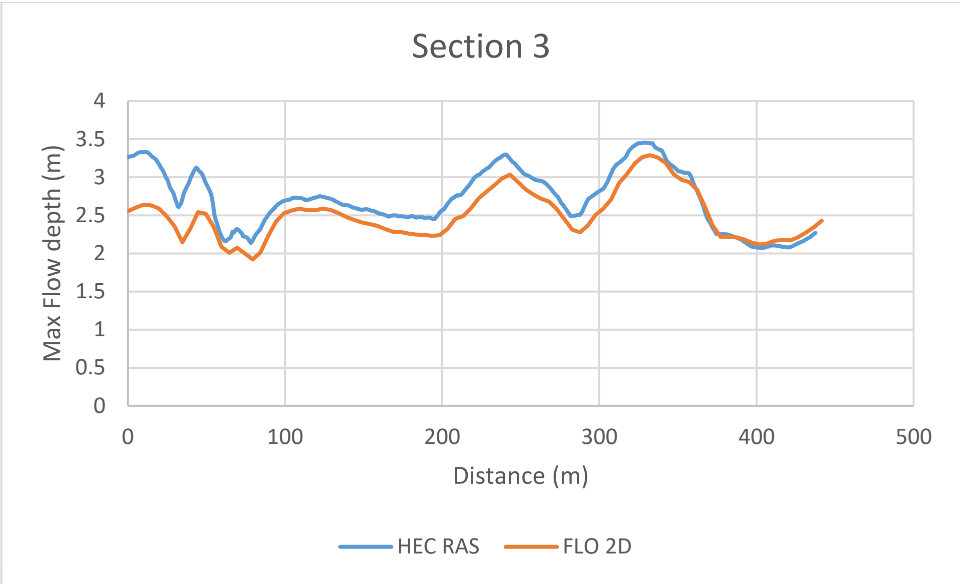

Figure 5-14 Comparison of Max Flow depth at Section-3 for HEC-RAS and FLO-2D (S1, 5 m)

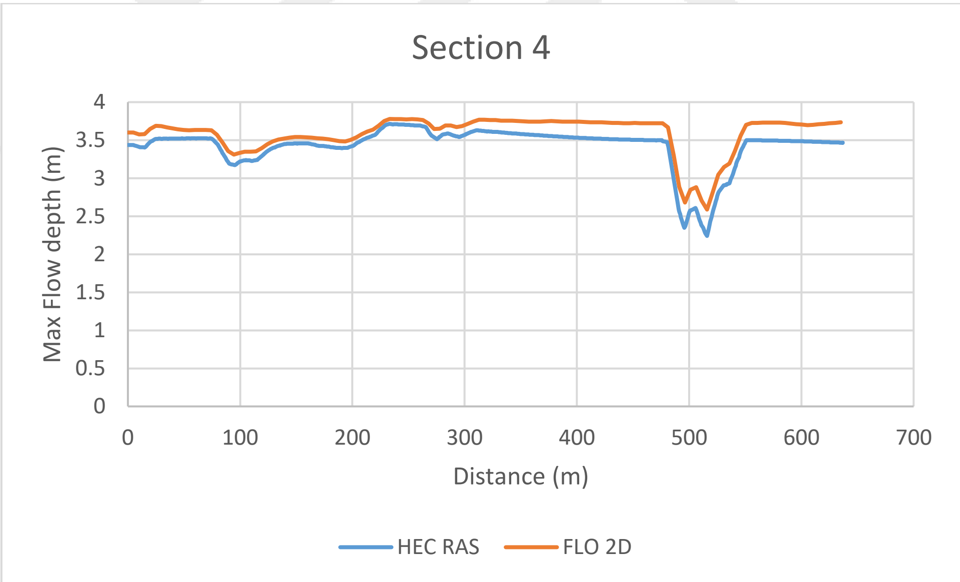

Figure 5-15 Comparison of Max Flow depth at Section-4 for HEC-RAS and FLO-2D (S1, 5 m)

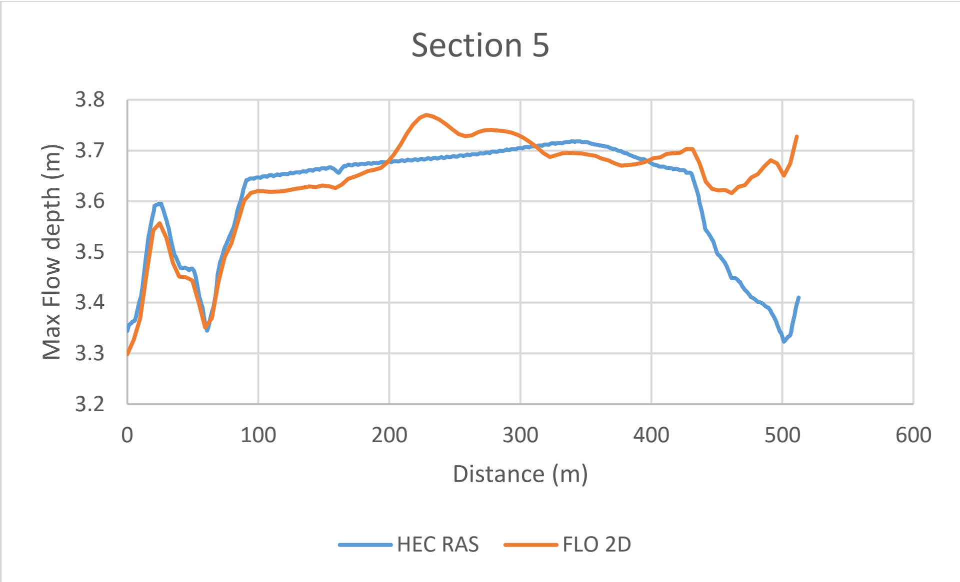

Figure 5-16 Comparison of Max Flow depth at Section-5 for HEC-RAS and FLO-2D (S1, 5 m)

From the graphs, it can be seen that at most of the sections, HEC-RAS and FLO-2D flow depth profiles are approaching each other. At Sections 2 and 3, HEC-RAS gives higher depth than FLO-2D, while at Sections 1, 4, and 5, FLO-2D gives higher depths. The differences can be due to the different governing equations and computational methods used in each model, and also the way the terrain information is incorporated into each model computations. HEC-RAS uses sub-grid bathymetric, in which for each computational grid hydraulic properties are calculated, while FLO-2D is a raster-based model in which each grid has a single value for elevation and roughness. The way that topography is interpreted by each model can have influence in determining the flow direction, thus effecting the flow depth at the sections.

Table 5-6 gives a comparison of the maximum velocity and arrival time of maximum depth at the sections for HEC-RAS and FLO-2D.

Table 5-6 Max velocity and Arrival time for Max depth at the sections for HEC-RAS and FLO-2D (S1, 5 m)

Sections	HEC-RAS		FLO-2D	
	Max Velocity (m/sec)	Arrival Time of Max depth (hr)	Max Velocity (m/sec)	Arrival Time of Max depth (hr)
Section 1	10.778	0.503	12.000	0.483
Section 2	3.885	0.548	4.008	0.526
Section 3	6.363	0.573	6.900	0.558
Section 4	3.078	0.790	3.418	0.795
Section 5	2.524	0.815	3.034	0.824

The flood extents obtained from HEC-RAS and FLO-2D at 5 m simulations give an F-statistic value of 0.98995, which means both models show almost 99% overlapping flood extents.

5.2.3 Sensitivity of Grid Resolution

In the part of the analysis, the effect of grid resolution on the flood inundation results is studied using 10 m, 25 m, and 50 m grid sizes. The simulations are run with breach hydrograph S1 and calibrated Manning's roughness shapefile. The understand the effect of change in grid resolution, RMSE values of flow depth are calculated in comparison to base 5 m simulation results.

The results of the sensitivity of grid resolution for both HEC-RAS and FLO-2D are presented distinctly below. The results are presented as graphs of the change in flow depth with respect to grid resolution.

HEC-RAS:

The flood extents obtained from HEC-RAS simulations at coarser grid resolution are compared with the extent obtained at 5 m grid resolution by calculating the F-statistic values as presented in Table 5-7.The values show that there is a minimal change in flood extent with an increase in grid resolution. Table 5-7 also shows the model runtime for routing a breach hydrograph of 3 hours duration over the downstream floodplain of İhsaniye Dam.

Table 5-7 F-statistic value and model runtimes for (HEC-RAS, S1)

Grid Resolution	F-Statistic (base 5 m)	Model Runtime (min)
5 m	--	1918
10 m	0.99312	244
25 m	0.98463	14
50 m	0.97382	3

Table 5-8 gives the RMSE values calculated for each section in comparison to 5 m simulation results. It can be seen that the lowest RMSE values for flow depth are for 10 m resolution, and as the grid resolution is increasing in RMSE is also increasing slightly.

Table 5-8 Flow depth RMSE values calculated with base 5 m flow depth for each section (HEC-RAS, S1)

Sections	Flow depth RMSE		
	10 m	25 m	50 m
Section 1	0.0912	0.3721	0.6764
Section 2	0.0722	0.0818	0.1459
Section 3	0.0474	0.1057	0.1044
Section 4	0.3511	0.3481	0.3275
Section 5	0.0090	0.0112	0.0095

Figure 5-17 to Figure 5-21 shows results obtained from HEC-RAS simulations in terms of the change in flow depth with grid resolution for sections 1 to 5.

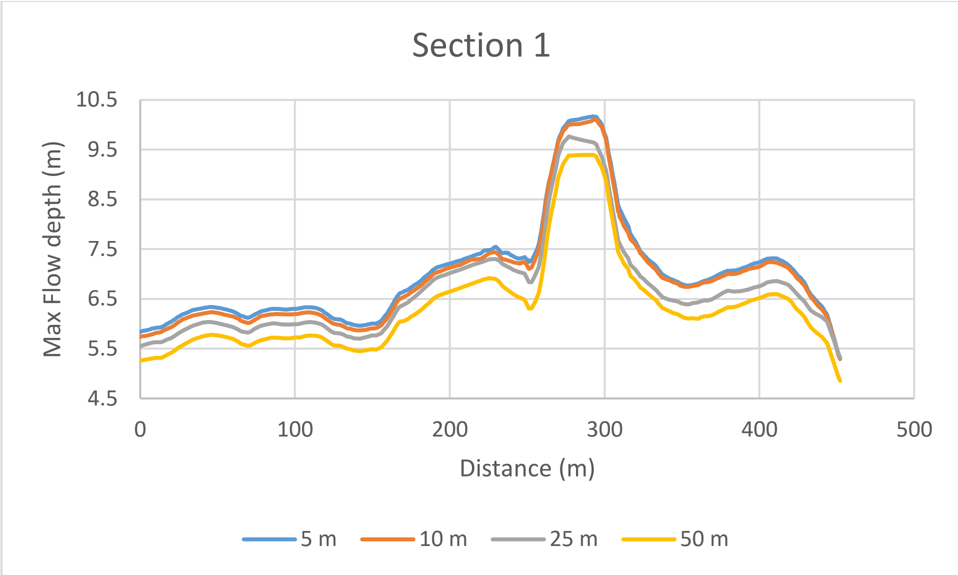

Figure 5-17 Change in flow depth at Section-1 with grid resolution (HEC-RAS, S1)

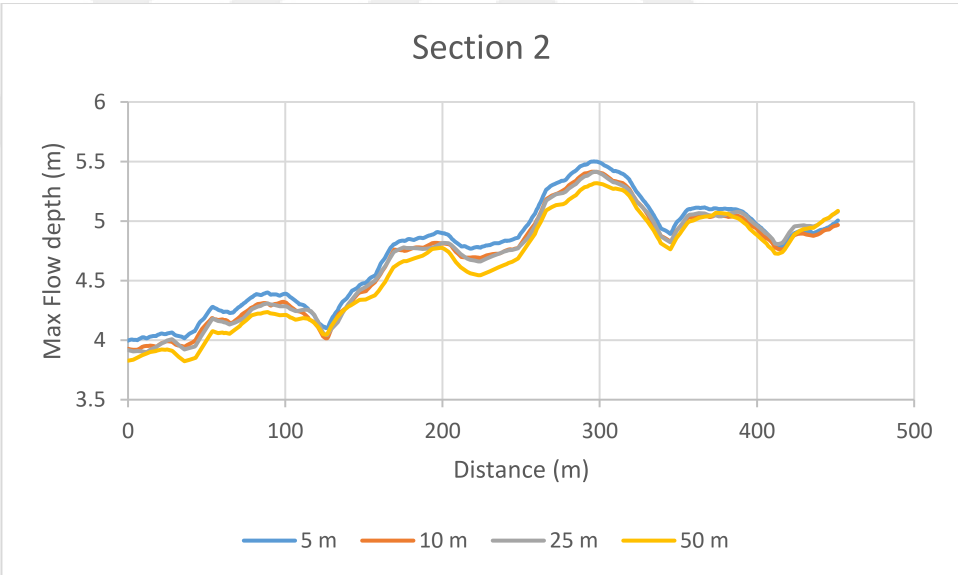

Figure 5-18 Change in flow depth at Section-2 with grid resolution (HEC-RAS, S1)

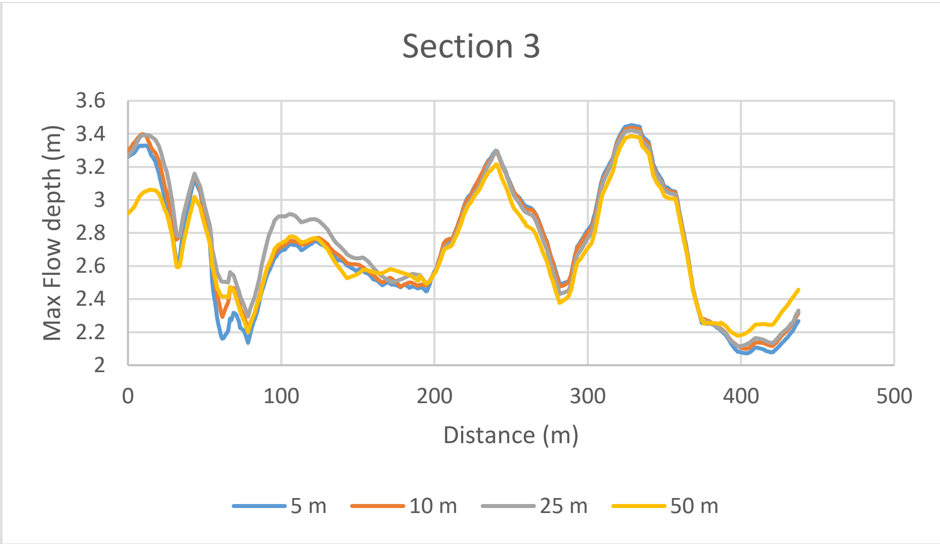

Figure 5-19 Change in flow depth at Section-3 with grid resolution (HEC-RAS, S1)

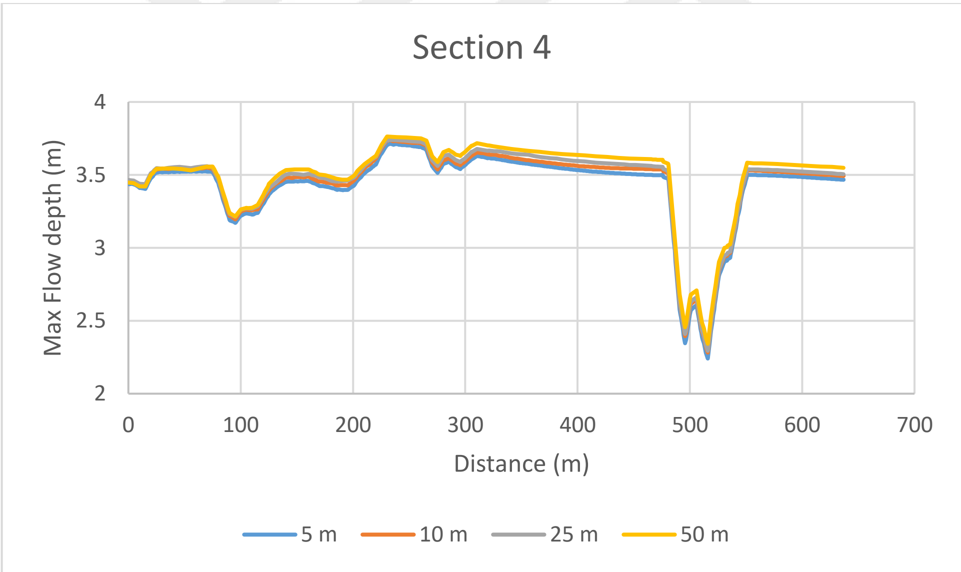

Figure 5-20 Change in flow depth at Section-4 with grid resolution (HEC-RAS, S1)

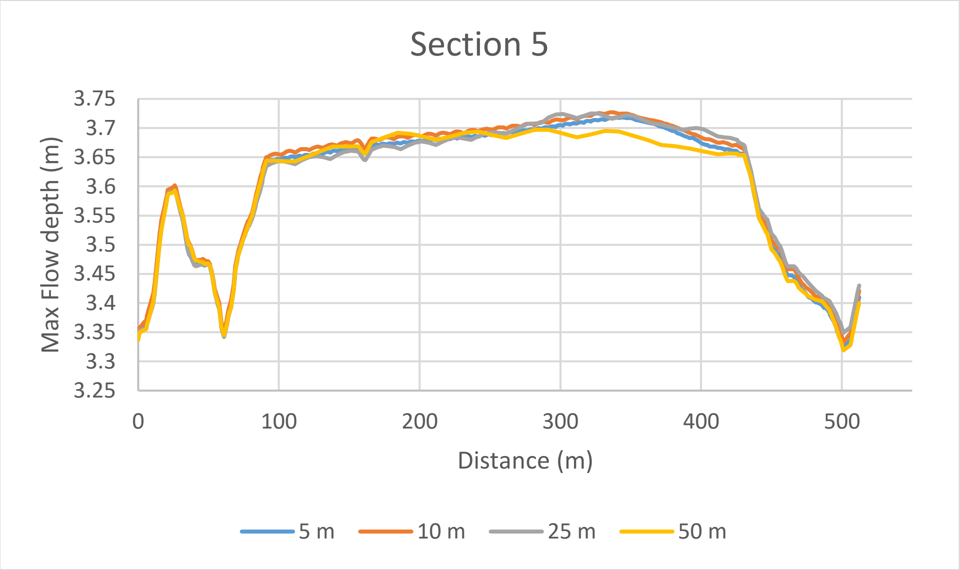

Figure 5-21 Change in flow depth at Section-5 with grid resolution (HEC-RAS, S1)

The graphs show that the calculated flow depth profile obtained at coarser resolution displays consistency with the flow depth profile of 5 m grid resolution at all sections. The flow depth obtained at 5 m and 10 m grid resolutions are almost approaching each other. It can be seen that for 25 m and 50 m resolution, there is a decrease in flow depth at all sections, except Section 4 where a slight increase is observed. The inundation maps for coarse grid resolution simulations are given in Appendix.

FLO-2D:

Table 5-9 shows the F-statistic value for flood extent by taking the flood extent of 5 m simulation as base. The FLO-2D simulation results show that as the grid size is getting coarser, the overlap area is decreasing. The FLO-2D runtime for the routing of 3-hour breach hydrograph is also given in Table 5-9.

Table 5-9 F-statistic value and Model runtimes for FLO-2D (S1)

Grid Resolution	F-Statistic (base 5 m grid)	Model Runtime (min)
5 m	--	580
10 m	0.98251	65
25 m	0.97326	6
50 m	0.94643	1

Table 5-10 shows the calculated RMSE values for each section in comparison to 5 m simulation results. The lowest RMSE values for flow depth are seen for 10 m resolution, and as the grid resolution is increasing in RMSE is also increasing slightly.

Table 5-10 Flow depth RMSE values calculated with base 5 m flow depth for each section (FLO-2D, S1)

Sections	Flow depth RMSE		
	10 m	25 m	50 m
Section 1	0.1957	0.2693	0.3877
Section 2	0.0660	0.1066	0.1615
Section 3	0.1184	0.1510	0.3027
Section 4	0.3011	0.3123	0.3243
Section 5	0.2483	0.2933	0.2951

Figure 5-22 to Figure 5-26 shows results the change in flow depth with grid resolution for Sections 1 to 5, obtained from FLO-2D simulations.

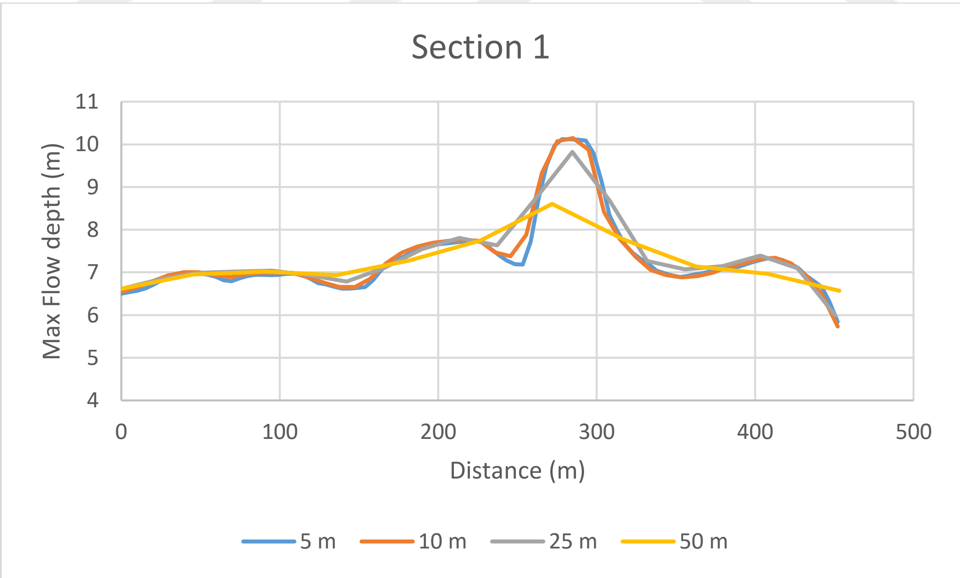

Figure 5-22 Change in flow depth at Section-1 with grid resolution (FLO-2D, S1)

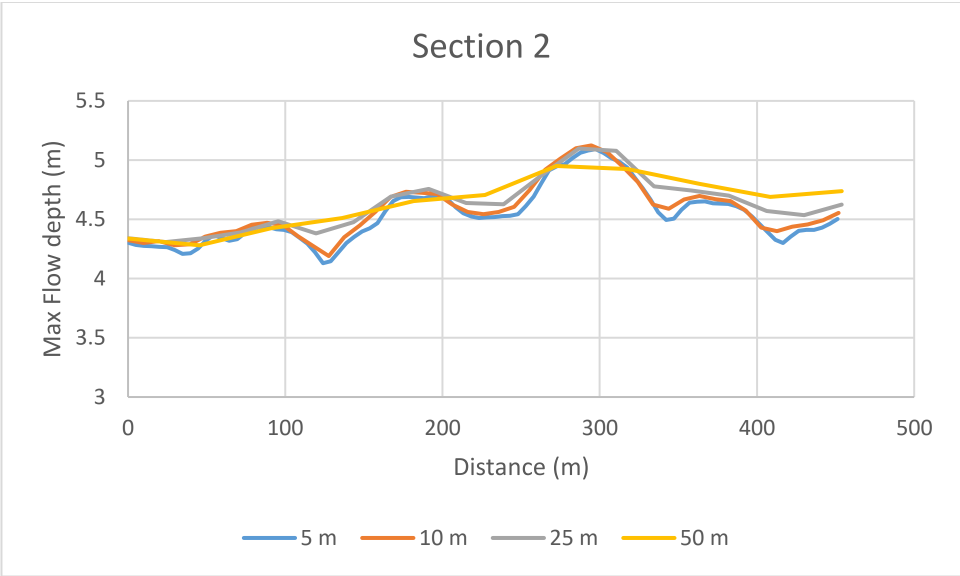

Figure 5-23 Change in flow depth at Section-2 with grid resolution (FLO-2D, S1)

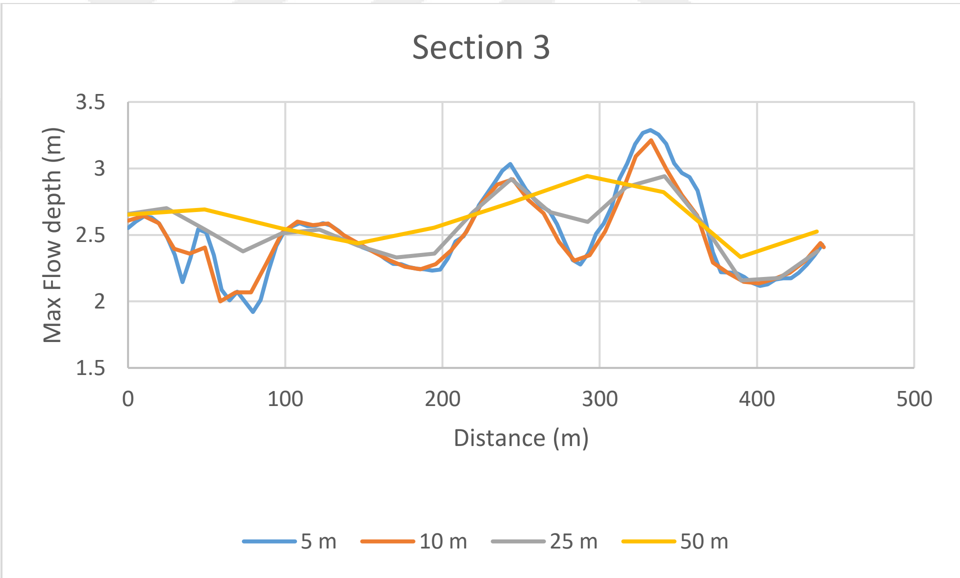

Figure 5-24 Change in flow depth at Section-3 with grid resolution (FLO-2D, S1)

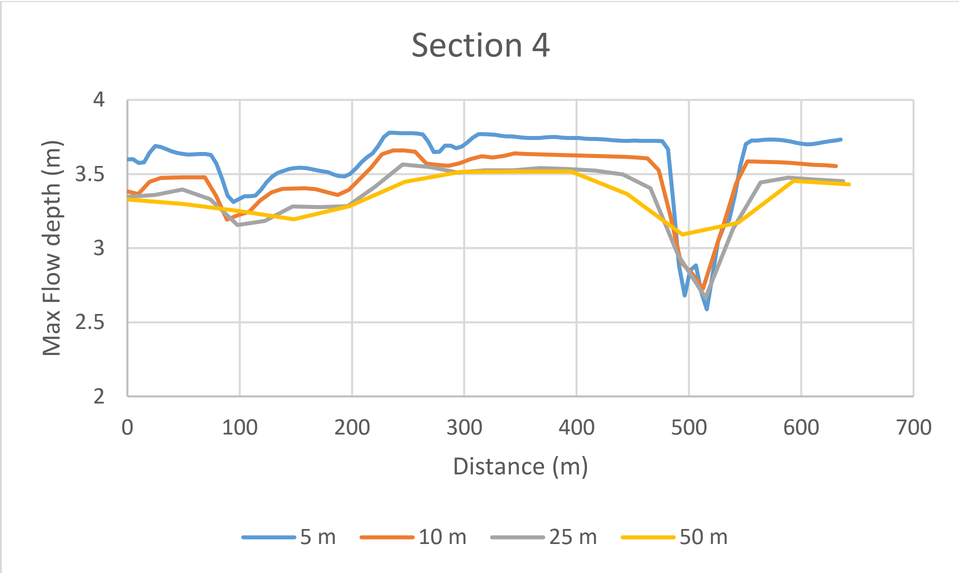

Figure 5-25 Change in flow depth at Section-4 with grid resolution (FLO-2D, S1)

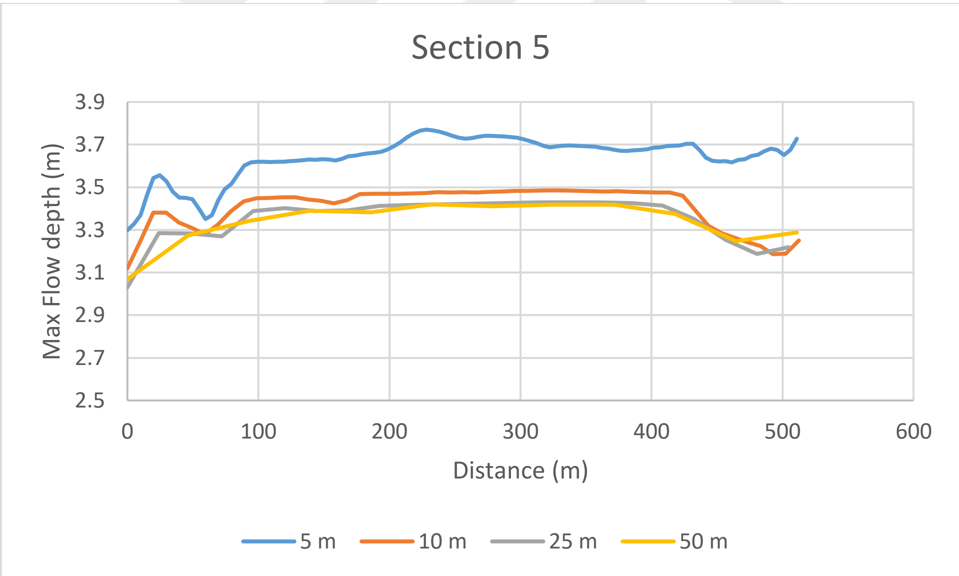

Figure 5-26 Change in flow depth at Section-5 with grid resolution (FLO-2D, S1)

In the graphs, it can be seen that as the grid size is changing, the flow depth is also changing. There is a consistency of results between finer resolutions. For coarser resolution, the calculated flow depth is not consistent and there are significant differences in flow depth at each section. It can be due to the fact that FLO-2D is a raster-based model, in which there is a single elevation value for each grid and topographic features which are smaller than the grid size is ignored in the computations.

5.2.4 Sensitivity of Roughness Values

The sensitivity of the roughness values to the flood inundation simulation is examined by varying the base values. The base roughness values upon which the model was calibrated are increased and decreased by 20%, to study the impact on the flow depth. Both model simulations were run at 5 m grid resolution using the breach hydrograph S1.

HEC-RAS:

The sensitivity of roughness values to the flood extent is calculated by means of F-statistic value in comparison to the flood extent obtained at 5 m resolution, as shown in Table 5-11. It shows that flood extent is less sensitive to the roughness values, meaning there is no major change in flood extent with a change in roughness values.

Table 5-11 F-statistic value at different roughness values for HEC-RAS (S1)

Roughness value	F-Statistic (Base n)
0.8* n	0.99012
1.2*n	0.99324

Figure 5-27 presents the change in flow depth with the roughness parameter for HEC-RAS simulations at 5 m grid size.

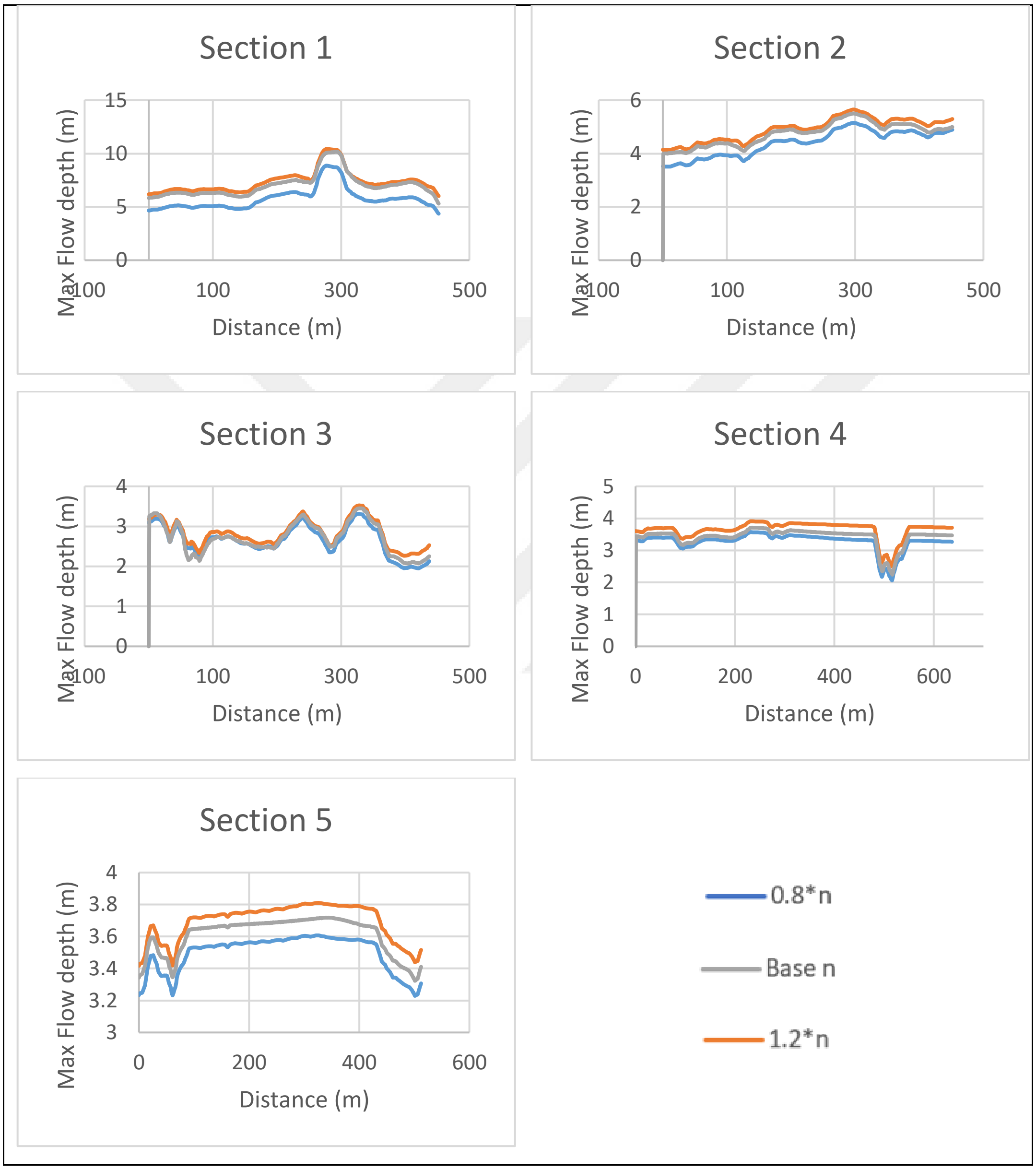

Figure 5-27 Change in Max flow depth with roughness values at sections (HEC-RAS, S1)

In these graphs, it can be seen that the model is quite sensitive to the Manning roughness values. With increase in the roughness values (1.2*n) the flow depth is increasing, while decreasing the roughness values (0.8*n) results in decrease in flow depth.

FLO-2D:

The F statistic values for flood extent at different roughness values is calculated in comparison to flood extent at base roughness values as shown in Table 5-12. It shows that in FO 2D, flood extent is less sensitive to the roughness values.

Table 5-12 F-statistic value for flood extent at different roughness parameter for FLO-2D (S1)

Roughness value	**F-Statistic (Base n)**
0.8* n	0.98521
1.2*n	0.98387

Figure 5-28 presents the change in flow depth with the roughness parameter for FLO-2D simulations at 5 m grid size.

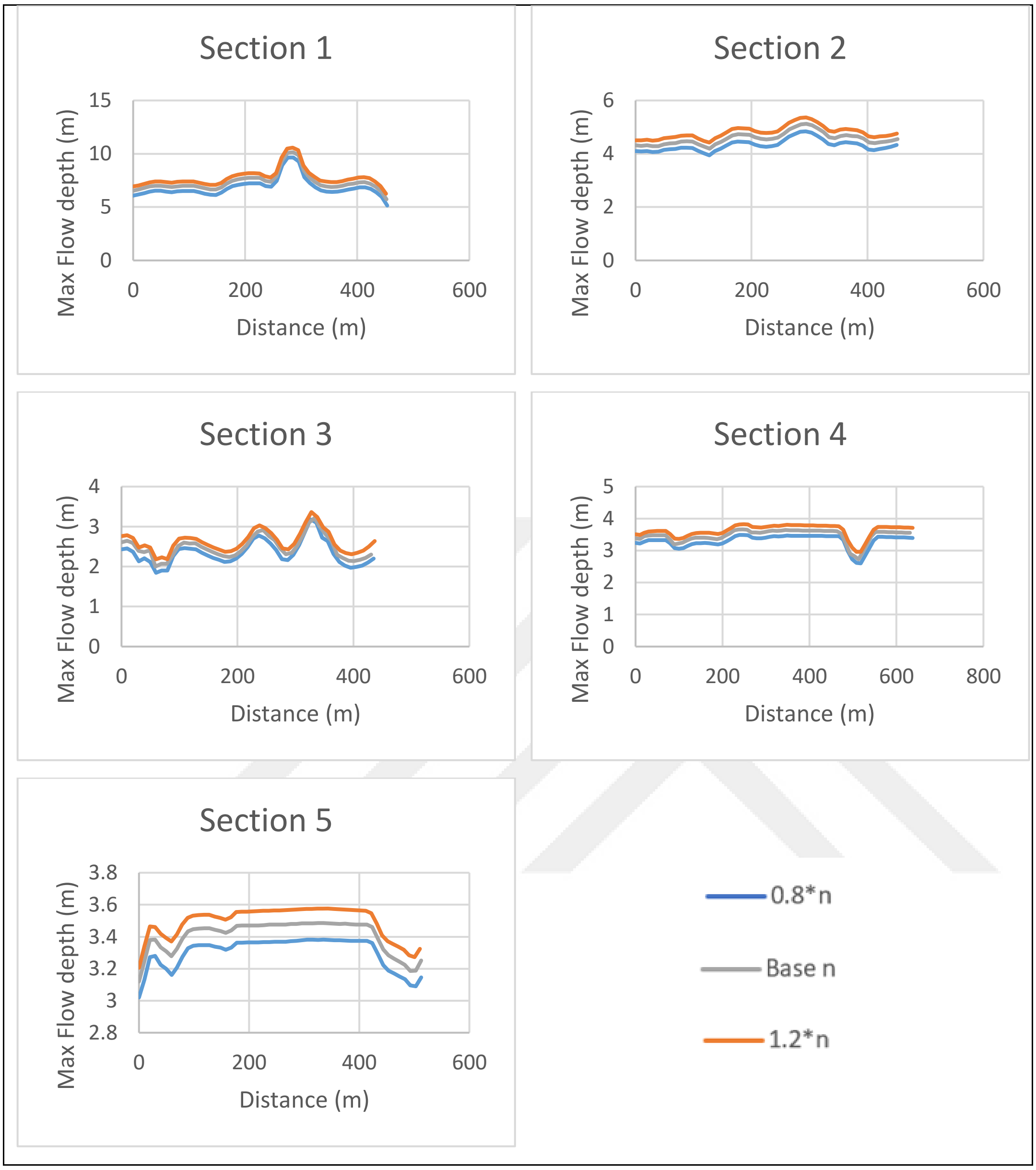

Figure 5-28 Change in Max flow depth with roughness values at sections (FLO-2D, S1)

These graphs shows that FLO-2D model is also very sensitive to the roughness values. An increase in the roughness values (1.2*n) results in higher flow depth in comparison to base flow depth, while decreasing the roughness values (0.8*n) results in lower flow depth.

5.2.5 Sensitivity of Breach Hydrograph

In this part of analysis, flood routing simulations are carried out at 5 m grid resolution using the breach hydrographs S2 and S3 along with the calibrated Manning roughness values with both models. The results are presented in terms of comparison of flow depth with S1 breach hydrograph.

HEC-RAS:

Table 5-13 shows the inundation area calculated by HEC-RAS at 5 m grid resolution for S1, S2, and S3 breach hydrographs.

Table 5-13 Ondokuz Mayıs Dam inundation area (HEC-RAS) for breach hydrographs (S1, S2, and S3)

Breach Hydrograph	Inundation Area (m^2)
S1	23308687
S2	23095773
S3	21548357

Figure 5-29 shows the comparison of flow depth for different breach hydrographs at the selected section for HEC-RAS simulations at 5 m grid size.

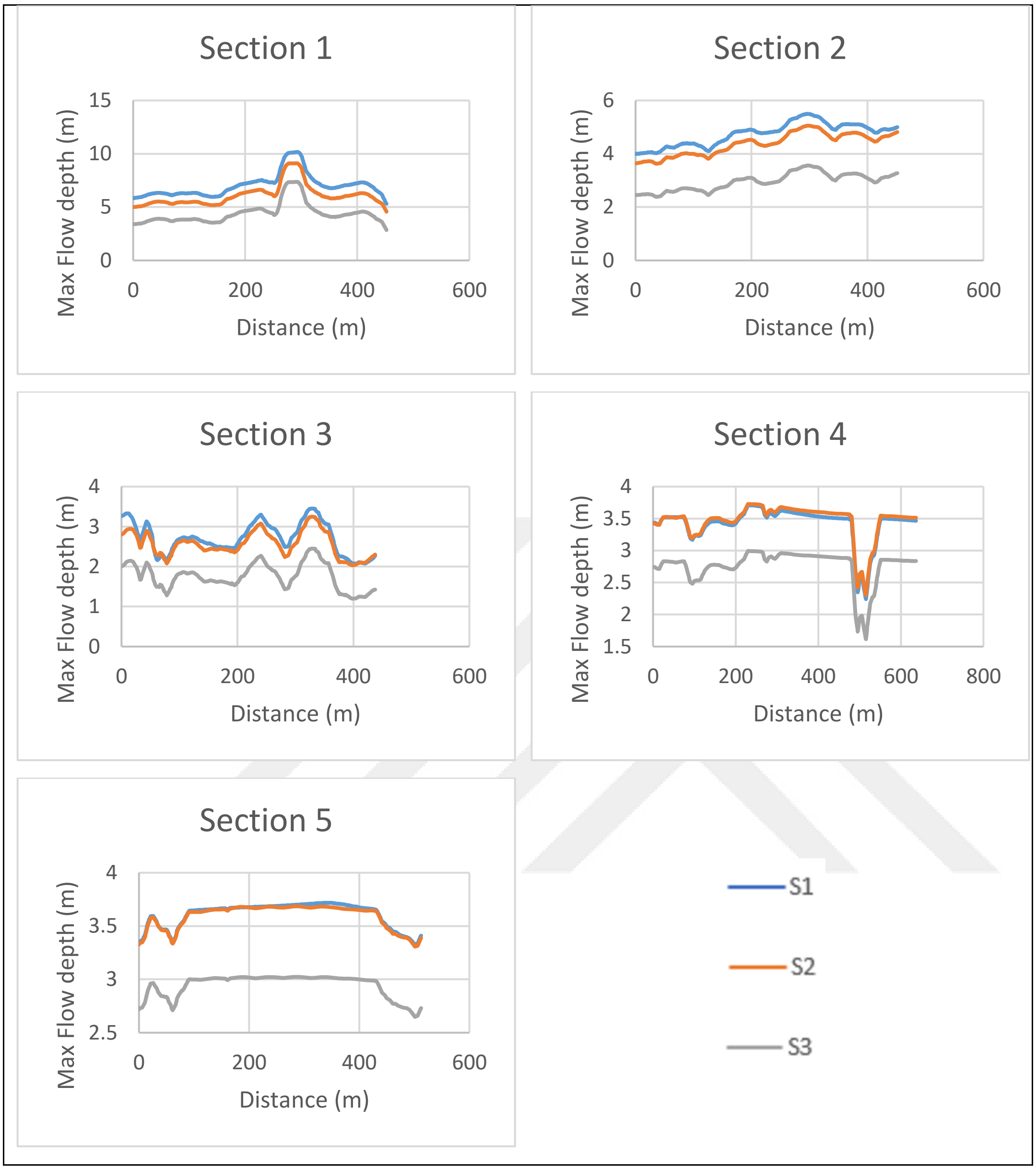

Figure 5-29 Change in Max flow depth with breach hydrograph at sections (HEC-RAS)

From the graph, It can be seen that there are significant differences in flow depth at each section. At Sections 4 and 5, which are located close to the boundary, the difference between flow depth for S1 and S2 is quite small. In general, it can be stated that with a decrease in peak flow, there is a decrease in flow depth at each section.

FLO-2D:

Table 5-14 shows the inundation area for FLO-2D at 5 m grid resolution for S1, S2, and S3 breach hydrographs.

Table 5-14 Ondokuz Mayıs Dam inundation area (FLO-2D) for breach hydrographs (S1, S2, and S3)

Breach Hydrograph	Inundation Area (m^2)
S1	23642413
S2	23214967
S3	21693467

Figure 5-30 shows the comparison of flow depth for different breach hydrographs at the selected section for FLO-2D simulations at 5 m grid size.

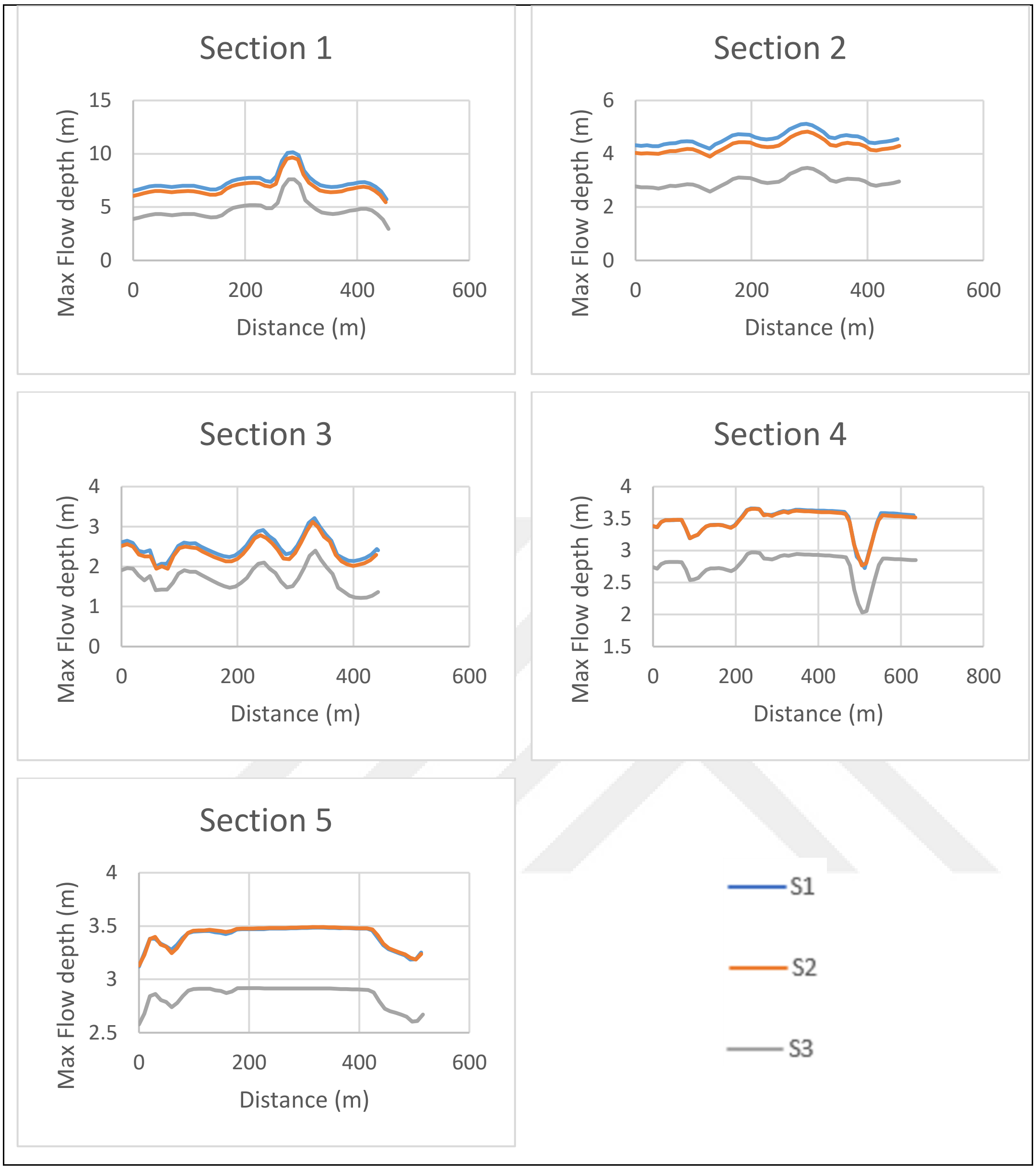

Figure 5-30 Change in Max flow depth with breach hydrograph at sections (FLO-2D)

The graph shows that the difference between flow depths of S1 and S2 is much smaller at Sections 4 and 5 (located near the downstream boundary), while the differences is quite significant for S3.

5.3 Breach Hydrograph Routing: İhsaniye Dam

For İhsaniye Dam, the flood routing of the breach hydrograph S1, is carried out by both HEC-RAS and FLO-2D models. In this part, first the results are presented in terms of inundation maps of maximum flow depth, maximum flow velocity, and arrival time for maximum depth. Then a comparison of flow depth obtained from the 5 m grid simulation of both HEC-RAS and FLO-2D is presented. The results of sensitivity of grid, roughness values and breach hydrograph are also discussed. The comparison of flow depth is made at sections located in the vicinity of the Yalakdere Town as shown in Figure 5-31.

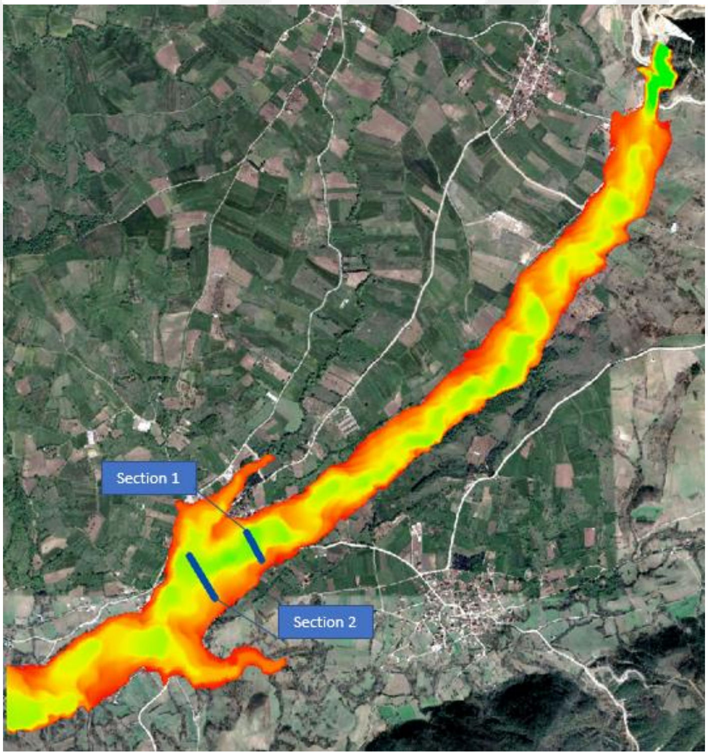

Figure 5-31 Location of Sections 1 and 2 (Yalakdere Town)

Figure 5-32 to Figure 5-34 show the maximum flow depth, maximum velocity, and arrival time for maximum depth maps for HEC-RAS and FLO-2D.

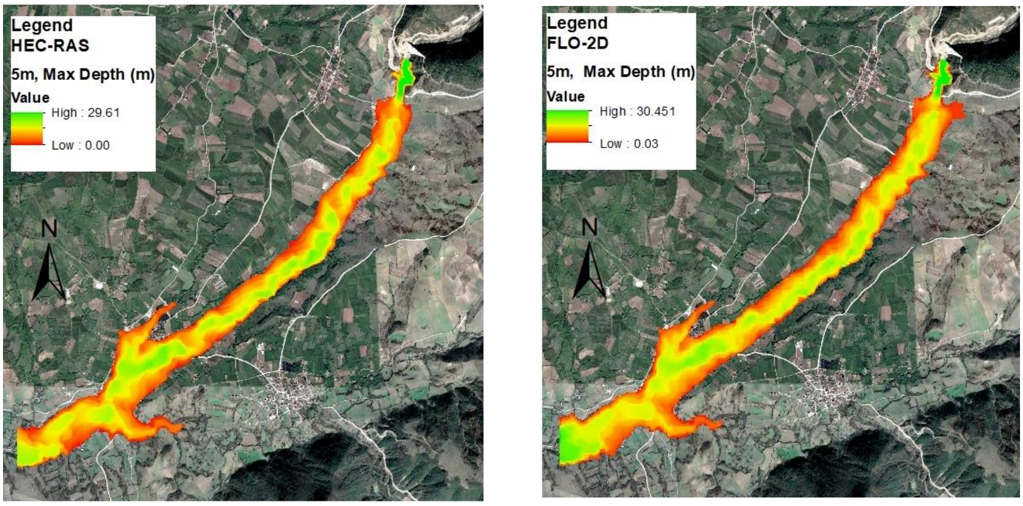

(a) (b)

Figure 5-32 Max flow depth for S1 at 5 m (İhsaniye Dam) (a) HEC-RAS (b) FLO-2D

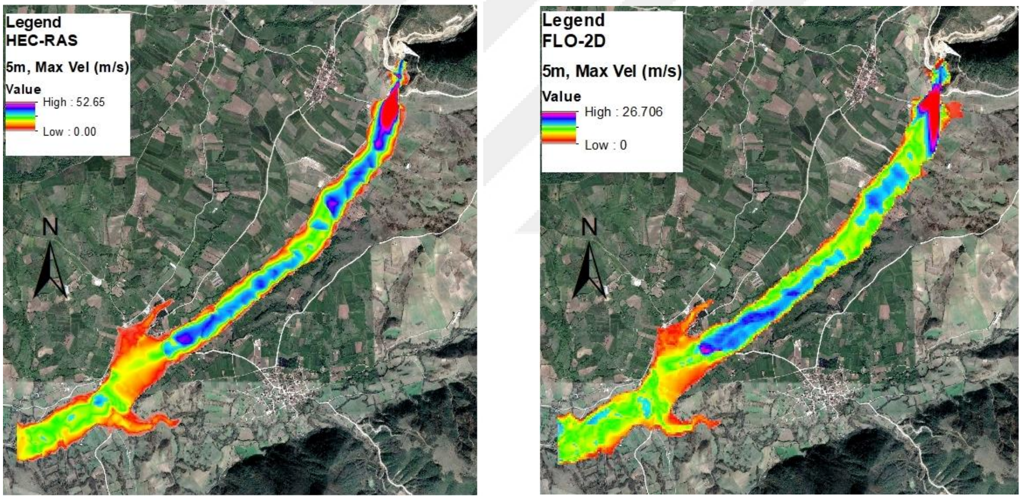

(a) (b)

Figure 5-33 Max flow velocity for S1 at 5 m (İhsaniye Dam) (a) HEC-RAS (b) FLO-2D

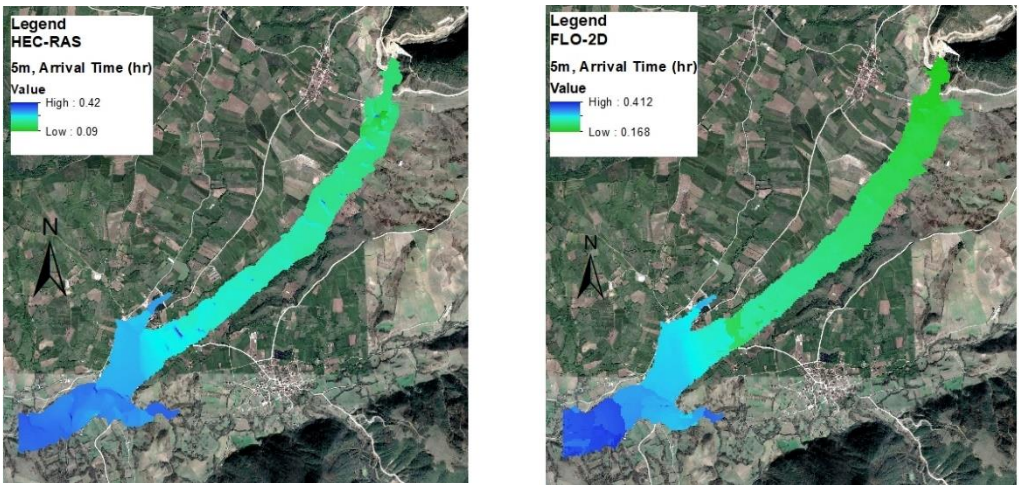

(a) (b)

Figure 5-34 Arrival Time for Max depth for S1 at 5 m (İhsaniye Dam) (a) HEC-RAS (b) FLO-2D

The comparison of maximum flow depth for Section 1 and 2 is shown below in Figure 5-35 and Figure 5-36, respectively.

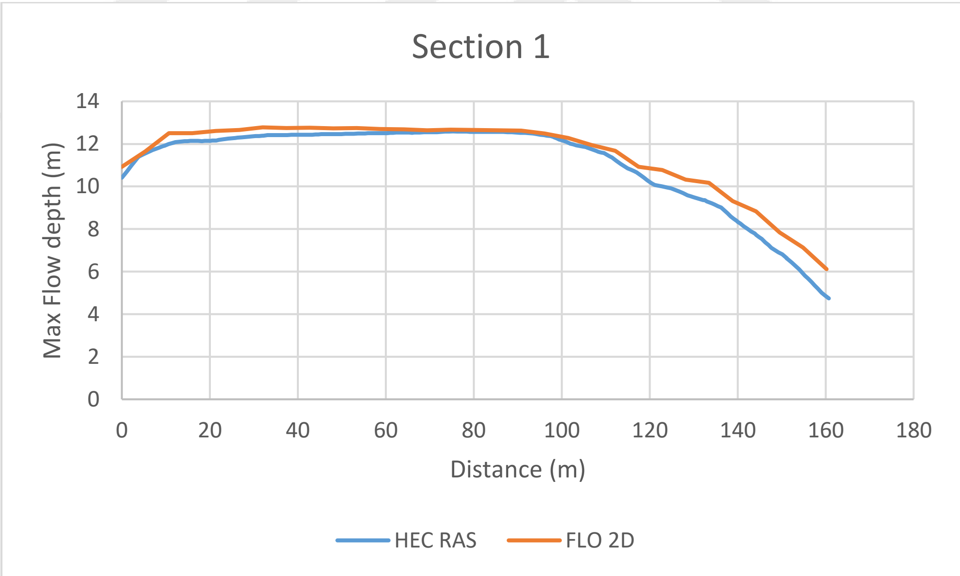

Figure 5-35 Comparison of Max Flow depth at Section-1 for HEC-RAS and FLO-2D (S1, 5 m)

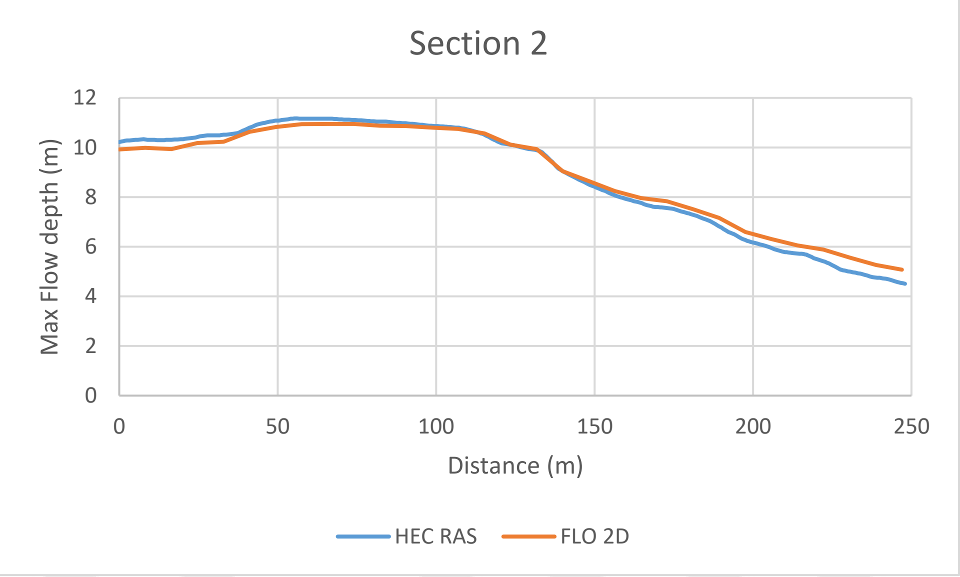

Figure 5-36 Comparison of Max Flow depth at Section-2 for HEC-RAS and FLO-2D (S1, 5 m)

The graphs show a consistency of the results in terms of maximum flow depths between HEC-RAS and FLO-2D at both sections. It can be seen that FLO-2D gives slightly higher flow depths in comparison to HEC-RAS at both sections. The terrain downstream of Ihsaniye Dam is a straight valley, and flow is confined within the valley. The consistency of results can be due to the fact that both models are using almost similar topographic details in the flow depth calculations.

Table 5-15 gives the maximum velocity and arrival time of maximum depth at each section for HEC-RAS and FLO-2D.

Table 5-15 Max velocity and Arrival time for Max depth at the sections for HEC-RAS and FLO-2D (S1, 5 m)

Sections	HEC-RAS		FLO-2D	
	Max Velocity (m/sec)	Arrival Time of Max depth (hr)	Max Velocity (m/sec)	Arrival Time of Max depth (hr)
Section 1	7.678	0.254	10.949	0.275
Section 2	6.041	0.291	6.890	0.305

Th F Statistic value of 0.90818 is obtained for flood extent of HEC-RAS and FLO-2D at 5 m grid resolution by taking HEC-RAS flood extent as the base. It shows that both models give more than 90% similar inundation area.

5.3.1 Sensitivity of Grid Resolution

In this part of the analysis, the impact of the sensitivity of grid resolution on the inundation results is analyzed by carrying out flood routing simulations at 10 m, 25 m, and 50 m grid resolution. The inundation results are presented below in terms of flood extent and comparison of flow depth at the sections for both models.

HEC-RAS:

The flood extents obtained from HEC-RAS simulations at coarser grid resolution are presented in terms of F-statistic value in Table 5-16. The values show that there is a minimal change in flood extent with an increase in grid resolution.

Table 5-16 also shows the model runtime for routing a breach hydrograph of 3 hours duration over the downstream floodplain of İhsaniye Dam.

Table 5-16 F-statistic value and Model runtimes for HEC-RAS (S1)

Grid Resolution	F-Statistic (base 5 m)	Model Runtime (min)
5 m	--	155
10 m	0.98346	26
25 m	0.96991	2
50 m	0.96426	0.66

Table 5-17 gives the calculated RMSE values for flow depth at each section in comparison to 5 m flow depth. For both sections, it shows that the lowest RMSE values for flow depth are for 10 m resolution, and an increase in RMSE is seen for coarser grids.

Table 5-17 Flow depth RMSE values calculated with base 5 m flow depth for each section (HEC-RAS, S1)

Sections	Flow Depth RMSE		
	10 m	25 m	50 m
Section 1	0.0713	0.1788	0.3174
Section 2	0.0394	0.1175	0.2691

Figure 5-37 and Figure 5-38 shows results obtained from HEC-RAS simulations in terms of the change in flow depth with grid resolution for Sections 1and 2.

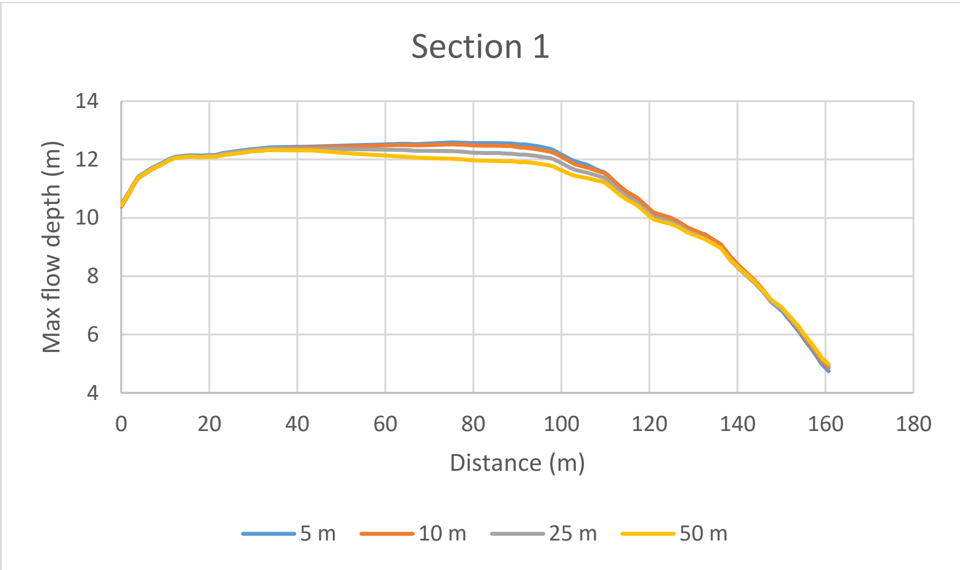

Figure 5-37 Change in flow depth at Section-1 with grid resolution (HEC-RAS, S1)

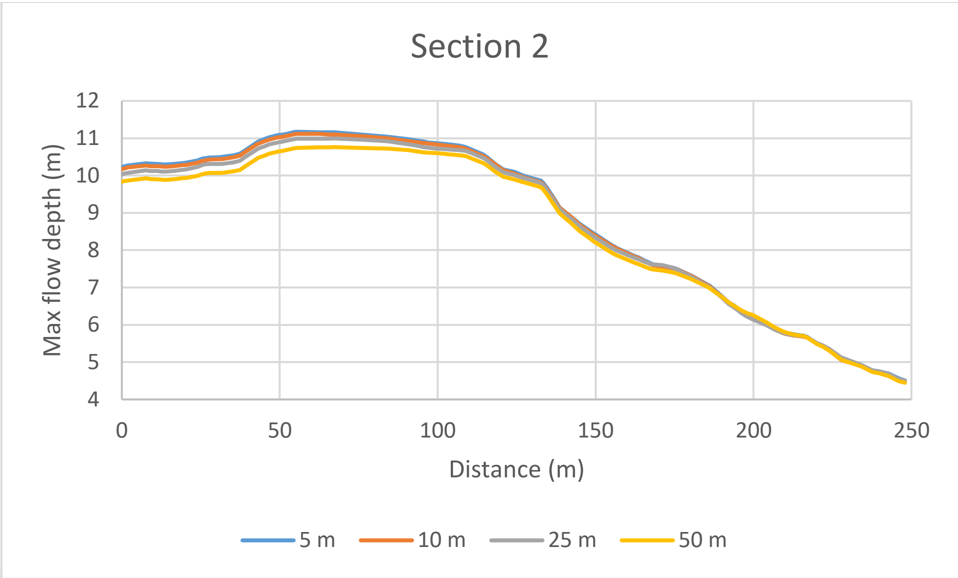

Figure 5-38 Change in flow depth at Section-2 with grid resolution (HEC-RAS, S1)

The graphs display a consistency of results between finer and coarser resolution results. It can be seen that the flow depth is decreasing slightly at both sections for coarser resolution. The downstream floodplain of İhsaniye Dam consists of a narrow valley, the increase in grid resolution in HEC-RAS has very little effect on the flow depth. The inundation maps for coarse grid resolution simulations are given in Appendix.

FLO-2D:

Table 5-18 shows the F-statistic value for flood extent by taking the flood extent of the 5 m simulation as the base. The FLO-2D simulation results show that as the grid size is getting coarser, the overlap area is decreasing. The FLO-2D runtime for the routing of a 3-hour breach hydrograph is also shown in Table 5-18.

Table 5-18 F-statistic value and Model runtimes for FLO-2D (S1)

Grid Resolution	F-Statistic (base 5 m)	Model Runtime (min)
5 m	--	27
10 m	0.96509	5
25 m	0.94332	2
50 m	0.88826	0.11

Table 5-19 presents the RMSE values for sections calculated in comparison to 5 m simulation results. It shows that the lowest RMSE values for flow depth are for 10 m resolution, and as the grid resolution is increasing in RMSE is also increasing.

Table 5-19 Flow depth RMSE values calculated with base 5 m flow depth for each section (FLO-2D, S1)

Sections	Flow Depth RMSE		
	10 m	25 m	50 m
Section 1	0.3581	0.5894	1.0265
Section 2	0.1241	0.2917	0.4505

Figure 5-39 and Figure 5-40 shows results obtained from FLO-2D simulations in terms of the change in flow depth with grid resolution for Sections 1 and 2.

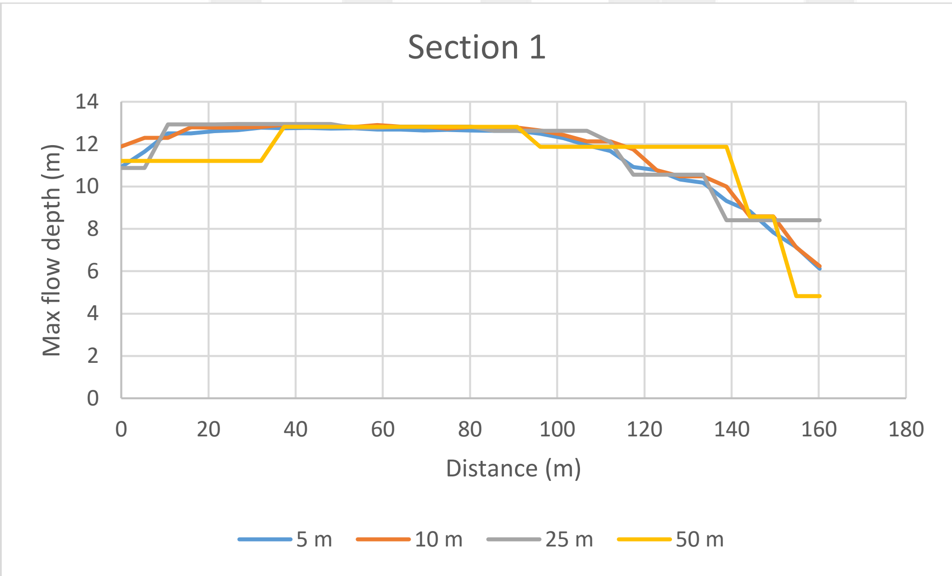

Figure 5-39 Change in flow depth at Section-1 with grid resolution

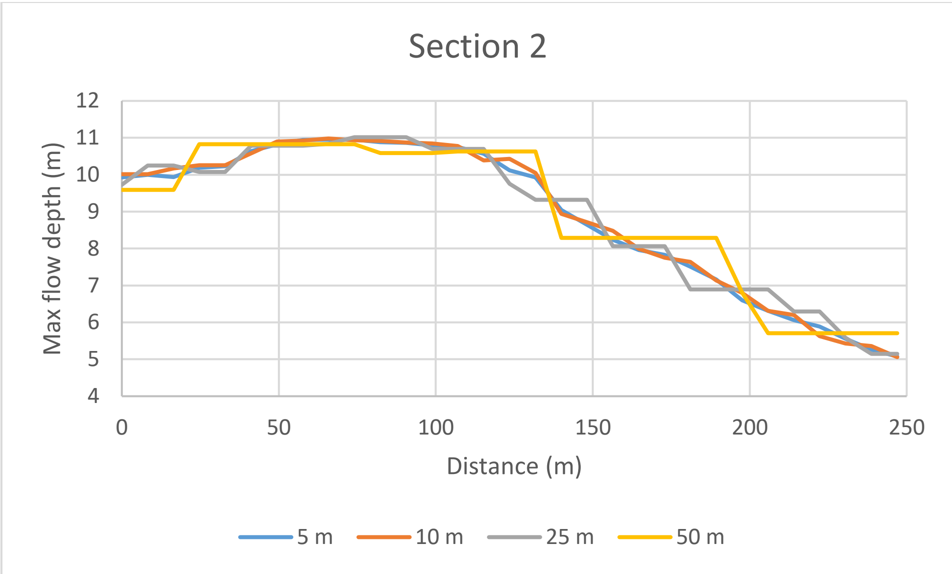

Figure 5-40 Change in flow depth at Section-2 with grid resolution

The graphs show that for finer resolutions the results are consistent. For coarser resolution, the calculated flow depth is not consistent and a significant difference in flow depth can be seen. The main reason for the occurrence of significant differences is in the presentation of the topographic features at the coarser grid in FLO-2D. As there is one elevation value for each grid, so as the grid size is increasing the topographic details are lost, which affects the model output.

5.3.2 Sensitivity of Roughness Values

In this segment, the sensitivity of the roughness parameter to the flood inundation simulation is analyzed by varying the base roughness values. The base values upon which the model was calibrated are increased and decreased by 20%. The simulations were run at 5 m grid resolution using the breach hydrograph S1 in both HEC-RAS and FLO-2D.

HEC-RAS:

The sensitivity of roughness values to the flood extent is calculated by means of F-statistic value, as shown in Table 5-20. It shows that flood extent is less sensitive to the roughness values.

Table 5-20 F-statistic value at different roughness values for HEC-RAS (S1)

Roughness value	F-Statistic (Base n)
0.8* n	0.97584
1.2*n	0.97791

Figure 5-41 and Figure 5-42 presents the change in flow depth with the roughness parameter at Sections 1 and 2 for HEC-RAS simulations at 5 m grid size.

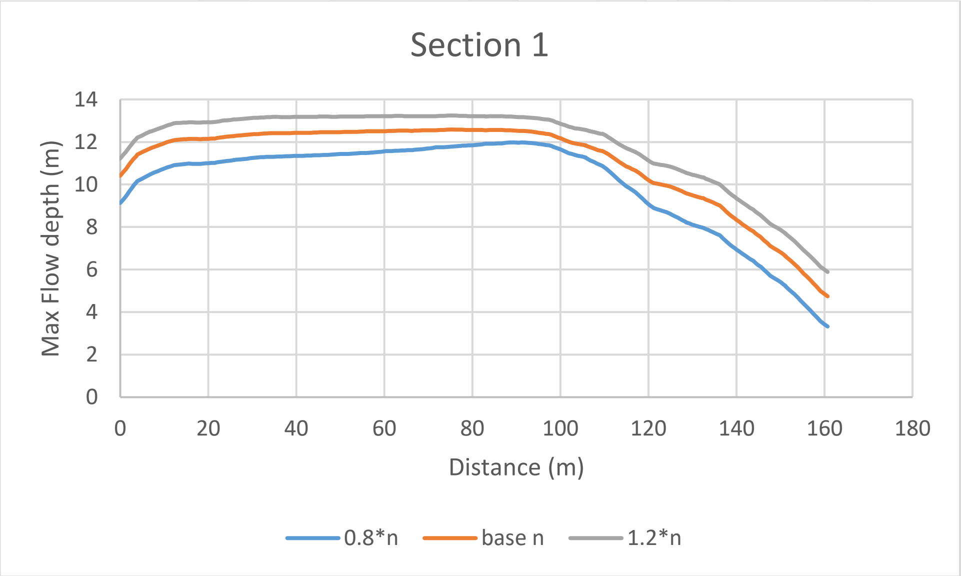

Figure 5-41 Change in Max flow depth with roughness values at Section-1 (HEC-RAS, S1)

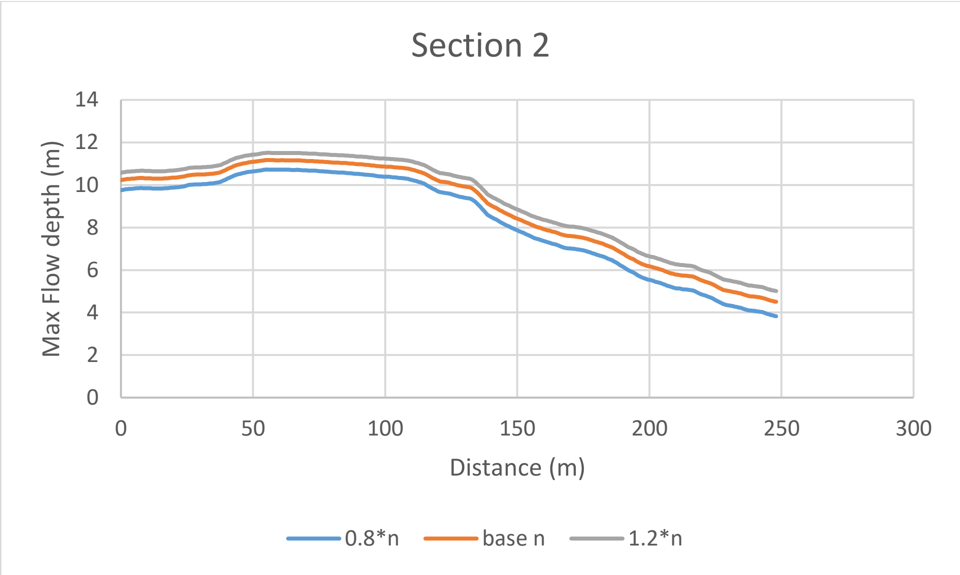

Figure 5-42 Change in Max flow depth with roughness values at Section-2 (HEC-RAS, S1)

The graphs show that the model is very responsive to the change in roughness values. With increase in the roughness values (1.2*n) the flow depth is increasing, while decreasing the roughness values (0.8*n) results in decrease in flow depth.

FLO-2D:

The sensitivity of roughness values to the flood extent is calculated by means of F-statistic value, as shown in Table 5-21. It shows that flood extent is less sensitive to the roughness values in

Table 5-21 F-statistic value for flood extent at different roughness parameter for FLO-2D (S1)

Roughness value	**F-Statistic (Base n)**
0.8* n	0.98223
1.2*n	0.97618

Figure 5-43 and Figure 5-44 presents the change in flow depth with the roughness parameter at Sections 1 and 2 for FLO-2D simulations at 5 m grid size.

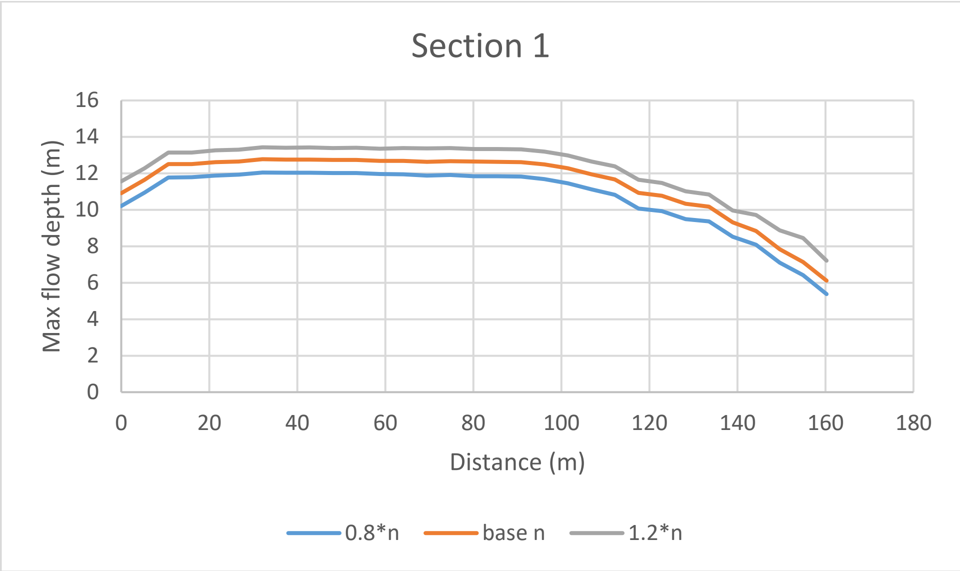

Figure 5-43 Change in Max flow depth with roughness values at Section-1 (FLO-2D, S1)

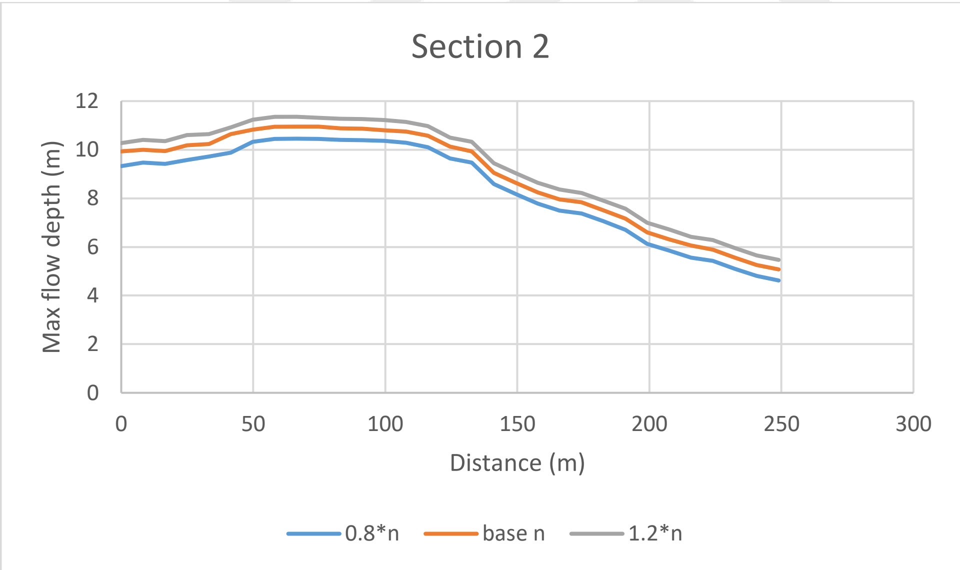

Figure 5-44 Change in Max flow depth with roughness values at Section-2 (FLO-2D, S1)

These graphs shows that FLO-2D model is also very sensitive to the roughness values. The increase in the roughness values results in higher depth than the base flow depth, while decreasing the roughness values results in lower flow depth.

5.3.3 Sensitivity of Breach Hydrograph

In this part of analysis, flood routing simulations are carried out at 5 m grid resolution using the breach hydrographs S2 and S3 along with the calibrated Manning roughness values with both models. The results are presented in terms of inundation area and the comparison of flow depth at selected.

HEC-RAS:

Table 5-22 shows the inundation area calculated by HEC-RAS at 5 m grid resolution for S1, S2, and S3 breach hydrographs.

Table 5-22 İhsaniye Dam inundation area (HEC-RAS) for breach hydrographs (S1, S2, and S3)

Breach Hydrograph	Inundation Area (m^2)
S1	1439849
S2	1382632
S3	1323026

Figure 5-45 and Figure 5-46 shows the comparison of calculated flow depth for S1, S2, and S3 breach hydrographs at the Sections 1 and 2.

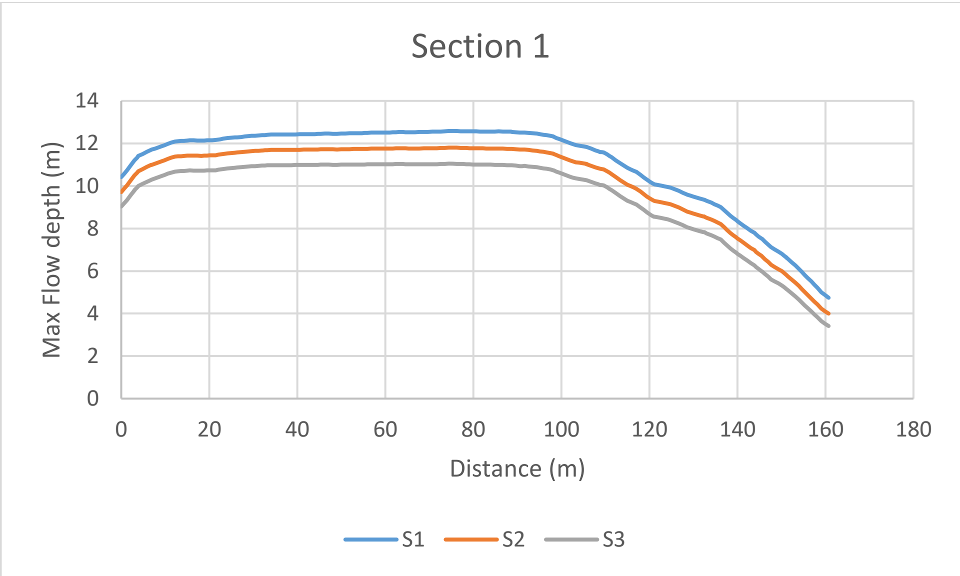

Figure 5-45 Change in Max flow depth with breach hydrograph at Section-1 (HEC-RAS)

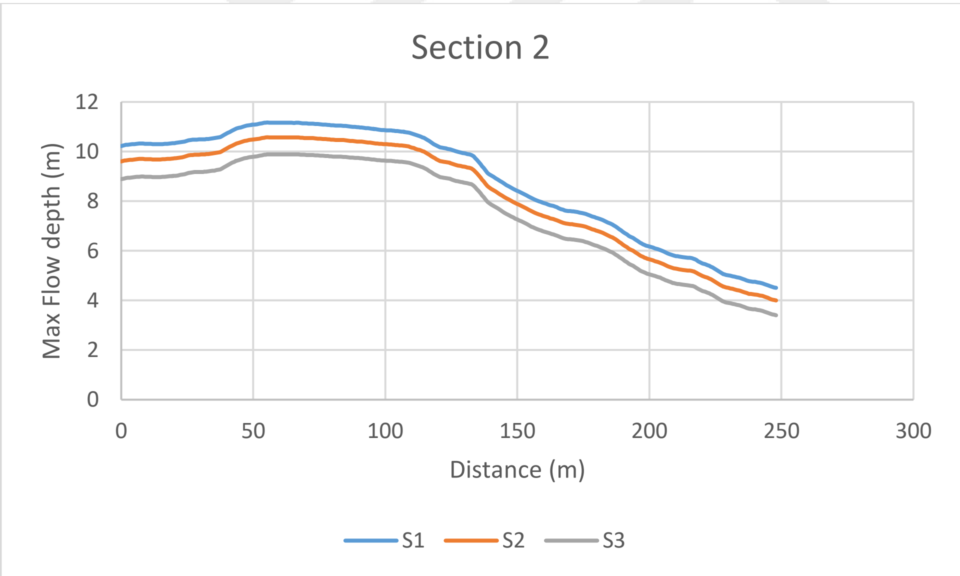

Figure 5-46 Change in Max flow depth with breach hydrograph at Section-2 (HEC-RAS)

From the graphs it can be seen that as the peak flow is decreasing from S1 to S3, the flow depth is also decreasing at both sections.

FLO-2D:

Table 5-23 shows the inundation area for FLO-2D at 5 m grid resolution for S1, S2, and S3 breach hydrographs.

Table 5-23 İhsaniye Dam inundation area (FLO-2D) for breach hydrographs (S1, S2, and S3)

Breach Hydrograph	Inundation Area (m^2)
S1	1546700
S2	1459400
S3	1381400

The comparison of flow depth for S1, S2, and S3 breach hydrographs at the selected section for FLO-2D simulations at 5 mis presented in Figure 5-47 and Figure 5-48.

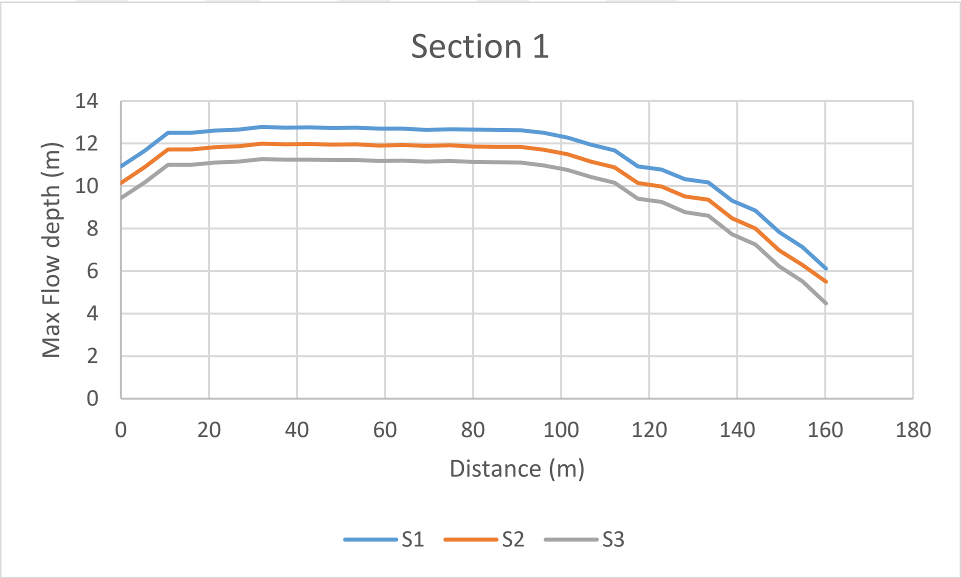

Figure 5-47 Change in Max flow depth with breach hydrograph at Section-1 (FLO-2D)

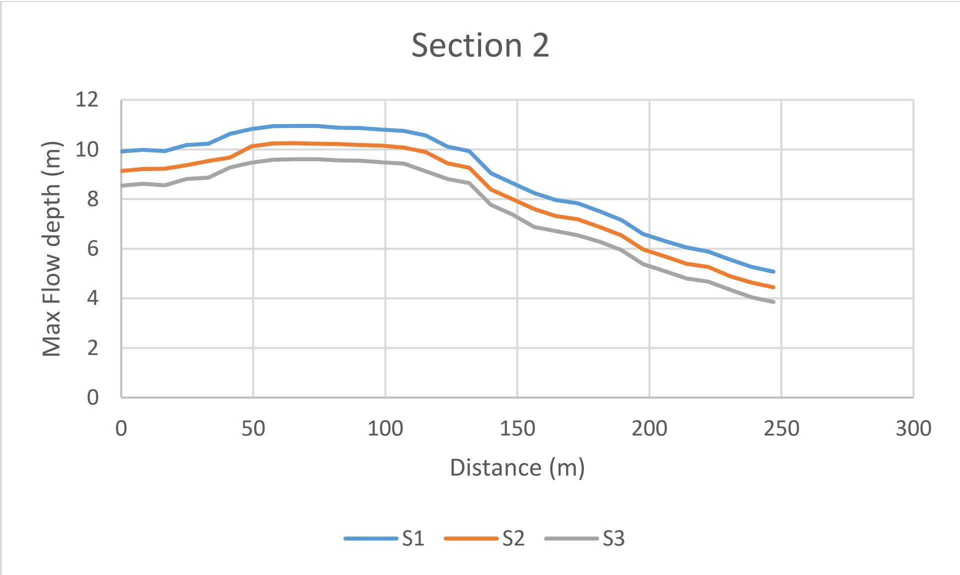

Figure 5-48 Change in Max flow depth with breach hydrograph at Section-2 (FLO-2D)

The graphs show that as the peak flow is decreasing from S1 to S3, the flow depth is also decreasing.

5.4 Breach Hydrograph Routing: Avcıdere Dam

The breach flood routing of Avcıdere Dam is simulated with both HEC-RAS and FLO-2D models using the breach hydrograph and Manning roughness shapefile. Initially, the results of 5 m grid simulation are presented in terms of inundation maps of maximum flow depth, maximum flow velocity, and arrival time for maximum depth. Then a comparison of flow depth for both HEC-RAS and FLO-2D is presented at selected sections. The Section 1 is located in Avcıköy Town, while Section 2 is located in the Yalakdere Town (Figure 5-49).

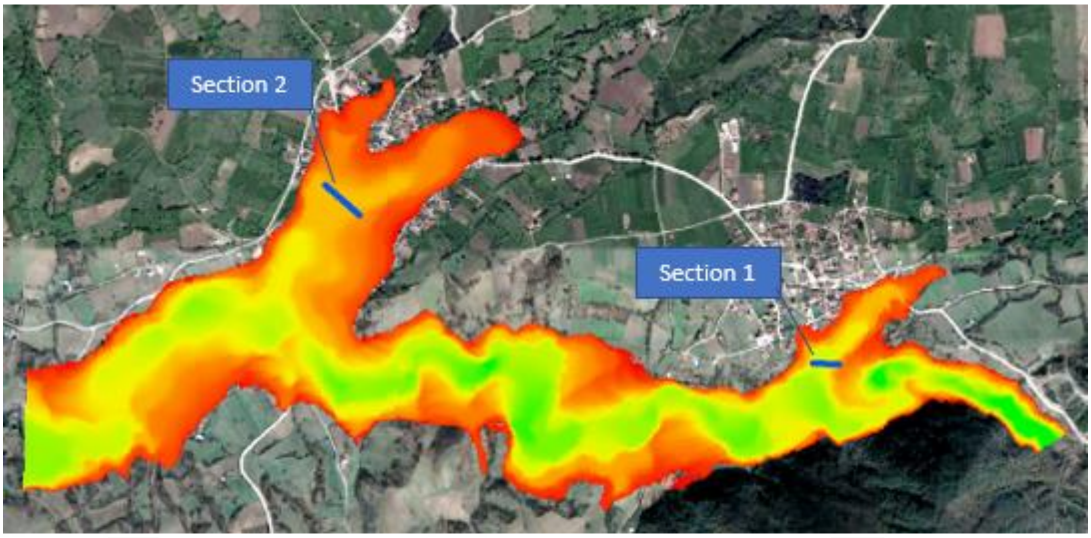

Figure 5-49 Location of Section 1 (Avcıköy town) and Section 2 (Yalakdere town)

Figure 5-50, Figure 5-51, and Figure 5-52 show the maximum arrival depth, maximum flow velocity and arrival time for maximum flow depth maps for S1 breach hydrograph at 5 m grid resolution for HEC-RAS and FLO-2D.

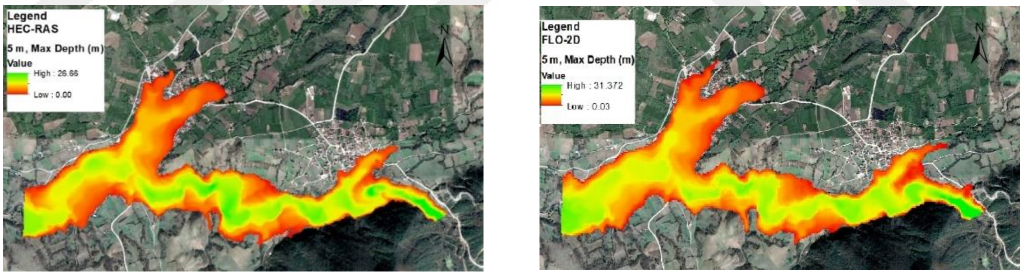

(a) (b)

Figure 5-50 Max flow depth for S1 at 5 m (Avcıdere Dam) (a) HEC-RAS (b) FLO-2D

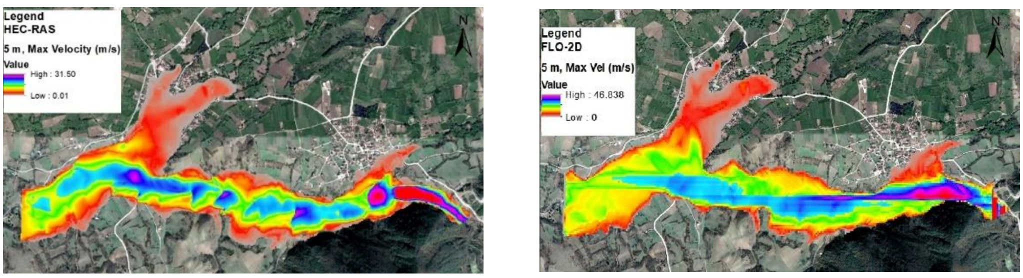

(a) (b)

Figure 5-51 Max flow velocity for S1 at 5 m (Avcıdere Dam) (a) HEC-RAS (b) FLO-2D

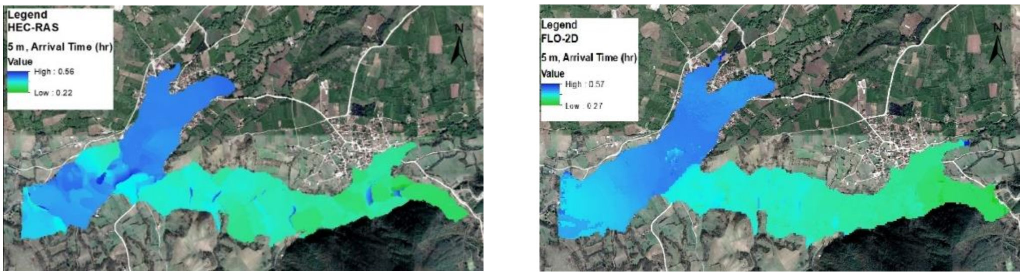

(a) (b)

Figure 5-52 Arrival Time for Max flow depth for S1 at 5 m (Avcıdere Dam) (a) HEC-RAS (b) FLO-2D

The comparison of Max flow depth at Section 1 and 2 is shown below in Figure 5-53 and Figure 5-54 respectively.

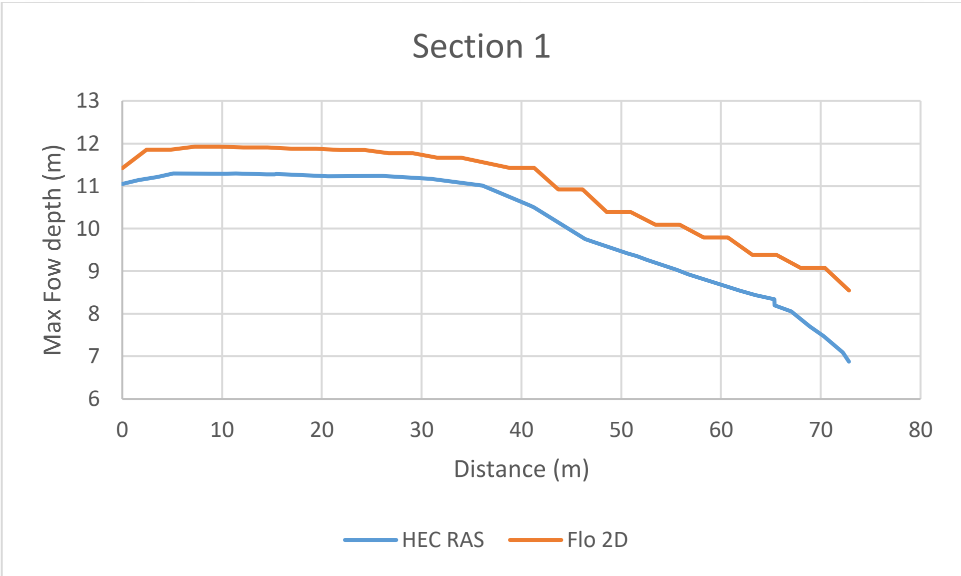

Figure 5-53 Comparison of Max Flow depth at Section-1 for HEC-RAS and FLO-2D (S1, 5 m)

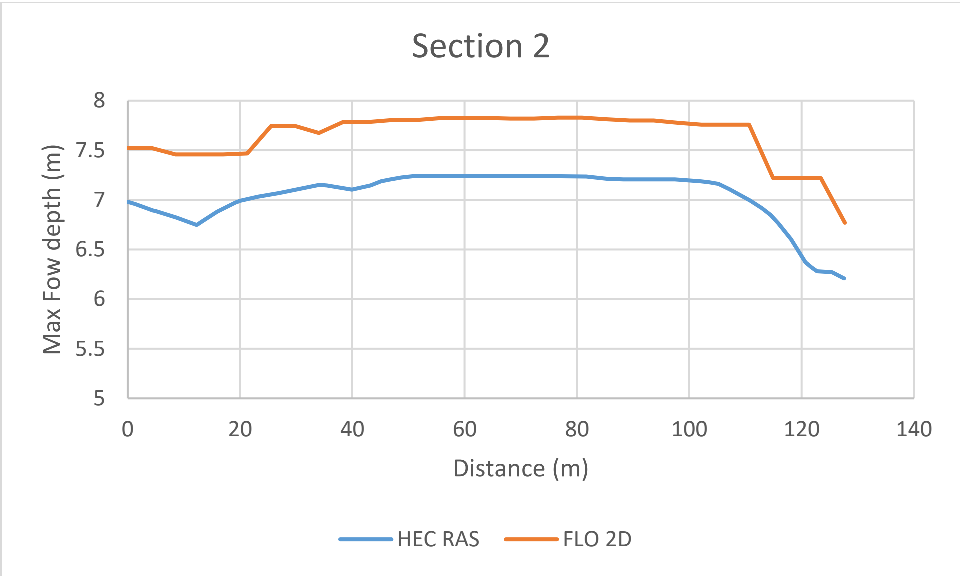

Figure 5-54 Comparison of Max Flow depth at Section-2 for HEC-RAS and FLO-2D (S1, 5 m)

It can be seen that FLO-2D gives higher flow depth at both sections in comparison to HEC-RAS. It can be due to the reason that the downstream floodplain of the Avcıdere Dam consists of hilly terrain with a meandering channel and both models incorporate the terrain in a different way in the calculations which can be affecting the flow patterns. Also one more thing to be considered is that both of the sections are located on the right side of Avci Creek and are flooded as a result of the backwater effect.

Table 5-24 gives a comparison of the maximum velocity and arrival time of maximum depth at the sections for HEC-RAS and FLO-2D.

Table 5-24 Max velocity and Arrival time for Max depth at the sections for HEC-RAS and FLO-2D (S1, 5 m)

Sections	HEC-RAS		FLO-2D	
	Max Velocity (m/sec)	Arrival Time of Max depth (hr)	Max Velocity (m/sec)	Arrival Time of Max depth (hr)
Section 1	11.473	0.349	5.850	0.345
Section 2	1.747	0.477	2.135	0.457

Th F Statistic value of 0.915309 is obtained for flood extent of HEC-RAS and FLO-2D at 5 m grid resolution by taking HEC-RAS flood extent as the base, meaning that both models give almost 91% of similar flood extent.

5.4.1 Sensitivity of Grid Resolution

In this part, the sensitivity of grid resolution on the inundation results is examined by carrying out flood routing simulations at 10 m, 25m, and 50 m grid resolution. The results are then compared with the results of 5 m resolution. The simulation results are presented for both HEC-RAS and FLO-2D models. The results are presented in terms of F statistic values for flood extent and comparison of flow depth at selected sections as shown in Figure 5-50.

HEC-RAS:

The flood extents obtained from HEC-RAS simulations at coarser grid resolution are presented in Table 5-25 in terms of F-statistic value, calculated by taking the 5 m flood extent as the base. The values show that there is a minimal change in flood extent in HEC-RAS, as the grid is getting coarser. Table 5-25 also shows the model runtime for routing of a 3-hour breach hydrograph over the downstream floodplain of İhsaniye Dam.

Table 5-25 F-statistic value and Model runtimes for HEC-RAS (S1)

Grid Resolution	F-Statistic (base 5 m)	Model Runtime (min)
5 m	--	87
10 m	0.97982	18
25 m	0.97068	1.50
50 m	0.95222	0.66

Table 5-26 provides the RMSE values calculated for each section in comparison to 5 m simulation results. For both sections, it shows that the lowest RMSE values for flow depth are for 10 m resolution, and as the grid resolution is increasing in RMSE is also increasing.

Table 5-26 Flow depth RMSE values calculated with base 5 m flow depth for each section (HEC-RAS, S1)

Sections	Flow Depth RMSE		
	10 m	25 m	50 m
Section 1	0.8162	0.8592	0.5866
Section 2	0.0796	0.0168	0.2479

Figure 5-55 and Figure 5-56 shows results obtained from HEC-RAS simulations in terms of the change in flow depth with grid resolution for sections 1 and 2.

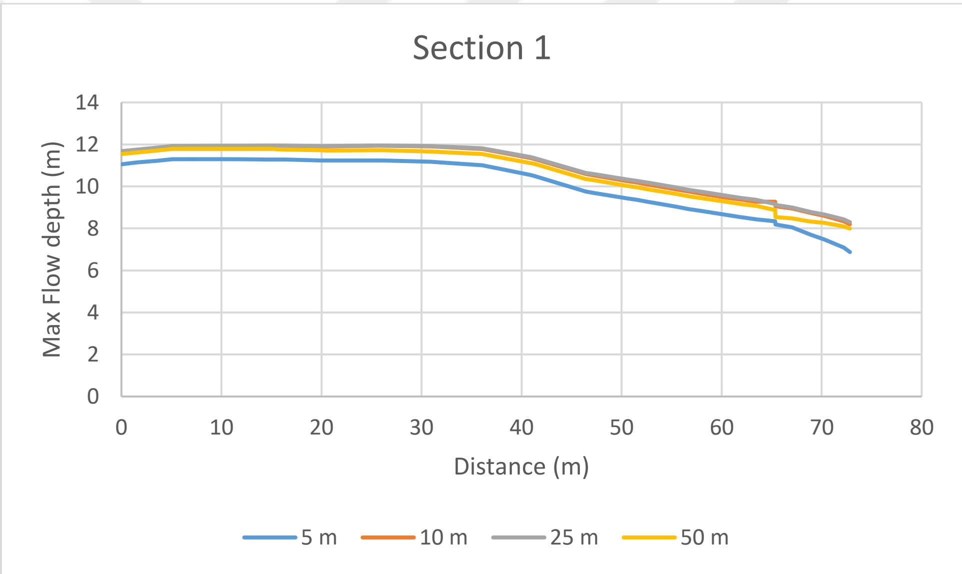

Figure 5-55 Change in flow depth at Section-1 with grid resolution (HEC-RAS, S1)

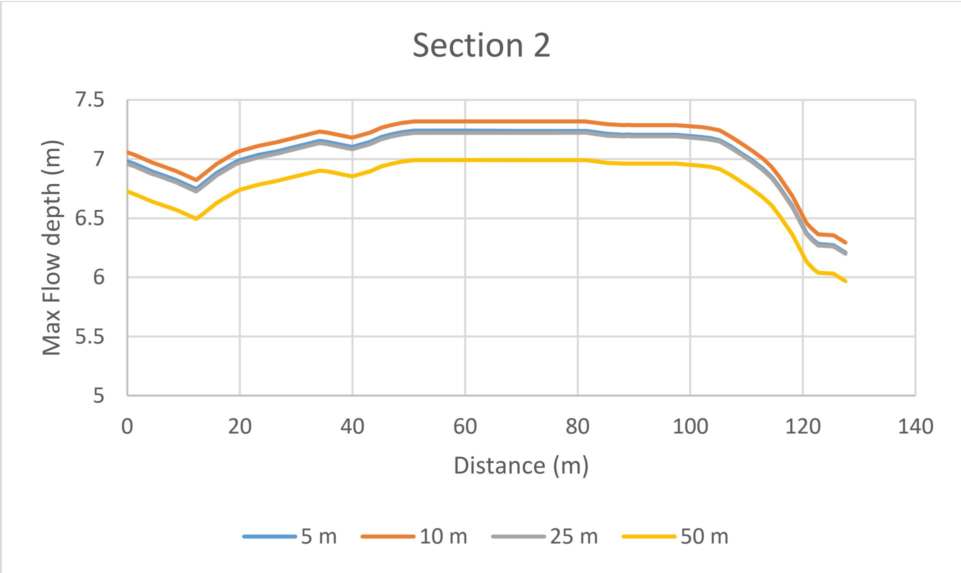

Figure 5-56 Change in flow depth at Section-2 with grid resolution (HEC-RAS, S1)

The graphs display a consistency of results as the grid resolution is increasing. It can be seen that the calculated flow depth at both sections is significantly affected by the grid resolution. The main reason can be the way how the terrain is captured at each grid resolution. In HEC-RAS, if the cell face of the grid is not aligned with the key terrain feature which can influence the flow, then the feature is not ignored in the computations. This way model cannot identify the terrain feature and route the flow in the neighboring cells, thus resulting in leakage which is a known limitation in the HEC-RAS two-dimensional model. The downstream floodplain of the Avcıdere Dam is hilly terrain with a meandering channel, for such types of terrains proper care must be taken while choosing the grid resolution.

FLO-2D:

Table 5-27 shows the F-statistic value for flood extent by taking the flood extent of the 5 m simulation as the base. The FLO-2D simulation results show that as the grid size is getting coarser, the overlap area is decreasing. The FLO-2D runtime for the routing of 3-hour breach hydrograph is also shown in Table 5-27

Table 5-27 F-statistic value and Model runtimes for FLO-2D (S1)

Grid Resolution	F-Statistic (base 5 m grid)	Model Runtime (min)
5 m	--	24
10 m	0.96118	4
25 m	0.92120	0.53
50 m	0.85772	0.11

Table 5-28 presents the RMSE values for sections calculated in comparison to 5 m simulation results. It shows that the lowest RMSE values for flow depth are for 10 m resolution, and as the grid resolution is increasing in RMSE is also increasing.

Table 5-28 Flow depth RMSE values calculated with base 5 m flow depth for each section (FLO-2D, S1)

Sections	Flow Depth RMSE		
	10 m	25 m	50 m
Section 1	0.4730	1.1875	1.3659
Section 2	0.1105	0.1977	0.4108

Figure 5-57 and Figure 5-58 shows results obtained from FLO-2D simulations in terms of the change in flow depth with grid resolution for Sections 1 and 2.

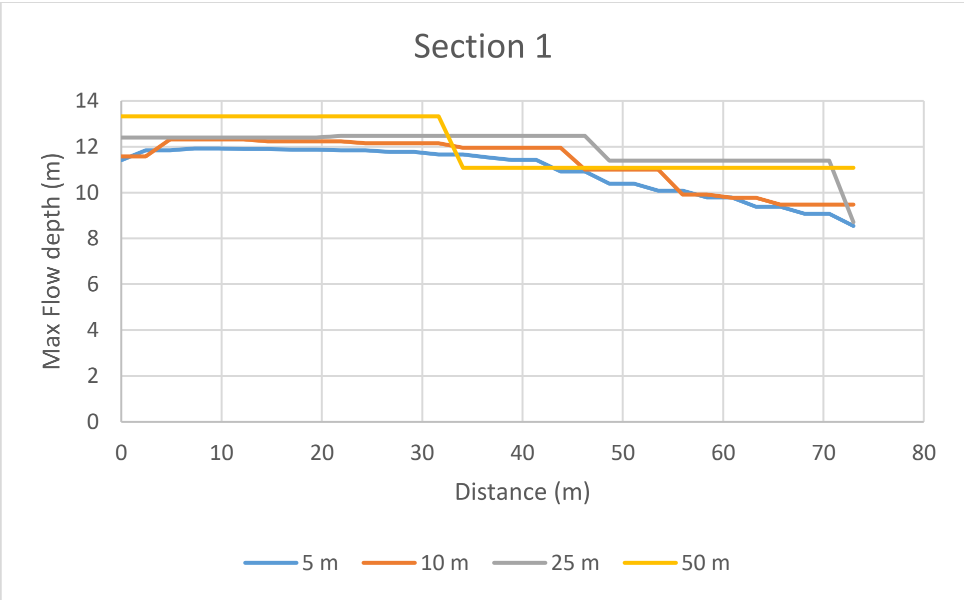

Figure 5-57 Change in flow depth at Section-1 with grid resolution (FLO-2D, S1)

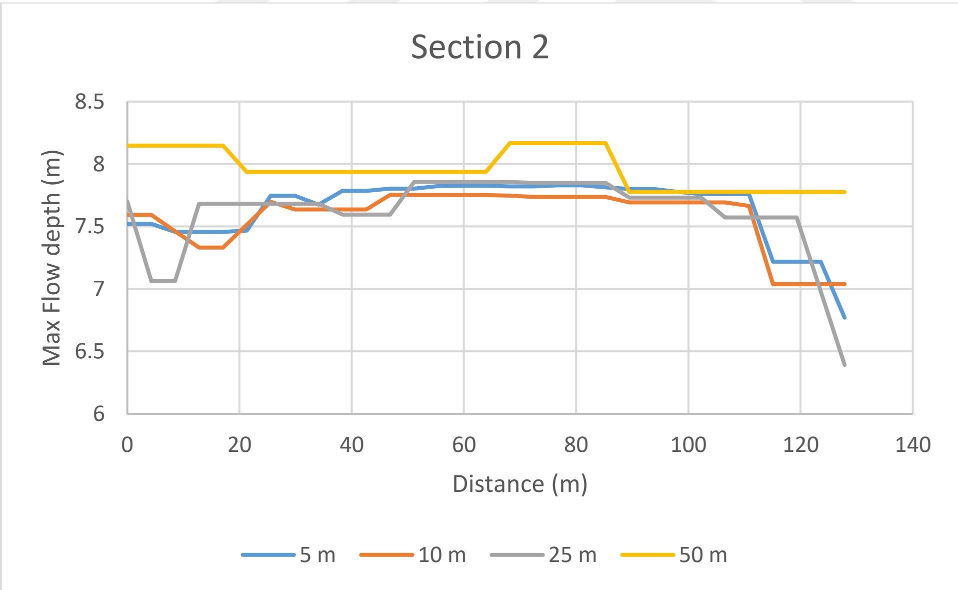

Figure 5-58 Change in flow depth at Section-2 with grid resolution (FLO-2D, S1)

The graphs show that as the grid resolution is getting coarser, flow depth at both sections is increasing. There is a consistency of results for finer resolutions, but for coarser resolutions there are significant differences in the calculated flow depth. The main reason for the occurrence of significant differences at coarser resolution is the way topography is represented in FLO-2D at the coarser grid. For meandering channel in hilly terrain, proper care must be taken to choose the grid resolution which is an important factor in capturing the topographic details, which can influence the flow patterns. As in FLO-2D, there is one elevation value for each grid, and for coarser grid resolution the topographic features smaller than the grid resolution are lost, thus affecting the model calculations.

5.4.2 Sensitivity of Roughness Values

In this part of the analysis, the sensitivity of the roughness parameter to the flood inundation simulation is analyzed by varying the base roughness values. The base values upon which the model was calibrated are increased and decreased by 20%. The simulations were run at 5 m grid resolution using the breach hydrograph S1 in both HEC-RAS and FLO-2D.

HEC-RAS:

The sensitivity of roughness values to the flood extent is calculated by means of F-statistic value, as shown in Table 5-29. It shows that in HEC-RAS, the flood extent is less sensitive to the increase and decrease in roughness values.

Table 5-29 F-statistic value at different roughness values for HEC-RAS (S1)

Roughness value	F-Statistic (Base n)
0.8* n	0.97852
1.2*n	0.97299

Figure 5-59 and Figure 5-60 presents the change in flow depth with the roughness parameter for HEC-RAS simulations at 5 m grid size.

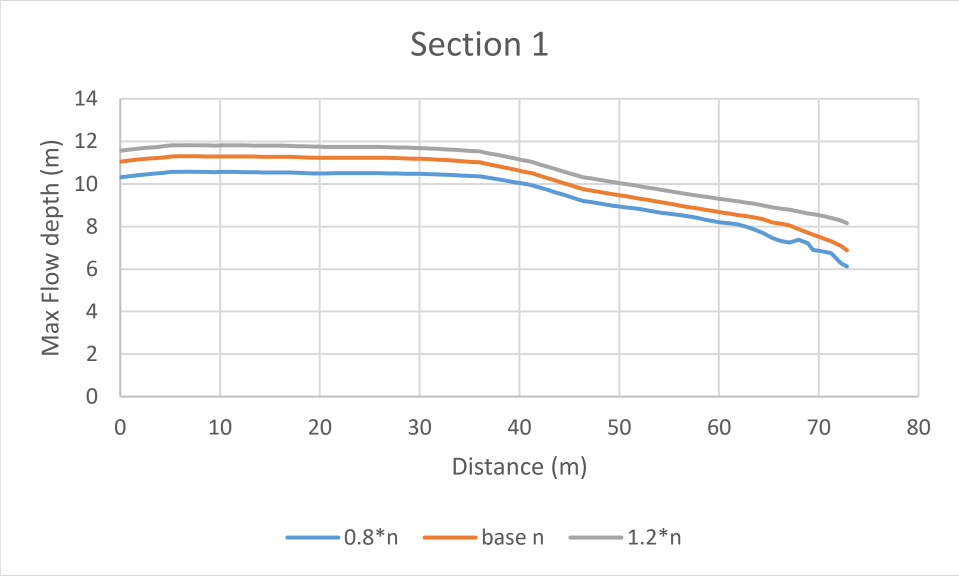

Figure 5-59 Change in Max flow depth with roughness values at Section-1 (HEC-RAS, S1)

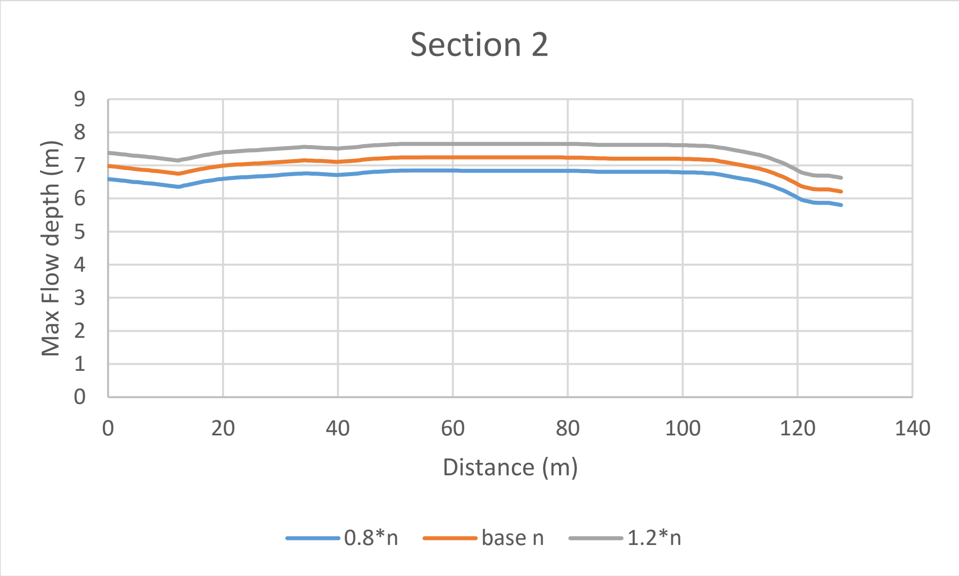

Figure 5-60 Change in Max flow depth with roughness values at Section-2 (HEC-RAS, S1)

The graphs show that the model is very responsive to the change in roughness values. With increase in the roughness values (1.2*n) the flow depth is increasing, while decreasing the roughness values (0.8*n) results in decrease in flow depth.

FLO-2D:

The sensitivity of roughness values to the flood extent are calculated by means of F statistic value, as shown in Table 5-30. It shows that in FLO-2D, a 20% decrease in base roughness values gives 97% same flood extent, while 20% increase in roughness values yields 94% similar flood extent.

Table 5-30 F-statistic value for flood extent at different roughness parameter for FLO-2D (S1)

Roughness value	F-Statistic (Base n)
0.8* n	0.97545
1.2*n	0.94955

Figure 5-61 and Figure 5-62 presents the change in flow depth with the roughness parameter for FLO-2D simulations at 5 m grid size.

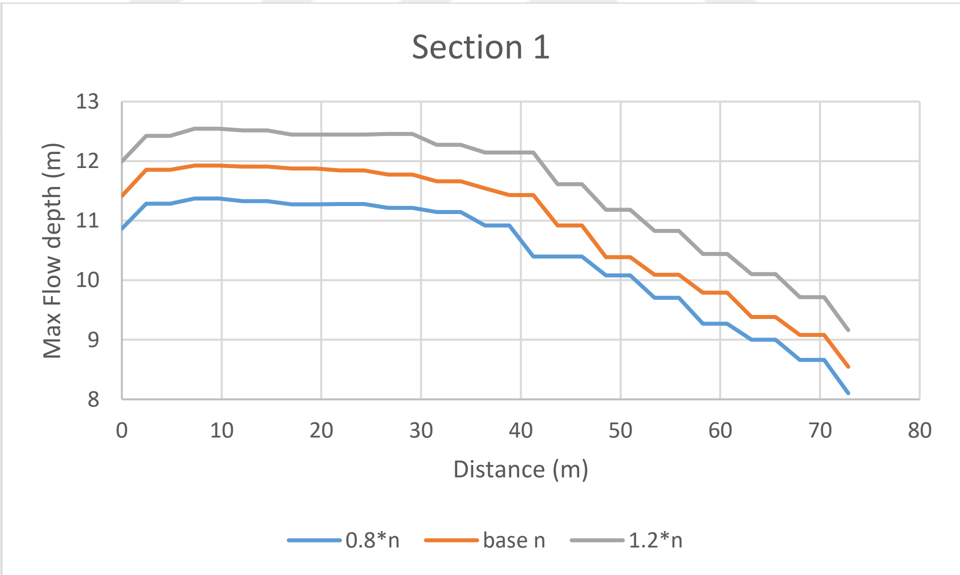

Figure 5-61 Change in Max flow depth with roughness values at Section-1 (FLO-2D, S1)

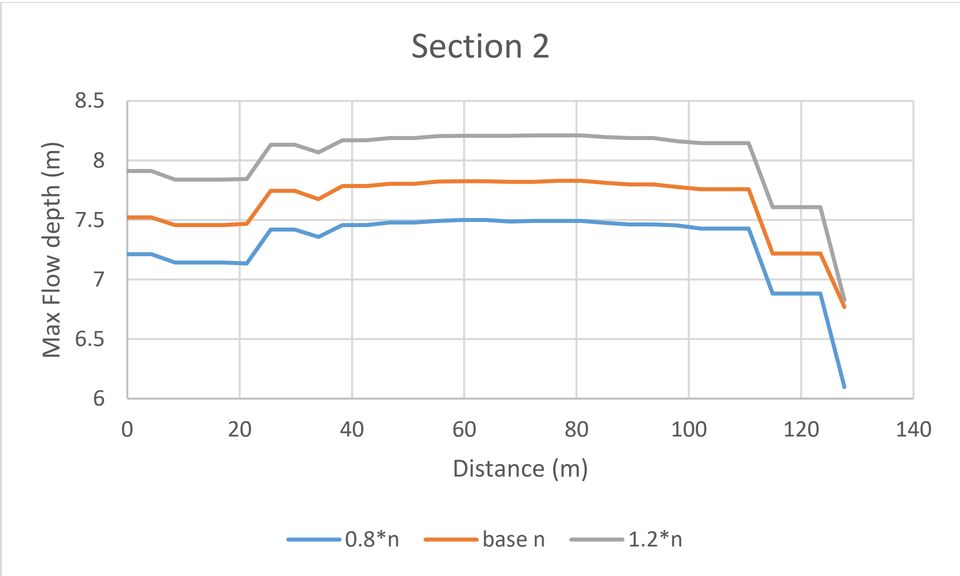

Figure 5-62 Change in Max flow depth with roughness values at Section-2 (FLO-2D, S1)

These graphs display the sensitivity of the FLO-2D model to the roughness values. It shows that an increase in roughness values from 0.8* n t0 1.2*n results in an increase in flow depth.

5.4.3 Sensitivity of Breach Hydrograph

In this segment, flood routing simulations are carried out at 5 m grid resolution using the breach hydrographs S2 and S3 along with the calibrated roughness values in both models. The results are presented in terms of comparison of flow depth with S1 breach hydrograph.

HEC-RAS:

Table 5-31 shows the inundation area calculated by HEC-RAS at 5 m grid resolution for S1, S2, and S3 breach hydrographs.

Table 5-31 Avcıdere Dam inundation area (HEC-RAS) for breach hydrographs (S1, S2, and S3)

Breach Hydrograph	Inundation Area (m^2)
S1	1138372
S2	935825
S3	819581

Figure 5-63 and Figure 5-64 shows the comparison of simulated flow depth for S1, S2, and S3 breach hydrographs at the selected section for HEC-RAS simulations at 5 m grid size.

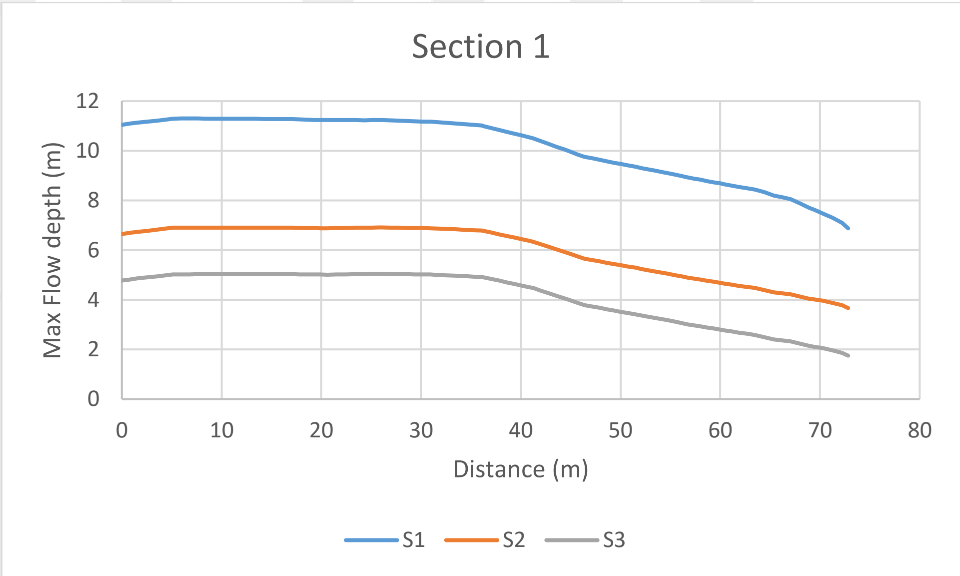

Figure 5-63 Change in Max flow depth with breach hydrograph at Section-1 (HEC-RAS)

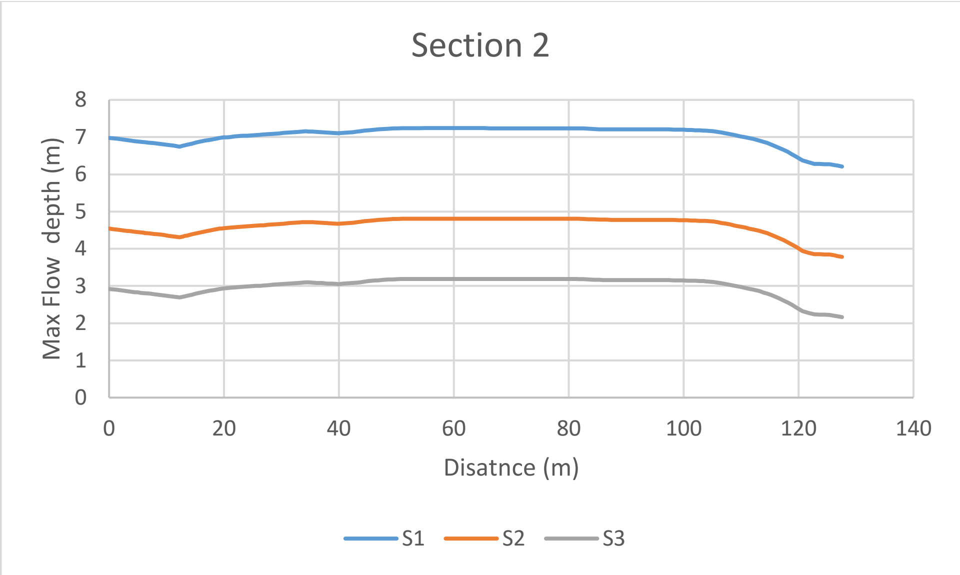

Figure 5-64 Change in Max flow depth with breach hydrograph at Section-2 (HEC-RAS)

From the graphs it can be seen that as flow depth at both the sections is quite sensitive to the breach hydrograph peak flow. The smaller the peak flow, the smaller the calculated flow depth and vice versa.

FLO-2D:

Table 5-32 shows the inundation area for FLO-2D at 5 m grid resolution for S1, S2, and S3 breach hydrographs.

Table 5-32 Avcıdere Dam inundation area (FLO-2D) for breach hydrographs (S1, S2, and S3)

Breach Hydrograph	Inundation Area (m^2)
S1	1199500
S2	1050425
S3	861225

Figure 5-65 and Figure 5-66 show the comparison of flow depth for S1, S2, and S3 breach hydrographs at the selected section for FLO-2D simulations at 5 m grid size.

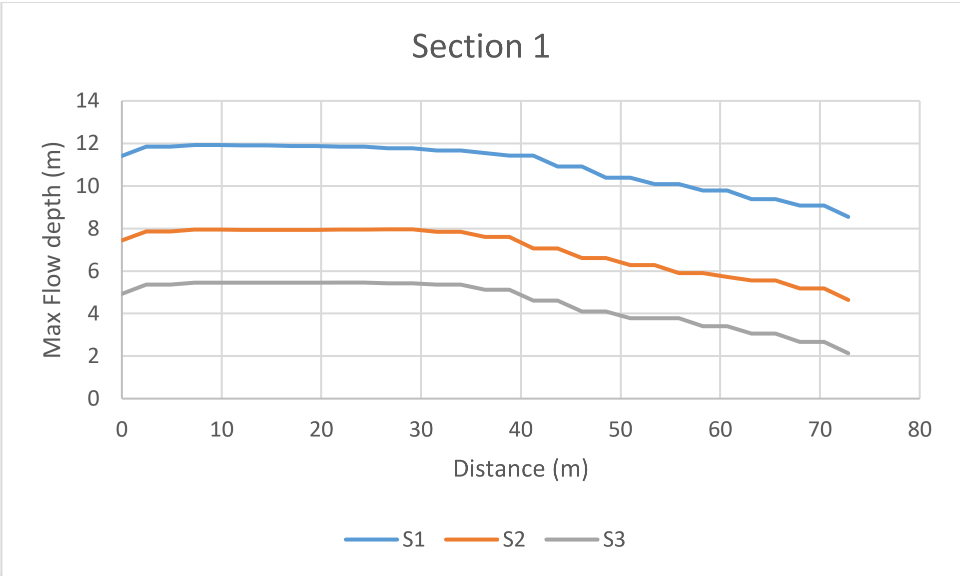

Figure 5-65 Change in Max flow depth with breach hydrograph at Section-1 (FLO-2D)

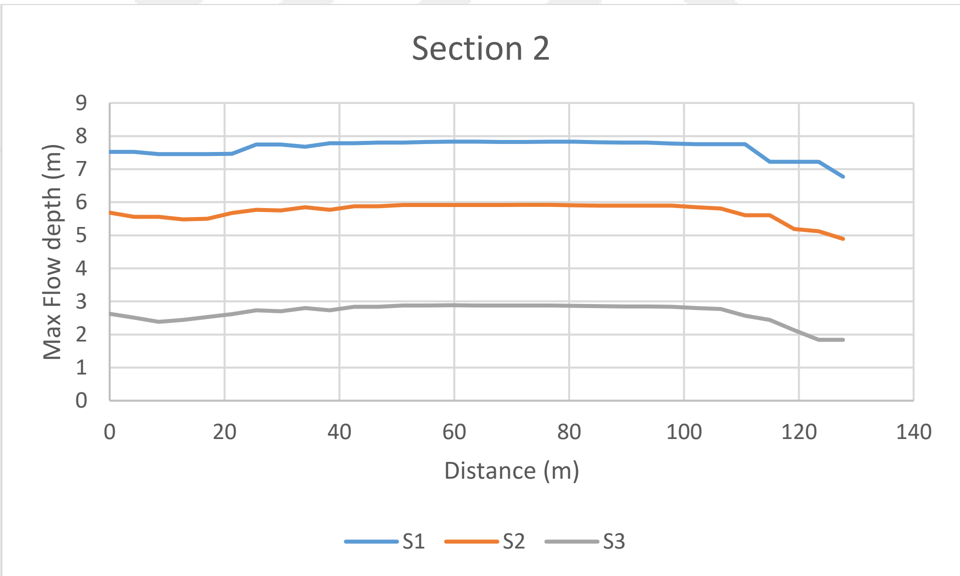

Figure 5-66 Change in Max flow depth with breach hydrograph at Section-2 (FLO-2D)

The graphs show that as the calculated flow depth at both of the sections is directly proportional to peak flows of the breach hydrographs. As the peak flow is decreasing from S1 to S3, the flow depth is also decreasing. It can said that the inundation results are very much sensitive to the breach peak flows.

5.5 Flood Hazard Maps

In this study, Flood hazard maps were prepared using Mapper ++ software which is provided along with the FLO-2D pro Model. The method used to develop hazard maps is based on (García et al, (2003, 2005)).

At a specific location, flood hazard level is a function of flood probability (Frequency) and intensity. Flood frequency is inversely proportional to the magnitude of flood. The frequency of occurrence of large floods is low. Flood intensity is determined by the flow depth and Velocity.

The flood hazard map consists of three hazard levels high, medium, and low. The high hazard level (red) shows the area in which the population is at risk both inside and outside of the houses. There is a possibility of buildings being destroyed. In medium hazard level area (orange) the person outside of their houses are in danger and structures may be destroyed or suffer damage based on construction characteristics. In low hazard area (yellow), there is very low or no danger to the population, and the structure might suffer little damages.

5.5.1 Flood Hazard Maps for Ondokuz Mayıs Dam Breach

Flood hazard maps obtained from each breach scenario are presented. The hazard maps shown in Figure 5-67 to Figure 5-69 are based on the results of breach hydrograph modeling for S1, S2, and S3 at a grid size of 5 m. The blue lines show the densely populated areas in Ondokuz Mayıs District.

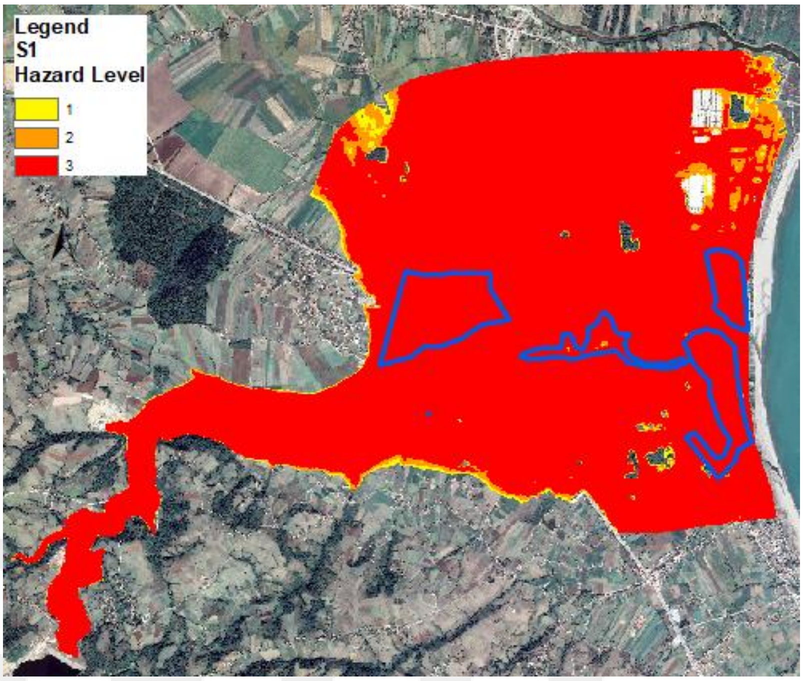

Figure 5-67 Flood hazard map for Ondokuz Mayıs Dam (S1)

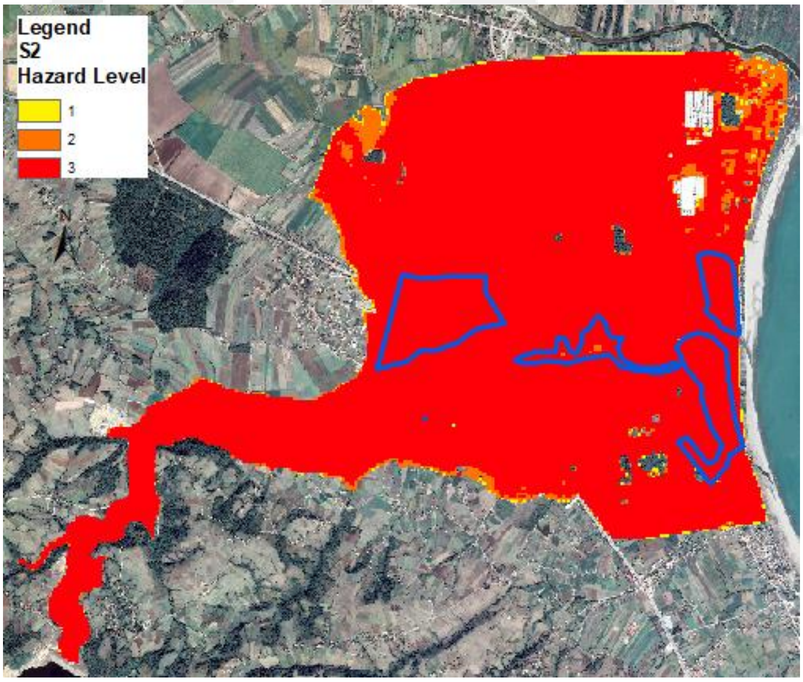

Figure 5-68 Flood hazard map for Ondokuz Mayıs Dam (S2)

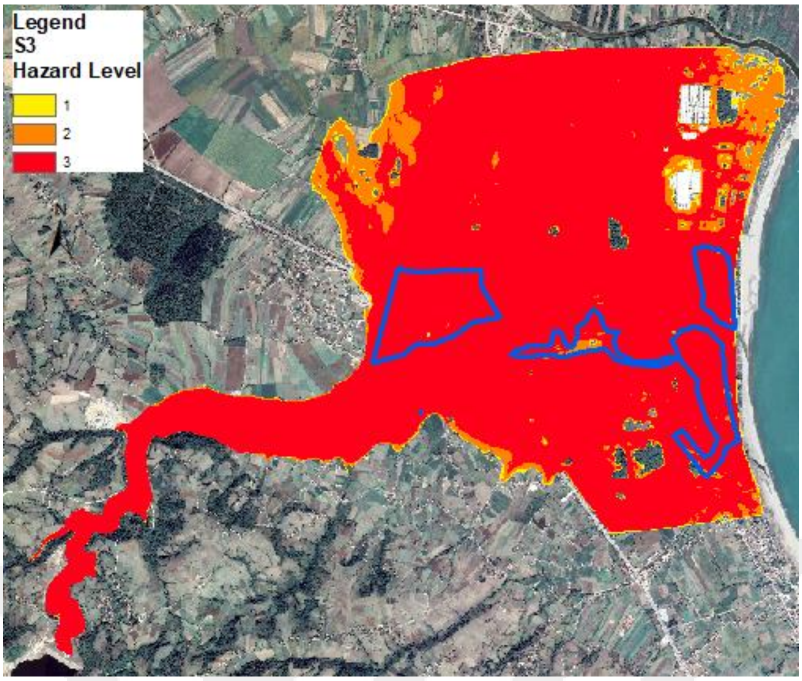

Figure 5-69 Flood hazard map for Ondokuz Mayıs Dam (S3)

The flood hazard maps shows that the Ondokuz Mayıs District is at high hazard level in case of breach of Ondokuz Mayıs Dam for all three breach scenarios. The population of the Ondokuz Mayıs District should be educated about the danger and emergency action plans should be developed for minimizing the losses which can occur in case of any mishap.

5.5.2 Flood Hazard Maps for İhsaniye Dam Breach

Figure 5-70 to Figure 5-72 shows the flood hazard maps developed for the İhsaniye Dam breach. These maps are based on the results of dam breach simulation for S1, S2, and S3 failure scenarios at 5 m grid size. The blue polygon represents the Yalakdere town boundary.

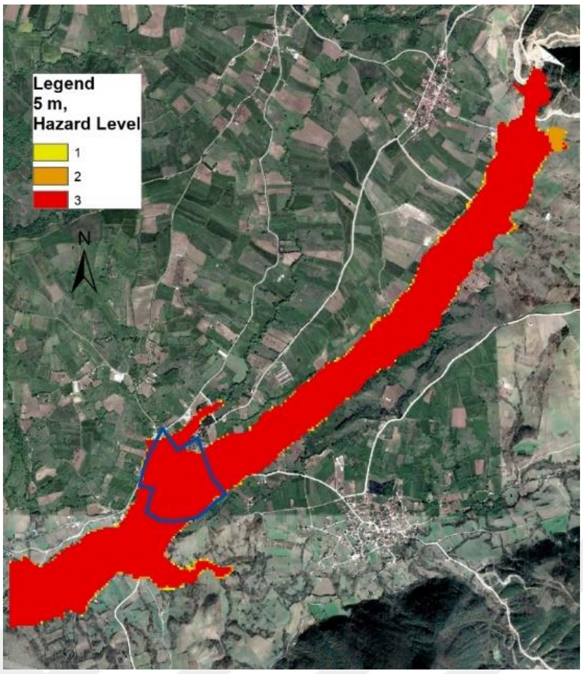

Figure 5-70 Flood hazard map for İhsaniye Dam (S1)

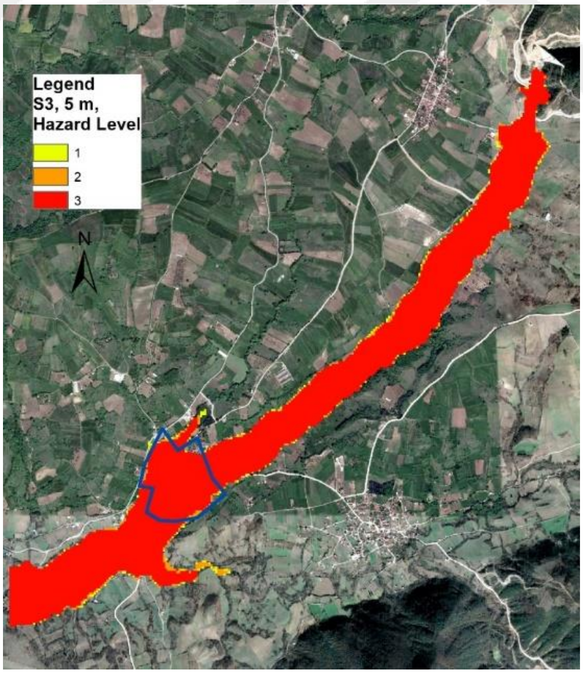

Figure 5-71 Flood hazard map for İhsaniye Dam (S2)

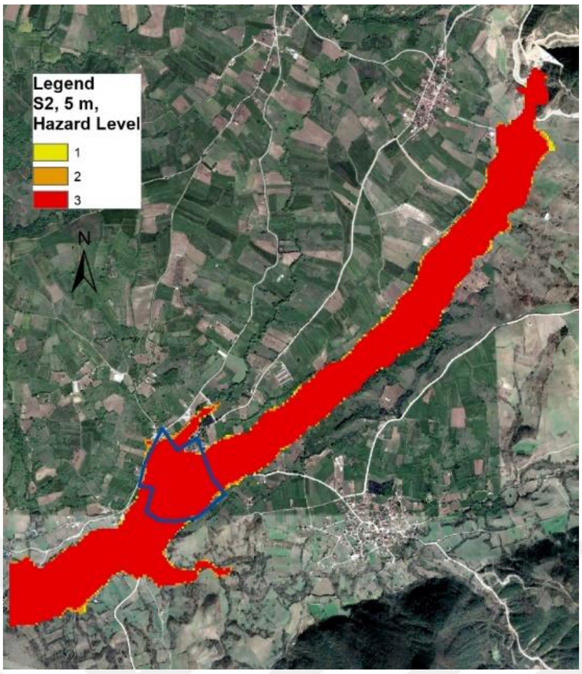

Figure 5-72 Flood hazard map for İhsaniye Dam (S3)

The flood hazard maps show that almost all of the Yalakdere town is at a high hazard level in case of the İhsaniye Dam breach. The residents of the Yalakdere town should be educated about the danger and action plans to take in case of emergency so that precious lives can be saved.

5.5.3 Flood Hazard Map for Avcıdere Dam Breach

In the case of Avcıdere Dam failure, flood hazard maps were developed from the simulation results for S1, S2, and S3 failure scenarios at 5 m grid resolution, as can be seen in Figure 5-73 to Figure 5-75. The blue polygon on the right side is the Avcıköy town, while the polygon on the left side is the Yalakdere town.

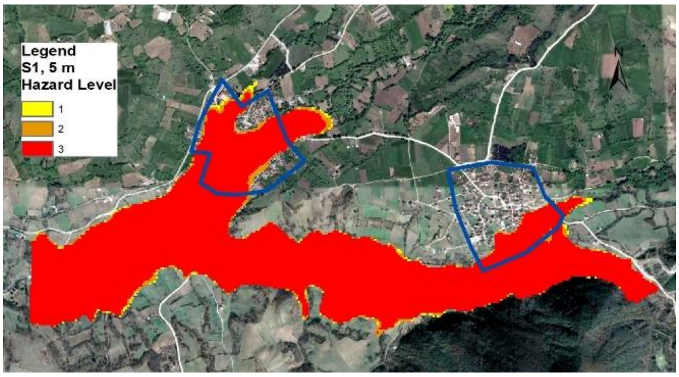

Figure 5-73 Flood hazard map for Avcıdere Dam (S1)

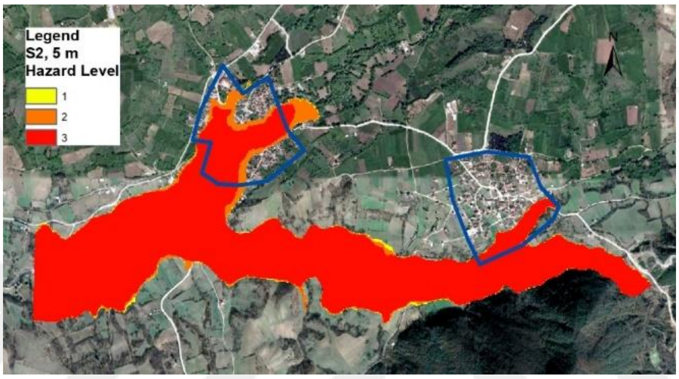

Figure 5-74 Flood hazard map for Avcıdere Dam (S2)

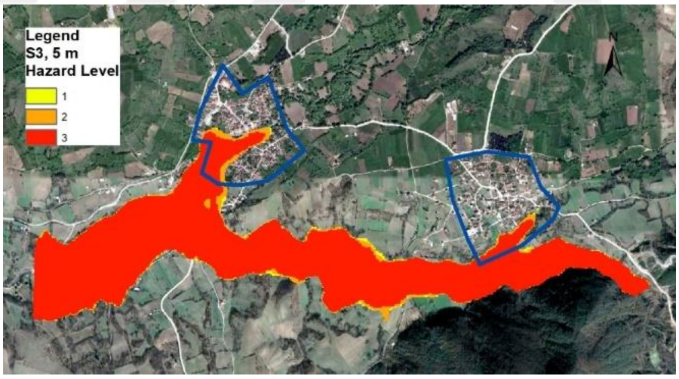

Figure 5-75 Flood hazard map for Avcıdere Dam (S3)

It can be seen in flood hazard maps that for all the three breach hydrographs, the population in the towns of Avcıköy and Yalakdere are at a high hazard level, especially the residents of the southern part of both towns which is closer to the Avci

Creek. The population should be educated about the danger and emergency action plans, so that precious lives can be saved.

5.6 Flood Damages Calculation

Flood inundation boundary and the water depth information obtained from flood routing simulations of dam-break were used in the calculation of the flood damages. In this study, damage calculations were made for the buildings and agriculture as discussed below.

5.6.1 Flood Damages for Buildings

In order to calculate the flood damages for buildings, the area of buildings that are affected by the flood is required. The type of building i.e., housing, commercial, industrial is helpful in determining the correct values of the economic losses. In this study, the calculations are made by considering all the buildings in the affected area as residential buildings. The building located in the inundation boundary are digitized and their area is calculated using GIS software. After calculating the building area, the maximum flow depth surrounding the buildings is taken for flood modeling results. The flood damages are then calculated using the methodology discussed in Section 4.7.1.1. The calculated flood damages for buildings are:

Ondokuz Mayıs Dam: The number of buildings in the flooded area for Ondokuz Mayıs Dam is calculated to be 2818 (The building area calculated using GIS software is 834,245 m^2) from the GIS software. Using the maximum flow depth, the damages were calculated for the areas accordingly. For S1, the flood damage to buildings is estimated to be about 288,099,829 Tl. For S2 it is about 258,331,562 Tl and S3 it is 212,628,144 Tl.

İhsaniye Dam: The number of buildings in the flooded area of İhsaniye Dam is 325 (36855 m^2). The damages caused to the building by S1 were 13,355,007 Tl, by S2 12,722,691 Tl, and by S3 is 11,792,434 Tl.

Avcıdere Dam: For Avcıdere Dam, the number of buildings in the flooded area is 282 (31911 m^2). The calculated flood damages caused to the building by S1 were 10,386,703 Tl, for S2 is 9,506,950 Tl, and for S3, is 8,528,891 Tl.

5.6.2 Flood Damages for Agriculture

The calculation of flood damages for agriculture depends upon a lot of factors, such as type of crop, age of crop, duration of the flood, flood depths, etc. In dam-break scenarios, there are larger flows in a short period of time which can be quite dangerous for both short-term and long-term crops. For the flood Damage calculation, it is assumed that both long-term and short-term crops are 100% affected by the dam breach floods and calculations re made accordingly.

In the Ondokuz Mayıs District, there are different types of crops such as rice, hazelnuts, vegetable (pepper, tomato, eggplant, cucumber, beans), watermelon, and some other types of fruits. In this study, flood damages are calculated based on the most valuable crops in the area i.e., Rice and Hazelnuts. For the year 2020, from TURKSTAT website, the income from long-term products is about 1745 Tl per 1000 m^2. For rice, the income is about 2238 Tl per 1000 m^2 (TURKSTAT, 2020). According to the flood modeling simulation results, the inundated area covers about 13,241,385 m^2 of cultivated area. Flood damage calculations were made for rice crops and hazelnut crops. Total damages to agriculture were calculated to be 26,630,696 Tl.

For the İhsaniye Dam breach, about 392,206 m^2 of the cultivated area is under floodwater. In this area, dry beans are cultivated, so the flood damage calculation is done with the assumption the whole area is covered with a fully mature dry beans crop. For dry beans, the price per 1000 m^2 of the crop is 4444 Tl (TURKSTAT, 2020). The calculated flood damages for dam breach are 1,743,220 Tl.

For the Avcıdere Dam breach, 87,937 m^2 of the cultivated area is underwater and the flood damages calculated in terms of loss to dry beans crop will be 390,849 Tl.

5.7 Dam-Break Risk Management

Over the years the safety of dams has increased due to progress made in engineering knowledge and the better quality of construction, but even then dam failure can occur, prompted by natural hazards, human actions or several other factors. For the protection of the population, economic and environmental resources along the downstream valley, dam-break risk management is promoted by the concerned authorities through safety legislation and technical guidelines.

In dam-break risk assessment, there are two important phases: First is the prediction of the likelihood of dam failure and the associated losses through risk assessment, and the second one is finding suitable mitigation measures with the main purpose to reduce the loss of life and downstream damages resulting from dam failure through both structural and non-structural measures.

The mitigation measures include the steps taken to reduce the probability of occurrence of dam failure by applying structural measures such as strengthening of the dam body, and non-structural measures, which are usually linked with the safety of dam and monitoring control systems. Emergency action plans, a non-structural measure can be developed to reduce the vulnerability of the downstream valley population. The emergency action plan is prepared for the pre-emergency phase of the disaster management cycle. It highlights the potential emergency conditions at the dam and presents the action to be taken to reduce the loss of life and property.

The first mandatory step during emergency events is the detection of a real problem that can affect the dam safety. The dam safety monitoring systems along with the visual inspection of dam body are the key aspects in the detection of a problem. After an emergency is encountered or reported, the responsible person at dam should classify the scale of the emergency level and alert the concerned authorities using the notification system. Depending upon the scale of emergency level, the population in the risk area is warned using warning systems. The warning system is commonly implemented to minimize the impact caused by floods on the population in the most dangerous zones of the downstream areas. It also plays a vital role in crisis management and helps in reducing the risk. In densely populated areas, which are at higher risk, a warning system based on sirens should be envisaged. For areas with a small population and located outside of the dangerous zone, the use of load speakers and personal warnings can be envisaged. Television and radio networks are also very effective means to inform the public during an emergency. No single warning system is enough to meet the desired outcome as each system has its own advantages and disadvantages. The main aspect to be considered is the reliability of the warning system and the surety that the message is clearly understood by the public. Evacuation plans should also be devised as it helps to relocate people to safer areas in case of any hazard. The success of evacuation plans greatly depends upon the level of organization, preparedness, testing and public awareness in a crisis context. The strategies for risk communication need to be properly selected, tested, and effectively implemented.

In this study, the downstream area of all the three dams i.e., Ondokuz Mayıs Dam, İhsaniye Dam, Avcıdere Dam, are at a high hazard level and there is a serious risk to the population in these areas. The population living in Ondokuz Mayıs District, Yalakdere Town, and Avcıköy Town should be educated about the emergency action plans, so that in case of any accident loss of lives and property can be avoided.

CHAPTER 6

SUMMARY AND CONCLUSIONS

6.1 Summary and Conclusions

In this study, the dam-break analysis of Ondokuz Mayıs Dam, İhsaniye Dam, and Avcıdere Dam was done using HEC-RAS and FLO-2D models. The hydrological and hydraulic data needed for the breach modeling was collected from DSI. The point elevation data was obtained from Tapu Kadastro and DSI at a scale of 1/5000. The elevation data was converted into DEM of 5 m resolution using the inverse distance weighing interpolation methods in ARC GIS. The land use roughness values were selected using a model calibration study for Engiz Creek in Ondokuz Mayıs Dam, and the roughness values for İhsaniye Dam and Avcıdere Dam, downstream terrain were taken by analyzing the Google Earth images.

For Ondokuz Mayıs Dam, a quality check of the elevation data is done by comparing the Tapu Kadastro data with the DSI data. The point elevation data was converted into DEM using the interpolation methods available in the Spatial Analyst tool of the ARC GIS software. The cross-section obtained from the DEM of Tapu Kadastro and DSI were compared. It was observed that both data sets give consistent elevation profiles for relatively flat terrain, and significant differences were observed for cross-sections located in the hilly region. So, for better representation of the terrain in the hilly region, a new DEM was developed using the elevation data of both Tapu Kadastro and DSI. This DEM was then used in the model calibration of Engiz Creek.

The model calibration for the Engiz Creek against the available flow measurement data at gauging station D15A026 on Engiz Creek, located upstream of Ondokuz Mayıs District. For the model calibration, the maximum flow rate of 211 m^3/sec observed in the year 2010 was selected and a flow depth of 2.735 m was taken from the provided rating curve of the gauging station. The inflow hydrograph with a for model calibration was obtained using breach parameters at dam location, so that the maximum flow passing through the gauging station is close to 211 m^3/sec. After obtaining the inflow hydrograph, calibration simulations were carried out by changing the roughness values with the hit and trail method, until the desired gauging station flow depth is obtained. These calibrated roughness values along with the DEM from Tapu Kadastro and DSI data were then used in breach hydrograph routing simulations of Ondokuz Mayıs Dam.

The breach hydrograph for the three dams was obtained from HEC-RAS. The reservoirs are modeled with dynamic wave routing as a 2D flow area. For each dam, three different sets of breach parameters were used along with overtopping and piping failure modes to obtain the breach hydrographs. The breach hydrographs were categorized as S1, S2, and S3. S1 being the worst case with the highest peak flow in the shortest time, S2 being the average case with peak flow and time to peak in between S1 and S3, while S3 has the smallest peak flow and is slowest to peak among the three hydrographs. For Ondokuz Mayıs Dam, the resulting peak flows for S1, S2, and S3 breach hydrographs are 62592 m^3/sec, 50993 m^3/sec, and 22179 m^3/sec, for İhsaniye Dam it is 13535 m^3/sec, 10584 m^3/sec, and 8485 m^3/sec and for Avcıdere Dam it is 19758 m^3/sec, 10587 m^3/sec, 6324 m^3/sec, respectively. These breach hydrographs were then used as an inflow hydrograph into the flood routing over the downstream terrain in HEC-RAS and FLO-2D.

From the breach hydrograph routing results for the Ondokuz Mayıs Dam breach, it was observed that for S1 breach hydrograph, the flood wave takes about 22 min to reach the Ondokuz Mayıs District (located at 7 km from the dam), for S2 about 33 min, and for S3 about 55 min. The maximum depth and its arrival time at the district are 10.11 m in approximately 30 min for S1, 9.10 m in 48 min for S2, and 7.35 m in 98 min for S3.

For the İhsaniye Dam breach, the comparison of flow depth at selected sections shows that FLO-2D is calculating higher flow depths with a slower arrival time than HEC-RAS. The flood wave resulting from İhsaniye Dam breach takes about 12 min to reach the Yalakdere town (located at 3.5 km from the dam) for S1 hydrograph, 16 min for S2, and 19 min for S3. The maximum depth and arrival time at Yalakdere town for breach hydrograph S1 is 12.57 m in 15 min, for S2 11.76 m in 20 min, and for S3 10.92 m in 26 min.

For the Avcıdere Dam breach it was found that two towns, Avcıköy and Yalakdere will be affected, Avcıköy town is located 1 km from the dam on the right bank of Avci creek and Yalakdere town is located 3 km from the dam also on the right side of Avci Creek. The breach flood wave from the dam will take about 9 min to reach Avcıköy Town for S1 hydrograph, 13 min for S2, and 29 min for S3. For Yalakdere town, the flood wave will take about 16 min for the S1 hydrograph, 23 min for S2, and 41 min for S3. The maximum depth and its arrival time at Avcıköy town for breach hydrograph S1 are 11.30 m in 21 min, for S2 is 6.90 m in 33 min, and for S3 is 5.02 m in 62 min. For Yalakdere town, the maximum depth and its arrival time for S1 breach hydrograph is 7.23 m in 28 min, for S2 is 4.80 m in 39 min, and for S3, 3.18m in 68 min.

The comparison for flow depth was made for 5 m grid resolution for both HEC-RAS and FLO-2D. For the Ondokuz Mayıs Dam study, it was seen that the calculated flow depth profiles were approaching each other, with FLO-2D calculating higher depth than HEC-RAS at Sections 1, 4, and 5, while HEC-RAS calculating higher depths at Section 2 and 3. For the İhsaniye Dam study, it was observed that FLO-2D calculated a higher flow depth than the HEC-RAS at both sections, and both flow depth profiles are approaching each other.

For the Avcıdere Dam study, it was seen that there are significant differences in the calculated flow depth of both models, with FLO-2D calculating significantly higher flow depths in comparison to HEC-RAS at both sections.

The results obtained from the sensitivity of grid resolution analysis from both models for all the three types of terrains (for Ondokuz Mayıs Dam: first a meandering channel in hilly terrain then a relatively flatter terrain, for İhsaniye Dam: a straight valley, for Avcidre Dam: a meandering channel in hilly terrain) show that FLO-2D is more sensitive to grid resolution than HEC-RAS. In HEC-RAS calculated flow depths at coarser resolution are consistent with the finer resolution, while in FLO-2D, significant differences are observed in calculated flow depths for coarser resolutions. Therefore, proper care should be taken in the selection for grid resolution. The results of the sensitivity of roughness values and breach hydrograph show that both HEC-RAS and FLO-2D are quite sensitive to change in the roughness values and breach hydrograph.

Flood hazard maps show that for Ondokuz Mayıs Dam breach: Ondokuz Mayıs District, and the adjoining population downstream of the district will be at high hazard level, for İhsaniye Dam breach: Yalakdere Town will be at a high hazard level, and for Avcıdere Dam breach: all of Yalakdere town and southern part of Avcıköy town will be at high hazard level.

The flood damages calculation was done for the damages to the building and agricultural product, based on the calculated flow depth for each area. The total calculated flood damages for the Ondokuz Mayıs Dam breach were approximately 314 million Turkish Lira. For the İhsaniye Dam breach, the calculated flood damages were approximately 15 million Turkish Lira. For the Avcıdere Dam breach, flood damages were calculated to be approximately 10 million Turkish Lira.

6.2 Recommendations

Based on the study, it can be recommended that there is an urgent need to develop a warning system and emergency action plan in all three study areas, as the downstream population is at a high hazard level. The responsible authorities at the dam must be efficient in identifying any problem, so that the warning can issues timely, and also through public awareness programs, the public should be educated about the evacuation plans, save evacuation spots, escape directions and evacuation routes, so that in the unfortunate incident of dam failure, precious lives can be saved.

HEC-RAS model can be used for future studies as it gives consistent results at coarser resolution in comparison to FLO-2D, while in the case of FLO-2D proper care must be taken while using coarser resolutions.

REFERENCES

Akkaya, U., & Doğan, E. (2016). Generation of 2D flood inundation maps of Meriç and Tunca Rivers passing through Edirne city center. *Geofizika*, *33*(1), 15–34. https://doi.org/10.15233/gfz.2016.33.7

Almeida, A. B., & Viseu, T. (1997). *Dams and valley safety: a present and future challenge, Dams and safety management in downstream valleys* ((eds A.B.). Rotterdam: A.A. Balkema.

Anees, M. T., Abdullah, K., Nawawi, M. N. M., Ab Rahman, N. N. N., Piah, A. R. M., Zakaria, N. A., … Mohd. Omar, A. K. (2016). Numerical modeling techniques for flood analysis. *Journal of African Earth Sciences*, *124*, 478–486. https://doi.org/10.1016/j.jafrearsci.2016.10.001

Babister, M., Ball, J., Barton, C., Bishop, W., Gray, S., Jones, R. H., … Weeks, B. (2012). Australian Rainfall & Runoff Revision Project 15: Two dimensional Modelling in Urban and Rural Floodplains. In *AR&R Report Number P15/S1/009*.

Bates, P. D., & De Roo, A. P. J. (2000). A simple raster-based model for flood inundation simulation. *Journal of Hydrology*, *236*(1–2), 54–77. https://doi.org/10.1016/S0022-1694(00)00278-X

Beden, N., Demir, V., Alrayess, H., & Ulke, A. (2018). Comparison of 2D hydraulic models for flood simulation on the mert river Turkey. *5th International Symposium on Dam Safety*, (December), 489–496.

Bozkuş, Z., & Güner, A. I. (2001). Pre-event dam failure analyses for emergency management. *Turkish Journal of Engineering and Environmental Sciences*, *25*(6), 627–641.

Bozkuş, Z., & Bağ, F. (2011). Virtual Failure Analysis of the Çınarcık Dam. *Teknik Dergi/Technical Journal of Turkish Chamber of Civil Engineers*, *22*(4), 5675–5688.

Bozkuş, Z., & Kasap, A. (1998). Comparison of physical and numerical dam-break simulations. *Turkish Journal of Engineering and Environmental Sciences*, *22*(5), 429–443.

Brunner, G. W. (2014). Using HEC-RAS for Dam Break Studies, TD-39. *Us Army Corps of Engineers Hydrologic Engineering Center (Hec)*, (August), 74.

Brunner, G. W. (2016). *HEC-RAS 5.0 Hydraulic Reference Manual Version 5.0*. Davis, CA: Hydrologic Engineering Center.

Brunner, G. W. (2018). *Benchmarking of the HEC-RAS Two-Dimensional Hydraulic Modeling Capabilities*. (April), 151.

Casulli. (2008). A high-resolution wetting and drying algorithm for free-surface hydrodynamics. *International Journal for Numerical Methods in Fluids*, *60*(2009), 391–408. https://doi.org/10.1002/fld

Chinnarasri, C., Jirakitlerd, S., & Wongwises, S. (2004). Embankment dam breach and its outflow characteristics. *Civil Engineering and Environmental Systems*, *21*(4), 247–264. https://doi.org/10.1080/10286600412331328622

Chow, V. . (1959). *Open Channel Hydraulics*, p. 680 p. New York: McGraw-Hill.

Compass PTS JV. (2019). *Rapid Response Flood Modeling Final Report*. Washington, DC.

Costa, J. E. (1985). Floods from dam failures. *Flood Geomorphology*, 439–463.

Dimitriadis, P., Tegos, A., Oikonomou, A., Pagana, V., Koukouvinos, A., Mamassis, N., … Efstratiadis, A. (2016). Comparative evaluation of 1D and quasi-2D hydraulic models based on benchmark and real-world applications for uncertainty assessment in flood mapping. *Journal of Hydrology*, *534*, 478–492. https://doi.org/10.1016/j.jhydrol.2016.01.020

DRIP. (2018). *Guidelines for Mapping Flood Risks Associated with Dams*. Central Water Commission Ministry of Water Resources, River Development & Ganga Rejuvenation Government of India, New Dehli.

DSI. (2013). Ondokuz Mayıs Dam reports. State Hydralics Works, Ankara, Turkey.

Environment Agency. (2018). *Preliminary Flood Risk Assessment for England*. Retrieved from https://www.gov.uk/government/publications/preliminary-flood-risk-assessment-for-england

Falter, D., Vorogushyn, S., Lhomme, J., Apel, H., Gouldby, B., & Merz, B. (2013). Hydraulic model evaluation for large-scale flood risk assessments. *Hydrological Processes*, *27*(9), 1331–1340. https://doi.org/10.1002/hyp.9553

Farooq, M., Shafique, M., & Khattak, M. S. (2019). Flood hazard assessment and mapping of River Swat using HEC-RAS 2D model and high-resolution 12-m TanDEM-X DEM (WorldDEM). *Natural Hazards*, *97*(2), 477–492. https://doi.org/10.1007/s11069-019-03638-9

Federal Energy regulator Commission (FERC). (1988). *USA Federal Regulatory Commission – Notice of Revised Emergency Action Plan Guidelines*, *Federal Energy Regulatory Commission (FERC)*. Washington, DC.

FEMA. (2004a). Federal Guidelines for Dam Safety: Hazard Potential Classification System for Dams, Washington, DC: FEMA. Retrieved from http://www.fema.gov/library/viewRecord.do?id=1828.

FEMA. (2004b). *Federal Guidelines for Dam Safety: Selecting and Accommodating Inflow Design Floods for Dams (FEMA 94).* Washington, DC: FEMA.

FEMA. (2013). *Federal Guidelines for Inundation Mapping of Flood Risks Associated with Dam Incidents and Failures.* (Vol. 3).

FEMA. (2017). *Technical Advisory: Risk Reduction Measures for Dams*.

Fletcher, C.A.J. (1990). *Computational Techniques for Fluid Dynamics, Volume I, 2nd ed.,*. Springer-Velag, New York.

Forest, M. (2020). HEC-RAS Sub-grid Bathymetry Theory and Application. Retrieved December 13, 2020, from hecrasmodel.blogspot.com/search/label/Leaking

Foster, M. A., Fell, R., & Spannagle, M. (1998). Analysis of embankment dam incidents. In *UNICIV Rep. No. R-374*.

Fread, D. (1988). *BREACH: An Erosion Model for Earthen Dam Failures. Technical report*.

Fread, D. L. (1989). National Weather Service Models to Forecast Dam-Breach Floods. *Hydrology of Disasters*, pp. 192–211.

Froehlich, D. C. (1995). Peak outflow from breached embankment dam. *Journal of Water Resourses Planning and Management*, *121(1)*, 90–97.

Funnemark, E. et al. (1998). Consequence analysis of dam breaks. *Proceedings of the International Symposium on New Trends Guidelines on Dam Safety (Ed L. Berga)*, 329–336. A.A. Balkema, Rotterdam.

García-Martínez, R., & López, J. L. (2005). Debris flows of December 1999 in Venezuela. In *Debris-flow Hazards and Related Phenomena* (pp. 519–538). https://doi.org/10.1007/3-540-27129-5_20

Garcia, R., López, J. L., Noya, M., Bello, M. E., Bello, M. T., González, N., … O'Brien, J. S. (2003). Hazard mapping for debris-flow events in the alluvial fans of northern Venezuela. *International Conference on Debris-Flow Hazards Mitigation: Mechanics, Prediction, and Assessment, Proceedings*, *1*, 589–599.

Gee, D. M. (2009). Comparison of dam breach parameter estimators. *Proceedings of World Environmental and Water Resources Congress 2009 - World Environmental and Water Resources Congress 2009: Great Rivers*, *342*, 3360–3369. https://doi.org/10.1061/41036(342)339

George, A. C., & Nair, B. T. (2015). Dam Break Analysis Using BOSS DAMBRK. *Aquatic Procedia*, *4*(Icwrcoe), 853–860. https://doi.org/10.1016/j.aqpro.2015.02.107

Haltas, I., Elçi, S., & Tayfur, G. (2016). Numerical Simulation of Flood Wave Propagation in Two-Dimensions in Densely Populated Urban Areas due to Dam Break. *Water Resources Management*, *30*(15), 5699–5721. https://doi.org/10.1007/s11269-016-1344-4

Haltas, I., Tayfur, G., & Elci, S. (2016). Two-dimensional numerical modeling of flood wave propagation in an urban area due to Ürkmez dam-break, İzmir, Turkey. *Natural Hazards*, *81*(3), 2103–2119. https://doi.org/10.1007/s11069-016-2175-6

Horritt, M. S., Bates, P. D., (2001). Effects of spatial resolution on a raster based model of flood flow. *Journal of Hydrology*, *253(1-4)*,.

Horritt, M. S., Bates, P. D., & Mattinson, M. J. (2006). Effects of mesh resolution and topographic representation in 2D finite volume models of shallow water fluvial flow. *Journal of Hydrology*. https://doi.org/10.1016/j.jhydrol.2006.02.016

Horritt, M. S., Bates, P. D., (2002). Evaluation of 1D and 2D numerical models for predicting river flood inundation. *Journal of Hydrology*, *268*(6), 87–99.

ICOLD. (1998a). *Dam-Break Flood Analysis – Review and Recommendations. Bulletin 111*. Paris.

ICOLD. (1998b). *World Register of Dams*. Paris.

Issakhov, A., & Imanberdiyeva, M. (2019). Numerical simulation of the movement of water surface of dam break flow by VOF methods for various obstacles. *International Journal of Heat and Mass Transfer*, *136*, 1030–1051. https://doi.org/10.1016/j.ijheatmasstransfer.2019.03.034

Jam, S., & Engle, S. (2012). *Guidance for 2-Dimensional Model Development in Riverine Systems*. Urban Drainage and Flood Control District, South Jamaica Strret Englewoo.d CH2M HILL, INC.

Jin, M., & Fread, D. L. (1997). Dynamic Flood Routing with Explicit and Implicit Numerical Solution Schemes. *Journal of Hydraulic Engineering*, *123*(3), 166–173. https://doi.org/10.1061/(asce)0733-9429(1997)123:3(166)

Kalinina, A., Spada, M., Marelli, S., Burgherr, P., & Sudret, B. (2016). Uncertainties in the risk assessment of hydropower dams: state-of-the-art and outlook. *ETH Zurich*, (CH-8093 ZURICH).

Khosravi, K., Rostaminejad, M., Cooper, J. R., Mao, L., & Melesse, A. M. (2019).

Dam break analysis and flood inundation mapping: The case study of Sefid-Roud Dam, Iran. In *Extreme Hydrology and Climate Variability: Monitoring, Modelling, Adaptation and Mitigation*. https://doi.org/10.1016/B978-0-12-815998-9.00031-2

Kiyici, E. (2019). Sensitivity analysis of 2-D flood inundation model LISFLOOD-FP with respect to spatial resolution and roughness parameter, (MSc Thesis), Department of Civil Engineering METU, Ankara

Luo, Y., Chen, L., Xu, M., & Tong, X. (2012). Review of dam-break research of earth-rock dam combining with dam safety management. *Procedia Engineering*, *28*(2011), 382–388. https://doi.org/10.1016/j.proeng.2012.01.737

MacDonald, T. and J. L.-M. (1984). Breaching characteristics of dam failures. *J. Hydraul. Eng*, (110(5)), 567–586.

FLO 2D Reference Manual. (2012). *FLO-2D Reference Manual*.

Manville, V. (2001). *Techniques for evaluating the size of potential dam-break floods from natural dams*. Lower Hutt: Institute of Geological & Nuclear Sciences.*Institute of Geological & Nuclear Sciences science report 2001/28* 72 p.

Meyer V, M. F. (2005). *National Flood Damage Evaluation Methods, A Review of Applied Methods in England, the Netherlands, the Czech Republic and Germany,.*

Morales-Hernández, M., Petaccia, G., Brufau, P., & García-Navarro, P. (2016). Conservative 1D-2D coupled numerical strategies applied to river flooding: The Tiber (Rome). *Applied Mathematical Modelling*, *40*(3), 2087–2105. https://doi.org/10.1016/j.apm.2015.08.016

Néelz, S., & Pender, G. (2009). *Desktop Review of 2D Hydraulic Modelling Packages. DEFRA/Environment Agency, UK.*

Ongdas, N., Akiyanova, F., Karakulov, Y., Muratbayeva, A., & Zinabdin, N. (2020). Application of hec-ras (2d) for flood hazard maps generation for yesil (ishim) river in Kazakhstan. *Water (Switzerland)*, *12*(10), 1–20. https://doi.org/10.3390/w12102672

Parker, D. J., Green, C. H., & Thompson, P. M. (1987). *Urban flood protection benefits: A project appraisal guide*. Aldershot, UK: Gower Technical Press.

Penning-Rowsell E C, Johnson C, Tunstall S, Tapsell S, M. J., & Chatterton J, Coker A, G. C. (2003). *The Benefits of flood and coastal defence: techniques and data for 2003,*. Flood Hazard Research Centre, Middlesex University.

Pilotti, M., Maranzoni, A., Milanesi, L., Tomirotti, M., & Valerio, G. (2014). Dam-break modeling in alpine valleys. *Journal of Mountain Science*, *11*(6), 1429–1441. https://doi.org/10.1007/s11629-014-3042-0

Pinos, J., & Timbe, L. (2019). Performance assessment of two-dimensional hydraulic models for generation of flood inundation maps in mountain river basins. *Water Science and Engineering*, *12*(1), 11–18. https://doi.org/10.1016/j.wse.2019.03.001

Quirogaa, V. M., Kurea, S., Udoa, K., & Manoa, A. (2016). Application of 2D numerical simulation for the analysis of the February 2014 Bolivian Amazonia flood: Application of the new HEC-RAS version 5. *Ribagua*, *3*(1), 25–33. https://doi.org/10.1016/j.riba.2015.12.001

Říha, J., Kotaška, S., & Petrula, L. (2020). Dam break modeling in a cascade of small earthen dams: Case study of the Cizina River in the Czech Republic. *Water (Switzerland)*, *12*(8). https://doi.org/10.3390/w12082309

Robinson, D., Zundel, A., Kramer, C., Nelson, R., DeRosset, W., Hunt, J., … Lai, Y. (2019). Two-Dimensional Hydraulic Modeling for Highways in the River Environment Reference Document. *FHWA Reference Document*, *Publicatio*(October), 301. Retrieved from https://www.fhwa.dot.gov/engineering/hydraulics/pubs/hif19061.pdf

Şahin, A. N. (2016). Performance of FLO-2D software on flood inundation analysis, (MSc Thesis), Department of Civil Engineering METU, Ankara.

Salt, D. V. (2019). A comparison of HEC-RAS and DSS-WISE LITE 2D hydraulic models for a Rancho Cielito Dam breach. (MSc Thesis) California State University.

SEPA. (2018). *Flood Modelling Guidance for Responsible Authorities*. 166. Retrieved from https://www.sepa.org.uk/media/219653/flood_model_guidance_v2.pdf

Shrestha, A., Bhattacharjee, L., Baral, S., Thakur, B., Joshi, N., Kalra, A., & Gupta, R. (2020). Understanding Suitability of MIKE 21 and HEC-RAS for 2D Floodplain Modeling. *World Environmental and Water Resources Congress 2020: Hydraulics, Waterways, and Water Distribution Systems Analysis - Selected Papers from the Proceedings of the World Environmental and Water Resources Congress 2020*, 237–253. https://doi.org/10.1061/9780784482971.024

Shustikova, I., Domeneghetti, A., Neal, J. C., Bates, P., & Castellarin, A. (2019). Comparing 2D capabilities of HEC-RAS and LISFLOOD-FP on complex topography. *Hydrological Sciences Journal*, *64*(14), 1769–1782. https://doi.org/10.1080/02626667.2019.1671982

Shustikova, I., Neal, J. C., Domeneghetti, A., Bates, P. D., Vorogushyn, S., & Castellarin, A. (2020). Levee breaching: A new extension to the LISFLOOD-FP model. *Water (Switzerland)*, *12*(4), 1–17. https://doi.org/10.3390/W12040942

Singh, K. P., & Snorrason, A. (1984). Sensitivity of outflow peaks and flood stages to the selection of dam breach parameters and simulation models. *Journal of Hydrology*, *68*(1), 295–310. https://doi.org/https://doi.org/10.1016/0022-1694(84)90217-8

Sinha, R. (2005). GIS in Flood Hazard Mapping : a case study of. *GIS Development*, (July), 1–8. https://doi.org/10.13140/RG.2.1.1492.2720

Smith, K., & Ward, R. (1998). Floods: Physical Processes and Human Impacts. In *Book* (p. 394). Retrieved from http://eu.wiley.com/WileyCDA/WileyTitle/productCd-0471952486.html

Tayefi, V., Lane, S. N., Hardy, R. J., & Yu, D. (2006). A comparison of one- and two-dimensional approaches to modelling flood inundation over complex upland floodplain. *Hydrological Processes*, (Hydrol Process 21), 3190-3202 (2007).

TOB. (2019). *Kizilirmak Basin Flood Management Plan*.

TURKSTAT. (2020). Turkey Statistical Institute. Retrieved from https://www.tuik.gov.tr/Home/Index

Ünal, Ç. I. (2019). Two-dimensional dam break analyses of Berdan Dam, (MSc Thesis), Department of Civil Engineering METU, Ankara.

Urzică, A., Mihu-Pintilie, A., Stoleriu, C. C., Cîmpianu, C. I., Huţanu, E., Pricop, C. I., & Grozavu, A. (2021). Using 2D HEC-RAS modeling and embankment dam break scenario for assessing the flood control capacity of a multireservoir system (Ne Romania). *Water (Switzerland)*, *13*(1), 1–28. https://doi.org/10.3390/w13010057

USACE. (1979). Appendix D, Recommended Guidelines for Safety Inspection of Dams, National Program of Inspection of Dams, ER 1110-2-106. Retrieved from Office of the Chief of Engineers, Corps of Engineers, Washington DC website: http://www.mde.state.md.us/programs/Water/DamSafety/TechnicalReferences/Documents/www.mde.state.md.us/assets/document/damsafety/COE/Guidelines for Safety Inspections of Dams.pdf.

USACE. (1997). Dam Safety Assurance Program (ER-1110-2-1155). Retrieved from http://140.194.76.129/publications/eng-regs/er1110-2-1155/entire.pdf.

USACE. (2009). The National Inventory of Dams. Retrieved from http://nid.usace.army.mil/.

USACE. (2014) Using HEC-RAS for a dam break studies. Davis: Institute of Water Resources, Hydrological Engineering Center.

USBR. (1995). *Emergency planning and exercise guidelines, Volume I: guidance documents*. Denver, USA.

USBR. (1998). *Emergency Action Planning, Proceedings of the International Technical Seminar "Dam and Safety Operation and Maintenance."* Denver, USA.

Vinet, F. (2017). Introduction. *Floods: Volume 1 - Risk Knowledge*, xv–xxvii. https://doi.org/10.1016/B978-1-78548-268-7.50022-5

Viseu, T., Palma, J., Oliveira Costa, C. (2007). *Alqueva dam early warning system. Proceedings of the 5th International Conference on Dam Engineering*. Lisbon, Portugal.

Wahl, T. L. (2010). Dam Breach Modeling – an Overview of Analysis Methods. *2nd Joint Federal Intragency Conference Las Vegas, NV*, 1–12.

Wikipedia. (2020). (https://en.wikipedia.org/wiki/Dam_failure).

Wing, O. E. J., Bates, P. D., Neal, J. C., Sampson, C. C., Smith, A. M., Quinn, N., Krajewski, W. F. (2019). A New Automated Method for Improved Flood Defense Representation in Large-Scale Hydraulic Models. *Water Resources Research*, *55*(12), 11007–11034. https://doi.org/10.1029/2019WR025957

Xu, Y., & Zhang, L. M. (2009). Breaching Parameters for Earth and Rockfill Dams. *Journal of Geotechnical and Geoenvironmental Engineering*, *135*(12), 1957–1970. https://doi.org/10.1061/(asce)gt.1943-5606.0000162

Yalçın, E. (2020). Assessing the impact of topography and land cover data resolutions on two-dimensional HEC-RAS hydrodynamic model simulations for urban flood hazard analysis. *Natural Hazards*, *101*(3), 995–1017. https://doi.org/10.1007/s11069-020-03906-z

Zaifoğlu, H. (2018). Implementation of a Flood Management System for Nicosia, (PhD Thesis), Department of Civil Engineering METU, Ankara.

Zeleňáková, M., Fijko, R., Labant, S., Weiss, E., Markovič, G., & Weiss, R. (2019). Flood risk modelling of the Slatvinec stream in Kružlov village, Slovakia.

Journal of Cleaner Production, *212*, 109–118. https://doi.org/10.1016/j.jclepro.2018.12.008

Zhang, L., Peng, M., Chang, D., Xu, Y. (2016). *Dam failure Mechanisms and Risk Assesment* (1st ed.). John Wiley & Sons, Singapore 473 pp.

Zolghadr, M., Hashemi, M. R., & Zomorodian, S. M. A. (2011). Assessment of MIKE21 model in dam and dike-break simulation. *Iranian Journal of Science and Technology*, *Transaction B: Engineering*, *35*(C2), 247–262.

APPENDICES

Appendix: Inundation Maps

Ondokuz Mayıs Dam Inundation maps

HEC-RAS

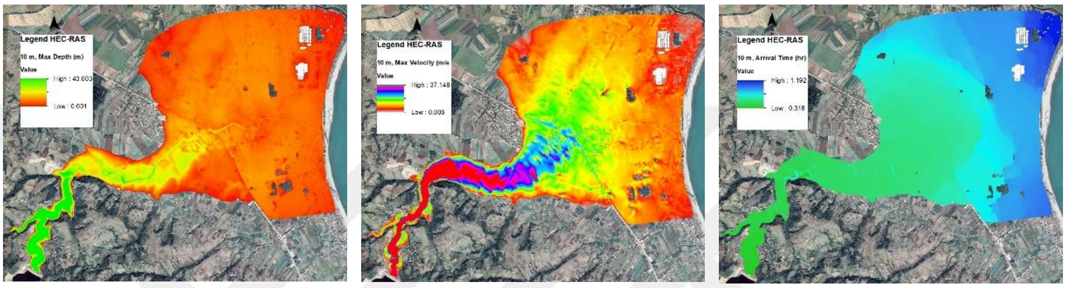

10 m

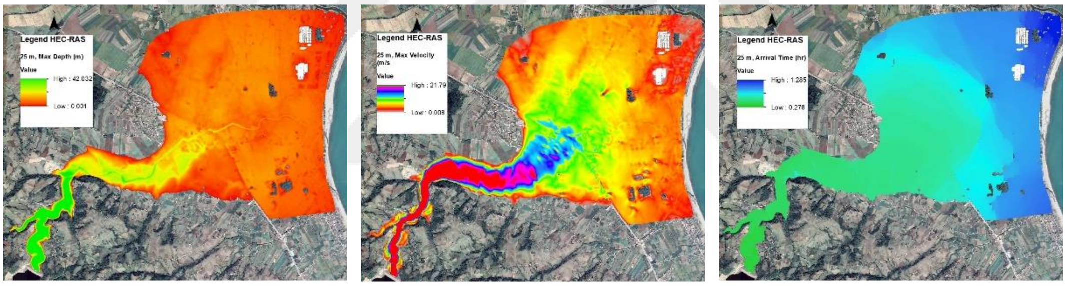

25 m

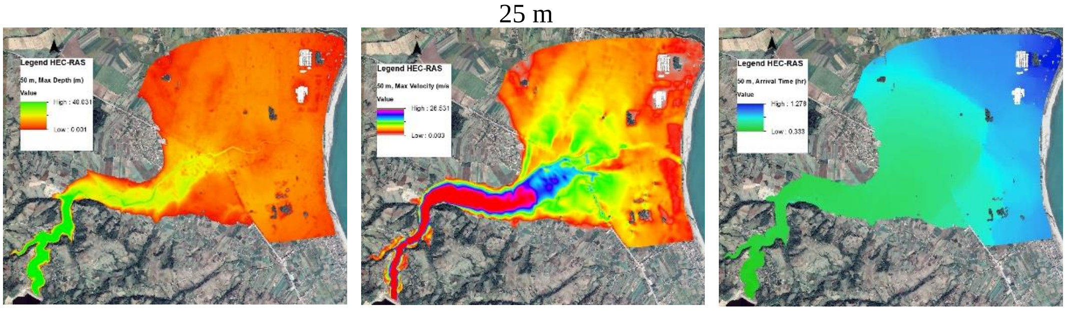

50 m

(a) (b) (c)

Figure A-1 Ondokuz Mayıs Dam. HEC-RAS, S1, (10m, 25m, & 50m)
(a) Max depth (b) Max velocity (c) Arrival time

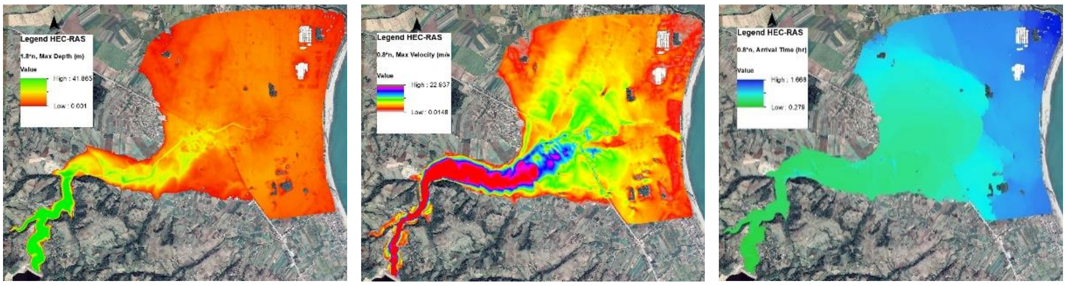

0.8* n

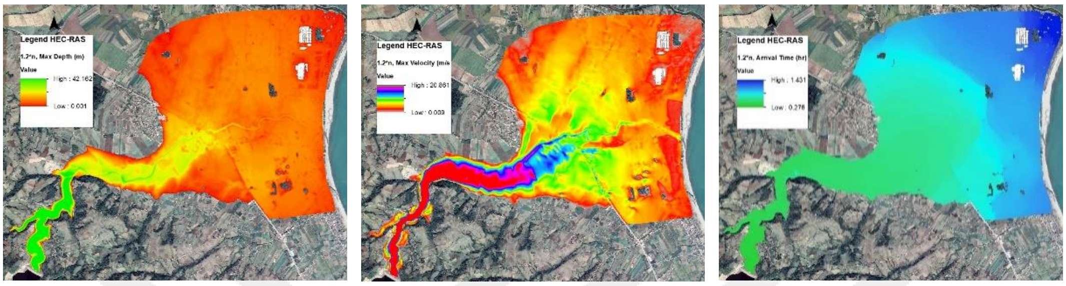

1.2* n

(a) (b) (c)

Figure A-2 Ondokuz Mayıs Dam. HEC-RAS, S1, 0.8*n & 1.2*n (5m)
(a) Max depth (b) Max velocity (c) Arrival time

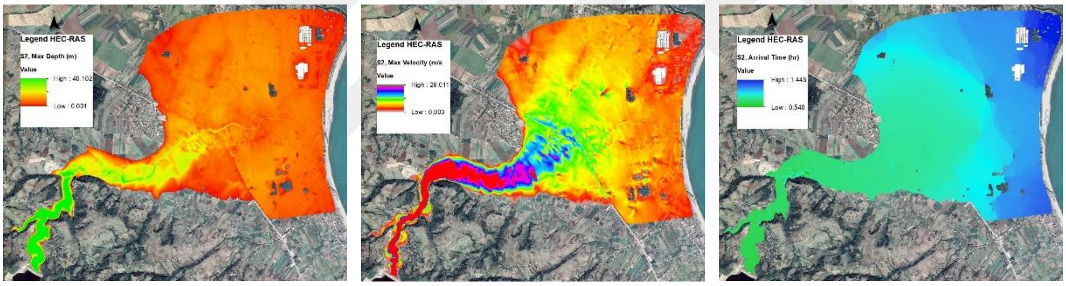

S2

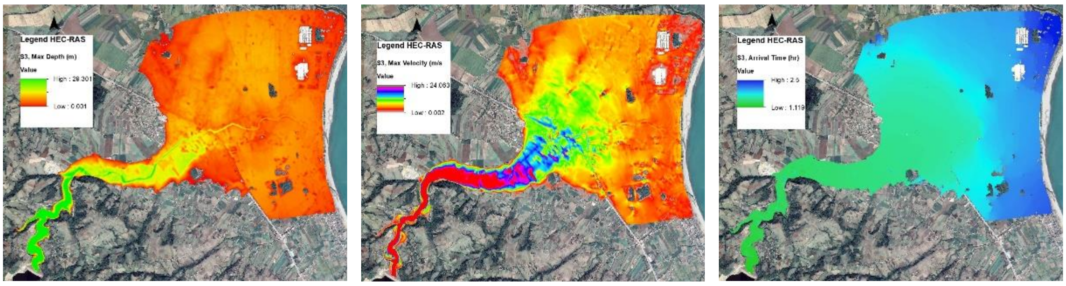

S3

(a) (b) (c)

Figure A-3 Ondokuz Mayıs Dam. HEC-RAS, S2 & S3 (5m)
(a) Max depth (b) Max velocity (c) Arrival time

FLO-2D

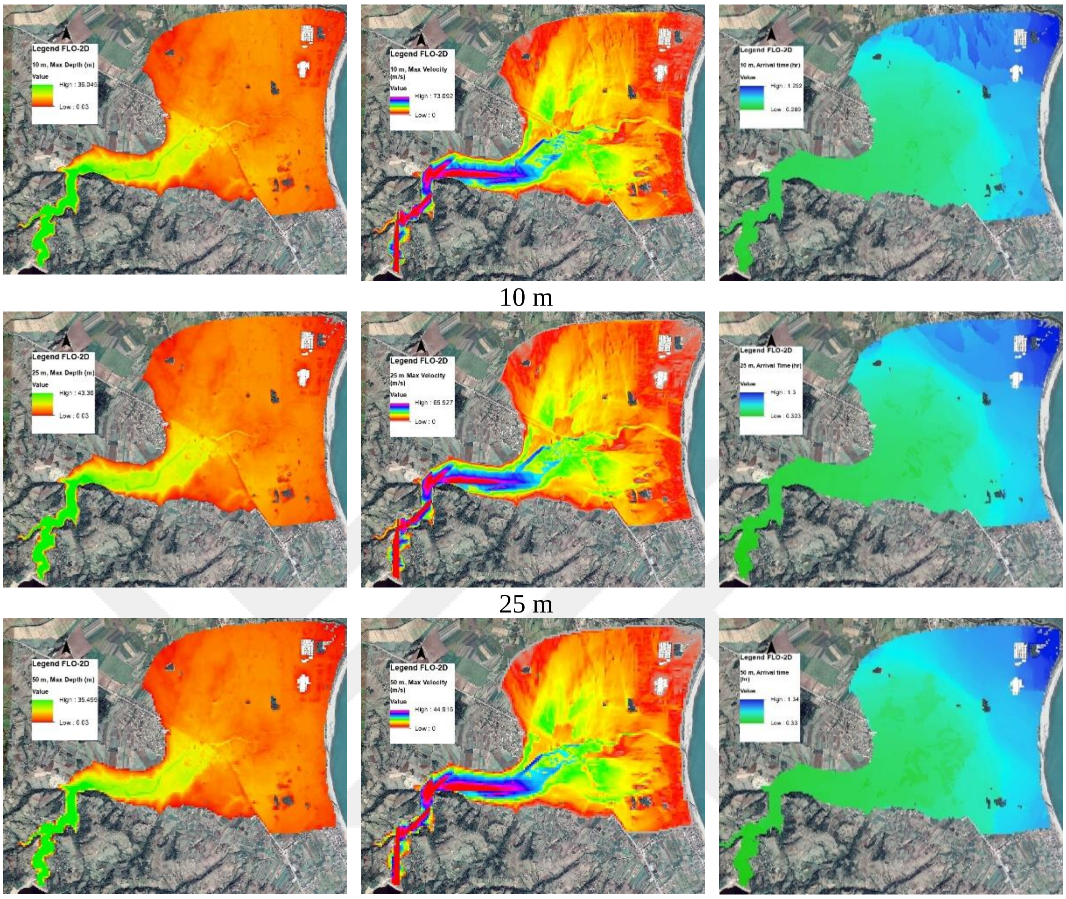

(a) (b) (c)

Figure A-4 Ondokuz Mayıs Dam. FLO-2D, S1, (10m, 25m, & 50m)
(a) Max depth (b) Max velocity (c) Arrival time

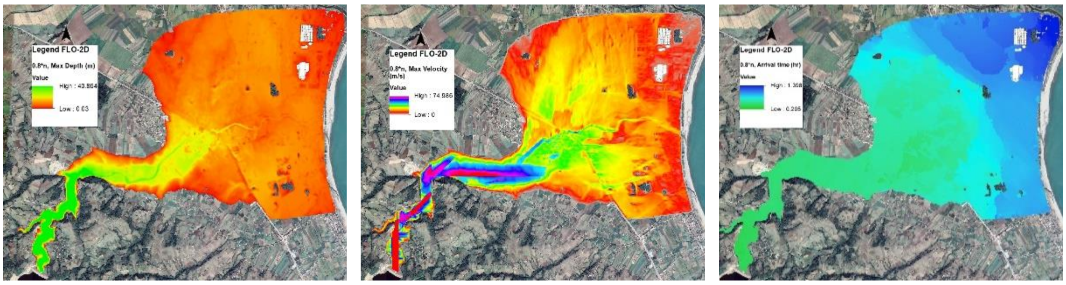

0.8* n

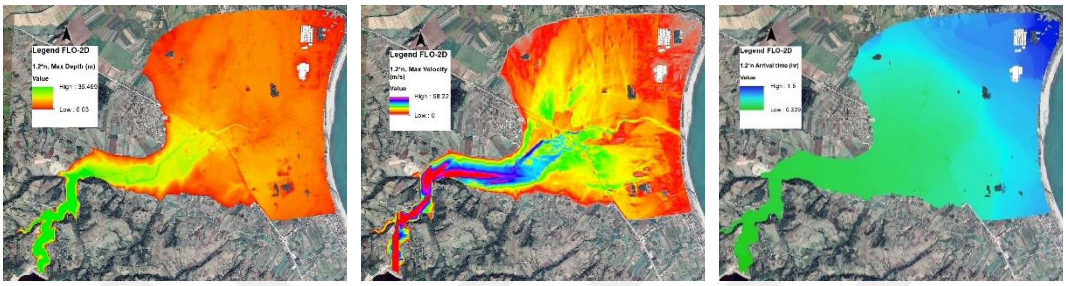

1.2* n

(a) (b) (c)

Figure A-5 Ondokuz Mayıs Dam. FLO-2D, S1, 0.8*n & 1.2*n (5m)
(a) Max depth (b) Max velocity(c) Arrival time

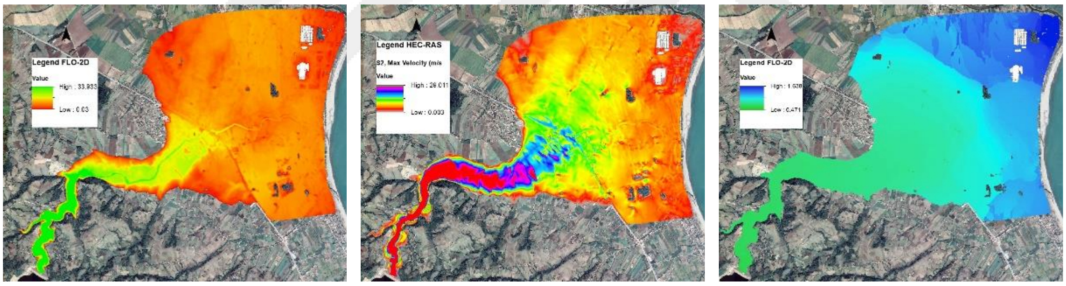

S2

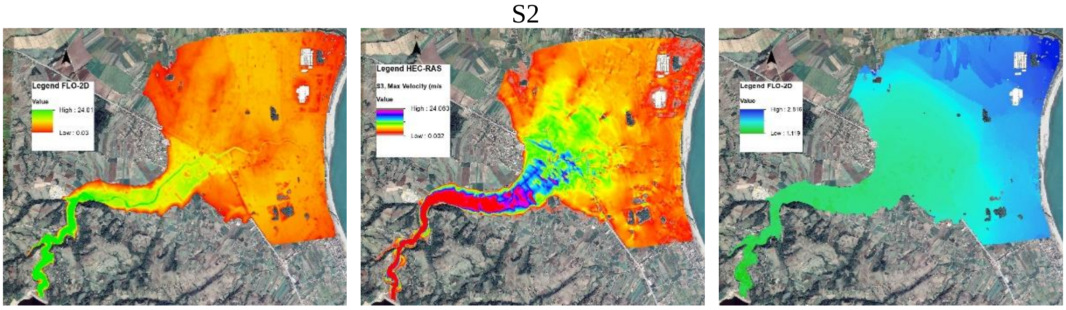

S3

(a) (b) (c)

Figure A-6 Ondokuz Mayıs Dam. FLO-2D, S2 & S3 (5m)
(a) Max depth (b) Max velocit y(c) Arrival time

İhsaniye Dam Inundation maps

HEC-RAS

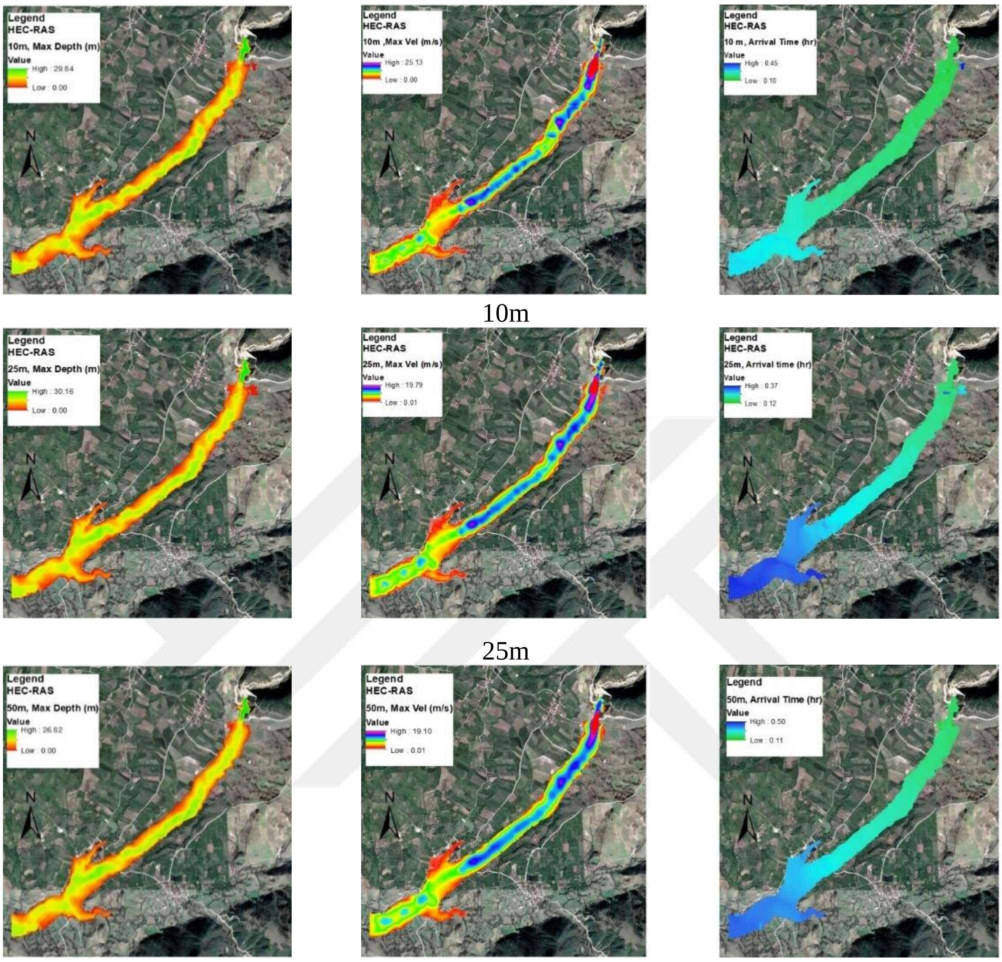

50 m

(a) (b) (c)

Figure A-7 İhsaniye Dam. HEC-RAS S1, (10m, 25m, & 50m)
(a) Max depth (b) Max velocity (c) Arrival time

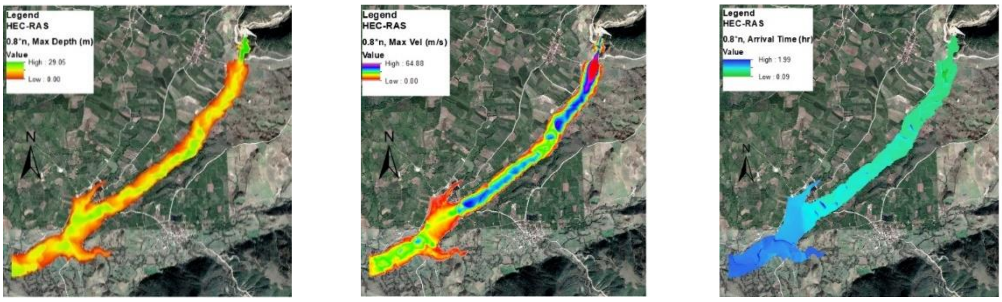

0.8* n

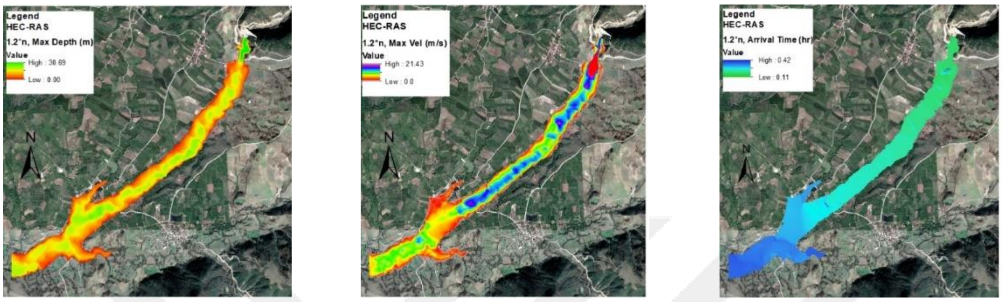

1.2*n

(a) (b) (c)

Figure A-8 İhsaniye Dam. HEC-RAS, S1, 0.8*n & 1.2*n (5m)
(a) Max depth (b) Max velocity (c) Arrival time

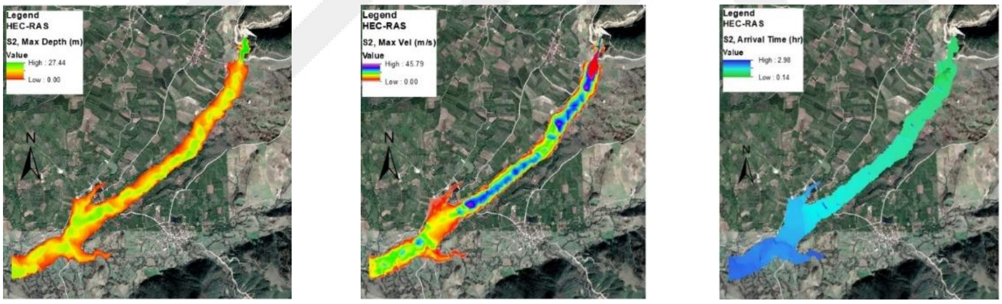

S2

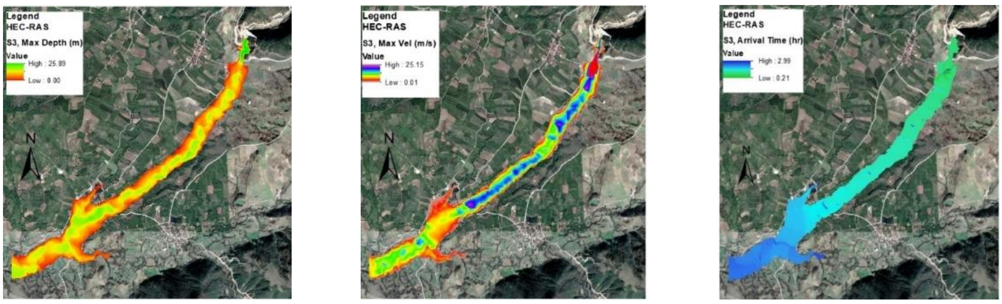

S3

(a) (b) (c)

Figure A-9 İhsaniye Dam. HEC-RAS, S2 & S3 (5m)
(a) Max depth (b) Max velocity (c) Arrival time

FLO-2D

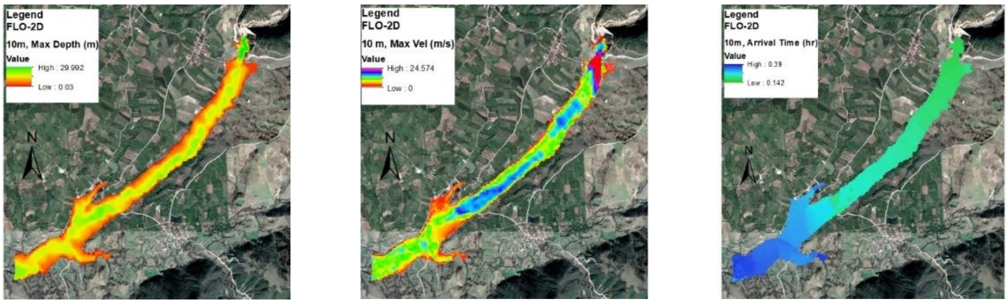

10 m

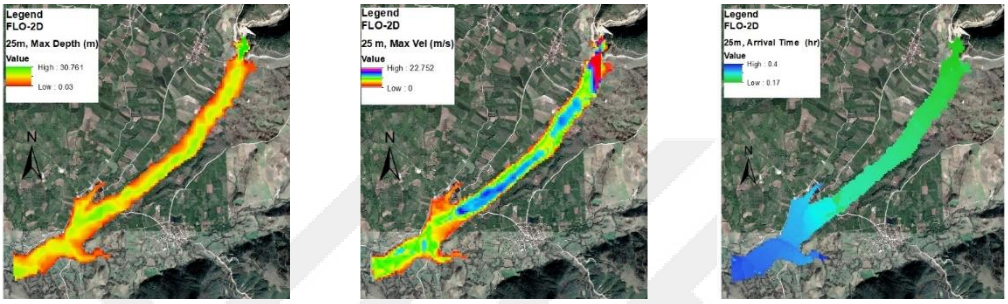

25 m

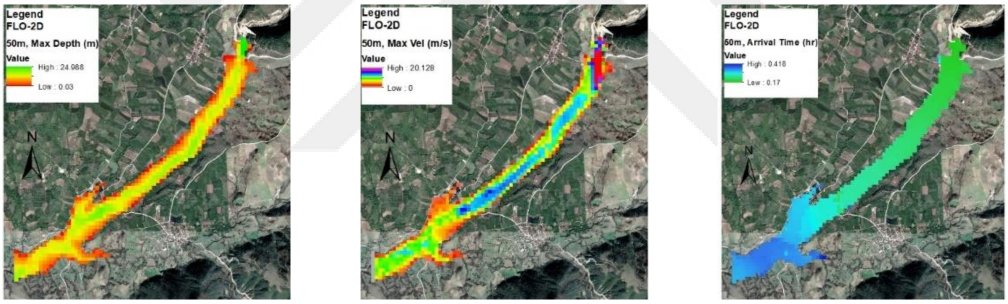

50 m

(a) (b) (c)

Figure A-10 İhsaniye Dam. FLO-2D, S1, (10m, 25m, & 50m)
(a) Max depth (b) Max velocity (c) Arrival time

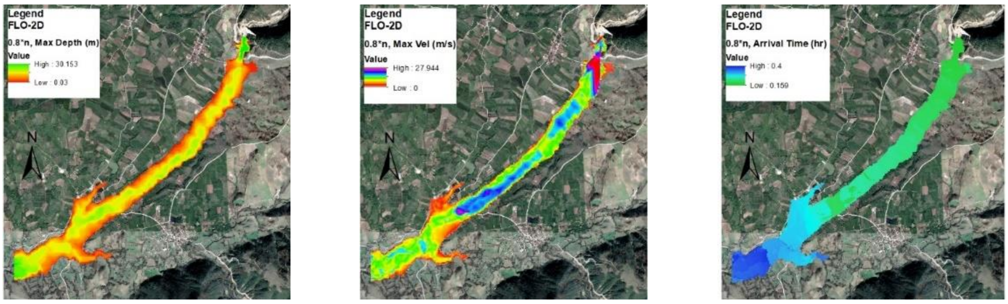

0.8*n

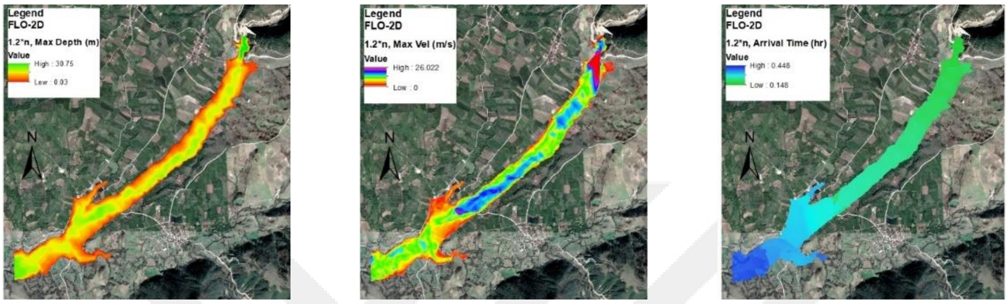

1.2*n

(a) (b) (c)

Figure A-11 İhsaniye Dam. FLO-2D, S1, 0.8*n & 1.2*n (5m)
(a) Max depth (b) Max velocity (c) Arrival time

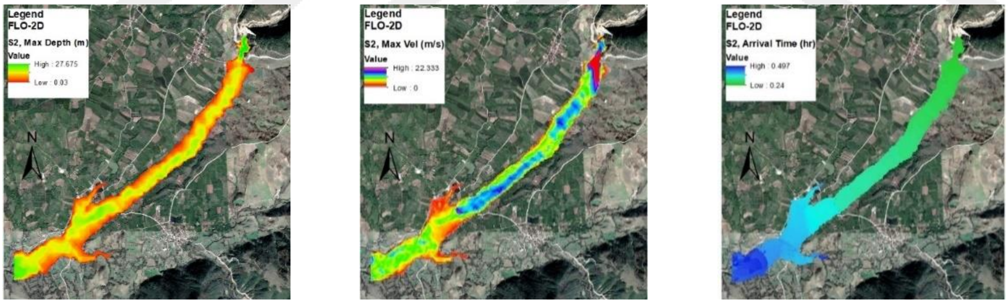

S2

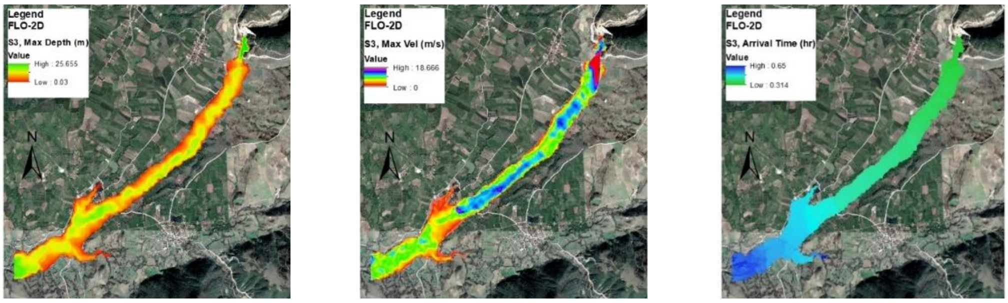

S3

(a) (b) (c)

Figure A-12 İhsaniye Dam. FLO-2D, S2 & S3 (5m)
(a) Max depth (b) Max velocity (c) Arrival time

Avcidere Dam Inundation maps

HEC-RAS

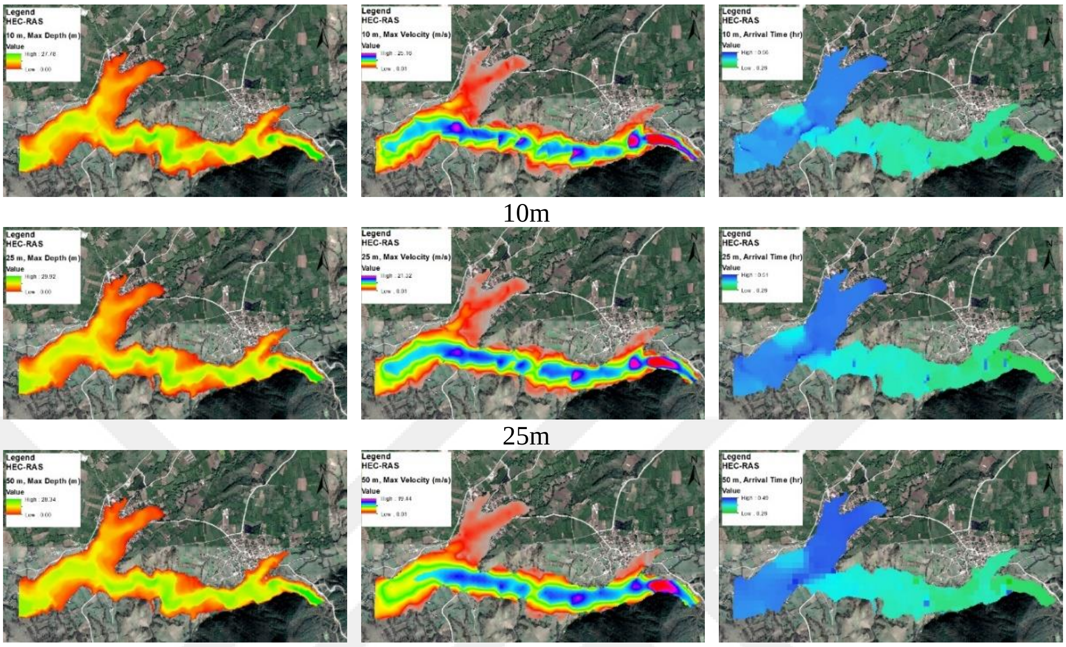

(a) (b) (c)

Figure A-13 Avcıdere Dam. HEC-RAS, S1, (10m, 25m, & 50m)
(a) Max depth (b) Max velocity (c) Arrival time

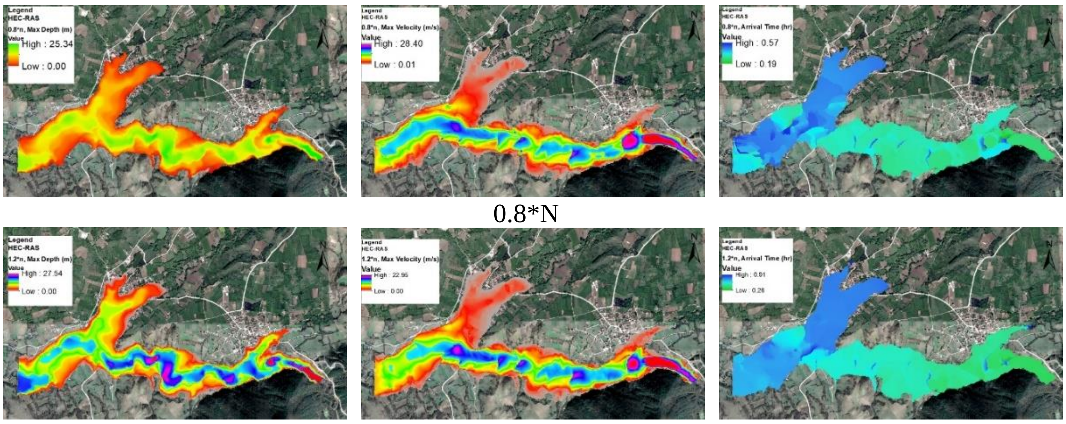

(a) (b) (c)

Figure A-14 Avcıdere Dam. HEC-RAS, S1, 0.8*n & 1.2*n (5m)
(a) Max depth (b) Max velocity (c) Arrival time

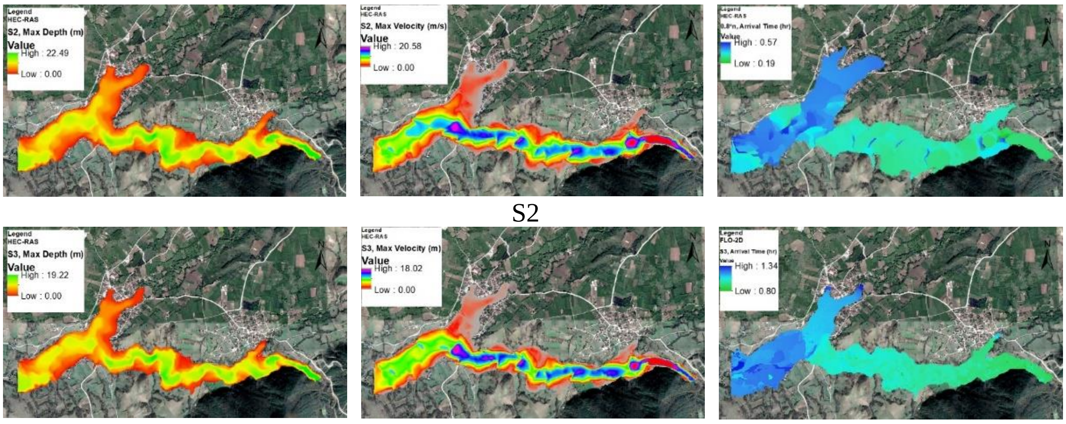

S2

S3

(a) (b) (c)

Figure A-15 Avcıdere Dam. HEC-RAS, S2 & S3 (5m)
(a) Max depth (b) Max velocity (c) Arrival time

FLO-2D

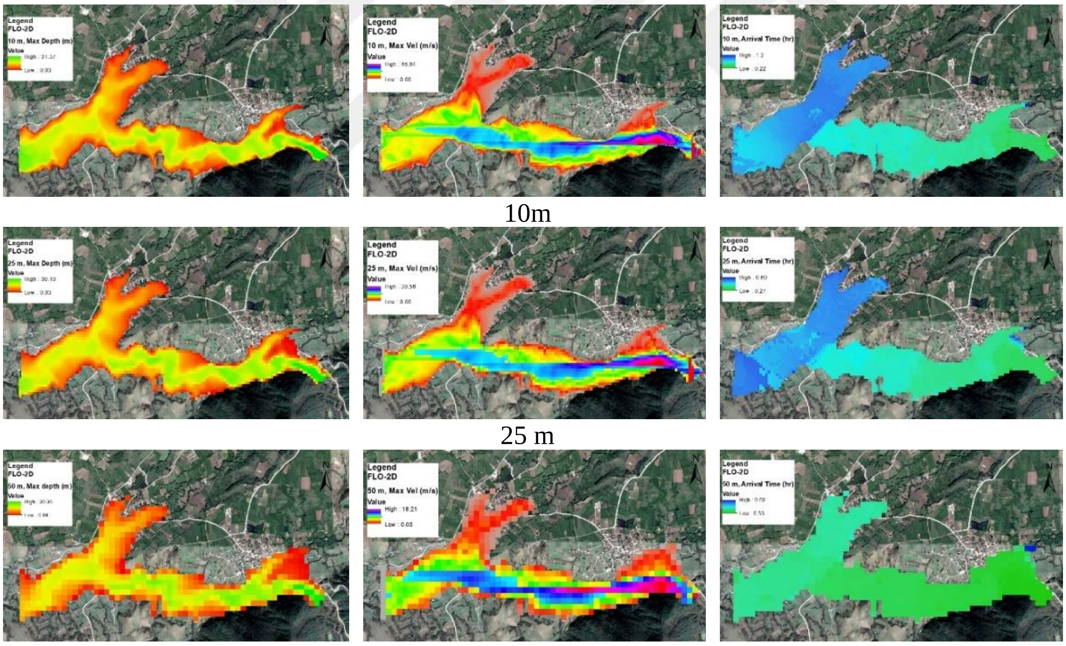

10m

25 m

50m

(a) (b) (c)

Figure A-16 Avcıdere Dam. FLO-2D, S1, (10m, 25m, & 50m)
(a) Max depth (b) Max velocity (c) Arrival time

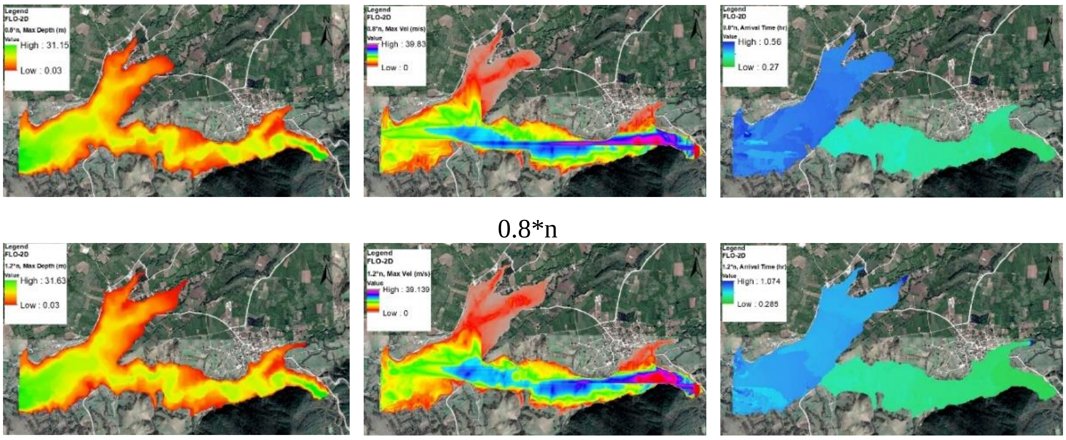

0.8*n

1.2*n

(a) (b) (c)

Figure A-17 Avcıdere Dam. FLO-2D, S1, 0.8*n & 1.2*n (5m)

(a) Max depth (b) Max velocity (c) Arrival time

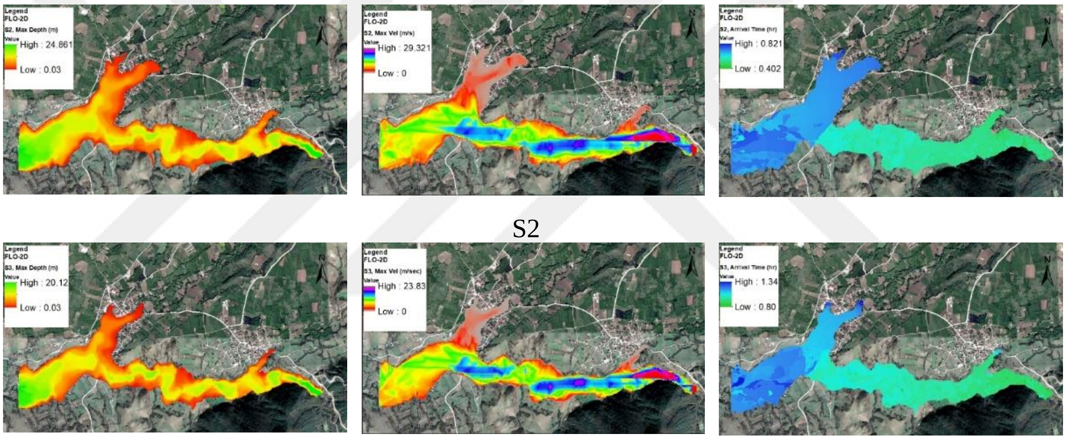

S2

S3

(a) (b) (c)

Figure A-18 Avcıdere Dam. FLO-2D, S2 & S3 (5m)

(a) Max depth (b) Max velocity (c) Arrival time

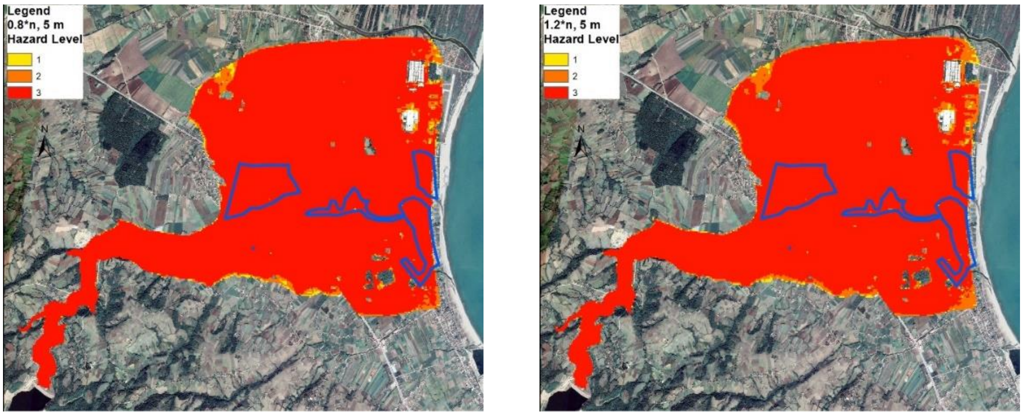

(a) (b)

Figure A-19 Flood Hazard map: Ondokuz Mayıs Dam, S1 (a) 0.8* n (b) 1.2* n

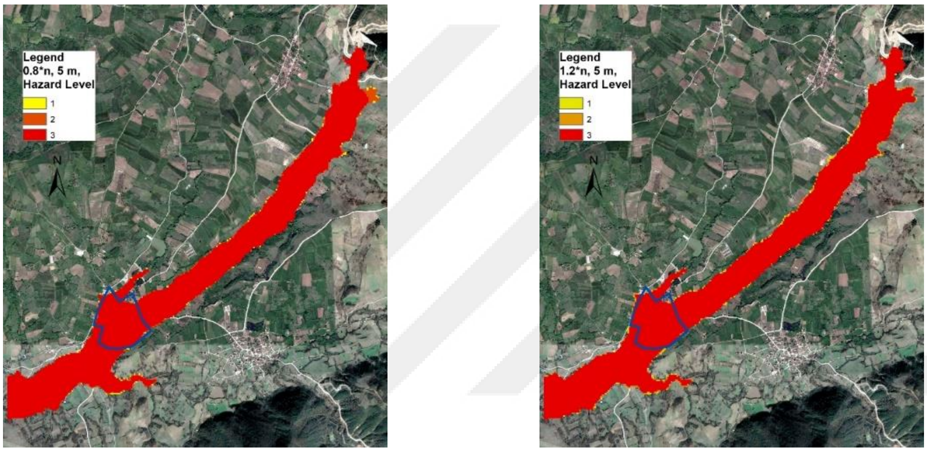

(a) (b)

Figure A-20 Flood Hazard map: İhsaniye Dam, S1 (a) 0.8* n (b) 1.2* n

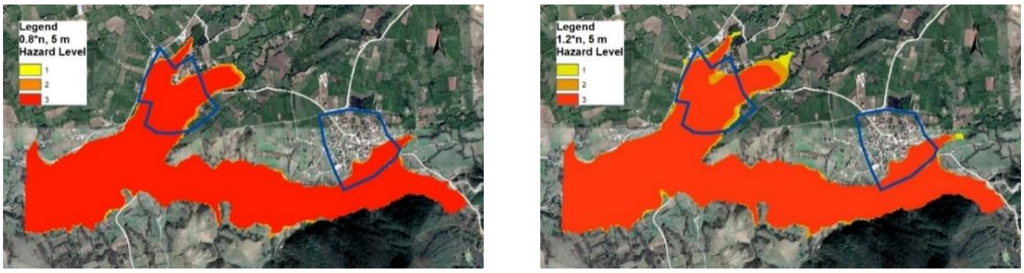

(a) (b)

FigureA-21 Flood Hazard map: Avcıdere Dam, S1 (a) 0.8* n (b) 1.2* n

CURRICULUM VITAE

PERSONAL INFORMATION